SIMULATION-BASED PROCESS DESIGN AND INTEGRATION FOR RETROFIT

A thesis submitted to the

University of Manchester

for the degree of

Doctor of Philosophy

in the Faculty of

Engineering and Physical Sciences

2010

by

Aurora Hernández Enríquez

School of Chemical Engineering and Analytical Science

Under the direction of

Dr. Jin-Kuk Kim

Contents

Word count: 53,086 words

List of tables

Table Page

List of figures

Figure Page

Nomenclature and abreviations

ACC_{HE}	Annualized capital cost for heat exchangers (£/Year)
ACC_i	Annualized capital costs (£/Year)
$ACC_{NewUnits}$	Annualized capital cost for new units (£/Year)
AF	Annualization Factor (Y^{-1})
$AirE_i$	Air emission of i (Tonnes i /Mt HC)
ANOVA	Analysis of variance
BC	Base Case
$_C$ =	Cold stream
CC	Composite curve
CCC	Cold composite curve
CCD	Central composite design
CC_{HE}	Capital Cost of the HE (£)
$CC_{NewUnit}$	Capital Cost of the new unit (£)
CIPA	Index of capital investment over plant assets (%)
$CI(X_i)$	Capital investment of i (£)
COP	Coefficient of performance
CO_2T	Annualized benefit from reduction in CO_2 emissions´tax (£/Y)
Cp	Heat capacity (kJ/(°C kg))
CP	Heat capacity flowrate (kJ/s)
DCS	Distributed control system
DoE	Design of experiments
EAs	Evolutionary algorithms
EI	Energy Improvements (£/Y)
EOS	Equation-oriented simulation
EPA42 factor	EPA-42 emissions´factor (MMTon CO_2/MMBtu)
ER	Energy recovery (kW)
ET	Energy targeting (kW)
FD	Factorial designs
FFD	Fractional factorial designs
Fi	Factor in EPA 42 for compound i [(Tonnes i*s) / (Mt HC*kJ)]
FOB	Free on board investment cost (£)
Fr_{FG}	Flowrate of fuel gas (kg/s)
Fr_{SGP}	Flowrate of sweetened gas processed (Tonne HC processed/Y)
GAs	Genetic algorithms
GCC	Grand composite curve
GCV	Gross calorific value (kJ/kg)
GHG	Greenhouse gas
GRG2	Generalised reduced gradient
$_H$	Hot stream
HC	Hydrocarbon
HCC	Hot composite curve
HCF	Hydrocarbon fractionation process
HE	Heat exchanger
HEN	Heat exchange network
H_i	Enthalpy intervals (kJ/kg)

HPS	High-pressure steam (P=100 kg/cm^2)
HUR	Hot Utility Reduction (MMBtu/Y)
IMP	Mexican Institute of Petroleum
IPCC	The Intergovernmental Panel on Climate Change
IPS	Intermediate pressure steam (P=24 kg/cm^2)
LP	Linear programming
MaPr	Marginal profit (£/Year)
MaPr*	Marginal profit normalised (Absolute Units/Year)
MARR	Minimum acceptable rate of return (%)
MER	Maximum energy recovery (kW)
MF	Mass flowrate (kg/s)
MINLP	Mixed integer nonlinear programming
MPCA	Marginal profit capital affected (£/Year)
MPCA*	Marginal profit capital affected normalised (Absolute Units/Year)
MPS	Medium-pressure steam (P=43 kg/cm^2)
N/A	Not available
NGL	Natural gas liquid recovery process
NLLS	Nonlinear least squares
NLP	Nonlinear programming
N_2Pe	Nitrogen penalty (£/Year)
NPr	Net profit (£/Year)
NPW	Net present worth (£)
LLS	Linear least squares estimation
LPG	Gas liquified from petroleum
LPS	Low-pressure steam (P=4.5 kg/cm^2)
OD	Operating data
PA	Plant assets (£)
PEMEX	Petroleos Mexicanos
PI	Process integration
PLP	Project Life Period (10 years)
PP	Payback period (Y)
PSE	Process systems engineering
PV	Variation in the value of the parameter from the base case (%)
PV_{BC}	Parameter value in the base case (parameter unit)
PV_S	Parameter value in the simulated case (parameter unit)
R^2	Statistic for model validation
RG	Residue gas
RGHP	Residue gas high pressure
RGLP	Residue gas low pressure
RMSE	Root mean square error
RSM	Response surface methodology
SA	Simulated annealing algorithms
SCC	Estimated social cost of carbon (£)
$SCCO_2$	Estimated Social Cost of CO_2 ($USD/Ton CO_2)
S_{CO}	Profit from the sales of co-product (£/Year)
SEC	Specific energy consumption (GJ/Tonne HC processed)
SG	Sweetened gas
SM	Simulated results

SMS	Sequential modular simulation
S_P	Profit from the sales of product (£/Year)
S_{RGHP}	Sells of RGHP (£/Year)
T_{COND}	Temperature for the condenser (°C)
TEC	Total energy consumption $(Electricity + FuelGas + Steam)$ (GJ/Year)
T_{EVAP}	Temperatures for the evaporator (°C)
T_i	Temperature intervals (°C)
TS	Supply temperature (°C)
TT	Target temperature (°C)
VC_E	Variable cost of energy (£/Year)
VC_{RM}	Variable cost of raw material (£/Year)
VF	Vapour fraction
α	Relative volatility
Φ	Diameters (m)
ΔQ_C	Minimum cold utilitiy energy needed (kW)
ΔQ_H	Minimum hot utilitiy energy needed (kW)
ΔT_{min}	Minimum temperature difference (°C)
ε	Error term
C_2+	Cryogenic liquids from internal supplier
C_3+	Cryogenic liquids from external supplier
C_5+	Light Naphtas
C_6+	Heavy Napthas

Abstract

This research proposes a novel Retrofit Design Approach based on process simulation and the Response Surface Methodology (RSM).

Retrofit Design Approach comprises: 1) a diagnosis stage in which the variables are screened and promising variables to improve system performance are identified through a sensitivity analysis, 2) an evaluation stage in which RSM is applied to assess the impact of those promising variables and the most important factors are determined by building a reduced model from the process response behaviour, and 3) an optimisation stage to identify optimal conditions and performance of the system, subject to objective function and model constraints. All these stages are simulation-supported.

The main advantages of the proposed Retrofit Design Approach using RSM are that the design method is able to handle a large industrial-scale design problem within a reasonable computational effort, to obtain valuable conceptual insights of design interactions and economic trade-off existed in the system, as well as to systematically identify cost-effective solutions by optimizing the reduced model based on the most important factors. This simplifies the pathway to achieve pseudo-optimal solutions, and simultaneously to understand techno-economic and system-wide impacts of key design variables and parameters.

In order to demonstrate the applicability and robustness of the proposed design method, the proposed Retrofit Design Approach has been applied to two case studies which are based on existing gas processing processes. Steady-state process simulation using Aspen Plus TM® has been carried out and the simulation results agree well with the plant data. Reduced models for both cases studies have been obtained to represent the techno-economic behaviour of plants. Both the continuous and discrete design options are considered in the retrofitting of the plant, and the results showed that the Retrofit Design Approach is effective to provide reliable, cost-effective retrofit solutions which yield to improvements in the studied processes, not only economically (i.e. cost and product recovery), but also environmentally linked (i.e. CO_2 emissions and energy efficiency). The main retrofitting solutions identified are, for the first case, column pressure change, pump-around arrangement and additional turbo-expansion capacity, while for the second case, columns pressure change, trays efficiency, HEN retrofit arrangements (re-piping) and onsite utility generation schemes are considered. These promising sets of retrofit design options were further investigated to reflect implications of capital investment for the retrofit scenarios, and this portfolio of opportunities can be very useful for supporting decision-making procedure in practice. It is important to note that in some cases a cost-effective retrofit does not always require structural modifications.

In conclusion, the proposed Retrofit Design Approach has been found to be a reliable approach to address the retrofit problem in the context of industrial applications.

Declaration

No portion of the work referred to in this thesis has been submitted in support of an application for another degree or qualification of this or any other university or other institution of learning.

Aurora Hernández Enríquez

COPYRIGHT STATEMENT

Dedicated to

This thesis is dedicated to God for everything I am and to my parents for their love, endless support and encouragement in all the way since the beginning of my life.

Finally, this thesis is dedicated to you bb, who always believe in me and all those who believe in the richness of learning.

Acknowledgments

I am deeply grateful to my supervisor, Doctor Jin-Kuk Kim, for his detailed and constructive comments, for his patience and for his important support throughout this work.

The financial support of the “Consejo Nacional de Ciencia y Tecnologia de Mexico (CONACyT)” is gratefully acknowledged.

My warm thanks are due to Professor Martin Tanco for his kind support and guidance in the application of RSM studies.

Chapter 1. Introduction

1.1 Motivation of the research

It has been suggested that the world is in a period of transition towards a sustainable energy system (Hekkert et al., 2005). The best strategy for this transition seems to be in two parallel forms – by reducing current greenhouse gas (GHG) emissions and implementing changes that are flexible enough for future innovations in the energy sector. More sustainable fuels need to be used, but this requires significant capital investment in restructuring of current plants, distribution systems, and a great deal of time to achieve the strategy of transition. Carbon dioxide emissions therefore become an important evaluation criterion, as stated in several international environmental activities: The 1987 Montreal Protocol (UNO, 1987), The Agenda 21 Initiative in June of 1992 at the Rio de Janeiro United Nations Convention on Climate Change (UNO, 1999), and The Intergovernmental Panel on Climate Change in 1988 (IPCC, 1988).

As a result, some government entities in the European Union, the USA and the Canadian province of British Columbia have started applying a carbon tax (Helm, 2009). Others, such as Australia and New Zealand, have adopted carbon emission trading, or "cap and trade", through which polluters can trade some or all of their permits with others (cap-and-trade) based on carbon credits, domestically or internationally. A hybrid instrument involving a cap and a carbon tax by creating a price-floor and a price-ceiling for emission permits has also been proposed (Hepburn, 2006). At the time of undertaking this research, a controversial discussion about the right regulations to set for the reduction of GHG emission levels across the world is underway, but there is no unique instrument to evaluate any outcomes (Kanter, 2009). What is for sure is that more and more companies are looking for solutions to reduce their GHG emissions or even to make no net contribution to global warming.

Globalisation has also encouraged the industry to look at increasing profits, reducing environmental impacts, being safer and developing a commitment to sustainability in order to be competitive. Therefore, many chemical companies have turned their attention

towards finding areas of opportunity and addressing these with a view to taking them forward. Such opportunities include energy savings, cost reductions, increasing quality standards and eliminating bottlenecks, while others seek acquiring new equipment or changing old processes for new ones.

In this context, simulation and optimisation techniques have been utilised as a tool in the process for decision-making, both of which are based primarily on the translation of a real engineering problem into mathematical equations that represent the process studied, the performance criterion or criteria and the constraints (Edgar et al., 2001). This procedure is commonly known as mathematical modelling. Once the model is built, simulation is used to verify the validity of the model to reproduce real data. After this, the optimisation process follows, in order to find the values of the variables in the model that yield the best value(s) of the performance criterion/criteria, which means the best possible solutions to the engineering problem are established. The process optimisation can be executed to support two options, the named "grassroot process design" and the "retrofit process design". The former applies to new process plants and the last deals with already set production plants.

This is not such an easy process, though, because the more variables and kinds of equations involved in the model, the more complex the mathematical algorithms used to find the solutions and the more difficulties and time taken to converge on a solution. In addition to that, in most cases there also exists a trade-off between the issues considered in the performance criterion/criteria. On the other hand, a model that contains unknown and immeasurable parameters does not have value in real life thus available experimental and operational evidence are important for modelling.

Previous studies have identified that a good deal of work has been done with advanced algorithms to solve multi-objective optimisation problems (Pintaric and Kravanja, 2004, Pintaric and Kravanja, 2000, Toffolo and Lazzaretto, 2002, Jia et al., 2006). However, it is still difficult to obtain a realistic operational model of a plant that includes not only the intrinsic process issues, but also the complementary issues previously mentioned (i.e. financial, environmental, safety, reliability). In addition, computational difficulties arise when attempts are made to solve more complex problems such as a global optimisation algorithm.

Hence, further research should be undertaken to explore these issues in the context of site-wide process retrofit designs, in order to determine the most cost-effective and practical solutions and provide a reliable design tool that can be applied across the industry. This has become the main motivation of the present work.

1.2 Objectives and novelty of the research

Following the motivation for this research work, the current study aims to develop a reliable and practical design approach which generates cost-effective and environmental-friendly retrofit design options. The design approach is a direct response of the industrial needs and it is intended that its generated options are used as a decision-support tool by the management team of the company. Therefore, the retrofit opportunities portfolio resulting from the design approach must be clear, conscise and well understood by the management team.

As a consequence of this, the proposed approach should be able to:

- Provide useful and reliable information of the retrofit options generated
- Generate solutions with a reasonable computational effort and acceptable computing time
- Be widely applicable in industry

By considering the limitations found in literature which were briefly mentioned in previous section 1.1 and which will be detailed in chapter 2, the research work done has implicit the novelties stated as follows:

“To combine two design methods, namely, process simulation and a response surface methodology, but rarely used together, in the field of chemical engineering for the execution of retrofit studies in the context of process integration.” This is considered novel because, as found in the literature surveys carried out in the response surface methodology, most of the studies in the chemical engineering field haven been done either on fitting mathematical models based on experiments performed, or in the

optimisation of products or processes based on process conditions; on the other hand, the application to simulation data has been mainly found in mechanical design studies (Laura Ilzarbe, 2008, Tanco et al., 2008, Tanco et al., 2009, Gaia Franceschini, 2008). Consequently, the focus of response surface methodology to plant retrofit design and the use of process simulation data can be considered as the main originality in this work.

One additional novelty resides in the same response surface methodology, which proposes the optimal search method based on ascending or descending slopes with stepsizes manually set and the repetitive evaluation of the model obtained under these until reaching a maximum or minimum point (Montgomery, 2005). In this work this stage is replaced by direct optimisation of this model using a numerical optimisation algorithm, linear or nonlinear according to the case. This speeds up the rate of solution and helps to improve the globality of solutions found.

In order to consider the intrinsic effects that the retrofit changes produce in the heat exchange system of the process, and to reduce the extra-work derived from these changes, a combined objective function is proposed. This includes both, the effect in the economic impacts (profit) and the effect in the energy targets (reduction of energy targets) to be applied in the first sensitivity analysis stage. This consideration can be translated as a two-objective function which is other originality of this approach because it differs from the commonly used economic benefit; this improves the efficiency of the optimum solution search by considering only the promising options in the searching space.

A further novelty of this work resides in the intrinsic estimation of environmental indexes from the simulation results. Although this is not either fully accurated or considered in the proposed approach at this point, it gives an insight of those indexes and the process simulation is already prepared to deal with future regulations. The remaining steps need to be focused on improvements to the calculator inside the simulation flowsheet in order to get better and reliable estimations.

The previously stated novelties of this approach yield to reliable, realistic and cost-effective retrofit solutions without heavy computational efforts.

1.3 Research significance and benefits

As it can be inferred from the motivation of this work, the concept of retrofit design is deeply involved in the decision-making process of the industry as this has been of great interest towards a more efficient and cleaner production. A large number of process design concepts in combination with optimisation methodologies have been developed and retrofit design is by now well established in process system engineering research. This will be detailed in chapter 2 but in general it can be shortly mentioned that the process design options comprise of chemical reaction alternatives, separation methodologies, separation sequencing, and energy recovery systems (power and heat exchange).

In addition to that, there are three main branches developed and used as the optimisation methodologies according with the type of problem to be solved. The first are the deterministic techniques such as the nonlinear programming (NLP), linear programming (LP) and the mixed integer nonlinear programming (MINLP). The second branch is comprised of the stochastic techniques such as evolutionary algorithms (EAs), genetic algorithms (GAs), and simulated annealing algorithms (SA). There is a third branch named as the experimental techniques in which the "design of experiments" (DoE) and the "response surface methodology" (RSM) are the options available to carry out the optimisation. Although all of those process design options and optimisation algorithms are found to be widely applied to the industrial scale case, it is found that a practical and reliable approach is still missing along the work done.

This research proposes a methodology for retrofit design which is based on the application of process simulation and RSM simultaneously. In general, this will treat the process simulation as physical experiments and will be capable of producing reduced models that reproduce the specified objective function (named "response" in RSM nomenclature) within an acceptable level of confidence. For this purpose, the most important factors will be firstly identified by the application of a screening design of experiments in combination with the process integration concepts. This will generate the knowledge of the variables that mostly affect the process response. The reduced models can then be optimised with far reduced time, as the form of the equations will be mostly quadratic and continuous in the parameters, yielding to the retrofit design options.

The approach is based on three stages and it can be briefly summarized as follows: the first is a diagnosis stage in which the potential variables for the retrofit design are identified and assessed by a sensitivity analysis; the process design options are taken into account for this selection. The second is the evaluation stage, which applies RSM to the promising options identified in the diagnosis stage. The process involves a first statistic-based screening in order to find the most important factors or variables which strongly affect the objective fuction; this screening comprises both, a design of experiments and an analysis of variance (named "DoE" and "ANOVA" in RSM) which will be detailed in chapter 3. Following to this selection there is a fitting process to reach a reduced mathematical model capable to represent the whole plant performance through the studied objective function. The final stage deals with the optimisation of the reduced model obtained to yield to the best retrofit options. The approach will help in reducing computational programming of the problem by applying the surface response methodology and optimizing the reduced model obtained from it to yield to reliable optimal results. The application of RSM to the industrial problem solving is broaden as such simulation-oriented work has proved, in the two study cases, to be particularly valuable for those industrial processes which parameters are difficult to move in order to find optimal conditions. With final optimisation solution, further detailed analysis can be carried out to enhance quality of solutions. The two study cases in which the approach was tested are the natural gas liquid recovery (NGL) and hydrocarbon fractionation (HCF) processes, giving satisfactory and promising application results. The proposed approach has a tool integration capacity able to be implemented in any company (i.e. Matlab, Minitab or any statistical software can be used for the statistical analysis).

The main benefits of the research can be summarised as follows:

- To provide a practical and reliable retrofit approach that has the capacity to handle a large production plant,
- To generate a reliable retrofit design portfolio which considers economic and environmental aspects for improvements,
- To require a reasonable amount of time to reach pseudo-optimal solutions by optimising reduced models,

- To quantify the effects of the most important factors towards the improvements, which helps understanding of the process,
- To have model flexibility in the proposed approach with tools integration capacity
- To be simple and generic enough to be applicable in the wide range of industrial applications.

However, it has some limitations regarding the time available to perform the simulations needed in the approach, which can be extremely high. An additional limitation deals with model uncertainty. However, when analysing the bases in the development of the approach, the pseudo optimal results identified can be considered statistically confident enough to proceed the generation of the best retrofit design solutions.

1.4 Thesis outline

Chapter 1 outlines the motivation that yields to this work along with the objectives, the novelty and the research significance of the research approach. Chapter 2 presents a brief literature review of the available works associated with the current research. The integrated process design concepts, optimisation methodologies and economic evaluation that support retrofit design are discussed. Chapter 3 introduces the design methodology proposed. It explains in detail the response surface methodology and how it can be applied to the retrofit design. A complete description of the methodology proposed, its steps, benefits and limitations is given. Chapter 4 presents the first case study. It illustrates the application of the proposed approach to an existing natural gas liquid (NGL) recovery plant. The results obtained are shown and a discussion was made. Chapter 5 demonstrates the application of the approach in the second case study, a hydrocarbon fractionation process (HCF). Chapter 6 summarises the conclusions of this work and discusses the future work required to improve the research.

Chapter 2. Literature Review

This review will consider some of the relevant literature associated with the current research study. In the first part, integrated process design concepts that support the retrofit process design are introduced, and then concepts of automated design based on mathematical optimisation techniques are presented. In the first section, the integrated process design methodologies, including distillation sequencing, distillation heat integration and design of heat exchanger networks, are briefly discussed. The second section describes the deterministic, stochastic and experimental optimisation techniques. A literature survey for the work carried out in the area of optimisation is also given in this part. The third section offers insights into the previous studies and design methodologies specifically relevant to the retrofit of a gas processing plant. Finally, in the last section, a brief review of the economic evaluation is focused on.

2.1 Integrated process design

In order to succeed in a global market with a high commitment towards cleaner production, the concept of process systems engineering (PSE) has emerged in the industry. As Westerberg and Grossmann (Westerberg and Grossmann, 2000) defined, PSE includes the discovery, design, manufacture and distribution of chemical products with many conflicting aims, and involves decision-making processes looking for an improvement that applies to the creation and operation of the chemical supply chain. The PSE area comprises many disciplines that focus on the optimal design and operation of process systems. Zhelev (Zhelev, 2007) pointed out that in the conceptual strategy of PSE there has been two main approaches in the design of complex systems, namely the mathematical and conceptual approaches. The former is represented by modelling, simulation and optimisation methods, while the second is established on the basis of fundamental principles, thermodynamic laws, heuristics and engineering evolution. Nowadays, there is a trend for the followers of each approach to explore the advantages of the other approach. Mathematical approach supporters can obtain a first approximation from the fundamental principles, heuristics and engineering concepts, used by the

conceptual approaches and reduce the searching space to find solutions. On the other hand, their conceptual counterparts are guaranteed to find global optimal solutions with the use of advanced mathematical searching algorithms. This fact was also remarked upon by Anantharaman et al.(Rahul Anantharaman, 2006), who stated that two systematic design methods most used in process industries are graphical diagrams based on thermodynamic insights and mathematical modelling and optimisation. By recognising the advantages of the two perspectives, the current work aims at using both.

Process integration has been of interest to researchers for over 35 years and it was defined as "a family of methodologies for combining several processes to reduce consumption of resources or harmful emissions to the environment" (Friedler, 2010). It has been stated that the pinch analysis is a simple concept which has proven to be efficient and effective through decades of use (Mubarak Ebrahim, 2000). Currently, a large variety of extensions have been developed that address combined heat and mass transfer processes (El-Halwagi and Manousiouthakis, 1989, Wang and Smith, 1994, Ntlhakana and Zhelev, 1999, Bhaw and Zhelev, 2000, Liu, 2001, Mubarak Ebrahim, 2000, Audun Aspelund, 2007); however, due to the interests of the present study the focus is placed on the heat integration. A brief summary of what was described by Smith (Smith, 2005) for process design is as follows. A chemical process can be divided into a number of generic sections to provide a structured basis for understanding and design. The hierarchy of these sections can be represented symbolically by the layers of the named "onion diagram", shown in Figure 2.1, which comprises the sequential nature of process design.

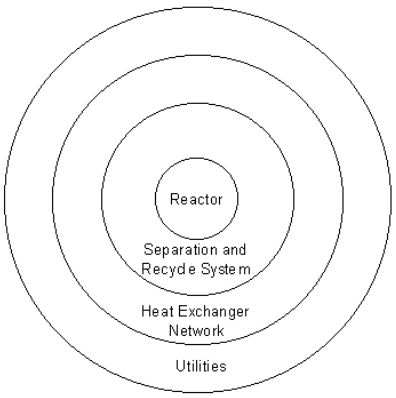

Figure 2.1 The onion model for process design from Smith (Smith, 2005).

In this onion model, the generic sections reactor, separation and recycle system, heat exchanger network and utilities directly involved in the chemical process normally

operate as part of an integrated system consisting of a number of individual units serviced by a common utility system that generates interactions among the different processes that go through it. These system interactions need to be exploited to maximise the performance of the site as a whole. Consequently, the design and optimisation of efficient process plants require tools that enhance the understanding of the users of the complex interactions between process plants and utility systems and facilitate the generation of optimal solutions.

Two situations are encountered in process design – the new design of a plant (i.e. grassroot design) and the design carried out to modify an existing plant (i.e. retrofit or revamp). This work will focus on the second situation, the retrofit design.
In general terms, and based on the onion model, there are two approaches to chemical process design and integration:

1. **Irreducible Structure.** This starts from the reactor and then moves outward by adding the individual processes described in the onion model. With the support of enough information in each stage, decisions must be made. The structure in this first approach is kept as irreducible, and additional features cannot be included.
   There are two main drawbacks to this approach. One is that in order to obtain the best decisions made, many designs must be drawn up and optimised at each stage. The other downside is that there is no guarantee of obtaining the best or near-best design after completing and evaluating many options. Besides this, there is the possibility that there will be complex interactions between different parts of the diagram, and if simplicity is required in the early stages of design, the benefits that some of these interactions may have brought might be lost.
   On the other hand, the main advantage of this approach is that engineers have full control in the decision making process, and in particular design assumptions can be included in this procedure.

2. **Reducible structure (superstructure).** This second approach is based on a superstructure that includes all the possible process options and interconnections. If covering all feasible solutions is necessary, redundant features can be embedded within the superstructure. A few issues need to be considered carefully when this superstructure approach is applied in process design: a) the optimum

structure will only contain options and features considered in the superstructure. If a particular feature is not implicitly embedded in the beginning, this feature will never appear in the final solution. Therefore, the more options considered, the more likely it is to obtain a better solution, b) design complexities and associated computational efforts increase significantly when the problem size is big, for example when a large number of unit operations and/or very detailed mathematical models are employed (rigorous models). Nevertheless, many optimisation methodologies have been developed to overcome these drawbacks, so the only remaining issue is the computational time necessary to find the optimum solution. The clear advantage of a superstructure approach is that many different options can be tested at the same time, and the procedure can be fully automated and may produce high quality solutions within a reasonable computational time.

Both approaches can handle the complex multiple trade-offs found in process design, and present advantages and disadvantages; thus, choosing which one to employ depends mainly on the features of the problem to solve, the tools available to be used on it and the preferences of the final users. For a retrofit study, the existing structure of the original plant provides a basic configuration to begin with, which promotes the use of the irreducible structure approach. Nevertheless, in order to achieve the advantage of the superstructure approach, it would be very useful to systematically identify further structural changes that can create cost-effective improvements in process performance. Moreover, it is important to consider the effect of interactions between the parameters present in the structure, as the optima point may be within. High confidence in the solutions is desired, which suggests that the solutions selected and tested must be evaluated under certain criteria. The complexity of the models involved impacts on the computational time needed to solve the problem; therefore, the use of commercial non-rigorous models where possible in the irreducible structure may relax this complexity level and reduce the time required to find a solution. This section has given a brief outline of the PSE concept with the two main approaches used to chemical process design and integration. The retrofit design and the features that need to be taken into account in the present study have been introduced. There is no chemical reaction involved in the research cases; therefore, when referring to the onion model, the inner layer of

reaction is not taken into account. The following sections describe the process design options considered in the current study.

2.1.1 Distillation sequencing

One of the most widely used methods for the separation of homogeneous mixtures is distillation, which, depending on the components involved, recovery and the purities required, often comprises a series of simple or complex column configurations. The simple column deals with one feed used to produce two product streams. The complexity of separation increases with the number of products, and when mixtures of components need to be separated, a series of columns in sequences are used. Table 2.1 is taken from Smith (Smith, 2005), and contains the relationship between the number of products and the number of possible distillation sequences involved in separation. When distillation sequencing uses columns with more than two products, the number of possible sequences is exponentially increased.

Number of products	Number of possible sequences
2	**1**
3	**2**
4	**5**
5	**14**
6	**42**
7	**132**
8	**429**

Table 2.1 Number of possible distillation sequences using simple columns.

Distillation involves two main sequences, direct and indirect, which are shown in Figure 2.2. The level of separation achieved (purity) may or may not be similar in all alternative sequences, while the cost for each sequence (capital and operation) may be significantly different, even when similar separation levels are reached. The energy efficiency of the separation performed is a key factor in the design. The following rules of thumb for simple columns sequencing have been mentioned, and verified effective in some cases, by Smith (Smith, 2005):

1. To do the most difficult separation last, this refers to where the relative volatility of the key components is close to the unity.

2. To favour the direct sequence.
3. To remove the component with the largest fraction first.
4. To favour near equal splits in molar flows between the bottom and top of a column.

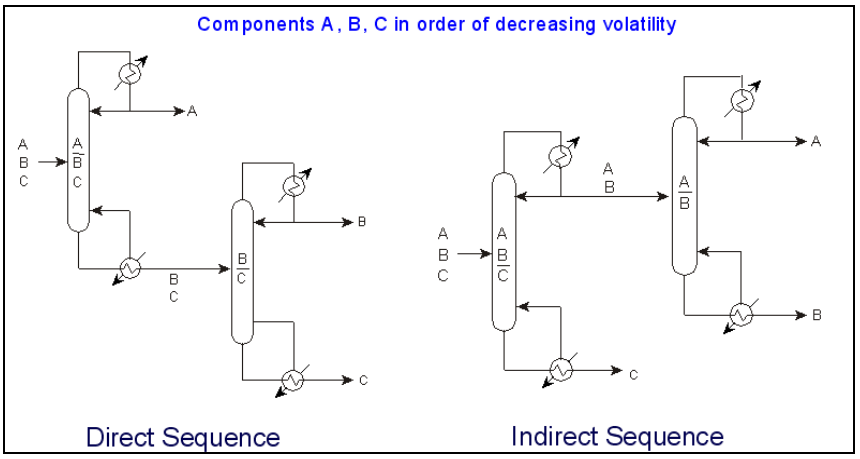

Figure 2.2 The direct and indirect sequences for simple columns taken from Smith (Smith, 2005).

In addition to the simple columns arrangements, complex column arrangements are available which is able to reduce energy demands when compared with simple columns arrangements. Figure 2.3 presents an example of these arrangements with three products.

1. A single-column sidestream arrangement that may be useful when the middle volatility product is in excess with respect to the other two products. A heuristic says that for a pure sidestream product coming from an inlet stream of 3 components (i.e. A, B and C), side-stream columns are preferred when either middle component (B) composition is bigger than 50% of feed and bottom component (C) composition is less than 5% of feed, or when middle component (B) composition is bigger than 50% of feed and top component (A) composition is less than 5% of feed.

2. A distributed distillation or sloppy distillation arrangement can be applicable where flexible operating pressures and distribution of the middle component are permitted as additional degrees of freedom. This added freedom may lead to better heat integration of reboilers and condensers in the arrangement, improving its energy efficiency.

3. A prefractionator arrangement is achieved when, in a sloppy distillation arrangement, the second and third columns are operated at the same pressure, both columns are joined and the middle product becomes the sidestream of this last column. This arrangement,

similar to sloppy distillation, reduces energy consumption by 20-30% when compared with conventional arrangements for the same separation process. This is a direct consequence of the reduction in the mixing effects for the middle product, which occurs when the simple distillation columns are used. In order to improve performance and energy efficiency in the design of process distillation systems, all of those arrangements can be used alone or in combination.

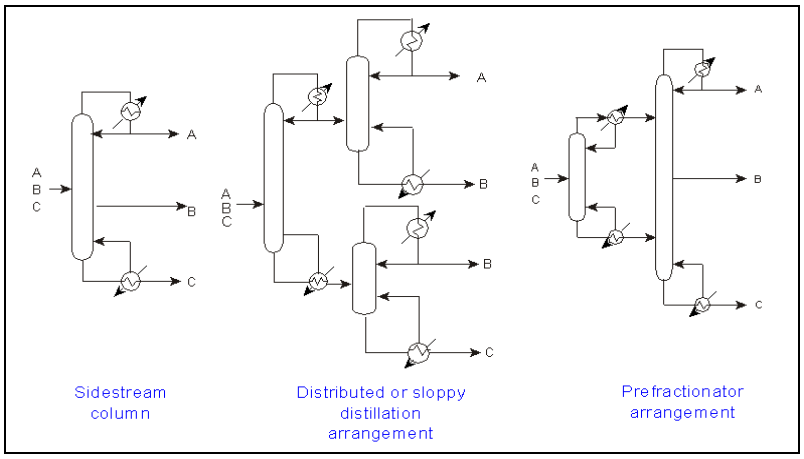

Figure 2.3 Distillation columns with 3 products taken from Smith (Smith, 2005).

It has been concluded that thermal coupling of distillation columns, when feasible, is an effective way of reducing energy consumptions (Rev et al., 2001, Khalifa and Emtir, 2009, Mizsey et al., 1998, Peter Mizsey, 1998, Mizsey P., 1998). Figure 2.4 are the most used, and its features are listed as follows:

1. Heat-integrated direct or indirect sequences – Figures 2.4a and 2.4b –can be formed by heat-integrating the condenser of one column with the reboiler of the other. The operating pressures in the first and second columns are matched so that there exists the possibility to have better heat integration opportunities.
2. Thermally-coupled columns as shown in (b) and (c) in Figures 2.4a and 2.4b are similar to the previous heat-integrated columns, but these two columns are integrated by eliminating the heat exchangers between them (i.e. the reboiler or condenser). Thus, the heat is transferred by direct contact. This makes these arrangements more energy-efficient than the previous heat-integrated columns.
3. Prefractionator arrangements, heat-integrated and thermally-coupled – in Figure 2.4c - are based on a prefractionator or preflash base, and connect the reboilers with the condensers of the columns in the heat-integrated case, or eliminate the intermediate heat exchangers in the thermically-coupled case. These

arrangements have proven to be the most energy efficient systems showing significant reduction of energy consumption when compared with the rest of the arrangements under the same feeding conditions and product specifications (Khalifa and Emtir, 2009); the presented slopppy double heat integrated arrangement in d) of Figure 2 .4c yielded a 16-23% of energy reduction and the Petlyuk obtained a 39-46% of energy reduction. On the other hand, it is mentioned that serious control problems can be expected in the operability of the Petlyuk system when inlet conditions are very unstable, as it is highly dependent on the feed composition (Rev et al., 2001).

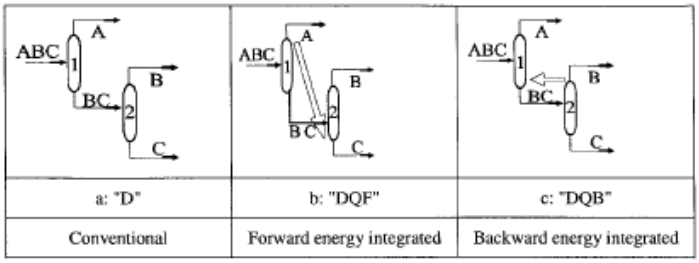

Figure 2.4a.

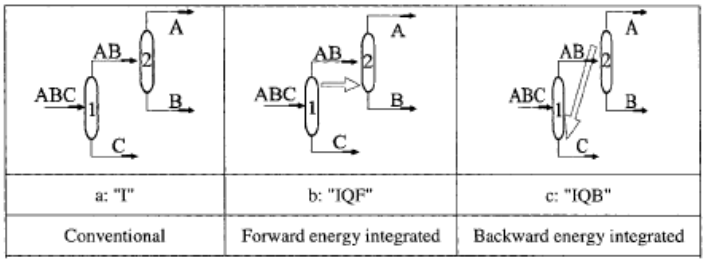

Figure 2.4b.

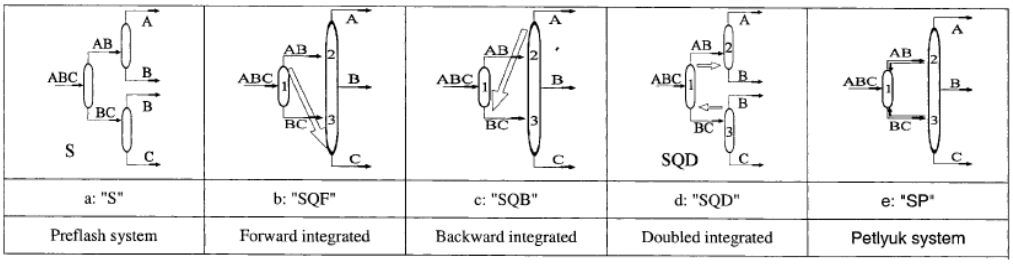

Figure 2.4c.

Figure 2.4. The thermal coupled columns arrangements taken from E. Re´v et al. (Rev et al., 2001).

Two further arrangements are shown in Figure 2.5 namely sidestream stripper/rectifier arrangements and partitioned side-stripper/side-rectifier arrangements (Annakou and Mizsey, 1996). These, when compared with the heat-integrated system discussed in the

previous section, have been shown to reduce energy consumption as a result of heat transfer by direct contact in a part of the system.

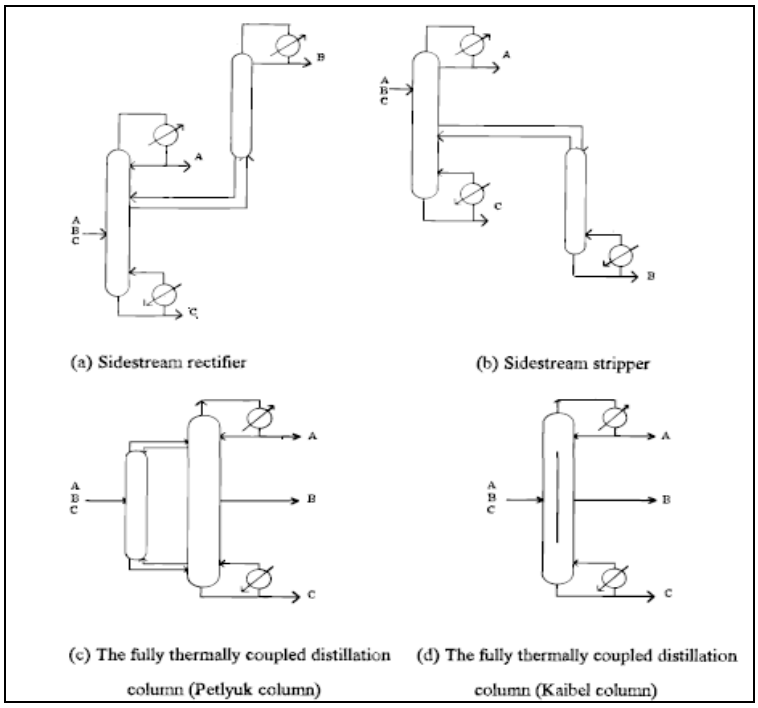

Figure 2.5 The thermal coupled columns arrangements taken from Mizsey et al. (Annakou and Mizsey, 1996)

Shah and Kokossis (Shah and Kokossis, 2002) proposed a synthesis framework for screening complex distillation sequences using a supertask model, instead of a superstructure representation, which is based on simple (simple column) and hybrid (complex columns and sloppy splits) tasks, instead of units. The methodology was tested in the industrial cases of light alcohol separation, light hydrocarbon separation (C_4-C_7), paraffin separation, refinery light-end separation and the separation of a C_4 mixture. The results suggested that the approach is a useful tool for screening to select favourable designs and integrated flowsheets before proceeding to more detailed design. Gadalla et al. (M. Gadalla, 2003) developed shortcut models for retrofit design applicable for various configurations of distillation columns. The results agreeded with rigorous simulation results in Hysys software providing a basis for optimising and improving the operating conditions of existing distillation columns. Wang and Smith (Wang and Smith, 2005) presented a new synthesis framework for screening low-temperature, heat-integrated separation systems. Task representation to the separation options including flash drums, dephlegmators, simple and complex distillation columns, is applied. The methodology proposed is illustrated by various case studies. The major

disadvantage of the presented approach is considerable run time required by the calculations.

Bek and Gani (Erik Bek-Pedersen, 2004) described a framework based on the driving force approach for the synthesis, design and operation of distillation-based separation schemes. A set of algorithms has been developed within the framework for the design of simple as well as complex distillation columns, for the sequencing of distillation trains, the determination of appropriate conditions of operation and for the retrofit of distillation columns. The optimal conditions can be visualized from the integrated algorithms and both, the feasibility of different separation techniques for a given separation task and the optimum methods of separation can be defined. The authors concluded that the easiest separation in a distillation column, which requires less energy, is the one carried out in the components´ split at the highest driving force. The limitations of the method are that the two adjacent products in the distillation column must be set on each side of the maximum driving force, which may be difficult to reach in operating units and that the method was applied to isolated distillation columns. Therefore, it is missing to test the method in complete plants where process integration applies.

From this section it is clear that the use of complex distillation arrangements combined with the proper distillation sequencing in the process is capable of achieving an average of 30% in energy savings compared with a conventional sequence. The capital cost is another important factor in identifying cost-effective solutions. A specific retrofit case must look for feasible options to be analysed and proposed in order to yield improvements in the process. It is important to comment that it is not straightforward to evaluate systematically the large number of options simultaneously and their design interactions within the whole process.

2.1.2 Retrofit for energy recovery systems

The total amount of energy saving is a function of the level of heat integration achieved in the whole plant. The ideal scenario aims to use a minimum of energy supplied with minium capital investment. The key concepts used in energy integration methodologies are: 1) ΔT_{min}, composite curves (CC), and 2) grand composite curves (GCC) and utilities,

and 3) heat exchange network (HEN) design and retrofit, all of which will be explained briefly in the following subsections.

1) ΔT_{min}, composite curves (CC), and energy targeting (ET):

A production plant consists of various process streams, which need to be heated up (i.e. cold streams) or cooled down (i.e. hot streams). Both types of streams can be characterised with a supply temperature (TS) (initial temperature), a target temperature (TT) (the final temperature) and heat capacity flowrate (known as CP, which is a mass flowrate (MF) multiplied by heat capacity (Cp). It is possible to separate all the streams into two sets by grouping hot streams and cold streams. In this manner, if all of the hot streams are plotted over temperature-enthalpy diagram and the hot composite curve (HCC) can be obtained. The same method applies to the cold streams, resulting in the cold composite curve (CCC). When the two CCs are plotted together, the pinch point can be identified at given minimum temperature difference (ΔT_{min}) as in Figure 2.6 (Linnhoff et al., 1979).

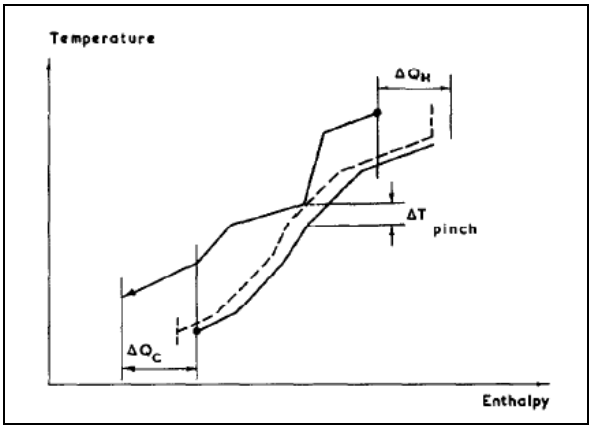

Figure 2.6 The heat recovery pinch from Linnhoff et al. (Linnhoff et al., 1979).

This plot identifies the maximum energy recovery (MER) when both ΔQ_C and ΔQ_H are minimised at given ΔT_{min}. By varying the $\Delta T_{min,}$ the relative position of the CC changes along with the ΔQ_C and ΔQ_H. There is a trade-off between the cost of utility consumption (operating cost) and the cost of the heat exchangers needed (capital cost).

An important conclusion can be drawn from this part: in both extremes, hot and cold, it is possible to estimate the minimum utilities energy needed in the process before any heat

exchanger network design is undertaken. These ETs can be used as a base reference to measure the effectiveness of the ER achieved in the process after each change in retrofit design. The Plus-Minus Principle is based on guidelines that propose changes to the system(Linnhoff and Vredeveld, 1984): 1) to decrease the total hot load below the pinch, as well as the cold utility needed, 2) to increase the total hot load above the pinch and thus decreasing the hot utility needed, and 3) to apply the same movements but in the opposite direction to the cold streams. If process changes which comprise shifting the hot and cold streams increase overlapping of the hot and cold composite curves, energy recovery increases in the system. The stated guidelines are described as follows:

- Increases the total hot stream heat load above the pinch;
- Decreases the total cold stream heat load above the pinch;
- Decreases the total hot stream heat load below the pinch;
- Increases the total cold stream heat load below the pinch.

To illustrate this, a hot stream can be shifted from below the pinch to above it with change in distillation column pressure. Various options can be identified in the first instanceand the complexity of the resulting structures to be evaluated may grow, but it can be worthwhile evaluating potential benefits and associated impacts.

2) Grand composite curves (GCC) and utilities:

CCs are a useful tool for estimating the MER and gaining a conceptual understanding of the system, and Linnhoff and Hindmarsh (Linnhoff and Hindmarsh, 1983) proposed a Grand Composite Curve (GCC) constructed from a problem table algorithm which allows systematic placement of utilities to be employed. The problem table calculates an enthalpy balance and identifies heat deficits or surplus for the hot and cold streams; then, the feasibility of complete heat exchange between streams by a stream cascading from higher to lower temperatures can be seen. An example of a problem table is given in Figure 2.7, while Figure 2.8 presents the GCC with utility targets.

SUBNETWORK	STREAMS AND TEMPERATURES: COLD STREAMS (3) (4)	T(°C)	HOT STREAMS (1) (2)	1 DEFICIT	2 ACCUMULATED INPUT	3 ACCUMULATED OUTPUT	4 HEAT FLOWS INPUT	5 HEAT FLOWS OUTPUT
		150						
SN1		125 145		- 10	0	10	107.5	117.5
SN2		100 120		+12.5	10	-2.5	117.5	105
SN3		70 90		+ 105	-2.5	-107.5	105	0
SN4		40 60		- 135	-107.5	27.5	0	135
SN5		25		+82.5	27.5	-55	135	52.5
SN6		20		+12.5	-55	-67.5	52.5	40

Figure 2.7 A Problem Table example from Linnhoff and Hindmarsh (Linnhoff and Hindmarsh, 1983).

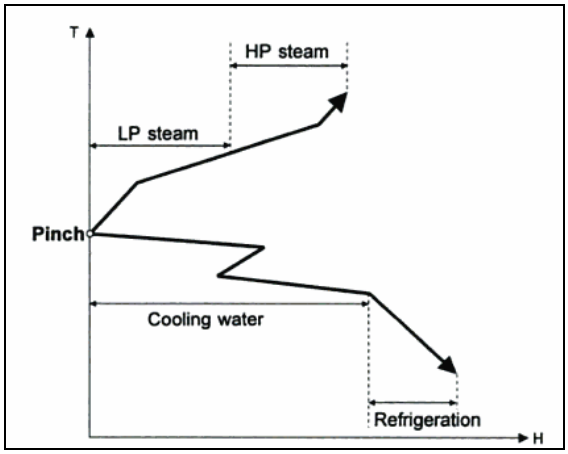

Figure 2.8 The Grand Composite Curve with utility targets from Linnhoff and Hindmarsh (Linnhoff and Hindmarsh, 1983).

The problem table is constructed, first, by shifting the supply and target temperatures of hot streams by subtracting $\Delta T_{min}/2$, and those of cold streams by adding $\Delta T_{min}/2$. Next, the temperature intervals (T_i) are listed in the table, together with the heat capacities (Cp), mass flowrates (MF) and its multiplication (CP) for each stream. The enthalpies are calculated for each temperature interval (H_i) as:

$$\Delta H_i = \left[\sum CP_C - \sum CP_H\right] \bullet \Delta T_i \qquad (2.1)$$

where $_C$ = Cold stream and $_H$ = Hot stream. At this point, the deficit or surplus of enthalpies are identified as + or - respectively. The values H_i are added or subtracted (cascaded) depending on the sign from higher to lower temperature intervals. The maximum heat deficit identified from the cascade procedure is added at the top, which avoids any heat deficit in any temperature intervals. Finally, the GCC can be graphed

from accumulated heat (H_i) and corresponding temperature (T_i). With GCC, process-to-process energy recovery (.e. pocket) is clearly visualised, and the amount of energy to be supplied or discharged and their levels and requirements can be systematically identified.

3) Heat exchange network (HEN) design and retrofit:

The capital cost of the HEN can be estimated from the area required for transferring heat in the HEN, which is often referred to as Area Targeting (Linnhoff and Ahmad, 1990). The pinch methodology states that the minimum heat exchanger area is obtained from setting all the heat exchangers to match in both CCs vertically, as seen in Figure 2.9, i.e. by assuming all heat transfer coefficients are equal. Therefore, it is worthwhile looking for the position of the existing heat exchangers in these CCs and finding those that are in a crossed position, as in Figure 2.9. There is also the need to find heat exchangers that provide a heat transfer across the pinch, coolers above the pinch or heaters below the pinch. These are critical violations to the pinch methodology, which leads opportunities for improving heat recovery systems. Nordman and Berntsson (Nordman and Berntsson, 2009b, Nordman and Berntsson, 2009a) applied these points in their two industrial case studies, together with their suggested graphical method for HEN retrofit, and found that the knowledge of heat exchanger placement in the existing network within the CC is important, in order to identify qualitatively the potential changes which can be considered in a retrofit design.

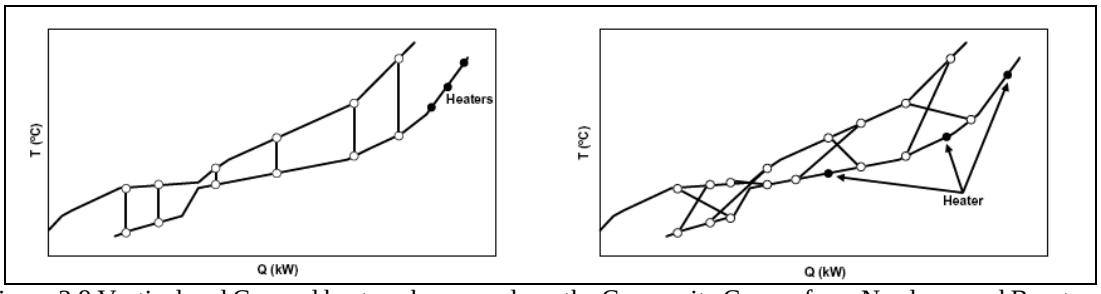

Figure 2.9 Vertical and Crossed heat exchangers along the Composite Curves from Nordman and Berntsson (Nordman and Berntsson, 2009a) .

Another important issue to consider when dealing with the retrofit of HENs is the network pinch which is a heat recovery limit within the HEN and it does reflect the

structure of the existing HEN (topology) and the process streams; this is independent of the area of individual exchangers in the network and it is different from the process pinch, which is only defined by process conditions, stream temperatures and heat capacity flowrates.

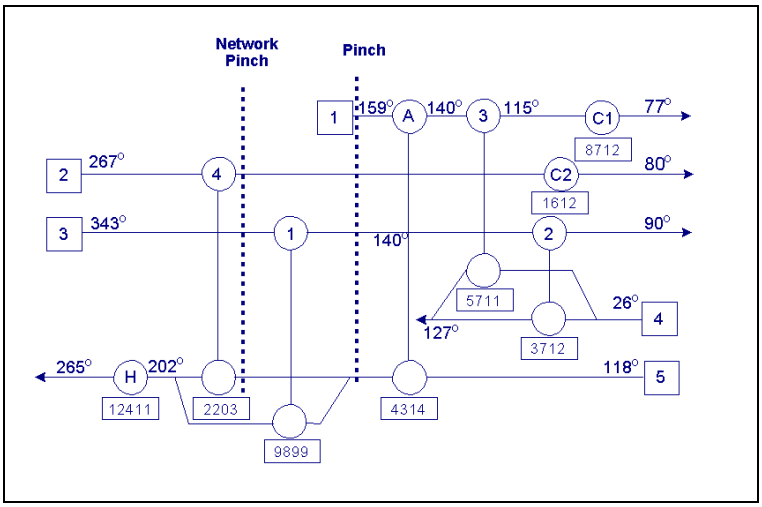

Figure 2.10 Heat Exchanger Network Grid: Network pinch vs pinch

The retrofit methods are mainly based on identifing the pinching matches (i.e. units that constrain heat recovery) and exploiting utility loops to improve systems' energy recovery (Smith, 2005, Kin-Lung Maa, 2000, Osman et al., 2009, Mahmoud et al., 2009). The retrofit can be done with either"retrofit by inspection" or "retrofit by automated design". The former has the advantage of incorporating the user's insights. However, design problem is likely to be complicated when dealing with large-size heat recovery systems (e.g. the large number of streams or multiple pinches). Possible options for retrofit in the HEN include to add a new match, to eliminate an existing match, to re-pipe a heat exchanger to re-sequence a heat exchanger, to add or remove a stream split, and to adjust the duty of an existing heat exchanger. Additional costs from the introduction of new heat exchange area and re-piping should be considered. The main objective for the retrofit design is to get an optimum balance between heat recovery and the capital cost to be invested, and there is a trade-off to deal with. The final solutions are obtained after many design modifications, as represented schematically in Figure 2.11, which schematically illustrates retrofit path of HEN based on the iteration of structural changes and operational optimisation. The iterations are repeated in the same manner until there is no significant energy saving achieved.

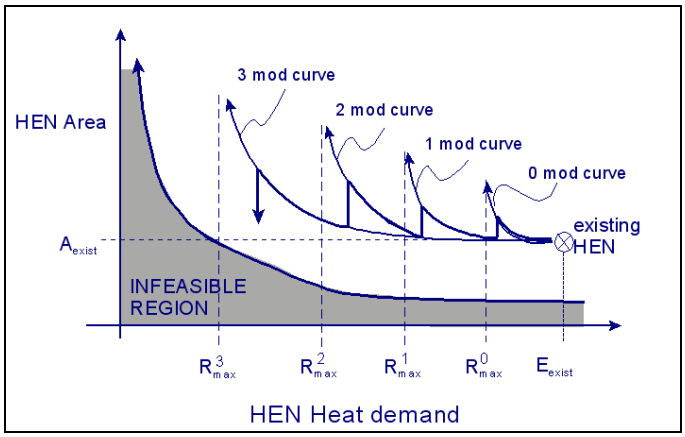

Figure 2.11 The HEN optimal retrofit path from Azante and Zhu (NDK. Asante and Zhu, 1997).

The present retrofit study aims to apply this methodology due to its proven cost-effective results in the industry. Nevertheless, it is extremely important to remark that any process changes undertaken to improve system performance (i.e. composition specification, split of streams, column pressure, etc.) will impact on the heat recovery and its retrofit of HEN.

2.2 Process Optimisation

As mentioned in the previous section, mathematical modelling and optimisation are extremely important tools for the design and retrofit of chemical processes. The optimisation of processes is considered as a powerful strategy because it can support users to screen a set of alternatives and to determine the most appropriate solution. Modelling is the first step to be carried out if an optimisation is going to be performed. The simulation of the process relies on a set of equations, or mathematical models, that attempt to predict the process behaviour. Two basic types of models used are shortcut and rigorous, and their application depends on a trade-off between the accuracy of results and computational effort. For the process simulation, a plant-wide flowsheet, which consists of various unit operation models, can be mathematically solved either in equation-oriented simulation (EOS) or in sequential modular simulation (SMS) mode. The state of the system in time is highly important in building the modelling framework and solvingthem. Steady-state simulation is suitable for processes operated continuously at a fixed condition, or within an acceptable range of fluctuation in operating conditions. Dynamic-state, on the other hand, is applicable when operating conditions are

time-dependent. The selection of the state depends on both the nature of the process studied and the retrofit design purpose. This research focuses on operating plants that is based on steady-state conditions.

A wide spectrum of optimisation methodologies are available from the literature, and the choice of methodology to be applied is strongly influenced by the nature of the design problem. This section presents a general review of the basics of optimisation, and summarises the optimisation techniques most commonly applied in retrofit design approaches.

A problem can be stated as a function with the form $f(x;y)$ with n continous variables x and m integer values y, subject to $c(x;y) \leq 0$. Optimisation is focused on the optimal choice of variables x and y in a region ξ, those which give the maximum or minimum of the objective function and satisfy the constraint $c(x;y) \leq 0$.

The maxima or minima of a function can be either global (the highest or lowest value over the whole region of interest) or local (the highest or lowest value over some small neighbourhood). The most suitable methods to locate maxima or minima depend upon the nature of the function treated. There are two broad classes of algorithms:

1. **Local maximisers or minimisers** locate the highest or the lowest point on the space around a given a point in a "valley" of the function.
2. **Global maximisers or minimisers** search over a region of searching space in an attempt to find the top or the bottom of the valley.

A common practice for local and global methods is, where possible, to examine the problem by initialising a model on a global search, and once defining the promising areas where the optimal solutions may exist, moving to a local search about the current best estimate.

It is important to mention that the complexity given by the size and type of variables of the problem may affect the solution time dramatically when applying an optimisation method. The most widely used techniques for retrofit design can be classified into three categories.

1) Deterministic techniques.

These are optimisation methods widely used in retrofit designs. One issue with these methods resides on its tendency to converge on a single optimum close to the starting point. Problem initialisation is highly important to the solution found. One of the most common technique is the mixed integer nonlinear programming (MINLP) problem, which considers mathematical programming with continuous (operational parameters) and discrete variables (structure changes), and nonlinearities in the objective function and constraints. Methods for solving MINLPs include outer approximation (OA) methods (Duran and Grossmann, 1986, Fletcher and Leyffer, 1994), extended cutting plane methods (Westerlund and Petersson, 1995) and generalised bender's decomposition (GBD) (Geoffrion, 1972). These techniques are generally relied on by the iterative algorithm that successively solves NLP and LP (or MILP) sub-problems. These approaches have the feature of only guaranteeing global optimality under (generalised) convexity. Global optimisation of non-convex problems obtains sub-problems via convex relaxations of the initial problem in a branch-and-bound context and solves them. Its application in solving MINLPs (Floudas, 2000, Tawarmalani and Sahinidis, 2002) has given acceptable solutions. Grossmann and his co-workers (Lee and Grossmann, 2003, Karuppiah and Grossmann, 2008, Ponce-Ortega, 2008) proposed a global optimisation method in which applications were presented in the synthesis of integrated process water networks, complex distillation and crystallisation systems, HENs, bioethanol plants and integrated gasification combined cycle (IGCC) plants. The authors claim that the algorithm had been applied to case studies and global optimal solutions had been found with reasonable computational effort.

MINLP has been widely used for discrete-continuous optimisation problems, as it can give fast and reliable results when the problems studied are not highly complex and can be relaxed in sub-problems. However, the significant drawback of not giving a guarantee of convergence and finding the global optimum has been the principal reason for the urgent development of alternative optimisation techniques. Nowadays, developments in hybrid algorithms have regained the advantages of deterministic programming and combined these with the power of stochastic techniques.

2) Stochastic optimisation techniques.

Low dimensional or constrained problems are properly suited by local optimisers, which can be initiated from a set of possible starting points that are generated either randomly or systematically. However, this approach is less likely to locate the true optimum as the ratio of the volume of the search region to the number of starting points increases. Gradientless optimisation techniques, such as evolutionary algorithms (EAs) (Gross and Roosen, 1998), genetic algorithms (GAs) (Holland, 1975) and simulated annealing (SA) (Kirkpatrick et al., 1983) are commonly applied to problems with multiple local optima or processes, for which it is not straightforward to obtain gradient information. However, these approaches may fail to find the true optimal solution, due to the stochastic element involved.

EAs are optimisation algorithms that work in a similar manner to biological evolution, involving the steps of reproduction, mutation, recombination and selection. Retrofit promising solutions are randomly generated and treated as individuals in a population, the fitness of these options in the system is evaluated through the objective function together with the constraints; multiple individuals are selected based on its fitness, and other are modified by the application of operators to form a new population. The evolution takes place repetitively with the generations produced, and it terminates when either a maximum number of generations has been reached, or a satisfactory fitness level has been obtained for the population. The solution for a problem in GA is given in the form of binary strings (0s and 1s numbers) which represent the absence or existence of the final options. GAs is the most popular type of EA and represent a promising alternative to gradient-based optimisation techniques for certain classes of problems. However, the drawback of the GA is that, because of its stochastic nature, it is not possible to predict the required number of generations (levels of evaluation) for obtaining a solution to within a certain level of accuracy, which can result in an excessive computational burden (Kefeng Wang, 1998, Jang W. , 2005, Tayal and C., 1999, Gross and Roosen, 1998, Leboreiro and Acevedo, 2004). Most individuals of the next generation are selected from the population pool using the roulette wheel method (Hanagandi and Nikolau, 1998). In addition to this random element, the algorithm uses the best individual and passes this on to the next generation. Additionally, a few individuals, selected randomly, pass on to the next generation without taking fitness into account, which maintains population diversity. The

most commonly used genetic operators are crossover and mutation. While crossover improves the average quality of the population, mutation diversifies a population and ensures coverage over a large area of the variable space. On the other hand, this elitist strategy in GAs results in a cluster around the global optimum or promising local optima. This property often causes premature convergence in simple GAs.

Lately, as mentioned, a number of mixed algorithms have been developed by integrating deterministic and stochastic optimisation algorithms to reduce the computational cost of GAs. Jang et al. (Jang et al., 2005) studied a plant economic optimisation for a turbo expander process developed for the separation of natural gas liquids (NGL) from raw natural gas streams at cryogenic temperatures. The results indicated that the convergence of their deterministic-and-genetic algorithm was significantly faster than that for the GA. A two-level strategy for the stochastic synthesis of chemical processes under uncertainty with a fixed degree of flexibility by using MINLP was presented (Pintaric and Kravanja, 2000). The two examples presented were medium- and large-scale problems. One related to heat exchanger networks (HENs), where the uncertain parameters set were the temperatures of process streams, cooling water and steam. The other example was a flexible heat-integrated distillation sequence and its HEN, for which the prices of some products were set as uncertain parameters. The results showed that the proposed two-level optimisation strategy reduced the number of decision variables and, thus, the sizes of the mathematical models involved. The optimisation strategy is robust, reliable, efficient and, thus, able to reach solutions in a reasonable computational time.

SA has recently gained popularity in optimising problems where the goal is to find an high qualitysolutions within a reasonable computational time, although global optimiality is not guaranteed. The name and idea comes from the technique known as ‘annealing’ in metallurgy, which consists of the heating and controlled cooling of a metal to get bigger crystals sizes in order to reduce its defects; the cooling process gives the molecules more opportunities to find configurations with lower internal energy than the initial state. At a certain temperature the molecules tend to jump from a lower energy stage E_1 to a higher level E_2 in the system space. The probability of this happening is given by the Bolzmann formula and the optimal state is always looking for the minimum value of energy achieved (Li et al., 2000). In the case of optimisation problems, the approach is similarly developed, the variables are like the metal molecules, and the states of variables are the

molecules distributions respectively. Artificial temperature is introduced. In this way, SA uses a random search of the solution space that generates distributions of optimal solutions, which are independent of the initial guess and close to the global optimum solution. This process implicitly develops a trade-off between the level of satisfaction from the results obtained and the computational time consumed.

SA algorithms have been developed widely and applied to HEN grassroot and/or retrofit designs (Dolan et al., 1990, Nielsen et al., 1996, Athier et al., 1998, Athier et al., 1996, Dolan et al., 1989). Recently, a series of combined optimisation algorithms have been proposed by integrating different optimisation technologies, in order to fully exploit the advantages of each method (Tantimuratha et al., 2000, Yu et al., 2000, E. S. Fraga, October 2001, Fraga et al., 2001). Case studies include ethylene plant heat integration (Yu et al., 2000), HEN retrofit, water minimisation applications and threshold problems (Tantimuratha et al., 2000) through to HEN synthesis (Fraga et al., 2001). The results show a notable reduction in computational time and improvements in the quality of the solutions found. These authors highlight the enormous potential that can be obtained from their methodologies and the need to do more research focused in this integration field.

It is clear from the work developed with stochastic techniques that they are able to handle large problems and can also produce good quality results. Nevertheless, there are drawbacks due to their stochastic nature, which include failing to find global optimum because of premature convergence or predicting an extremely large number of generations for obtaining a solution to within a certain level of accuracy, which results in an excessive computational efforts.

3) Experimental techniques.

"Design of Experiments" (DoE) is an important tool used not only to fit mathematical models based on experiments performed (Gaia Franceschini, 2008), but also as a powerful technique used in the optimisation of products and processes.

The DoE methodology is a systematic approach that varies levels of the evaluated factors in a wide range to cover most of the possibilities to get a response. The selection of designs used for experimental runs depends principally on aspects, such as the purpose of the study, the number of factors and minimum levels, restrictions on runs (experimental

costs), the effects (main or interactions) to be studied (resolution), the order of the model to be fitted and the restrictions on the design shape (corner restrictions). After setting the proper design to be used, the experimental or simulation runs are performed and an analysis of variance (ANOVA) is applied to the obtained responses. This helps to determine if the means in the set of data differ significatively from each other and from the corresponding group mean. If so, this is followed by a statistical distribution test to determine which factors, or combination of thereof, are associated with the differences identified in the ANOVA. A key piece in the ANOVA is the p-value; this is the probability of obtaining a value for a test statistic that can be in or out of the respective distribution (with the base in the null hypothesis). If the p-value of a factor is low, say less than 0.05 or 0.01, a null hypothesis is often rejected, which in the ANOVA test means that the factor is statistically significant for the behaviour of the studied system. The most important factors are then identified as main or as combination and their effects. The "response surface methodology" (RSM) can then be applied to fit a reduced model, based on the most important factors identified, which can satisfactorily reproduce the studied response. The reduced model can be used to find near optimal solutions in practical periods of time by applying the steepest ascendant approach which will be explained in detail in the Section 3.3(Montgomery, 1997). For now, though, a number of studies developed in this field are presented here.

The generalised response surface methodology (GRSM) is an extension of the classic RSM proposed by Box and Wilson (Box and Draper, 1987), which allows for the handling of multiple random responses by selecting one response as the goal and the other responses as constrained variables. To search for the optimum, local gradients are estimated by both GRSM and RSM. These gradients depend on local first-order polynomial approximations. RSM uses the steepest ascendant (STA) direction algorithm to perform the search function (Box and Draper, 1987, Montgomery, 1997). On the other hand, an adapted steepest ascent (ASA) search direction was developed by Kleijnen et al. (Kleijnen et al., 2004), who claimed to get a better estimation than the SA. In the study published by Kleijnen et al. (Kleijnen, 2008), the estimated gradients with this ASA were used in a bootstrap procedure in order to test whether the estimated solution was indeed optimal. It was also proposed that the optimisation of simulated (not real) systems relied on GRSM. They stated that, unfortunately, RSM, unlike some other search heuristics, has

not yet been implemented as an add-on to any of the commercial simulation software packages.

Davis and Ierapetritou (Davis and Ierapetritou, 2008) mentioned that when the models of the system are not known (i.e. black box model), these approaches are inefficient for solving MINLP, the relaxed NLP sub-problems of which are non-convex. It was suggested that this problem can be solved by fitting global models first, and then determining the best areas to apply local methods. On the other hand, it has been stated that "response surfaces have a tendency to capture globally optimal regions because of their smoothness and global approximation properties. Local minima caused by noisy response are thus avoided" (Kini, 2004), which is in contrast to the above and supports the work done here.

The main advantage of the experimental techniques is that they can provide a reduced model with a high level of confidence (if the experiments are statistically well based) to find near optimal solutions and explain the interrelations among the factors involved and responses. On the contrary, the main disadvantage is that it is time-consuming for the computation of DoE and relevant analysis, as this increases exponentially with the number of variables considered. However, once DoE and its analysis have been carried out, it does not require a significant amount of time to apply the results from DoE for the design.

2.3 Retrofit design studies

The optimisation methodologies mentioned in the previous section address multiple and complex trade-offs in the refrofit study. However, it is still not a straightforward process to solve practically large-sized problems, due to the large number of variables involved, the binary variables used for representing discrete decisions, and local optima problems. Similar to the combined optimisation algorithms referenced before, a number of studies are based on methodologies that combine both thermodynamic and optimisation approaches in order to address these complex large-sized problems.

A selection of summarised studies below gives a view of the type of retrofit studies found in the literature for the natural gas liquid recovery process. These cases show the specific methodologies available that have been applied to address the industrial scope as well as the scopes, limitations and tools employed.

An analysis was presented on different turbo-expansion processes, based on capital analysis and operating limitations, by using an ad hoc simulator and the MINLP optimisation technique (S. Diaz, 1996, M. S. Diaz, 1997).

A NGL unit was simulated using a commercial simulator (e.g. HYSYS®) and compared the results with an operating plant data (Mehdi Mehrpooya, 2006). Structural changes in the unit were proposed and tested looking for improvements. A stochastic optimisation algorithm (GA) in which the objective function was based on cost and maximising profit was applied to determine an optimal design. Optimisation variables were selected from the sensitivity analysis and comprised operating and changes in the unit. The MATLAB® software was linked with HYSYS® software.

An improved genetic algorithm (IGA) was proposed by Wang et al. (Kefeng Wang, 1998) to provide a systematic approach and tools for synthesis design and the retrofits of distillation systems. The algorithm, said to have inherited its main ideas from evolutionary computing, employed a distributed sub-population strategy to avoid local optima, and applied for a continuous variable space coding procedure. This has as the consequence of being computationally fast and stable in converging to global optima. In order to illustrate the suitability of the proposed algorithm for the design of the heat integrated distillation system, two examples were presented: the heat integration of propanol separation and the heat integration of the HDA separation problem. Energy recovery, heat loads, minimum approach temperature and stream matches were not fixed in these applications.

In summary, the literature shows in general studies of retrofitting for energy efficiency and studies for self-process improvements (e.g. recoveries, product purities, etc.). A wide range of methodologies have been applied, which vary from traditional methods to elaborate graphics and deterministic or stochastic programming. There is a marked trend to use hybrid approaches, which take advantage of each of the methodologies. The main

focus of most of the work found is to find a systematic methodology that provides reliable results; however, most of design strategies are based on decomposition of the overall problem into subproblems which then are sequentially solved. An inminent issue arising from this decomposition is due to the fact that the changes done in the process and the heat integration are directly linked, and there is no certainty that an improvement in one side (process) will reflect the same positive manner for the other side (heat integration). Therefore, it is needed a measure of the possible effects that the changes to the process may yield to the heat integration system. One of the examples for using a decomposed approach was published by Fraga et al. (Fraga et al., 2001), where, firstly, the process is considered by separating from heat integration and, secondly, the heat exchangers are evaluated and retrofitted. The visual tool they propose is a good starting point for joining the changes done to the process and the HEN retrofit; nevertheless, as they only worked with providing the hot and cold streams and did not linked it directly with the simulation of the process. Thus, it would be helpful to link the factors that affect the process improvement.

2.4 Economic metrics

Many factors need to be considered in the economic analysis of process design activities. Its outcome is heavily dependent on the objective function, which considers in the first instance the cost of the equipment to be installed as a consequence of the retrofit design requests. These costs are highly dependent not only on the type of units by nature, but also on the location and the operating conditions.

A survey of the types of economic functions used in the optimizing objective funcions was carried out by Pintaric and Kravanja (Pintaric and Kravanja, 2006). Among 64 cases, the minimisation of cost, e.g. the total cost, operating cost, logistical and investment cost was used as economic criteria for 36 cases, while the maximisation of profit or economic potential was found in 17 cases. The net present worth (NPW) criterion appeared in 7 cases. Other interesting but less common criteria were the maximisation of the cumulative cash flow, maximisation of the monetary value added, the minimisation of investment and inventory opportunity costs reduced for the benefit of the stockholders, and the method known as “real-options” to incorporate uncertainty in the prices.

Previous studies addressing energy systems for the economic model have assessed the component costs including maintenance and the cost of fuel consumption [(Toffolo and Lazzaretto, 2002), (Lazzaretto and Toffolo, 2004), (Pintaric and Kravanja, 2004)]; however, since the resulting formulation of the total cost of operation must depend on the optimisation variables of interest, they expressed the cost of each component as a function of thermodynamic variables. Pintaric and Kravanja (Pintaric and Kravanja, 2006) also highlighted the problem of selecting the most suitable criteria for the design and synthesis of process flow sheets. The main conclusion of the paper was that compromised criteria such as the maximisation of net present worth (NPW), minimisation of the equivalent annual cost and maximisation of the modified profit with the discount rate equal to the minimum acceptable rate of return (MARR), are the most appropriate criteria for the optimisation of process flow sheets, since an appropriate trade-off is established between the absolute terms of the future cash flows and the profitability of the investment.

In the case of an industrial plant, a couple of additional issues that need to be taken into account are the availability and reliability of the economic data. This research comprises operating plants that have production data available online; to build the objective function it was considered the unit prices from the financial statements and preliminary capital costs are used in the objective function based on annualised costs. Therefore, the promising economic benefits suggested by the retrofit analysis are highly likely to be reflected in the financial statements.

2.5 Concluding remarks

A large amount of research has been carried out on retrofit design. The issues identified in the literature in relation to retrofit problem designs can be summarised as follows:

1. Integrated process design: multiple tradde-offs are present between the benefits to be achieved (i.e. utilities reduction) and the implications involved in the promising retrofit changes (i.e. capital costs and spatial feasibility). The best approach to use depends strongly on: the features of the problem, the resources available, and the user requeriments; thus, there is no unique methodology that

fits all the problems. Moreover, the solutions reached by different approaches may differ, so a systematic way of validating its uncertainty is always required.

2. Process optimisation: a large number of mathematical programming tools are available for both deterministic and stochastic optimisation. Besides this, an alternative experimental optimisation is available. Nevertheless, most of these algorithms have important disadvantages regarding: a) a large computational burden that is highly time-consuming, b) an uncertainty on global optimality and c) lack of full control by the user in the decision making process. However, the advantages of those tools may be synergised positively through a proper combination of the algorithms.
3. Retrofit design: the effects of the structural changes carried out to the process in the objective function have been estimated in most of the cases reviewed by a sensitivity analysis. Nevertheless, the statistically based identification of the main factors and interactions existing between them would complement the reliability of the stated effects.

Therefore, there is always a trade-off to deal with in order to balance the stated issues. An additional issue is that resources available for conducting retrofit study are often limited. There has been a trend toward integrating the currently large number of methodologies available. The main focus has been given to find a systematic approach that can improve the quality of the results obtained and reduce the solution time. A valuable fact in such a systematic approach is that it can yield to practical and realistic solutions when optimising complex operational plants. An easy modification by the users and an effective understanding of the retrofit modifications effects is also desirable. This will lead to a more reliable and a better understanding of the portfolio of opportunities obtained.

Chapter 3. Design Methodology

It is important to state at this stage that the aim of this research is to provide a reliable and practical approach for generating cost-effective retrofit design options which yield to not only economic improvements (i.e. cost, product recovery), but also enhanced sustainability (i.e. CO_2 emissions, energy use efficiency). This chapter describes the approaches used to solve the retrofit problem, and is divided into two main sections. The first section introduces the response surface methodology (RSM) and explains how this experimental optimisation approach can be applied to address the retrofit problem. The definition and basic concepts used in experimental design and RSM are explained, and finally a detailed description of the generation of RSM models, along with a discussion on model accuracy. The second section of this chapter explains details of the proposed retrofit approach, including the reasons for choosing the RSM method for a retrofit study, main benefits and limitations of the proposed approach and the specific considerations done in the RSM applied. The steps involved in the proposed approach are described along the sequence to carry on them.

3.1 Response Surface Methodology

3.1.1 Overview

RSM is based on the work proposed by Box and Wilson (Box, 1951). Montgomery (Montgomery, 2005) defined it as a group of mathematical and statistical techniques applied to the modelling and analysis of problems that include a response of interest that is affected by several variables or factors and of which objective is to be optimised. Modelling can be performed by fitting quantitative data extracted from a set of experiments with an appropriated experimental design. Design of experiments (DoE) is used to set the systematic variations to the input parameters, which are performed to determine multi-variable equations. The statistics analysis of these equations helps in the understanding of the problem and generates the models which describe its behaviour and characterisitcs. The models generated are commonly called mechanistic or empirical

models, because these are obtained directly from experiments. However, it is also possible to develop shortened or reduced models from theoretical models through simulations if these are treated as experiments (computer experiments). In this manner, DoE efficiently explores the system of interest in order to extract useful information in a statistical sense, with reasonable time and resources.

RSM is therefore a sequential procedure that follows model generation (DoE-based) searches for its optimum along a path of improvement (gradients-based), which can be ascent or descent depending on the optimisation objective. This method has been widely used in various areas including chemistry, biology, electronics and manufacturing, in which its main applications are related with determining the factors and levels that satisfy a set of requested specifications throughout the searching space, and determine the optimum combination of factors at a desired response, setting the conditions for process stability, gaining an insight and achieving a quantitative understanding of the system's behaviour over the region studied. Some examples of RSM and DoE applied to simulation data found in the literature are the RSM of cellular manufacturing[1], in which a process optimisation was carried out, achieving savings of 20% in annual costs (Irizarry et al., 2001b, Irizarry et al., 2001a, Shang and Tadikamalla, 1998); multi-measures manufacturing models, which were reviewed in a survey by Rosen et al. (Rosen et al., 2008) proposing to generate metamodels[2] to guide the simulation end user in selecting the decision that incorporates their preference towards risk and uncertainty; for ink-marking machines performance optimisation (Yang and Tseng, 2002), in which both throughput and cycle time performance for ink-marking machines were successfully optimised; and manufacturing of missiles (Schonning et al., 2005) in which the design computational time for the missiles was reduced by 44%.

There were also attractive for solving industrial-type design problems; DoE for mechanical processes, such as the computational fluid dynamics of turbines that evaluated main and joint effects of input parameters on the turbine studied yielding to the

[1] Cellular manufacturing is a model for workplace design and it is an integral part of lean manufacturing systems.
[2] Metamodeling included the analysis, construction and development of the frames, rules, constraints, models and theories applicable and useful for modeling a predefined class of problems.

influences in the radial velocity at the inlet on the pressure recovery and energy loss factor (Cervantes and Engstrom, 2004); thermo-mechanical models (Davim and Cardoso, 2005) to predict the behaviour of a composite "polyetheretherketone" under thermal conditions; neuronal network-based models for crude oil distillation in which the effect of system input variables on oil product qualities was analysed by DoE (Liaua et al., 2004), and to determine optimal mould design parameters for electronic packages and the setting of process parameters (Tong et al., 2004), and even for probabilistic reservoir forecasting models where DoE was applied to do earth and flow-simulation modelling with high statistical significance (Kabir et al., 2002). Therefore, the results obtained from these studies show RSM as a promising tool for optimising simulation generated systems. The main advantages for RSM are its ability to facilitate the understanding of the main factors and interactions that affect the studied response, both as a systematic tool and to provide control of the user's decision in the solutions. This simplifies the optimisation procedure once the process model has been reduced, which reduces computational time invested on designs.

3.1.2 Experimental designs

A production system can be modelled as a series of processes, with input parameters that can be controlled or uncontrolled, and are dependent on output variables as in Figure 3.1. Parameters may vary due to measurement errors, variations in production, environmental conditions or equipment deterioration. This leads to uncertainties embedded in the experimental data that generate changes in the parameter values over time, following certain distributions of the input parameters and output variables. Nevertheless for the simulation results, different from the experimental data, those variations stated are not present, which means that there is no random error associated with the output; thus, the uncertainties are assumed to be zero (Myers et al., 2004b). The controllable parameters are commonly called "factors" and the uncontrollable named "co-factors". The different output variables are called "responses". The factors may be continuous or discrete according to their nature, and may involve certain levels of study. For design optimisation using RSM, the desired measure is identified (response) and the factors that may significantly influence the measure of the system selected. Initial experiments are carried out by screening and to determine whether non-linear terms would possibly improve the accuracy of the model. Following this, coefficients that integrate the model that predicts

the process are estimated through regression. Additional experiments are performed for the purpose of fitting the response surface model with an acceptable level of accuracy and confidence. The process model determined, as stated, in most of the cases is mechanistic or, occasionally, a reduced theoretical model.

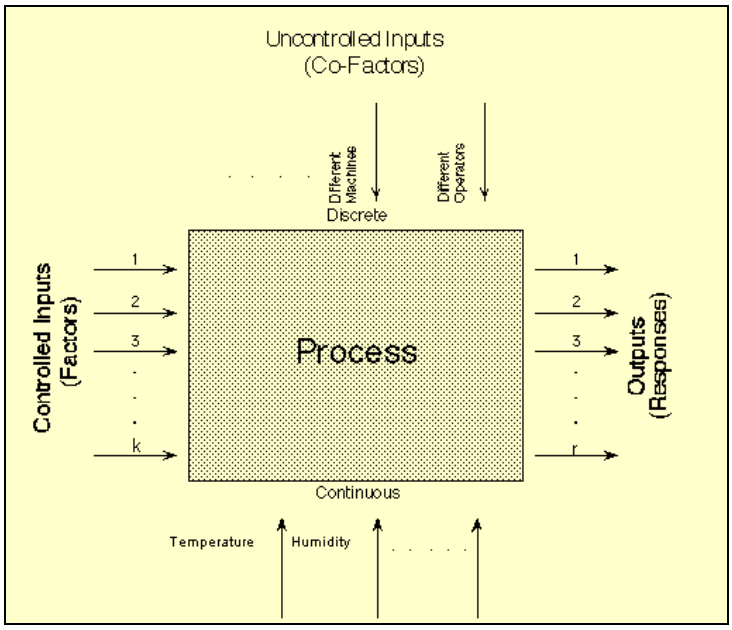

Figure 3.1 Production system modelling from Eng. Statistics Handbook (U.S.CommerceDepartment, 2006).

In order to extract the most useful information about the effects of the factors in the responses, it is necessary to perform experiments that comprise variations of one or more factors; criteria for setting the number and type of experiments may vary, but the larger the better, as this is likely to cover the most possibilities. On the other hand, carrying out experiments has implications on cost and time required. Thus, it is preferred that this be reduced to the minimum. Therefore, there is a trade-off and a systematic tool needs to be applied so that the number of experiments to be executed can be minimised, but at the same time the system behaviour can be effectively understood by estimating the possible effects of factors and its interactions. Additionally, it is also necessary for the variance of the coefficients of the model obtained through regression to be reduced to reach a good fit level, which is also improved by increasing the number of experiments. In consideration of obtaining such desired results, design of experiments (DoE) is used, which is based on the statistical sampling carried out in the studied space under geometric principles. In general, there are two classes of design:

1) Classic or “black-box” designs are applied if the levels can be set without any geometrical restriction in the outputs. For this class, factorial designs (FD) are the most efficient. The term “black-box” is given because in most of the cases the process equations are either unknown, due to the lack of developed first-principles models (i.e. the case of novel technologies) or inaccessible since its trademark registered codes do not allow direct access to the design models (i.e. the case of the commercial simulation software). Therefore, process behaviour is described as being a “black-box” because of the lack of closed-form equations. These designs have the advantage of geometrical forms that can be interpreted easily and can lead to simple interpretation of the factor effects. Moreover, some designs in this class such as fractional factorial designs (FFD) can be projected into larger designs in the subsets of significant factors of a previous design (projection property). It is also possible to sequentially combine the runs of two or more FFDs to estimate factor effects and interactions (sequential experimentation). However, in the cases of dynamic experiments or constraints on the outputs, these designs are not suitable.

2) Optimal or “model-based experiment” designs apply fully for the presence of geometrical restrictions and/or dynamic experiments. Optimal designs are a class of experimental designs that are optimal with respect to some statistical criteria. These request the explicit knowledge of the mathematical model of the system, and an optimisation framework is applied to both, the design of experiments and the solution of the problem (Gaia Franceschini, 2008). This feature allows parameters to be estimated with minimum deviations between estimations by the model and real values, leading to a lower number of experimental runs required to estimate parameters with the same precision as a classical design. As a result, when applying this optimal design, the appropriate model must be known in advance, as so does the suitable statistical criterion (i.e. understanding of the process and statistical theory beforehand). As a consequence, these designs are model-dependent. This is an important disadvantage when assessing many models because, while an optimal design is best for one model, it cannot work efficiently on other models. Another counterpart of the optimal designs is that these cannot be used for assessing the robustness of the process (design robustness). In this case, classic designs are suggested (Myers et al., 2004b, Myers RH, 2004).

The specific features in the present research are: not having geometrical restrictions in the searching space for the retrofit study, the necessity of understanding the relationship between the response and factors involved, simplicity and clearness of the methodology applied, and using available company commercial software. With these in mind, classic designs are considered the most suitable for application. This class will be detailed in the following paragraphs.

Among the most widely used designs of experiments are two, three, and five-level full factorial designs (FD), the forms of which are orthogonal. A two-level full FD (2^k), where *k* is the number of the design variables, is suitable for fitting linear response surface models. A three-level full FD (3^k) is used to generate quadratic polynomials. Both are useful for a small number of factors, but for higher order factorial design, the number of design points rises exponentially with an increase in the number of factors. In this case, fractional factorial designs (FFDs) are appropriate; these are applied mainly for screening purposes. FFDs are based on the idea of when several variables exist, the process is likely to be driven by main effects (single factors) and low order interactions (between two factors). Therefore, higher order interactions (among three or more factors) have a lower effect on the responses. The projection property and sequential experimentation features previously mentioned are two major advantages in the FFDs, as these can save time and costs when complementing previous screening experiments to fit models with further designs.

As stated, FFDs are formed by fractions or sections of the corresponding full FD 2^k or 3^k, which are arranged in blocks by a design technique known as "confounding" or "aliasing". FFDs at two levels are the most widely applied for screening purposes, because it is possible to achieve satisfactory results from a relatively low number of experiments. Therefore, FFDs are commonly referred to as screening DOE. The design is conformed by blocks of experiments or simulations, which are formed by selecting factor combinations called "generators"; the total collection of design generators for an FFD is called its defining relation. As a result of its common use, two-level designs will be exemplified. Figure 3.2 shows a two-level full FD with three factors (2^3) that has a cube shape by nature; the two levels are set in high and low for each factor, each of which is located in a side of the cube. Thus, due to its geometry the design has eight experiments to perform (one in each cube's corner). If for some reason it is necessary to reduce the

number of experiments by a half, an FFD can be set to take the half fraction of this full FD. As a result of the symmetry of the cube, it is possible to take either the dark-shaded corners or the unshaded corners, which will lead to a $2^{3-1} = 2^2$ design with four experiments to perform.

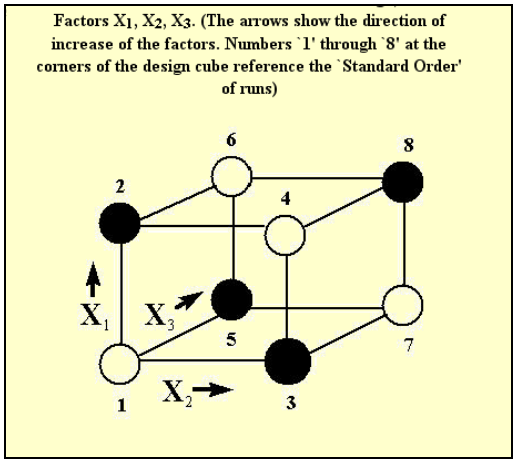

Figure 3.2 A 2^3 Full Factorial Design from Eng. Statistics Handbook(U.S.CommerceDepartment, 2006).

The resulting block size is smaller than the full FD (8), yielding to a reduction in the number of experiments from 8 to 4. On the other hand, with this reduction certain main factor effects become indistinguishable from or are confounded by other factor´s interactions, increasing the difficulties in the analysis. To illustrate this from the previous example, if the dark-shaded corners are taken, the design of the experiments can be presented in either of the following forms:

	X1	X2	X3
1	-1	-1	+1
2	+1	-1	-1
3	-1	+1	-1
4	+1	+1	+1

a) A 2^{3-1} FFD.

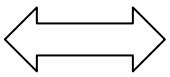

	X1	X2	X1*X2
1	-1	-1	+1
2	+1	-1	-1
3	-1	+1	-1
4	+1	+1	+1

b) A 2^2 FFD augmented with X1*X2.

Figure 3.3 A FFD taken from Eng. Statistics Handbook (U.S.CommerceDepartment, 2006).

The third column in both tables shows that main factor effect, X3, is combined (aliased) with the second order interaction between X1 and X2 (X1*X2). This fact increases difficulty in the analysis of the effects, but this is a consequence for having reduced the number of experiments. Therefore, the level of confounding is an important feature in the FFD for further analysis.

An identity column (I) in which all the levels are set in +1 by multiplying the three factors in each row and defining them as I=X1*X2*X3 can be generated. This is known as the defining relation, because with it the complete combination (confounding pattern) for the design can be generated (by multiplication). Usually, for an FFD, the defining relation will be the group of all the columns that are equal to the identity column. The block formed in Figure 3.3 came as a result of selecting factor combination X3=X1*X2, known as the "generator".

For designs with more factors, the number of possible combinations or generators that yield to other blocks increases. These will produce a different amount of experiments and confounding levels, but there will only be one defining relation. In general, for an FFD with k number of factors at two levels and p number of generators, there will be 2^{k-p} experiments. The defining relation is formed by the collection of all the p generators written in the identity form. The length of the shortest string of factors (generator) in the defining relation is called the "resolution" of the design. For instance, the specification for a 2^{8-3} design is given in Figure 3.4:

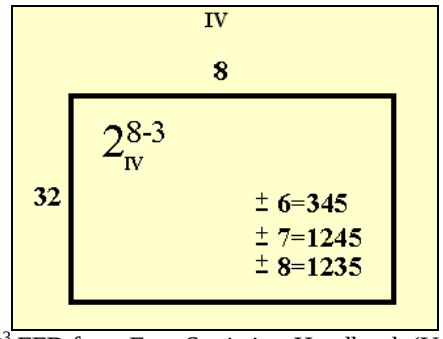

Figure 3.4 Specification for a 2^{8-3} FFD from Eng. Statistics Handbook (U.S.CommerceDepartment, 2006).

The number of factors k is 8, the number of chosen generators p is 3. These are shown on the lower-right corner. The FFD is at two levels, so the 2^{8-3} design has a total of 32 experiments (2^5). The defining relation is the generators group:

$$\{I = \pm 3456;\ I = \pm 12457;\ I = \pm 12358\}$$

The first of the three generators has the shortest string of factors I=X3*X4*X5*X6 in the defining relation and its length is 4 factors. In this case, the resolution is level IV.

The common resolutions are III, IV and V levels because, as stated before, FFD is based on the idea that the process is likely to be driven by main effects and low order

interactions; higher order interactions (more than 3) probably are not important and, hence, higher level resolutions (VI or more) are not commonly found.

A brief summary can be given to detail the resolution differences:

Resolution III Designs: The main effects are confounded with interactions between two factors (i.e. X1=X2*X3); thus it is difficult to estimate the main effects in isolation.

Resolution IV Designs: There are no main effects aliased with two-factor interactions, but two-factor interactions are aliased with each other (i.e. X1*X2=X3*X4). Therefore, it becomes easy to estimate the main effects in isolation, but difficulties arise in estimating second-order interactions.

Resolution V Designs: There is no main effect or two-factor interaction confounded with any other main effect or two-factor interaction, but two-factor interactions are aliased with three-factor interactions (i.e. X1*X2=X3*X4*X5). Consequently, an estimation of the main effects in isolation is easy, and so can carry out the estimation of the second-order interactions as higher order interactions are not considered important.

On the other hand, as already mentioned, an increase in the number of experiments is proportional to the increase in resolution level.

In conclusion, the higher the resolution level, the easier to analyse the effects; however, contrary to this, more experiments are needed.

The previous two levels of full factorial design or FFD (depending on the number of factors, as indicated previously) are frequently applied as the first screening designs in the response surface methodology. Following the identification of the most important factors by this screening, the most suitable response surface must be fit. To do this, the design of the experiments applied must minimise the variance of the coefficients of regression, which will be explained further in section 3.1.4. A first-order surface model (linear) can be fit by a full factorial design at two levels (2^k) or by an FFD of the 2^k series. To fit a second-order surface model (quadratic), the most usual class is the central composite design (CCD). Its widespread use relies on the fact that it can be constructed through a

sequential experimentation from a full factorial design, or an FFD, at two levels by adding some additional points to acquire spherical forms. The additional points yield up to three variants of this kind of CCD (U.S.CommerceDepartment, 2006) – the circumscribed has a centre and star points at some distance α from the centre, set larger than the limits (generally set as α =± (number of factors)^(1/4)); the inscribed has a centre where the star points are within the ±1 limits; and the faced has a centre and star points at the centre of each face of the factorial space (α = ± 1). Figure 3.5 shows the three variants of the CCD: Central Composite Circumscribed (CCC), Central Composite Face Centered (CCF), and the Central Composite Inscribed (CCI).

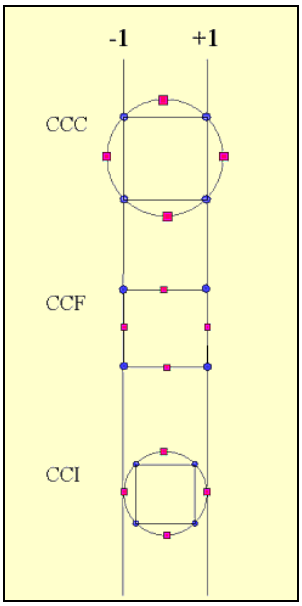

Figure 3.5 Central Composite Designs for 2 factors from Eng. Statistics Handbook (U.S.CommerceDepartment, 2006).

An important feature for providing good predictions in the region of interest for second-order response surface designs is rotatability, which assures that the model has a reasonably consistent and stable variance for the predicted response at points of interest. CCD – circumscribed or inscribed – are rotatable because the variance of the predicted response is constant on the spheres. In most cases, these designs are preferred over the faced option, as this is not rotatable. The final selection of CCD to be used depends on where the star points can be placed. It is important to note here that the number of design points for fitting the quadratic response surface models is still high if the number of design variables is more than 10.

Another type that can fit a full quadratic model is the Box-Behnken design, which is a fractional 3^k factorial formed by combining 2^k factorials with incomplete block designs, and are very efficient in terms of the number of required runs. They are either rotatable or nearly rotatable. These designs fill out a polyhedron while approximating a sphere, and are subsets of full three-level factorial designs. Therefore, Box-Behnken designs can be expected to have poorer prediction ability in the corners of the cube enclosing the design, because, unlike the CCD, they do not include points at the vertices of the cubic region. This could bring advantages when the corner points are factor-level combinations difficult to test due to physical restrictions or excessive cost (Montgomery, 2005).

The designs previously mentioned lead to a response surface fit. It is important to mention that the ranges of the designs available must be carefully selected to be appropriate for the sytem studied. Following this, to optimise the response surface fitted with a sequential approach based on gradients, searching can be performed to reach its maximum or minimum points.

Two main issues emerge from the literature regarding the use of integer variables and the globality of RSM. The publication by Davis et al. (Davis and Ierapetritou, 2008) stated that when the black-box models are functions of strictly integer variables, RSM cannot be applicable because of the infeasibility of fractional values; therefore, direct search, or branch and bound are proposed for the optimisation of these variables. RSM is classified as a local method which ensures a global optimal solution only under conditions of convexity. However, as the black-box functions cannot be determined in advance, there is an uncertainty in the results obtained, in terms of global optimality. To deal with the globality issue, Fan (Fan, 2003) developed an algorithm named ‘‘Ridge Analysis Algorithm’’ based on the trust region methods that locate and verify the global optimum within a spherical region of interest, within a response function that is in the quadratic form being this the common model used for the surface function fitting. This fact implies that RSM can lead to global solutions for some specific cases in which it can be proven to be in the trust region. However, it is often difficult for the industrial cases to apply a rigorous mathematical method to verify the trust region; the wide operational ranges and the models involved make it complex. Regarding the integer variables issue, the ranges of each design need to be carefully set and managed so that infeasibilities can be avoided. To clarify this, if, for instance, the effect of a pump that does not exist in the real process is

intended to be studied, a first screening DOE must be performed (i.e. FFD at two levels) and the pump should be considered. The design levels for the pump should be set as the +1 level with the pump flow capacity value given (i.e. 100 kg/h) and the -1 level with the pump set as non-existent (i.e. not considered in the process flowsheet). If following the first screening DOE the pump is one of the most important factors that improve the studied response (driving factor), then the response surface to be optimised should be fitted with the consideration of the pump; hence, this factor (pump) should be set in the continuous range (i.e. from 10 to 100% capacity) along the levels in the design so that it does not have infeasibilities. Of course, the considered range should be set according to the user criteria in respect to feasibility, capital costs and availability in the market.

3.1.3 Fitting RSM models

Response surfaces are the final models, either empirical or reduced from theoretical models, produced. Methods and tools are required for checking its appropriateness (i.e. fitness). The models may consider just the main effects and interactions, or may also need quadratic and possibly cubic terms to account for curvature. Therefore, these require linear, quadratic or cubic forms depending on the terms required for good accuracy of the response reproduction in the model. In most cases, higher order terms are not normally required, while for industrial applications, quadratic models have been stated as almost always sufficient (U.S.CommerceDepartment, 2006). Assume that there is one output, z, which is a polynomial function of two inputs, x and y. The function z = f(x, y) describes a two-dimensional surface in the space (x, y, z). In general, it is possible to have as many input variables as needed, and the resulting surface becomes a hyper-surface. It is also possible to have multiple output variables with a separate hyper-surface for each one.
To simplify the explanation, a response based on three inputs (x_1, x_2, x_3) is considered. The full equation of a cubic response surface is:

$$
\begin{aligned}
& y = b_0 + b_1x_1 + b_2x_2 + b_3x_3 + ... && \text{(Main terms)} \\
& b_{12}x_1x_2 + b_{13}x_1x_3 + b_{12}x_2x_3 + ... && (2^{nd} \text{ order interaction terms}) \\
& b_{11}x_1^2 + b_{22}x_2^2 + b_{33}x_3^2 + ... && \text{(Quadratic terms)} \\
& b_{123}x_1x_2x_3 + b_{112}x_1^2x_2 + b_{113}x_1^2x_3 + b_{122}x_1x_2^2 + ... && (3^{rd} \text{ order interaction terms}) \\
& b_{111}x_1^3 + b_{222}x_2^3 + b_{333}x_3^3 + ... && \text{(Cubic terms)} \\
& + \varepsilon && \text{(Experimental Error)}
\end{aligned}
\qquad (3.1)
$$

Where:

ε is the error term in the response observed (i.e. noise), which for data generated from simulations has a cero value, b_i's are the parameters that fit the experiment's or simulation's data (input variables and responses) within the surface model, and y is the expected value of the surface response. As stated, the form of the best surface fitted can be linear, quadratic or cubic, formed from equation 3.1 with the terms that apply. The estimated response surface can then be displayed by a graphical contour or surface plotting. The linear least squares (LLS) estimation is used to estimate the parameters (b_i's); it is essential to stress that "linear" stands for the unknown parameters to be estimated (b_i's) of the equation 3.1 that are linear. These are also known as the coefficients of regression, and in general any surface model that is linear in its parameters to estimate, such as the b_i's in equation 3.1, is a linear regression model – even though the surface shape is not. A brief review of the LLS tool is given below, and at the end of this section the general form for the non-linear case is mentioned briefly. To facilitate the illustration from equation 3.1, only the main terms are taken, which can be represented in a general form as:

$$y_i = b_0 + b_1 x_{i,1} + b_2 x_{i,2} + \ldots + b_k x_{i,k} + \varepsilon_i$$

$$= b_0 + \sum_{j=1}^{k} b_j x_{i,j} + \varepsilon_i \qquad i=1, 2, \ldots, n \qquad (3.2)$$

Where,

y_i is the group of responses (observations), x_i the group of input variables, b_0 the intercept of the plane, which together with b_j are the unknown parameters to be estimated (regression coefficients), and ε_i the random disturbances (error). Generalising this based on matrix represent tation (matrix notation) is equivalent to:

$$y = \hat{b}X + \hat{\varepsilon} \qquad (3.3)$$

Where,

$$y = \begin{bmatrix} y_1 \\ y_2 \\ . \\ . \\ . \\ y_n \end{bmatrix}, X = \begin{bmatrix} 1 & x_{1,1} & x_{1,2} & . & . & . & x_{1,k} \\ 1 & x_{2,1} & x_{2,2} & . & . & . & x_{2,k} \\ . & . & . & . & . & . & . \\ . & . & . & . & . & . & . \\ . & . & . & . & . & . & . \\ 1 & x_{n,1} & x_{n,2} & . & . & . & x_{n,k} \end{bmatrix}, \hat{b} = \begin{bmatrix} b_0 \\ b_1 \\ . \\ . \\ . \\ b_k \end{bmatrix}, and \qquad \hat{\varepsilon} = \begin{bmatrix} \varepsilon_1 \\ \varepsilon_2 \\ . \\ . \\ . \\ \varepsilon_n \end{bmatrix}$$

The LLS method searches for the $\hat{b}$ so that the sum of the squares of the errors, $\hat{\varepsilon}$, is minimised. Therefore, the LLS criteria used to estimate the unknown parameters can be defined as:

$$L = \sum_{i=1}^{n} \varepsilon_i^2 = \sum_{i=1}^{n} [y_i - (\hat{b}_0 + \hat{b}_1 X_i)]^2 \qquad (3.4)$$

which needs to be minimised by setting the partial derivatives of L with respect to $\hat{b}_0$ and to $\hat{b}_1$ (parameters to be estimated) equal to zero, and solving the resulting system of equations. This leads to the estimators for the parameters:

$$\hat{b}_1 = \frac{\sum_{i=1}^{n} (X_i - \overline{X})(y_i - \overline{y})}{\sum_{i=1}^{n} (X_i - \overline{X})^2} \qquad (3.5)$$

$$\hat{b}_0 = \overline{y} - \hat{b}_1 \overline{X} \qquad (3.6)$$

Where:

$\overline{X}$ is the average of the input variables and $\overline{y}$ the average of the responses. As the two parameters are functions of each other, the input and the response variables, these are not independent. For this reason, the solution implies an iterative approach in which initial values must be chosen for the parameters, after which values are obtained by successive approximation.

The majority of the surface models have proven to give a good fit with LLSs; however, in cases where linearity does not produce good results, non-linear least squares should be applied. The general form for the non-linear least squares (NLLS) case is similarly focused on the reduction of the residuals (r_i), which are similar to the errors (ε_i):

$$S = \sum_{i=1}^{n} r_i^2 \qquad (3.7)$$

In addition, the criteria are defined as:

$$r_i = \Delta y_i - \sum_{s=1}^{n} J_{i,s} \Delta \beta_s ; \Delta y_i = y_i - f\left(x_i, \beta^k\right) \qquad (3.8)$$

where y_i is the group of responses (observations), x_i the group of input variables, β the group of unknown parameters to be estimated (regression coefficients) and J_i the Jacobian or matrix of the partial derivatives of r_i with respect to β. The solution is similarly iterative, starting from initial estimations, by successive approximations, and finalising until the parameters are known. As already stated, this class of surfaces is not commonly found in industry therefore this NLLS will not be detailed in this section.

An important fact to mention is that the greater the number of the terms to be estimated, the more the experiments that are needed for estimation. Consequently, a balance must be made depending on the user's needs and the possibilities to perform more experiments or simulation runs.

The least square methods can fit the data to the response surface models, and then these models can be used to predict the behaviour of the specific response across the studied ranges. This can save time and cost in real experimentation or computational simulations. As stated previously, equation 3.1 is a standard model that may – most of the time – fit the response surfaces. Nevertheless, there might be processes where the experimenter knows in advance that the model to be fit is a non-standard model, such as a quartic model. In this case, the model formulation is different from equation 3.1, and an optimal design must be generated and applied (Montgomery, 2005).

3.1.4 Accuracy of the RSM model

The surface model must be capable of effectively predicting the behaviour of the process studied, and therefore, the validation of the surface model is important. For linear regression (based on LLS), the first step of the model validation is a numerical method which estimates the R^2 statistic. This is called the coefficient of determination and is a statistical measure of how well the fitted line approximates the real data points. It can be described as follows. After LLS, the regression coefficients are known, which means that the predicted values can now be estimated as:

$$f_i = (\hat{b}_0 + \hat{b}_1 X_i) \qquad (3.9)$$

The mean of the observed values y_i is estimated as:

$$\bar{y} = \frac{1}{n}\sum_{i=1}^{n} y_i \qquad (3.10)$$

Therefore, it is possible to define the error sum of squares:

$$SS_{err} = \sum_{i=1}^{n} (y_i - f_i)^2 \qquad (3.11)$$

Which is the same as equation 3.5 and the total sum of squares:

$$SS_{tot} = \sum_{i=1}^{n} (y_i - \bar{y})^2 \qquad (3.12)$$

Here, the R^2 is defined as:

$$R^2 = 1 - \frac{SS_{err}}{SS_{tot}} \qquad (3.13)$$

The possible values of R^2 are $0 \leq R^2 \leq 1$, while the maximum value of 1 indicates that the SS_{err} tends to be zero value; thus, the regression line fits the data perfectly. However, a high value for R^2 may not guarantee that the model fits the data well.

The root mean square error (RMSE) is an alternative statistic also used frequently to measure the differences between a model's predicted values (f_i) and actual observed

values (y_i). This is similar to R^2 in view of the fact that the deviation of the predicted vs. the observed values is assessed; however, the difference is that RMSE has the units of the response, and R^2 has no units. Hence, the deviation is related directly with the magnitude of the response. RMSE is then defined as:

$$RMSE = \sqrt{\frac{\sum_{i=1}^{n}(y_i - f_i)^2}{n}} \qquad (3.14)$$

As a consequence, the lower the RMSE the better, as the predicted values tend to be similar to the observed values. When comparing regression models that use the same dependent variable and estimation period, the RMSE goes down as the adjusted R^2 goes up. Therefore, the model with the highest adjusted R^2 will have the lowest RMSE.

The graphical residual analysis is an alternative tool to verify the adequacy of the model that has been used widely in process modelling studies for its usefulness and reliability. It has been stated that as graphical methods readily illustrate a broad range of complex aspects of the relationship between the model and the data, this is an advantage over numerical methods for model validation such as R^2 statistics and RMSE. The residual for the i^{th} observation in the data set is the difference between the observed value (y_i) and the predicted value by the model defined in equation 3.9 as f_i, and can be mathematically expressed as:

$$e_i = y_i - f_i \qquad (3.15)$$

The residuals should approximate the random errors that make up the relationship between the explanatory variables (x_i) and the response variable (y_i) if the model is correct. Accordingly, when the residuals appear to behave randomly, this suggests that the model fits the data well. Figure 3.6 shows a plot of residuals with random behaviour. Therefore, it is always useful to perform additional confirmation experiments or simulations after fitting the RSM model, in order to verify the accuracy of the model. Because of that this will be carried on this approach.

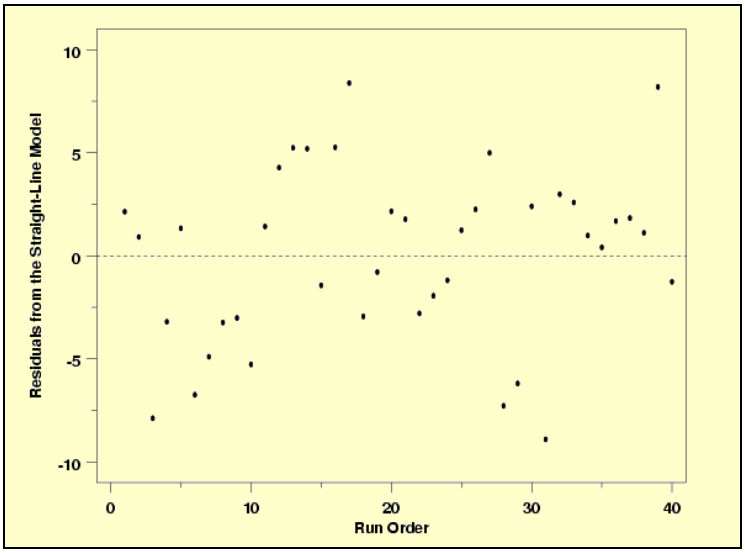

Figure 3.6 Plot of Residuals randomly scattered from Eng. Statistics Handbook(U.S.CommerceDepartment, 2006).

For the purpose of verifying the adequacy of how response surface models fit along this work, it was decided to use the three tools, namely R^2 statistic, RMSE and the plot of residuals, to support the reliability of the models.

3.1.5 Analysis of Variance (ANOVA)

The basic tool used to define the statistical importance of the factors involved in a DoE is estimated by the analysis of variance (ANOVA). This is confirmed by a series of statistics, the main focus of which is to assess the hypothesis of no differences in treatment means which can be understood as to assess the importance of factors in the studied response. The development of the test statistic used in the analysis is broad and goes beyond the scope of this work, so a brief summary is given below based on the standard ANOVA table of results. A complete description of the ANOVA can be found in Montgomery (Montgomery, 2005). Figure 3.7 shows the example of ANOVA results for 3 factors, which is illustrated in Matlab Statistics Toolbox (TheMathWorksInc., 2004).

Analysis of Variance

Source	Sum Sq.	d.f.	Mean Sq.	F	Prob>F
X1	3.781	1	3.781	0.82	0.4174
X2	199.001	1	199.001	42.95	0.0028
X3	0.061	1	0.061	0.01	0.914
Error	18.535	4	4.634		
Total	221.379	7			

Constrained (Type III) sums of squares.

Figure 3.7 ANOVA for 3 factors from Matlab Statistics Toolbox examples (TheMathWorksInc., 2004).

The analysis is based mainly on the evaluation of all the factors under an F-distribution, which is a continuous probability distribution and it is also known as the Fisher-Snedecor distribution. The F-distribution arises frequently as the null distribution of a test statistic therefore it is used to test if the null hypothesis of no difference in treatment (factors) is true. If this is true, then the analysed factor has no difference in the treatments, which can be understood as the factor not being important for the studied response.

The first column of Figure 3.7, named "Source", lists the factors studied, the errors and total rows. The second column presents the sum of squares (SS) for each factor, the error and the total SS. The third column represents the degrees of freedom for each one. The fourth is the mean square of each SS. The fifth is the F test value. The last column presents a comparison of the F value with the corresponding F distribution. These values are known as the p-values, which Montgomery (Montgomery, 2005) defined as "the smallest level of significance that would lead to the rejection of the null hypotheses H_o", which means the smallest level at which the studied factor is statistically significant or important enough to the response studied. It was suggested that a good level of significance is 99.5 which for the p-value represents < 0.005, so when the p-value of a factor is less than this number, it is statistically significant and becomes one of the most important factors for the studied response.

Note that the ANOVA model assumes that the error term should follow the assumptions for a normal and independent distribution. Thus, after performing an analysis of variance, the model should be validated by analysing the residual plot.

In some cases, software computations for the p-values are too low to be shown and the p-values are presented with 0 values by default in the software. When this happens and there is more than one most important factor, it may be necessary to determine the order of importance for these. For this purpose, the effect of each of the factors can be estimated directly from the experiment or simulations' responses. For both the 2^k full FD and 2^{k-p} FFD, the effect of factor i can be estimated with the following simplified form:

$$EffectOfFactor(i) = \bar{Y}(+) - \bar{Y}(-) \qquad (3.16)$$

with $\bar{Y}(+)$ denoting the average of all response values for which factor i is in the "+" level, and $\bar{Y}(-)$ denoting the average of all response values for which factor i is in the "-" level. The same equation can be applied for two factor interactions. Multi-factor interactions (three or more factors) were assumed to have a lower effect on the responses in section 3.1.2. Finally, a plot of the effect of the factors can be created for visualisation purposes (the effect of factor vs. factors). Factors that present the higher values from the base line (abscissa) will be the most important factor for the studied response.

3.2 The proposed retrofit design approach

3.2.1 General considerations

It is worthwhile restating that the present work has the aim of generating a reliable and practical approach to determine cost-effective modifications in the process to improve its base case design performance (not only economically, but also environmentally). To address this issue, the proposed Retrofit Design Approach is based on the application of process simulation and RSM for retrofit design. Workload does not allow the company to invest much time in the study of retrofit. Furthermore, personnel and policy changes require the application of tools that should be easily transferable and based mainly on commercial software simulators. Therefore, RSM was chosen because the user prefers a tool that could generate reliable retrofit design results, but at the same time could be applied practically in industry. The reasons for using commercial simulators are the guarantee of being certified by external standard organisations and their easy-to-use features. In Chapter 2, it was found that most of the methods used for retrofit require a large efforts for programming, but RSM is an alternative optimisation methodology that does not need to carry on programming to reach pseudo-optimal solutions and can yield to a high statistical confidence for its results. Additionally, it has been favoured for the design of experiments in the industry because of its promising cost-time reductions and obtaining the efficient and reliable results (Ilzarbe et al., 2008, Tanco et al., 2008, M. Tanco, 2009, Tanco et al., 2009). All of these considerations were the reasons behind why RSM was selected for the retrofit study in this research.

Therefore, the basic benefit from RSM that can be applied in this work is the fact that it does not require a considerable programming load to generate reliable optimal results. Additional advantages of RSM include, as stated in section 3.1.1, facilitating the understanding of the main factors and their interactions that affect the studied response. Being a systematic methodology and providing user's control in design procedure is favourable when compared with other conventional optimisation methods.

On the other hand, the main limitations for the RSM include that, firstly, the global optimality of the solutions found is not fully guaranteed, however, optimality is verified 1) by initialising the linear or nonlinear optimization problem of the surface model from different points to choose the best solution and 2) by carring out confirmational simulations in the space around the best solution found. Secondly, the computational time for simulation may be high, as a large number of simulations may be performed before achieving the optimal solutions depending on the number of factors and levels for the study. A third drawback of RSM application is regarding the integer variables managed for the structural changes implicit in a retrofit design – the ranges of each factor need to be set and managed carefully so that infeasibilities can be avoided in the DoE applied.

The previous sections in this chapter stated that the purpose of RSM is that when the coefficients of a satisfactory approximation function are found, the approximation function can then be used directly instead of involving every simulation model in the process flowsheet. Thus, the Retrofit Design Approach generates a reduced model (response surface model) of the production process, which is simulated by relating the variation in output parameters to the variations in input parameters. The time to perform a stochastic optimisation of the initial whole simulation model might range from minutes to hours or even days of computation time, unlike optimising a linear or quadratic function, which requires only a fraction of a second. This is also a considerable advantage of Retrofit Design Approach. Therefore, in the proposed Retrofit Design Approach, the reduced model is optimised in order to obtain pseudo optimal solutions based on the objective function (response of interest) to a desirable level. The approach can make suggestions on how to change operational variables (i.e. continuous variables) and potential structural changes (i.e. discrete variables) towards improving the objective response. As previously mentioned, while this method may substantially reduce the programming difficulties commonly faced in a retrofit problem, it may not reduce the

solution time signficantly. Nevertheless, the number of simulations may be decreased, as the RSM is executed if the experimental designs chosen are complementary of each other, as explained in section 3.1.2. An example would be a CCD constructed based on an FFD. It is important to notice that the RSM cannot solve the MINLP problem regarding the initial options in the superstructure; however, it can yield to a reasonable set of initial options based on process integration tools which are considered satisfactory for the user.

3.2.2 The approach used

In order to provide an insight and understanding how the proposed Retrofit Design Approach is carried on, Figure 3.8 schematises the sequence to carry on its steps – a description of each one is presented in the following lines.

Three main stages are applied in the Retrofit Design Approach: a diagnosis stage, an evaluation stage and an optimisation stage, all of which are supported by simulation software.

1. The diagnosis stage identifies potential variables to be changed or structural modifications which promise a cost-effective improvement in the process. The improvement is measured by the increases in profit, as the main response studied, and by an additional response regarding the effect on energy targets. Some variants of these responses may appear according to the focus of the process, but in general profit is estimated as the difference between sales of products and co-products minus the operating costs in which the raw material and the energy costs are considered. Energy targets are computed from the problem table algorithm. The data for both responses are taken directly from the simulation results in all the cases. The profit is estimated by a calculator built inside the simulator, and the energy targets are estimated by heat integration software.

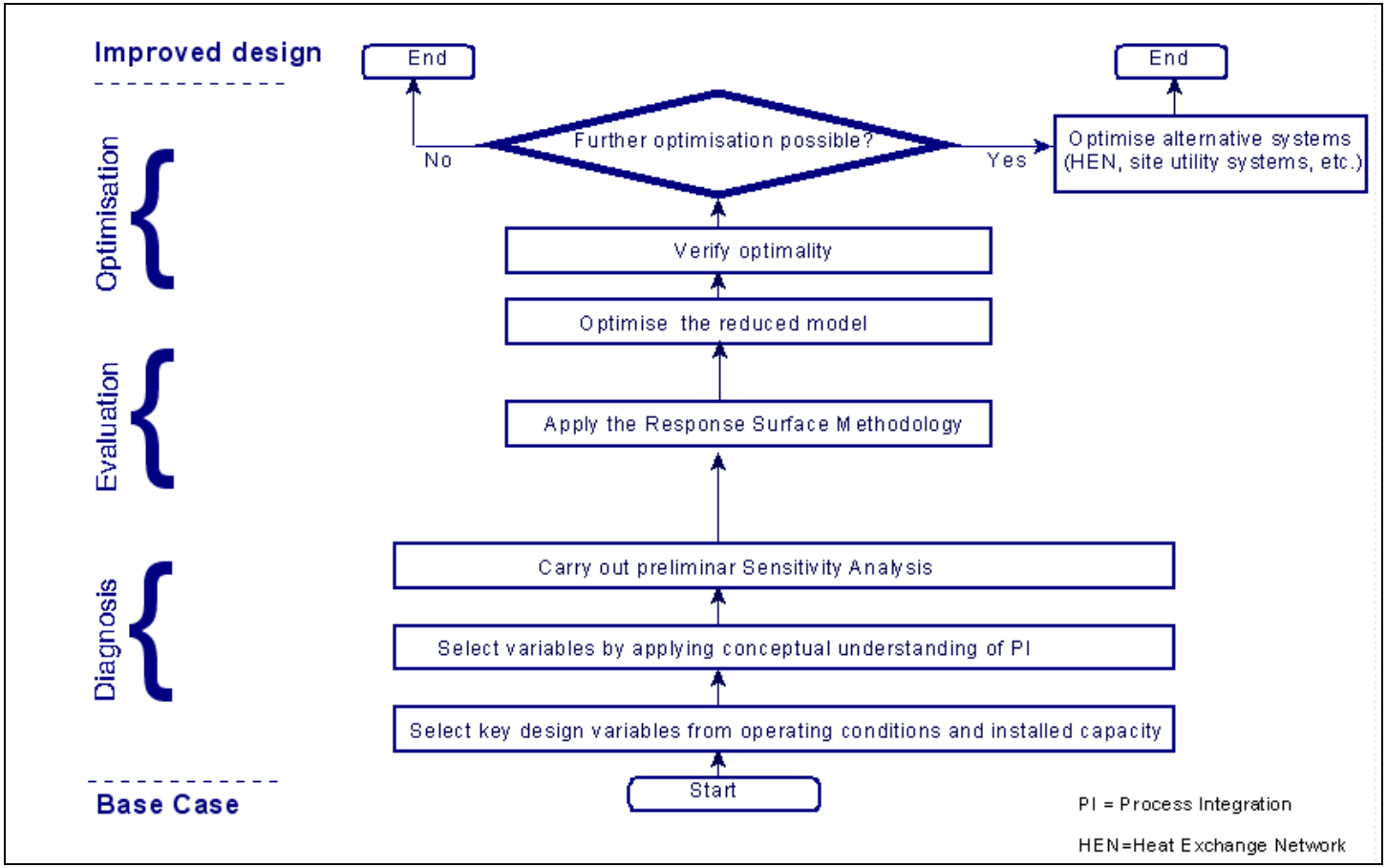

Figure 3.8 Steps involved in the proposed Retrofit Design Approach.

In general, the profit response is totally set by the user needs but it is suggested to apply the five types of profit defined here and to adapt these to the specific problem. The first is net profit (NPr), which represents overall profit from the sale of products and by-products (i.e. steam, condensates) after considering operating costs (raw materials, energy used (i.e. utilities)). The second is referred marginal profit (MaPr), which is the difference between the NPr for the simulated case and the NPr for the best case historically registered in the plant. The third is the marginal profit normalised (MaPr*), which is the MaPr estimated for each case divided by the MaPr of the base case to give absolute units. The fourth is the Marginal Profit Capital Affected (MPCA) which is defined as the MaPr minus the total Annualized Capital Costs (ACC_i) for the changes suggested to perform by the retrofit design (i.e. new units, modified units, heat exchangers). Finally for simplification purposes, MPCA* (MPCA normalised) was defined as the MPCA of the simulation divided by the MPCA of the base case to give absolute units.

These can be expressed as follows:

$$NPr = S_P + S_{CO} - VC_{RM} - VC_E \qquad (3.17)$$

where

NPr = Net profit [£ /Y]; S_P = Profit from the sales of product [£ /Y]; S_{CO} = Profit from the sales of co-product [£ /Y]; VC_{RM} = Variable cost of raw material [£ /Y]; VC_E = Variable cost of energy [£ /Y].

$$MaPr = NPr_{SC} - NPr_{HBC} \qquad (3.18)$$

where

MaPr=Marginal profit [£/Y]; NPr_{SC}= Net profit of studied case [£/Y]; NPr_{HBC}= Net profit of historical best case [£/Y].

$$Ma\,Pr^{*} = \frac{Ma\,Pr}{Ma\,Pr_{BC}} \qquad (3.19)$$

where

MaPr*=Marginal profit normalised [Absolute units/Y]; MaPr=Marginal profit of studied case [£/Y]; $MaPr_{BC}$=Marginal profit of base case [£/Y];

$$MPCA = Ma\,\mathrm{Pr} - ACC_i \qquad (3.20)$$

where

MPCA = Marginal Profit Capital Affected [£ /Y]; MaPr = Marginal Profit [£ /Y]; ACC_i = Annualized Capital Costs of "i" change suggested for retrofit (i.e. New Units, Modified Units, HE) [£ /Y].

$$MPCA^* = \frac{MPCA}{MPCA_{BC}} \qquad (3.21)$$

where

MaPr*=Marginal profit normalised [Absolute units/Y]; MaPr=Marginal profit of studied case [£/Y]; $MaPr_{BC}$=Marginal profit of base case [£/Y];

To consider the capital costs associated with the structural changes proposed by the retrofit, capital investment is estimated for new units considered in the study as the Annualized Capital Cost for new units ($ACC_{NewUnits}$):

$$ACC_{NewUnits} = CC_{NewUnit} \bullet AF \qquad (3.22)$$

where

$ACC_{NewUnit}$ = Annualized Capital Cost of the new unit [MM £ /Y]; $CC_{NewUnit}$ = Capital Cost of the new unit (acquisition cost plus piping cost plus installation cost) [MM £]; AF= Annualization Factor [Y^{-1}].

The effects on profit and energy targets are defined respectively as the differences between the profit or energy targets (hot and cold) in the case studies minus the profit or energy targets in the base case, divided by the profit or energy targets in the base case and reported as a percentage.

The diagnosis stage then comprises of:

a. Selection of key design variables This is done by exploring all the controllable design parameters of the plant within the allowable range or a possibility of adopting

reduced capacity (working load) and their impact. Structural changes available for de-bottlenecking in the plant installed capacity are also considered for assessment.

b. Conceptual understanding of Process Integration (PI): The promising options for operational changes or structural modifications based on process integration concepts are considered. These may be continuous variables such as stream splits, altering existing equipment bypasses, heat duty modifications, etc. or discrete variables such as adding or eliminating equipment, relocating or modifying existing equipment internally, etc. The feasibility of these structural modifications in the real physical location, based on the user's experience and knowledge, as well as practical constraints (e.g. plant layout), must be considered as an important aspect at this stage. The evaluation of potential options is carried out with process design methodologies, including process integration methods. Options for the distillation sequence reviewed in section 2.1.1 are tested in this stage for the columns existing in the process. The component flowrates through each column, in combination with the column composition profile, are checked to examine mixing effects, the feeding stage or the product extraction stage location, the feeding condition, and the number of stages or their overall efficiency. Complex column arrangements, such as side stream, sloppy or prefractionator, presented in the section 2.1.1, are also included for testing and to find out whether they can produce a considerable improvement in the process. The process integration techniques applied in this research were stated in section 2.1.2 and include the ET, MER, CC and GCC. The utilities used and their levels are also matched against the GCC. The plus/minus principle is then applied to find the process variables that can improve the energy recovered in the process by displacement of composite curves. Finally, a number of possibilities for utilities in situ generation schemes are explored and evaluated to assess viability and cost-effectiveness. If these are promising, they are also added to the final variables list. The exploration is focused either on recovering energy lost in the process or in improving profitability in the process by the feasible implementations. These process integration options are useful for evaluation because, as referred to in Chapter 2, they can certainly identify promising variable changes that may highly improve process performance in product recoveries, product specifications, energy recovered and utilities reductions.

The impact of each variable identified in the previous stages is assessed by a sensitivity analysis to select the most promising variable. It has been stated that this

class of analysis, which is commonly known as a one-to-one analysis, is not adequate for screening factors, as it does not consider interactions between factors that may be important for some cases (Myers et al., 2004a, Montgomery, 2005). It must be clarified that the sensitivity analysis carried out in this part does not account for the identification of the most important factors in the process response. This is only performed as a tool to gain the necessary knowledge of the process at this first diagnosis stage and, thus, to eliminate the parameters or structures that are highly improbable to account for an improvement. Otherwise, these factors without any worth may exponentially increase the size of the DoE.

This sensitivity analysis is carried out by executing perturbations to the variable studied and assessing the impact that these perturbances have in the two responses of interest (profit and energy targets). The ranges of the variable perturbance are established with base on the capacities of the existing equipment reported in the safety or process data sheets, or with base on the commercially available ranges for the structural changes or the new equipment in the plant.

The criteria to consider a variable as a "promising one" need to be based on the order of magnitude for the profit and energy targets of the plants studied, in order to effectively yield towards promising improvements. The levels for the criteria are set by the user needs. Specifically, for the case studies reviewed in this research, the levels of the criteria are set as:

1. If the perturbation of the variable yields to a minimum increase of 5% in the profit response when compared with the base case, although the energy targets are not reduced.
2. If the perturbation of the variable results in the combination of a minimum of a 1% increase in the profit response (compared with the base case) and a minimum 3% reduction in energy targets.
3. If the perturbation of the variable does not result in an increase in the profit response but yields a minimum reduction of 5% in the energy targets.

Following on from this sensitivity analysis, variables that show not to account for improvements in the process (criteria-based) are removed from the Retrofit Design

Approach. The remaining set of promising variables is then transferred to the evaluation stage. For the Retrofit Design Approach, this stage defines the initial size of the problem or possible design to be applied based on the list of variables (number of factors to study), the ranges in which these can be varied (the levels) and if there is any geometrical restriction in the outputs for the searching space (geometrical form).

2. The evaluation stage. In this stage, promising options transferred from the diagnosis stage are subjected to RSM investigation. The capital costs are estimated only for these options, which become a much simpler task than they would be if the cost estimates for all possible modification options were required prior to design. The response to be studied in this stage will only be the profit. A screening DoE is applied to indentify the most important factors from the promising variables set. Further to the selection of the most important factors, a reduced model is obtained by fitting the process response behaviour. If this is necessary, additional simulations are executed to account for a complementary DoE that accurately fits the surface model. The general procedure for the evaluation stage can be divided into two steps, detailed as follows:

a. *Preliminary screening* consists of a screening DoE, which is an FFD at "n" levels with "k" factors, where number of levels "n" can be any number chosen by the user and the "k" factors are given by the promising variables transferred from the diagnosis stage. In practice, it is recommended to set this FFD at two levels (n=2), as it was referred to in section 3.1.2 as one of the most useful DoE for screening purposes due to its simplicity and relatively low number of runs needed when compared with a full FD. The resolution and, thus, the confounding pattern are selected with base on the minimum number of runs needed for a simple and clear factor analysis, and will depend on a number of factors. This first screening DoE will result in a number of simulations to be performed and the subsequent estimation of the impact of factors in the objective response profit. For this purpose, the ANOVA is applied to the simulation's responses and the final result is the identification of the most important factors in which the surface model will be fitted.

b. *RSM* is put into practice in the second part of the evaluation stage. The methodology generates the input parameters with base on the most important factors found, and produces the results of its perturbations in the objective response from the simulation. Infeasibilities with integer parameters when present in the most important

factors' set must be avoided by setting the integer parameter in the continuous range along the levels in the response surface design, just as in the example given in Section 3.1.2. For this step, the surface response design proposed is a CCD, as this can be formed by completing, where possible, the previous FFD applied, yielding this to a fewer number of simulations than a completely new DoE and, subsequently, reducing the solution time. The results are then fitted by LLS to obtain a reduced model with a high level of confidence to reproduce data in the ranges studied. The accuracy of the reduced model and the validation of it are tested by the R^2, RSME and residual plots.

3. The optimisation stage:

This stage deals with the optimisation of the reduced model obtained from the RSM looking for the optimal values of the objective response in the parameter ranges studied. In this step, similar to the evaluation stage, the integer variable infeasibilities are avoided by setting the integer parameter in the continuous range along the optimisation, which range is inside of where the RSM model was obtained (as stated in the example given in Section 3.1.2). As the models are reduced and without integer variable infeasibilities, they are conformed mostly by linear or non-linear continuous variables, so LP or NLP solvers can be used most of the time. Optimisation can be carried with the Microsoft Excel Solver tool, which uses the generalised reduced gradient (GRG2) non-linear optimisation code developed by Lasdon (Waren and Lasdon, 1995) and for linear problems uses the simplex method with bounds on the variables, and the branch-and-bound method, implemented by Watson (Watson, 1995).

To verify optimality: One issue with the NLP solvers used in Excel is that they tend to converge on a single optimum close to the starting point, and Microsoft Excel Solver has no sure way of knowing if this is a global optimum point (FrontlineSystems, 2003). One way to find this out is to apply external knowledge of the problem. This can be done either through commonsense or through experimentation, which has already been done through the DoE where the region near to the pseudo-optimum point has been identified. Or, alternatively, Microsoft Excel Solver can be started from different and separated points to see which solution is best. From this step, the optimal conditions for operating and main process structure are reached. Additionally, a series of confirmatory simulation runs is performed around the optimal solutions reached

from the optimised reduced models to verify their optimality.

Further optimisation: In general, further optimisation of the process is required when following to the process changes set by the new optimised conditions, there is still a possibility for reduction in the energy recovered in the process. The main reason for this is that the process streams have been changed and a potential for energy improvement may remain. One of the most typical cases found is the HENs optimisation. Energy recovery in the HENs is influenced by process changes. After setting the optimal solutions found in the previous step, the process structure is no longer the same and operating condtions of some of streams are changed. Therefore, it would be ideal to consider process changes and HEN optimisation simultaneously, however, it is not straightforward to include all the possible options in a single design framework. It is adopted in this study to consider the design of heat recovey systems after accepting process changes. For some cases the existing design of heat recovery systems is highly integrated and, consequently, it is very difficult to employ any structural changes. Therefore, the revamping of heat recovery is preferably not considered in those cases and the approach ends. Nevertheless, for the rest of the cases HEN retrofit is strongly suggested, as it may yield to a highly profitable improvement derived from energy targets gap reduction. Before proceeding to any HEN optimisation, the final optimal conditions found in the previous stage are fixed in the process. Next, the new ET, CC, GCC and pinch point are obtained. As mentioned in section 2.1.2, knowledge about pinch violations is a useful starting point for the HEN retrofit; thus, the identification of HE in a crossed position, coolers that are above the pinch, heaters that are below it and heat transference between process streams across the pinch is carried out. The HEN pinch and the pinching matches are also checked. During this analysis, structural features of the network subjected to change such as re-piping, re-sequencing, changing bypasses, adding or deleting heat exchangers are proposed. After these retrofit changes are proposed, the area cost is updated with the new area or the area added to existing heat exchangers, while piping costs are added to new heat exchanger equipment for re-piped units. Several different topologies can be obtained and, as the structure is not the same after these changes, iterative methods must be applied for the optimisation. A general view of HEN optimisation solutions can be obtained initially from the inspection methodology. Then, a more complete HEN optimisation is carried out with the MINLP and GA algorithms in sequence. The

MINLP solutions are generally simpler (i.e. less expensive) than solutions generated by GA, although they reach significantly less enhancement that the GA obtained. Finally, both algorithms may complement each other.

It is important to state that HENs retrofit is just one of further enhancement options which can be applied to further optimisation. Other energy recovery options such as site utility systems design (steam or electricity generation), or water systems can also be addressed along this last stage. Their treatements, in general, will be similar to the HEN´s optimisation previously detailed. However, the number of options available is considerably large and very specific for each case; hence, these are not included in this text.

Finally, the payback periods and the carbon taxation reduction achieved with the proposed retrofit design options can be estimated.

The payback period for general profit improvements is estimated as:

$$PP = \frac{ACC \bullet PLP}{(PI)} \qquad (3.23)$$

Where,

PP= Payback period [Y]; ACC = Annualized Capital Cost [MM£ /Y]; PLP = Project Life Period [Y]; PI = General Profit Improvements [MM£ /Y].

The payback period for energy improvements is calculated as:

$$PP = \frac{ACC \bullet PLP}{(EI + \mathrm{CO_2T})} \qquad (3.24)$$

Where,

PP= Payback period [Y]; ACC = Annualized Capital Cost [MM£ /Y]; PLP = Project Life Period [Y]; EI = Energy Improvements [MM£ /Y]; CO_2T= Annualized benefit from reduction in CO_2 emissions´tax [MM£ /Y].

Energy improvements are directly quantified from the reduction of energy requirements multiplied by the utility unit cost.

The carbon taxation reduction is derived mainly from the energy reduction in the process. CO_2 emissions are estimated with base on this energy reduction by using the EPA 42 factor for furnace combustion ((EPA), 2006), and the resulting mass flowrate is multiplied by the updated tax of carbon per unit of mass, which is derived from the estimated social cost of carbon (SCC) for 2005 of USD $ 43 / tC, and from the consideration that one tC is roughly equivalent to 4 tCO_2, (Klein and Parry, 2007).

10.75 $USD per ton of CO_2 ($SCCO_2$)

CO_2 emission factors based on EPA-42 ((EPA), 2006) for the specific equipment involved in the emission, and its efficiency are used.

$$CO_2T = \frac{HUR \bullet EPA42\ factor \bullet \eta \bullet SCCO_2}{ExR} \qquad (3.25)$$

where

CO_2T= Annualized benefit from reduction in CO_2 emissions´tax [MM£ /Y]; HUR = Hot Utility Reduction [MMBtu/Y]; EPA42 factor = EPA-42 emissions´factor [MMTon CO_2/MMBtu]; η = Equipment efficiency [Addimensional]; $SCCO_2$ = Estimated Social Cost of CO_2 [$USD/Ton CO_2]. ExR = Exchange rate average of equivalent $USD to 1 GBP (£).

The results integration in the Retrofit Design Approach is executed by generating the final retrofit portfolio, which includes all the correspondent cost-effective changes proposed with improvements, capital costs, CO_2 tax reductions and payback periods. This portfolio is an important decision making tool delivered to the management team in the company as the final product of the Retrofit Design Approach.

3.3 Concluding remarks

A systematic approach to address the retrofit problem in the industry has been presented in this chapter. The principal advantages of the Retrofit Design Approach are as follows: it has the capacity to handle a large production plant, with less computational load, it is accessible to most of the unit employees due to its tools integration feature, the RSM results in a reduced model function of the most important factors which affect the process, the reduced model is capable of representing the optimisation response with a high confidence level. This simplifies the pathway to achieve pseudo optimal solutions. The effects of the most important factors towards the studied response can be quantified and, as a consequence, the system can be understood.

Finally, the time taken to perform the approach can be high during the first and second steps due to the large number of simulations generated, but this is offset by the considerable reduction of the optimisation time of the model derived from RSM.

Besides the limitations found, Retrofit Design Approach is considered a suitable approach to address the retrofit problem under the industrial scope, and consequently to test its applicability. In the next chapters the proposed approach will be tested in gas processing plants.

Chapter 4. Case Study I

In this chapter, the proposed design method described in the previous chapter is applied to the retrofit of natural gas liquid (NGL) recovery plant.

The first part describes the existing NGL process, as well as operating data and relevant specifications. Economic data used in the calculation of capital and operating costs including utilities, raw materials, products and co-products, are also given. The second part details the development of the simulation model and its validation. The assumptions considered are listed and the optimisation objective function is defined. The third section addresses the retrofit problem by executing the proposed Retrofit Design Approach. Finally, key findings and results obtained from the proposed approach are discussed.

4.1 Natural Gas Liquids (NGL) recovery process

4.1.1 Process description

NGL recovery is the process of extracting hydrocarbon liquids associated with natural gas coming from wells. The pre-purified natural gas stream is separated further, mainly into natural gas and associated liquids. Either ethane or propane is recovered, depending on their purposes, and the extraction of these products is generally based on low temperature separation, using external refrigeration, turbo expansion, Joule-Thompson expansion, absorption or a combination of these. During the early 1960s and until the 70s, lean-oil absorption processes were commonly applied with a low recovery of up to 40% ethane from the feed gas. Nowadays, the NGL procedure most commonly used is based on the turbo-expander process, and a number of these have been designed and evolved by companies, such as Ortloff Engineers Ltd. (John D. Wilkinson, 1998).

The Gas Subcooled Process (GSP), OverHead Recycle Process (OHR), Cold Residue Reflux process (CRR), Recycle Split-Vapor process (RSV) and Recycle Split-Vapor with Enrichment process (RSVE) are the processes most used under the ethane recovery mode. The Split-Flow Reflux process (SFR), Improved Overhead Recycle process (IOR) and

the Cascade Overhead REcycle (CORE) have been developed to offer better efficiency under propane recovery mode (John D. Wilkinson, 1998).

The case study in this research is directed at improving the economics and efficiency of the process for the recovery of natural gas liquids. The currently-operating unit is known as Cryogenic 1, and is a modified process from the original designed by Ortloff Engineers Ltd., which itself was adapted by the Mexican Institute of Petroleum (IMP) and rebuilt in 1997. Its owner is the gas and basic petrochemicals division (PGPB) of the company Petroleos Mexicanos (PEMEX). Its principal purpose is to separate sweetened gas (SG) into useful, saleable residue gas (RG) and cryogenic liquids (C_2+) products. The gas separation process uses high levels of cooling through the system, as well as successive auxiliary expansion to liquefy the feed SG stream and then separate the components by distillation in a demethanizer column.

Maximum design capacity is 173 kg/s of feed, with a design recovery efficiency of 75 % for the ethane (C_2) and 99 % for the propane (C_3). It is important to mention that, currently, the ethane separated in this plant is re-injected back into the residue gas stream in a subsequent plant due to transport limitations. Hence, although ethane's recovery is low at present, it will need to be increased due to future projects. This plant is one of the major energy consumers in the whole site[1] (30% on average). Figure 4.1 provides a schematic illustration of the general NGL process. It is divided into six sections: 1) pre-cooling; 2) dehydration; 3) cooling and expansion; 4) demethanization; 5) residue gas recompression; and 6) coolant cycle. The main plant equipment includes six flash drums, twenty three heat exchangers, two turbo-expanders, two Joule-Thompson valves, one simple distillation column with no condenser, three compressors, one gas dehydration and regeneration unit, and one furnace in the system.

[1] Gas Processing Centre: Cactus Chiapas, Mexico. PEMEX Gas y Petroquimica Basica.

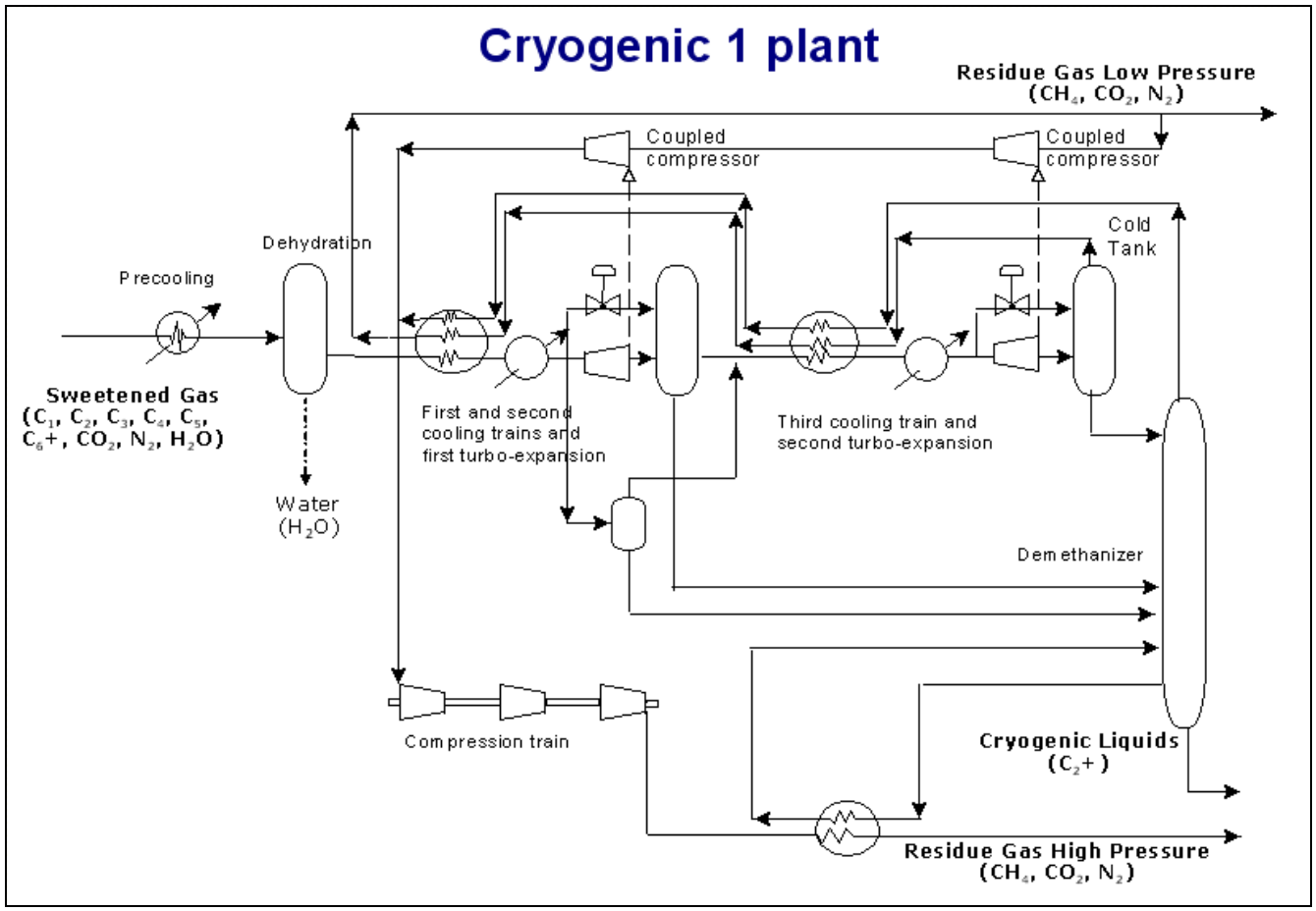

Figure 4.1 NGL process.

The inlet SG, treated in a previous process, enters at 65 Kg/cm^2 and 43 °C and is then fed to a first pre-cooling heat exchanger with cooling water, where the gas temperature is reduced to 35°C. The outlet gas flows then to a series of dehydrating columns, which reduce the humidity of the feed gas SG stream to less than 0.1 ppm.

Following this stage, the dried gas is fed first to a cooling train consisted of a series of four gas-to-gas and two gas-to-propane refrigerant heat exchangers, which are required for chilling the feed gas in the unit to about -10 °C. From this first cooling train a liquid stream is extracted and sent to a first separator tank, which sends the liquid to stage number 18 in the demethanizer column and its vapours to join the vapours outlet from the separator tank following the first turbo-expander. The process continues with a second cooling train with a series of two gas-to-gas and two gas-to-propane refrigerant heat exchangers, which chill the feed gas to about -37 °C. Next, a first turbo-expander expands the gas from 60 to ~37 kg/cm^2, followed by a separator tank from which a feeding stream to stage number 8 of the distillation column is obtained. A Joule-Thompson valve is set in parallel to the first turbo-expander to bypass the gas going through in case of failure. The outlet gas stream of this tank is joined with the first tank's vapours and sent to the third cooling train formed by two gas-to-gas heat exchangers placed to chill the feed gas to about -69 °C. The gas is then sent to the second turbo-expander to reduce its pressure from 35 to 20 kg/cm^2 approximately. A Joule-Thompson valve is set in parallel to this turbo-expander to bypass the gas going through in case of failure. The outlet stream goes to the final separator tank, which is also known as the "cold tank" because its pressure of about 20 kg/cm^2 and temperature of -89 °C make it the coldest point in the system. The top vapours of this cold tank are sent back to cool a part of the inlet stream and then to the fuel gas network as residue gas low pressure (RGLP). Part of this stream is sent through the coupled compressors with the expanders towards the high-pressure compression section. The cold tank liquid stream is pumped to the first stage of the demethanization column. The column normally operates at 25 kg/cm^2 and a temperature of -79 °C in the top. It is divided into two sections with different diameters, in which the number of stages in each is 17 and 13. Bottom demethanizer products – cryogenic liquids (C_2+) – are sent to final customers. The demethanizer has a reboiler which uses a low-pressure steam to provide the duty, but does not have a condenser. The reflux ratio to the column is controlled by the top inlet liquid stream coming from the cold tank; the overhead vapours produced in it, mainly methane (i.e. 93.5% mol CH_4), flow back to the first and second

turbo-expanders to a series of gas-to-gas heat exchangers, where it provides a heat exchange process to cool the inlet gas stream down. Following this stage, the gas is compressed by high pressure steam turbines to the desired pipeline pressure set by the final customers (i.e. 70 kg/cm^2), and is known as residue gas high pressure (RGHP). As the final pressure is high, its associated temperature is also high (i.e. 113 ^{o}C); thus, it is heat-integrated with the demethanizer column bottoms, which supply a part of the total duty requested by the column to perform the separation, while the complementing duty is given by the reboiler.

4.1.2 Process data and specifications

Table 4.1 presents the feed conditions, including flowrate and composition. Additionally, the key recoveries for methane and ethane are given, and in Table 4.2 the NGL recovery unit products specifications shown. Complementary information on the plant is given in the Appendix as Table A.1, which lists pressure, temperature and mass flow rate in normal operating conditions for the main pieces of equipment in the plant. Table A.2 lists the capacities and maximum and minimum operational parameters in the plant.

Components	Molar Fraction
N_2	0.0507
CO_2	0.0001
C_1	0.7742
C_2	0.1000
C_3	0.0438
NC_4	0.0143
IC_4	0.0065
NC_5	0.0042
IC_5	0.0039
C_6+	0.0021
H_2O	0
Flowrate, kg/s	149.27
Flowrate, m^3/s	170.26
T, ^{o}C	45.5
P, kg/cm^2	64.8
Propane Recovery, %	99.3
Ethane Recovery, %	65

Table 4.1 Feed stream and key recoveries in the Cryogenic 1 plant.

Product	Parameter	Unit	Limits
Cryogenic Liquids (C_2+)	**Methane content**	**% Vol**	**$\leq$ 0.8**
Residual Gas High Pressure	**Propane content**	**% mole**	**$\leq$ 0.2**
	CO_2 + N_2 content	**% Vol**	**1.4 - 3**
	Humidity	**ppm**	**$\leq$ 112**
	Total Sulfur	**ppm**	**$\leq$ 200**
	H_2S	**ppm**	**$\leq$ 4.4**
	Calorific Value	**kJ/m^3**	**$\geq$ 35,443**
	Oulet Pressure	**Kg/cm^2**	**66.792 $\pm$ 0.2**
Residual Gas Low Pressure	**Humidity**	**ppm**	**$\leq$ 112**
	H_2S	**ppm**	**$\leq$ 4.4**

Table 4.2 Product specification in the Cryogenic 1 plant.

4.1.3 Economic considerations

In order to estimate the annualised capital cost of the equipment required in the retrofit design, a ten-year project life with a 12 % interest rate is assumed.

A relevant consideration in this part concerns the profit used for this study. For the purpose of reflecting in the financial statements of the company with the same order of magnitude, it is preferred that the profit used for the plant should be referenced with the profit for the best case historically registered. This is the marginal profit defined in equation 3.18 and normalised in 3.19 in which the net profit of equation 3.17 (NPr) considers: three products (residue gas low pressure, residue gas high pressure and C_2+), three by-products (low pressure steam, medium pressure steam and condensates), one raw material (Sweetened Gas), three types of energy are used (high pressure steam, cooling water, electricity) and one penalty due to nitrogen content.

The equation 3.17 can be then expressed as:

$$NPr = S_P + S_{CO} - VC_{RM} - VC_E + N_2Pe \qquad (4.1)$$

where

NPr = Net profit [£ /Y]; S_P = Profit from the sales of product excluding RGHP sells

[£ /Y]; S_{CO} = Profit from the sales of co-product [£ /Y]; VC_{RM} = Variable cost of raw material [£ /Y]; VC_E = Variable cost of energy [£ /Y]; N_2Pe = Nitrogen Penalty [£ /Y].

with:

$$N_2Pe = S_{RGHP} * \left(\frac{GCV_{RGHP}}{GCV_{RGHP@5\%N_2}} \right) \quad (4.2)$$

where

S_{RGHP}=Sells of RGHP [£ /Y]; GCV_{RGHP}=Gross calorific value of RGHP at studied conditions [KJ /kg]; $GCV_{RGHP@5\%N2}$=Gross calorific value of RGHP at inlet content of 5% mole of nitrogen [KJ /kg].

This term estimates the penalty to the NPr related to the level of nitrogen content in the feed. It is considered to reflect the reduction of the gross calorific value (GCV) for the final RGHP, the selling price of which is based on its caloric value. The penalty is determined as the ratio between the GCV of the RGHP at the studied % mole of inlet nitrogen and that of the RGHP product with a 5% mole of inlet nitrogen (base case).

NPr, N_2Pe, MaPr, and MaPr* were calculated in units of Mexican Pesos (MXN) / day. These were further converted to GBP (£) using the exchange rate average of 20 MXN for 1 GBP.

Therefore, the objective function used in this study is defined based on maximization of the annualized MaPr. The number of annual working days for the plant is assumed to be 350 per year, as maintenance period is 30 days for every 2 years. Utilities with its available temperature and cost are shown in Table 4.3. The prices per unit of the individual raw-material and products are given in Table 4.4. These costs are based on the average cost of 2008.

The capital cost for the new equipment in this case study was considered the Free On Board (FOB) investment cost plus piping costs and associated arrangements, which is assumed to be 40% of the equipment cost.

Hot utilities	Available temperature, ℃	Cost, £/kW^{-1}.y^{-1}
Fuel Gas		**120**
High pressure steam	**450**	**379**
Medium pressure steam	**360**	**358**
Low pressure steam	**180**	**242**
Hot water	**90**	**33**
Cold utilities		
Cooling water	**25**	**25**
Propane	**-45**	**472**
Power		
Electricity		**300**

Table 4.3 Available utilities for Cryogenic 1 plant.

Component	Type	Unit Cost
Sweetened Gas (SG)	**Raw Material Gas phase**	**0.134, £/m^3**
Cryogenic Liquids (C_2+)	**Product Liquid phase**	**83.6, £/m^3**
Residual Gas(RG)	**Product Gas phase**	**0.109, £/m^3**

Table 4.4 Raw material and products' unit costs for Cryogenic 1 plant.

4.2 Process simulation

4.2.1 Simulation model

The simulation of the plant was performed in the Aspen Plus simulator 2006.5 SM (steady-state). The Peng-Robinson-Soave (PRS) equation of state was set for the calculation of thermodynamic properties. The standard modules available in the Aspen Plus library were used in the simulation, except the dehydration unit. However, to avoid hydrate formation problems in the system, the assumption of having the inlet stream water content at 0.1 ppm was always kept. This is supported by the hydration problems seldom registered in historical data during the last three years.

A number of assumptions made, based on the normal operating strategy of the plant, are as follows:

Modelling Assumptions

1. The propane coolant duty provided is not restricted.
2. To reduce the burden of the simulation flowsheet and thus the convergence time, the propane coolant loop is not represented explicitly in the flowsheet. However, its duty and power are estimated in the MaPr based on the duty requirements for refrigeration.
3. A coefficient of performance (COP) of 1.4 is estimated based on the plant's average temperatures for the evaporator of -45 ℃ (T_{EVAP}=228 ℉) and for the condenser of 50 ℃ (T_{COND}=323 ℉) in the refrigeration cycle (Smith, 2005):

$$COP = \frac{0.6 \bullet T_{EVAP}}{T_{COND} - T_{EVAP}} \tag{4.3}$$

4. Because of the assumption related to dehydrating system, the amount of fuel gas burned in the furnace was held constant.

4.2.2 Base-case simulation and validation

The base-case was simulated with average production data for 2008 – the inlet stream in Table 4.1 showed an average of 149.27 kg/s of SG processed from the current plant. The parameters used for the base-case simulation are given in Table 4.5. Table 4.6 presents the conditions and compositions of the outlet methane-rich product RG, both high-pressure and low-pressure, and C_2+ rich product streams at the base-case. The C_3+ recovery obtained in the unit is also shown in Table 4.6, while the difference (%Diff.) between the operating data (OD) and simulated results (SM) is estimated for each stream as:

$$\%Diff. = \left[\frac{(SM - OD)}{OD} \right] \bullet 100 \tag{4.4}$$

Equipment	Input parameters	Value	Output variables	Value
1st train propane coolers	Pressure, Kg/cm²	62	Refrigeration duty, MW	8.0
	Temperature, ºC	-6.6		
2nd train propane coolers	Pressure, Kg/cm²	61	Refrigeration duty, MW	9.3
	Temperature, ºC	-33.8		
1st Turboexpander	Discharge pressure, Kg/cm²	34.3	Power, MW	2.4
	Isoentropic efficiency	0.85	Outlet Temperature, ºC	-65
Tank from 1st turboexpander	Pressure, Kg/cm²	34.3	Vapour fraction	0.80
	Temperature, ºC	-65		
2nd Turboexpander	Discharge pressure, Kg/cm²	15.3	Power, MW	2.9
	Isoentropic efficiency	0.85	Outlet Temperature, ºC	-106
Cold Tank from 2nd turboexpander	Pressure, Kg/cm²	15.3	Vapour fraction	0.92
	Temperature, ºC	-106		
Demethanizer column	Top Pressure, Kg/cm²	22.4	Reflux Ratio (external)	0.3
	Number of stages	31	Top Temperature, ºC	-93.8
	Condenser	None	Bottom Pressure, Kg/cm²	21.7
	Boilup ratio	0.39	Bottom Temperature, ºC	22.3
	Murphree stages efficiency	0.58	Reboiler duty, MW	4.9
High pressure compressors	Discharge pressure, Kg/cm²	67	Power, MW	17.4
	Isoentropic efficiency	0.85	Outlet Temperature, ºC	90

Table 4.5 Main parameters in the Cryogenic I used for the base-case simulation.

The major operating cost of the plant comprises raw material (i.e. SG) and energy costs. From Table 4.5, the largest energy cost is related to high-pressure compressors, which are driven by shaft power generated from central utility systems requiring high-pressure steam (HPS @ P=100 kg/cm^2). Medium-pressure steam (MPS @ 43 kg/cm^2) is extracted from the turbines used to run both the compressors for refrigeration (the second largest

energy consumers) and the lubricant oil pumps. Note that, as stated in the modelling assumptions, the MPS used by the refrigeration compressors is estimated from the refrigeration duty needed. The unused MPS is exported as a co-product in the plant. Low-pressure steam (LPS @ 4.5 kg/cm^2) is extracted from the back pressure turbines coupled to the refrigeration compressors, which is then used in the demethanizer column reboiler and some ejectors, while a remaining amount of unused LPS and steam condensates are exported as co-products. Therefore, the more efficient this energy chain transformation, the higher amount of steam can be exported as co-products and a higher MaPr obtained.

Streams	Residue Gas High Pressure			Residue Gas Low Pressure			C_2+		
Molar Fraction	OD	SM	% Diff.	OD	SM	% Diff.	OD	SM	% Diff.
N_2	0.0586	0.0590	0.7	0.0737	0.0740	0.4	0	0	0
CO_2	0	0	0	0	0	0	0	0	0
C_1	0.9161	0.9186	0.3	0.9026	0.9037	0.1	0.0008	0.0008	0
C_2	0.0248	0.0220	-11	0.0228	0.0215	-6	0.4440	0.4457	0.4
C_3	0.0005	0.0004	-20	0.0009	0.0008	-10	0.2661	0.2658	-0.1
NC_4	0	0	0	0	0	0	0.1081	0.1077	-0.4
IC_4	0	0	0	0	0	0	0.0544	0.0539	-1
NC_5	0	0	0	0	0	0	0.0401	0.0399	-0.5
IC_5	0	0	0	0	0	0	0.0370	0.0370	0
C_6+	0	0	0	0	0	0	0.0495	0.0492	-1
H_2O	0	0	0	0	0	0	0	0	0
Rate, kg/s	92.0	92.2	0.2	10.2	10.2	0	47.0	46.9	-0.2
T, ºC	43.3	43.3	0	30.5	30.5	0	22.3	22.3	0
P, Kg/cm²	71.3	71.3	0	18.2	18.2	0	22.7	22.7	0
C_3+ Recovery, %							99.3	99.6	0.3

OD=Operating Data; SM = Simulation results

Table 4.6 Base case simulation: operating data vs. simulation results.
Operating data used is based on August 2008 when feed contains 5% mole nitrogen.

From Table 4.6, it can be observed that the simulation results show a good level of agreement with real operating data. On average, the higher deviations in compositions

found were -20% and -11% for C_3 and C_2 respectively in the residue gas high pressure; nevertheless, these deviations were not serious due to very low compositions. For the residue gas low pressure, the highest was -10% in C_3, but this is only trace component in that stream, and for the C_2+ stream of -1% in both iC_4 and C_6+ respectively. The C_3+ recovery yielded close results.

An additional Excel spreadsheet calculator was built in Aspen Plus. Note that it is not a direct part of the proposed approach, but can give the model the chance in the future to consider environmental emissions estimated from the simulation results. The emissions to air are estimated roughly by using the correlation factors stated in EPA AP-42 ((EPA), 2006) for uncontrolled furnaces with fuel gas and duty less than 100 MMBtu/hr. The general equations used to estimate the indexes are described as:

$$AirE_i = F_i \bullet Fr_{FG} \bullet GCV_{FG} \qquad (4.5)$$

Where

$AirE_i$=Air emission of i [Tonnes i /kt HC]; i includes SO_2, NOx, CO_2, and VOC; Fi= Factor in EPA 42 for compound i [(Tonnes i*s) / (kt HC*kJ)]; Fr_{FG}=Flowrate of fuel gas [kg/s]; GCV_{FG}= Gross calorific value of fuel gas [kJ/kg].

$$SEC = \frac{TEC}{Fr_{SGP}} \qquad (4.6)$$

where

SEC=Specific energy consumption [GJ/Tonne HC processed]; TEC=Total energy consumption which includes the energy in $(Electricity + FuelGas + Steam)$ [GJ/Y]; Fr_{SGP}=Flowrate of sweetened gas processed [Tonne HC processed/Y];

Table 4.7 presents these indexes, and the factors used for each emission are also listed Table 4.7. Water discharges and waste indexes cannot be estimated up to this level. Nevertheless, the fields in the environmental calculator are left in order that in future the cooling water data from laboratory and the waste data can be introduced in the calculator and those indexes can be broadly estimated as well. The European Integrated Pollution Prevention and Control Bureau ((EIPPCB), 2003) ranges proposed for these indexes and

the Mexican Law regulated limits (MexicanGovernment, 2007) are also presented as a reference.

Emission	EPA42 emission factor	EIPPCB	MX Law[1]	Cryogenic 1 unit simulation
SO_2 (Tonnes SO_2 / Mt HC)	0.0006	30-6,000	50	0
NOx (Tonnes NOx / Mt HC processed)	0.09804	60-500	190	0.979
CO_2 (Tonnes CO_2 / Tonne HC processed)	117.6471	0.02-0.82	N/A	0.001
VOC (Tonnes VOCs / Mt HC processed)	0.0054	50-6,000	N/A	44.244
T range (ºC)	Direct from laboratory	10-35	40	N/A
Oil (mg/l)	Direct from laboratory	0.05-9.8	15	N/A
BOD5 (mg/l)	Direct from laboratory	2-50	30	N/A
Suspended Solids (mg/l)	Direct from laboratory	2-80	40	N/A
Total nitrogen (mg/l)	Direct from laboratory	1.5-100	15	N/A
Lead (mg/l)	Direct from laboratory	0.2-0.5	0.2	N/A
Waste, (Tonnes Waste Generated / Mt HC processed)	Direct data	133 - 4,200	N/A	N/A
SEC, (GJ / Tonne HC processed)	Not needed in equation 4.8	1-4	N/A	1.066

1 NOM-001-SEMARNAT-1996

Table 4.7 Environmental indexes estimated for the Cryogenic I plant (Year 2008).

4.3 Application of Retrofit Design Approach

4.3.1 Diagnosis stage

The diagnosis stage was applied to identify potential variables which can be adjusted or modified for improving cost-effectiveness of the process. The existing designs for heat

recovery systems are highly integrated and, consequently, make it very difficult to employ any structural changes. Therefore, a revamping of heat recovery is not considered in this case study.

It is important to note that the case study in Chapter 5 includes the heat recovery study. The first part (a) of the diagnosis stage explores the impact of all the controllable variables of the plant within the allowable range.

Selection of key design variables: The impact of the independent variables existing in the distributed control system (DCS) of the plant is first explored. These comprise the initial parameters which are listed below. The nitrogen component in the inlet gas varies due to upstream adjustments; therefore, this factor is added to the initial list. The normal operating condition ranges for each one of these variables is shown in Table A.1 of the Appendix section.

The list of initial parameters is:

1. First cooler temperature at outlet
2. First separation tank temperature at outlet
3. First furnace temperature
4. Heat exchanger 1 (process/process) temperature at outlet
5. Heat exchanger 2 (process/process) temperature at outlet
6. Heat exchanger 3 (process/process) temperature at outlet
7. Heat exchanger 4 (process/process) temperature at outlet
8. First chiller temperature at outlet
9. Second chiller temperature at outlet
10. Second separation tank pressure
11. Third chiller temperature at outlet
12. Fourth chiller temperature at outlet
13. Heat exchanger 5 (process/process) temperature at outlet
14. Heat exchanger 6 (process/process) temperature at outlet
15. Third separation tank pressure
16. Fourth separation tank pressure
17. 1st turboexpander discharge pressure
18. Fifth separation tank pressure
19. Heat exchanger 7 (process/process) temperature at outlet

20. Heat exchanger 8 (process/process) temperature at outlet
21. Sixt separation tank pressure
22. 2nd Turboexpander discharge pressure
23. Seventh separation tank pressure
24. Demethanizer column pressure in top
25. High Pressure Compressors discharge pressure

To gain knowledge of the process at this first diagnosis stage, and thus to eliminate the parameters that are highly unlikely to account for an improvement in MaPr, the impact of the listed parameters was assessed by the sensitivity analysis described in section 3.2.2. The perturbances applied to the variables ranged from the low to high safe operational limits. Table A.2 of the Appendix presents these limits for selected variables. As there was a single response (MaPr) for this case, just the first criterion of the sensitivity analysis of the propossed Retrofit Design Approach for this diagnosis stage was applied to select the promising variables. Moreover, as the effects in the response were seen to be extremely low, the minimum increase in MaPr was set at 0.01 (i.e. any parameter that yielded to an increase in MaPr was selected). The analysis produced three final parameters and the inlet nitrogen composition, which are detailed below. The rest of the initial list showed either a null or negative improvement in MaPr. It should be noted that the inlet nitrogen content yielded a very negative effect on MaPr, and due to its high magnitude, variability and non-controllability, it was carefully considered it in the study. These parameters and the inlet nitrogen composition are detailed below.

Figures 4.2, 4.3 and 4.4 present the behaviour of the MaPr response obtained as a deviation from the base-case simulation of MaPr as follows:

$$EffectOnMa\ \Pr = \left[\frac{Ma\ \Pr_S - Ma\ \Pr_{BC}}{Ma\ \Pr_{BC}} \right] \bullet 100 \qquad (4.7)$$

Where

EffectOnMaPr=Variation in the marginal profit from the base case [%]; $MaPr_S$=Marginal profit estimated of the simulated case [£/Y]; $MaPr_{BC}$=Marginal profit of base case [£/Y];

versus the parameters: demethanizer column operating pressure (kg/cm^2), power recovery from the second natural gas turbo-expander (kW) and power recovery from the first natural gas turbo-expander (kW), presented as a deviation from the value of each corresponding parameter in the base-case simulation, respectively, as:

$$PV = \left[\frac{PV_S - PV_{BC}}{PV_{BC}} \right] \bullet 100 \qquad (4.8)$$

Where

PV= Variation in the value of the parameter from the base case [%]; PV_S=Parameter value in the simulated case [kg/cm^2, kW, and kW respectively]; PV_{BC}=Parameter value in the base case [kg/cm^2, kW, and kW respectively].

Figure 4.5 presents effect on MaPr due to the inlet nitrogen content (N_2).

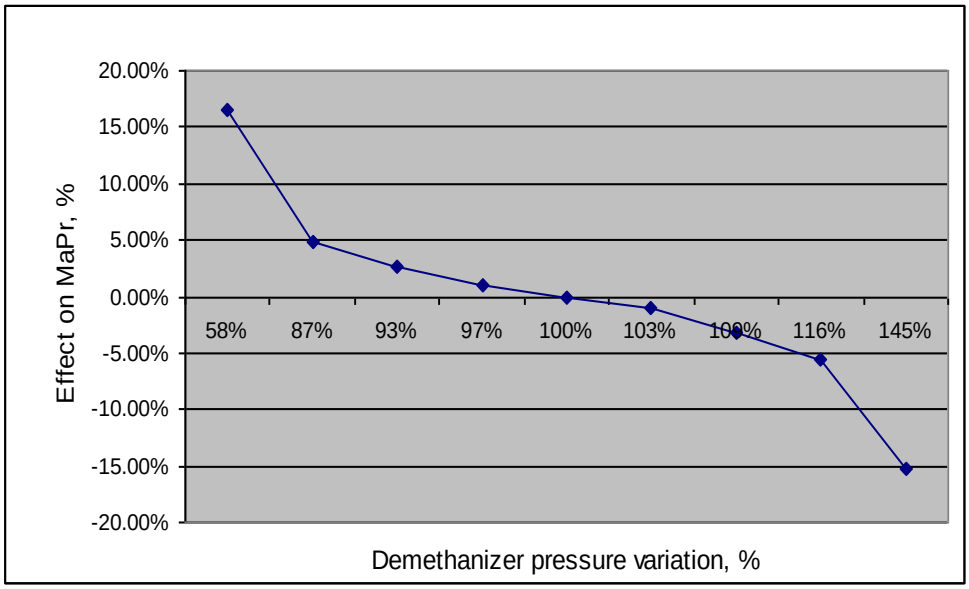

Figure 4.2 Effect of demethanizer pressure on the MaPr response.

As seen in Figure 4.2, the influence of demethanizer pressure on MaPr occurs when the column pressure is decreased, in which case the MaPr response value increases considerably. To understand this, the mean relative volatility C_2/C_3 (α) in the demethanizer is plotted versus the demethanizer pressure variation in Figure 4.6 and it will be reviewed later on this text.

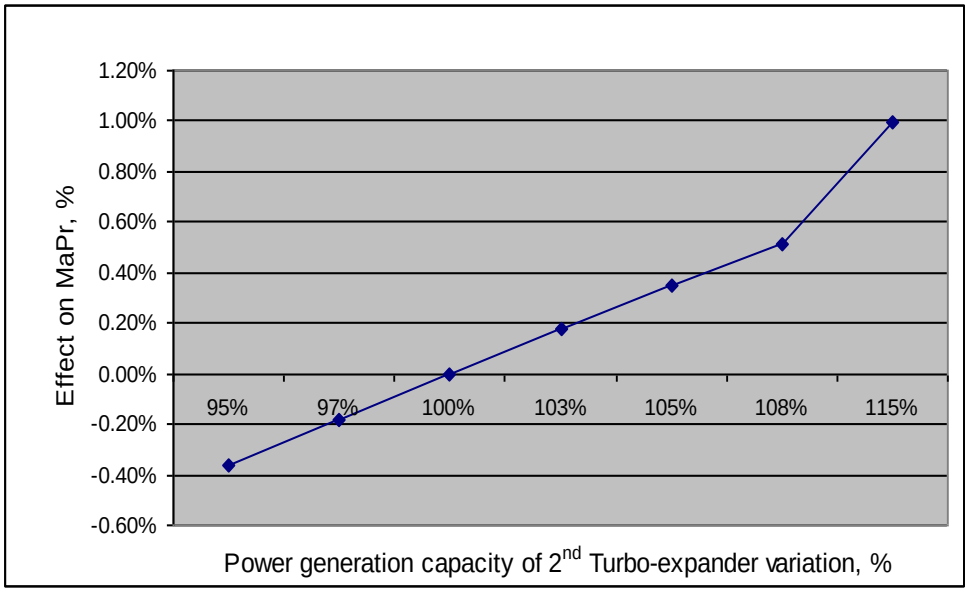

Figure 4.3 Effect of power generation capacity of 2nd turbo-expander on the MaPr response.

As shown in Figure 4.3, the objective function increases against the increasing power generation capacity of the second turbo-expander (>100%). From this point and beyond, it has a positive slope that increases by up to 115% of power generation capacity, which is the upper limiting value for this first sensitivity analysis.

From Figure 4.1, it can be observed that the outlet of the second turbo-expander is the cold tank, both the second and first turbo-expanders each have a coupled compressor and the coupled compressor of the second turbo-expander sends the RG product to the coupled compressor of the first turbo-expander, from where the RG is sent to the high pressure compressors in the unit. Based on this connectivity for the second turbo-expander, the effect seen in Figure 4.3 when increasing its power generation capacity occurs because of two facts. First, the outlet pressure in the expander is decreased, which increases the liquid recovered in the cold tank and sent to the demethanizer. The total liquid recovery in the plant is then increased and, as the price for C_2+ is higher than for the HPRG, the MaPr is improved. Second, the shaftwork provided by the second turbo-expander to its coupled compressor is increased and adds extra compression to the RG stream, which reduces the high-pressure steam consumed in the RG high-pressure compressors. As a result of both effects, the MaPr value is increased.

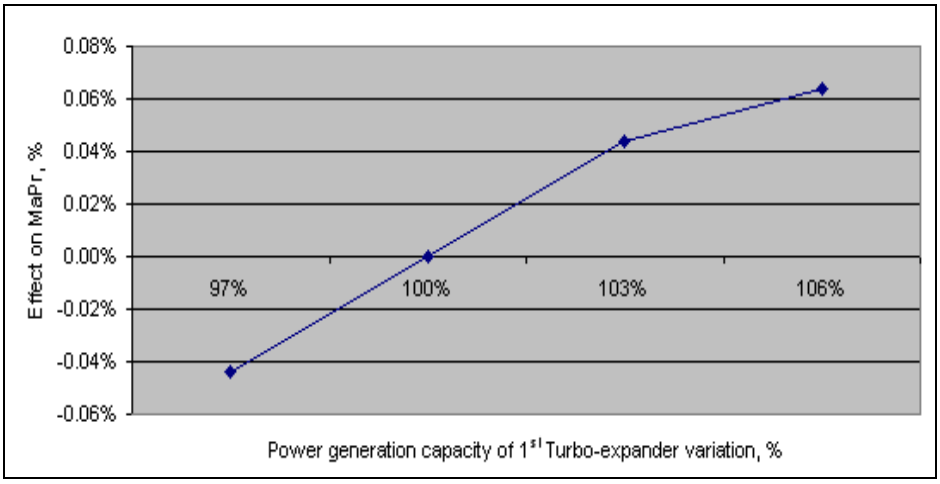

Figure 4.4 Effect of and power generation capacity of first turbo-expander on the MaPr response.

Figure 4.4 illustrates the relationship between the objective function and the power generation capacity of the first turbo-expander. This behaviour is similar to the previously explained second turbo-expander in that the MaPr response value rises from 100%, and continues increasing while the turbo-expander capacity increases. Thus, the reasons for this occurring are the higher shaftwork provided to its coupled compressor and the increase in liquid recovery, yielding increases in MaPr.

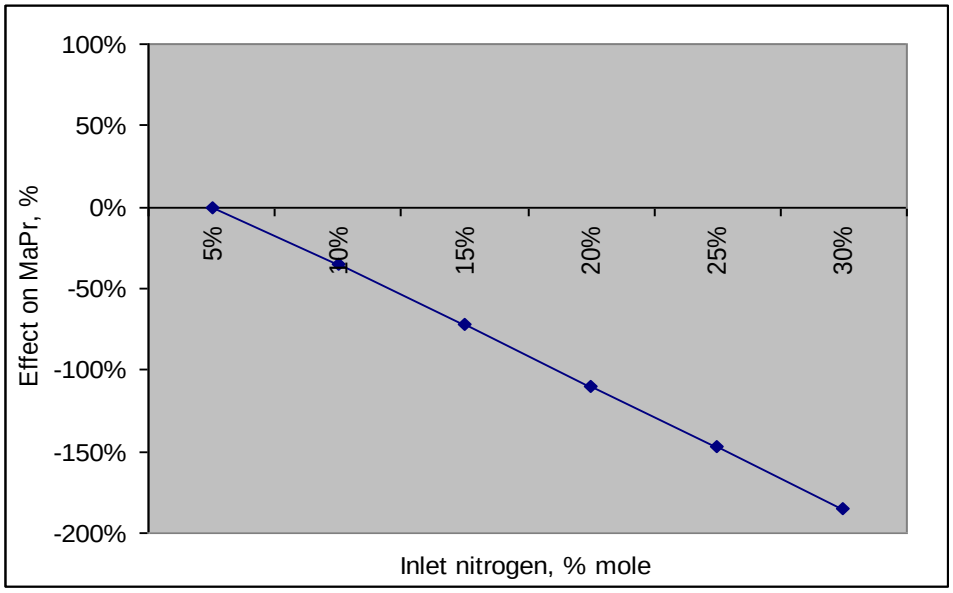

Figure 4.5 Inlet content nitrogen effect on the MaPr response.

Figure 4.5 shows that the nitrogen presence in the inlet SG reduces the MaPr achieved. To understand this effect, the properties of nitrogen are presented and compared with methane properties in Table 4.8.

Property	Nitrogen	Methane
Molecular weight, $g.mol^{-1}$	14.0067	16.042
Boiling point, °C	-195.8	-161.6
Gas density (1.03 kg/cm^2 and 15 °C), kg/m^3	1.185	0.68
Specific heat capacity at constant pressure (C_p), $J \cdot mol^{-1} \cdot K^{-1}$	29.124	35.0
Specific heat capacity at constant pressure (C_v), $J \cdot mol^{-1} \cdot K^{-1}$	0.020	0.027
Latent heat of vapourisation, $kJ \cdot mol^{-1}$	5.56	8.18

Table 4.8 Nitrogen properties compared with methane properties.

It can be observed from Table 4.8 that nitrogen and methane have similar molecular weights. On the other hand, nitrogen is denser than methane which means that for a stream with these two components and with the same mass, if this is richer in nitrogen it will occupy less volume than if this is richer in methane. The boiling point reflects nitrogen to be more volatile than methane. The latent heat of vapourisation and the specific heat capacity for nitrogen (C_p) are also lower than for methane.

All of these properties besides the N_2Pe set in equation 4.2 with respect to the reduction of the GCV in the final product RG, make nitrogen presence in the system (from 5 to 30% N_2) to have effects on MaPr response.

Effects that decrease the MaPr response:

1) As the nitrogen composition is increased in the inlet stream, the inert gas reduces the GCV of the RG product, this is reflected in the penalty (N_2Pe) estimated by equation 4.2 which reduces the MaPr.

2) As the nitrogen composition is increased in the system, the inert gas makes the amount of C_2+ to be reduced, thus the total liquid produced (C_2+) is decreased with respect to the base case causing a reduction in MaPr.

Effects that increase the MaPr response:

1) As the C_2+ inlet to the plant is reduced due to the increasing nitrogen content, which is noticeable in the increasing vapour fraction of the cold tank, this results in decreasing the total duty required by the reboiler, which means less low pressure steam

consumed.

2)) The significantly less total duty required by the reboiler reduce the temperatures profiles in the demethanizer; this increases the driving force temperature differences between the column top vapour and the inlet natural gas stream, and makes the heat integration in the system easier.

3) As inlet nitrogen is increased the total gas produced is heavier and its volume is decreased, which requires less power for compression.

Although these effects could increase the MaPr response, the negative effects are stronger than the positive yielding a reduction of MaPr when the nitrogen content is increased.

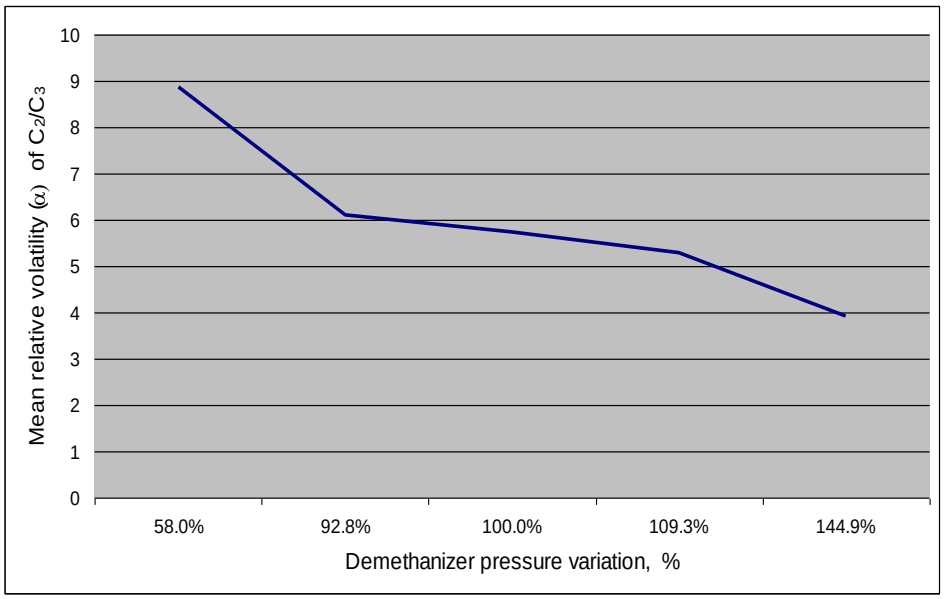

Figure 4.6 Effect of demethanizer pressure on the mean relative volatility C_2/C_3.

From Figure 4.6, it is clear that when the column operating pressure is decreased (demethanizer pressure variation < 100%), the mean relative volatility C_2/C_3 in the column increases, which makes fractionation easier and consequently decreases the reboiler duty in the column. On the other hand, the low pressure of the RG product from the top of the demethanizer requires extra compression power to be sent to the final customers, this fact increases the amount of HPS required in the RG high-pressure compressors. Hence, a trade-off exists when the pressure in the column is decreased. However, from Figure 4.2, the net result is that the MaPr is improved with lower demethanizer pressures.

Table 4.9 shows the results of the sensitivity analysis of all the initial list of parameters, its ranges studied, the maximum increase in MaPr obtained in that range, the parameter variation at which that occurred (best setting), and impact in C_3+ recovery and in high pression compressors power consumption. The nitrogen content is also presented in Table 4.9. Only the three first highlighted parameters plus the nitrogen content met the criteria of the sensitivity analysis and those were selected 9 as the promising continuous factors from this stage. Note that in the graphs the ranges were varied beyond +10% for some of those parameters, but due to safety reasons those were fixed at its lowest permited value.

Description	Unit	Range Disturbance	Best setting	Effect on MaPr, %	C_3+ recovery, %	High pressure compression power, %
Pressure in stage 1 of demethanizer	**Kg/cm²**	**-10 to +10%**	**-10%**	**2.6**	**0.06**	**-0.04**
Power generation capacity of second turboexpander	**MW**	**-5 to +15%**	**+15%**	**0.99**	**0.05**	**-3.45**
Power generation capacity of first turboexpander	**MW**	**-3 to +6%**	**+6%**	**0.06**	**0.03**	**-0.48**
% mole nitrogen	**% mole**	**5 to 30%**	**5% (base case)**	**0**	**0**	**0**
First cooler temperature at outlet	ºC	-10 to +10%	0%	0	0	0
2nd separation tank temperature at outlet	ºC	-10 to +10%	0%	0	0	0
3rd separation tank temperature at outlet	ºC	-10 to +10%	0%	0	0	0
4th separation tank temperature at outlet	ºC	-10 to +10%	0%	0	0	0
5th separation tank temperature at outlet	ºC	-10 to +10%	0%	0	0	0
6th separation tank temperature at outlet	ºC	-10 to +10%	0%	0	0	0
7th separation tank temperature at outlet	ºC	-10 to +10%	0%	0	0	0

N/A = Not Applicable

Table 4.9 Continuous factors in the Cryogenic I plant.

Continuation of Table 4.9:

Description	Unit	Range Disturbance	Best setting	Effect on MaPr, %	C_3+ recovery, %	High pressure compression power, %
First furnace temperature	ºC	-5 to +5%	0%	0	0	0
Heat exchanger 1 temperature at outlet	ºC	-10 to +10%	0%	0	0	0
Heat exchanger 2 temperature at outlet	ºC	-10 to +10%	0%	0	0	0
Heat exchanger 3 temperature at outlet	ºC	-10 to +10%	0%	0	0	0
Heat exchanger 4 temperature at outlet	ºC	-10 to +10%	0%	0	0	0
Heat exchanger 5 temperature at outlet	ºC	-10 to +10%	0%	0	0	0
Heat exchanger 6 temperature at outlet	ºC	-10 to +10%	0%	0	0	0
Heat exchanger 7 temperature at outlet	ºC	-10 to +10%	0%	0	0	0
Heat exchanger 8 temperature at outlet	ºC	-10 to +10%	0%	0	0	0
First chiller temperature at outlet	ºC	-5 to +5%	0%	0	0	0
Second chiller temperature at outlet	ºC	-5 to +5%	0%	0	0	0
Third chiller temperature at outlet	ºC	-5 to +5%	0%	0	0	0
Fourth chiller temperature at outlet	ºC	-5 to +5%	0%	0	0	0
High Pressure Compressors discharge pressure	Kg/cm²	-10 to +10%	0%	0	0	0

Table 4.9 Continuous factors in the Cryogenic I plant.

This first part of the diagnosis stage produced a first group of three parameters and the inlet nitrogen composition. The proposed approach continues then with the second part of the diagnosis stage, where the promising alternatives for operational changes or structural modifications based on process integration options are explored.

Conceptual understanding of retrofitting: The options for distillation columns reviewed

in section 2.1.1 were applied to the demethanizer, as there is only one column in the plant. The feasible options were:

1. Feed location: Changes to the position of the current inlet streams to the distillation column were considered.
2. The number of stages and their efficiency were also selected to determine whether there was a significant improvement, although high capital cost was implied.
3. Adding or adjusting pumparounds in the demethanizer: Although the existing designs for heat recovery systems are highly integrated and make it very difficult to employ any structural changes in the plant, two additional possible pumparounds to be set and one potential increase in the flow rate of the actual pumparound were identified. These would not be incurred in very complex structural changes and may feasibly be done if promising. The two feasible pumparounds could be placed to recover heat from the liquid outlet of second separator tank to the demethanizer and from the residue gas high pressure to the demethanizer.
4. Adding or adjusting power generation capacity in the turbo-expanders: The previous first part of the diagnosis stage identified that the power generation capacity of both turbo-expanders can improve the MaPr; therefore, the structural possibility of including two additional turbo-expanders was also tested for evaluation.

The specific options that did not apply to this case were the distillation arrangements together with the feed conditions and the heat integration of the plant. The distillation arrangements and feed condition changes were considered unrealistic because there are just two products in the column, which is placed at the last part of the separation process, and most of the separation work is done through refrigeration and turbo-expansion steps, consequently, the cost for these changes would be too high and there is limited space. Therefore, these structural changes were excluded in the plant. Regarding the heat integration of the plant, it was mentioned at the beginning of the diagnosis stage that for this case study the existing design of heat recovery systems was highly integrated, which would make it very difficult to employ any structural changes. As a consequence, revamping of heat recovery was not considered in this case study.

A good level of knowledge about the process was gained after performing the first part of the diagnosis stage, from which a first group of factors was generated. To identify the effects of the factors and interactions for the second part of the diagnosis stage, the previous four options could be set in a second group and be tested together with the first group. Hence, with the purpose of eliminating the unpromising options for improving the MaPr, the two groups of factors were directly transferred to the evaluation stage.

The initial group from the first part of the diagnosis stage were continuous parameters that have already been set a range of study, from which operational limits were used in the next evaluation stage. Of the four options comprising the second group, the ranges of study to be applied in the evaluation stage needed to be set at specific points, according to their nature (structure modifications).

Option 1 is the position of feed stages in the column. This parameter took the current feeding stages' position for the base-case (18, 8 and 6 stages), and was set at two stages above all inlets´ position in the demethanizer (16, 6 and 4 respectively). These changes were chosen randomly. The aim of this evaluation was to identify if there is any effect on changing the position of the feed stages. Hence, the positions changed to this point were irrelevant as long as the perturbation existed. Once the evaluation had been performed and if there was a considerable effect from this parameter, the sign and the magnitude of the effect would lead to the improvement.

Option 2 considered two parameters, namely the number of stages and their efficiency. The current number of stages is 30and this can be increased upto 48 stages (60% more). The efficiency had a value of 58% (Murphree efficiency) for the base-case and the upper limit was set at 63%, which is an efficiency currently offered by industries (Koch-Glitsch, 2010).

Option 3 had three implicit parameters. One is to increase pumparound flowrate – a continuous variable that for the base-case had a value of 4,536 kgmol/h. The low level was set at 50% of this value (2,268 kgmol/h), while the high level was set at 6,804 kgmol/h, a 150% of the base case value. This high value is approximately an 80% of what can be pumped through the existing heat exchanger, but is the maximum let by the column operation within hydraulic limits (e.g. dried tray) and product specifications. The

others are two additional pumparounds set at zero flowrates for the low level, as these additional pumparounds do not exist. For these pumparounds, the temperature profile in the column was matched with the operating temperature at the outlet from each one of the correspondent equipment (separator tanks and heat exchangers), and then leaving a minimum difference in temperature of 10°C. For the high level, maximum possible flowrates were estimated from the available liquid (holdup) in the stages from which they were extracted, starting from a minimum liquid flowrate and gradually increasing it until a value in which the column was not able to operate was reached (dried tray or out of specification product).

The first additional pumparound arrangement was set from stage 23 in the demethanizer to pre-heat the liquid stream at the outlet of the second separator tank, which is one of the inlet streams to the demethanizer. The flowrate range was between 0 and 4,536 kgmol/h. The last parameter in option 3 was another new pumparound from stage 28 of the demethanizer to cool the stream of RG at the outlet of the heat exchanger located following the high-pressure compressors, with maximum flowrate of 4,536 kgmol/h.

For the Option 4, the two parameters involved are the power generation capacity of the first and second turbo-expanders by either installing new ones in parallel, or by revamping the current ones, respectively.

From Figures 4.3 and 4.4, maximum allowable capacities for that extra power generation were 115% and 106% for the second and first turbo-expanders respectively. As the power generation capacity from each one was gradually increased, the outlet pressure of each turbo-expander was reduced, and an ascending trend of effect on MaPr was found. Therefore, the high levels set for the two parameters involved in option 4 were the double of the current capacity for each of the existing turbo-expanders, which were 2,466 kW for the first and 2,953 kW for the second. The final selection was made between the installation of two new turbo-expanders in parallel or increasing the current capacity as a revamp of the existing equipment. The parallel option was selected due to its easiness of maintenance and practical limitation associated with plant layout.

A single-response for MaPr was studied for this case. As a final result, the total factors transferred to the evaluation stage from the second part of the diagnosis stage were 8,

which added to the initial three parameters identified in the first part of the diagnosis stage and the inlet nitrogen composition yielded a total of 12 factors to be studied in the evaluation stage (X_i). Table 4.10 gives a short description for each factor.

Factor	Description
X_1	Pressure in stage 1 of demethanizer.
X_2	Power generation capacity of second turboexpander.
X_3	Power generation capacity of first turboexpander.
X_4	Nitrogen content at inlet stream.
X_5	Increasing the current amount of pumparound flowrate.
X_6	Adding one pumparound and one heat exchanger from stage number 23 in demethanizer to second separator tank liquid outlet.
X_7	Adding one pumparound from stage number 28 in demethanizer to the heat exchanger outlet of the high pressure compressors.
X_8	Varying the feeding stages position of the current ones in the demethanizer column.
X_9	Increase the number of stages in the demethanizer column.
X_{10}	Replace existing column trays with new one in the demethanizer column (type of trays) to increase its efficiency.
X_{11}	Increase power generation capacity of first turboexpander by installing other in parallel to the current one.
X_{12}	Increase power generation capacity of second turboexpander by installing other in parallel to the current one.

Table 4.10 Feasible changes for the Cryogenic I plant.

4.3.2 Evaluation stage

Promising variables listed in Table 4.10 are assessed to determine the impact of the factors considered. The problem has 12 factors, with at least two possible levels available for the evaluation of each factor. No geometrical restrictions in the outputs for the searching space (geometrical form) were found in the diagnosis stage. As explained in Section 3.2.2, for the evaluation stage, a first screening DOE was applied to identify the most important factors, which is followed by fitting a reduced model based on those.

Preliminary screening: The first screening DOE was a fractional factorial design (FFD) at two levels, with 12 factors for this case. The resolution and thus the confounding pattern were selected based on the simplicity of analysis for the 12 factors. For this purpose, Matlab® was able to automatically find and generate an FFD on two levels based on the requested number of factors, the maximum number of runs (2^{k-p}) and the resolution level by using the function "fracfactgen". A minimal resolution level of IV was

required to provide a good balance between the number of runs and the confounding level. The minimum number of simulations suggested by the generated design in Matlab® was 64. The complete data sheet given by Matlab®, including the confounding level, is shown in Table A.3 from the Appendix. The generators were: 'X_1', 'X_2', 'X_3', 'X_4', 'X_5', 'X_6', '$X_3X_4X_5X_6$', '$X_2X_3X_5X_6$', '$X_2X_4X_5X_6$', '$X_1X_4X_5X_6$', '$X_1X_3X_5X_6$' and '$X_1X_2X_3X_4X_5X_6$', while the screening two-level FFD obtained is visualised in Table A.4 from the Appendix in coded variables (levels for each factor) dictated by the design. Its corresponding natural variables (real operational value for each factor), according to the considerations made in the second part of the diagnosis stage for the two groups, are presented in Table 4.11. Therefore, Table A.4 and Table 4.11 present the condition of each simulation. As assumed in section 3.1.2, interactions between three or more factors had a lower effect on the MaPr response, so these were not taken into consideration.

Factor	Units	Level (-1)	Level (+1)
X_1	Kg/cm^2	22.5	26.5
X_2	kW	2,803	3,101
X_3	kW	2,391	2,541
X_4	%mole	5	30
X_5	Kgmol/h	2,268	6,804
X_6	Kgmol/h	0	4,536
X_7	Kgmol/h	0	4,536
X_8	Number	18, 8, and 6	16, 6, and 4
X_9	Number	30	48
X_{10}	%	58	63
X_{11}	kW	0	2,466
X_{12}	kW	0	2,953

Table 4.11 Natural variables for the 12 factors at 2 levels used in FFD.

The 64 simulations set in the screening design were carried out and the ANOVA for the simulation responses were made with the statistic toolbox of Matlab 7.0.1. Table 4.12 presents the results for the main factors, as detailed in section 3.1.5, from which the last column shows the p-values for each factor (Prob>F). Factors X_1, X_4, X_7 and X_{11} have a p-value less than 0.005; therefore, as stated in Chapter 3, these are statistically significant (most important factors). Besides this, X_{12} had a slightly higher value than 0.005, and was

also considered part of the most important factors, although strictly speaking, under the significance level defined in the Section 3.1.3 of the proposed approach (99.5%), it is not.

Factor	Sum of Squares	F test value	Prob>F (p-value)
X_1	8.5×10^{11}	51.51	0
X_2	3.0×10^{9}	0.18	0.6713
X_3	1.1×10^{10}	0.66	0.419
X_4	1.0×10^{15}	63136.67	0
X_5	8.0×10^{9}	0.49	0.4887
X_6	7.4×10^{10}	4.5	0.0388
X_7	8.4×10^{11}	50.85	0
X_8	8.3×10^{8}	0.05	0.8238
X_9	6.9×10^{10}	4.18	0.046
X_{10}	6.0×10^{8}	0.04	0.8492
X_{11}	3.1×10^{11}	19.05	0.0001
X_{12}	1.1×10^{11}	6.84	0.0117
Error	8.4×10^{11}		
Total	1.0×10^{15}		

Table 4.12 ANOVA results for main factors Cryogenic I.

On the other hand, Table 4.13 shows the ANOVA results for the second-order interactions for factor X_1. It is visualised that all the interactions with X_1 yielded p-values larger than 0.005; therefore, these interactions are not significantly important. The results were similar to all the second-order interactions for the 12 factors.

It can be observed from Table 4.12 that the p-values of X_1, X_4 and X_7 laid in the case mentioned for ANOVA in Section 3.1.3, where they are too low to be shown by the software, and these are set to be zero. Consequently, to properly rank them in their order of importance, and to verify the results provided by the ANOVA, the effect of each of the factors as a main or second-order interaction was estimated by equation 3.16. Once this was done, it was possible to rank the order of importance of the most important factors. Table 4.14 presents both p-values for the most important factors and its effect. The

magnitude of the factors' effect can be ranked based on its absolute values. The sign, on the other hand, provides the direction for the improvement.

Factor	Sum of Squares	F test value	Prob>F (p-value)
$X_1 X_2$	6.0×10^8	0	0.9957
$X_1 X_3$	3.4×10^{10}	0	0.9672
$X_1 X_4$	5.5×10^7	0	0.9987
$X_1 X_5$	1.9×10^8	0	0.9982
$X_1 X_6$	2.1×10^9	0	0.9918
$X_1 X_7$	3.2×10^7	0	0.999
$X_1 X_8$	5.1×10^9	0	0.9873
$X_1 X_9$	6.7×10^8	0	0.9954
$X_1 X_{10}$	3.9×10^8	0	0.9965
$X_1 X_{11}$	8.6×10^9	0	0.9836
$X_1 X_{12}$	1.9×10^{10}	0	0.9753
Error	1.0×10^{15}		
Total	1.0×10^{15}		

Table 4.13 ANOVA results for 2nd order interactions with X_1 factor.

Factor	**Description**	**P-value**	**Factor's Effect, £/D**
X_1	Pressure of demethanizer	0	-11,567
X_7	Additional pumparound from demethanizer to high pressure heat exchanger	0	11,493
X_{11}	Additional turboexpander in paralell with first turboexpander	0.0001	7,034
X_{12}	Additional turboexpander in paralell with second turboexpander	0.0117	4,215

Table 4.14 P-values and estimated effects for the most important factors.

The strongest effect on the MaPr response is given by factor X4 (inlet nitrogen) with a value of -404,981 £/D, and its negative effect agrees with what was found in Figure 4.5; however, it cannot be controlled by the user because it comes in the feeding for that reason it is not shown in Table 4.14. By carring out the analysis with the absolute values and the signs of the factors' effect in Table 4.14, the value of factor X_1 (pressure of the demethanizer) is the first in descending ranking order; this fact was found in Figures 4.2 and 4.6. Second in order of magnitude was factor X_7 (additional pumparound from the

demethanizer to the heat exchanger), the sign of which was positive, thus implying that the higher its flowrate, the better (at least up to the set high limit of (+1)). The main reason for this effect was a direct reduction in duty used by the demethanizer reboiler due to the heat transferred through the stated pumparound. The factor X_{11} (additional turbo-expander to the first existing turbo-expander) continued in the third place of the ranking order with a positive sign; this means that the higher the additional turbo-expander capacity, the better. Finally, the factor X_{12} (additional turbo-expander to the second existing turbo-expander) was last in the most important factors' order, and also had a positive effect which reflects that the more additional turbo-expander capacity, the better improvement achieved. As detailed in Figures 4.3 and 4.4, both additional turbo-expanders improved the MaPr due to reductions in high-pressure power compression and higher liquid recoveries. It is essential to point out that the capital cost of the factors (acquisition and installation when non-existent) was not considered in this part, but will be in the final stage.

Figures 4.7 and 4.8 visualize the effect of all the main factors and second-order interactions on MaPr respectively.

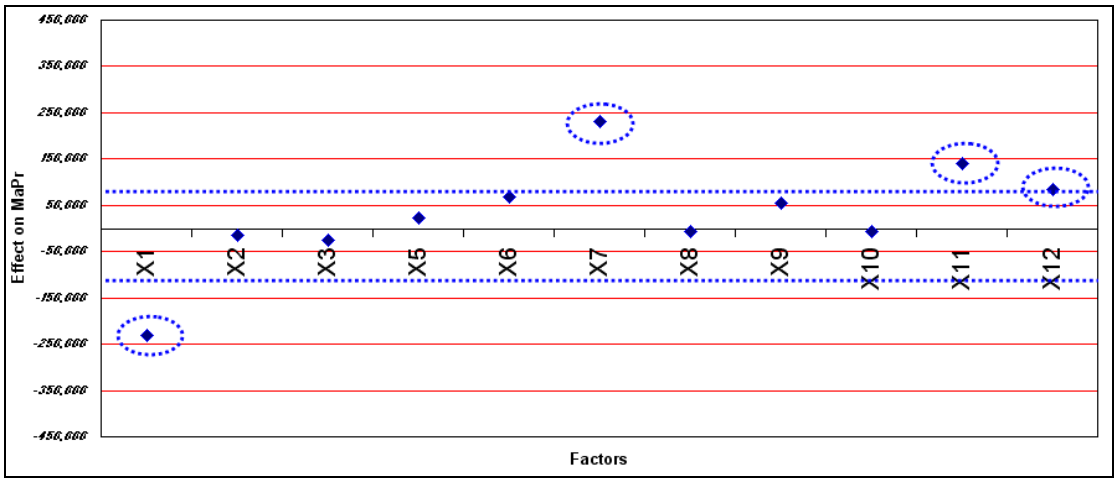

Figure 4.7 Effect of main factors on MaPr.

From Figure 4.7, it can be seen that factors X_1, X_7, X_{11} and even X_{12} fall outside the enclosed area below the base line for the response MaPr; these are marked in the figure with dashed circles for clarity. Therefore, this proves what ANOVA found, namely that these factors are really the most important factors for the response MaPr, while the remaining main factors do not produce any significant effect on MaPr.

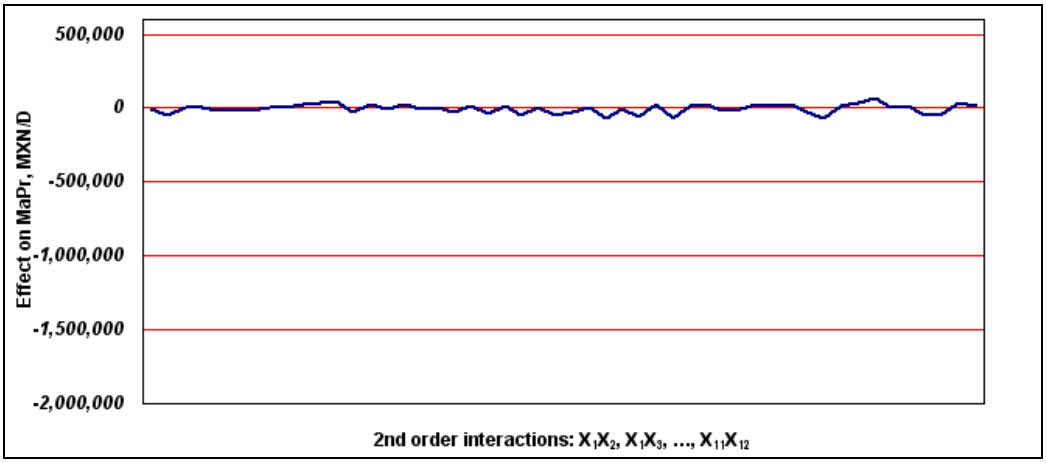

Figure 4.8 Effect of 2nd order interactions on MaPr.

Figure 4.8 shows on the y-axis the effect on MaPr estimated with equation 3.16 for each of the second-order interactions (50 in total) on the x-axis; the name of each factor on the x-axis is not shown because of a lack of space in the graph, but it is implied in the x-axis label. It can be clearly observed in this Figure 4.8 that none of the second-order interactions yielded a noticeable peak in the response MaPr from the base line. This also supports what the ANOVA found, namely that no interactions were seen to be statistically significant for the response MaPr.

It is important to mention that, as observed in Figures 4.7 and 4.8, besides X_1, X_4, X_7, X_{11} and X_{12}, the rest of the factors and second-order interactions did not show evidence of being most important factors, and this is the reason why they are not listed in Table 4.14.

The Retrofit Design Approach continues with the second part of the evaluation stage, where the application of the RSM was conducted based on the previously identified most important factors to obtain a reduced model.

Application of RSM: Before proceeding to the RSM, two main considerations were made in the methodology based on the results achieved in the last section. First, in order to cover the wide range of nitrogen composition at the inlet to the system for factor X4, and not to yield an infinite number of possible compositions (continuous factor), it was decided to fix with four levels of 5, 10, 15 and 20% mole. The second consideration was for factor X_1, for which Table 4.14 showed a negative effect for MaPr, and consequently the lower, the better. As this is a controllable continous factor in the demethanizer column, it was possible to set it at its lowest operating value of 22.5 kg/cm^2 (320 psia) to yield

improvement in MaPr. This also simplified the system, as the fixed factor X_1 became a constant value in the reduced model.

Note that these considerations have been possible because there were no interactions between MaPr important factors in the previous section, which means that factors can be set independently of each other; otherwise, the factors would not have been independent and the interactions involved with the respective factors should have been taken into account (Myers and Montgomery, 2002). Subsequently, once X_1 and X_4 were fixed, the RSM was applied to find a reduced model (for each nitrogen scenario), which predicted the MaPr response based on the remaining independent most important factors: X_7, X_{11} and X_{12}. In order to do this, and to re-use some useful data from the previous simulations, the CCD proposed by the approach (section 3.1.2) was built based on the previous FFD, and, as stated in the referred section, the circumscribed CCD was preferred. The additional points for the proposed design were placed at α values calculated as referred to in Section 3.1.2 of Chapter 3:

$$\alpha = \pm\left(NumberOfFactors\right)^{1/4} = (3)^{1/4} = 1.316$$

An additional central point was set to verify the calibration of the simulations along the design (i.e. no settings were moved away from the initial point). It was stated in Chapter 3 that in the response surface design when integer parameters are present in the most important factors, these must be set in the continuous range so as to avoid infeasibility (an example is given in section 3.1.2). This could be addressed easily in this stage, as all of the structural changes (integer factors) were found to improve MaPr when existing; therefore, all three factors were set in the continuous range. The simulations, based on the circumscribed CCD applied, are shown in Table 4.15 with both the coded variables (levels for each factor) dictated by the design, and its corresponding natural variables (real value for the factor) according to the considerations made in the second part of the diagnosis stage for these options. These give the condition of each run.

Number of simulation	Coded Variables			Natural Variables		
	X_7 absolute units	X_{11} absolute units	X_{12} absolute units	X_7 kgmol/h	X_{11} kW	X_{12} kW
1	-1	-1	-1	2,041	2,219	2,658
2	-1	-1	1	2,041	2,219	3,248
3	-1	1	-1	2,041	2,713	2,658
4	-1	1	1	2,041	2,713	3,248
5	1	-1	-1	2,495	2,219	2,658
6	1	-1	1	2,495	2,219	3,248
7	1	1	-1	2,495	2,713	2,658
8	1	1	1	2,495	2,713	3,248
9	1.316	0	0	2,566	2,466	2,953
10	-1.316	0	0	1,970	2,466	2,953
11	0	1.316	0	2,268	2,791	2,953
12	0	-1.316	0	2,268	2,141	2,953
13	0	0	1.316	2,268	2,466	3,342
14	0	0	-1.316	2,268	2,466	2,564
15	0	0	0	2,268	2,466	2,953

Table 4.15 CCD applied to Cryogenic I.

The 15 simulations were run following this CCD circumscribed design. For simplicity reasons absolute units were preferred thus, the MaPr* responses were obtained and the linear least squares (LLS) method carried out in Matlab for fitting the corresponding model. The same procedure was applied to each of the four fixed inlet nitrogen compositions, and best fit models obtained. These are presented in Table 4.16 for the MaPr* response, together with its root mean square error (RMSE). The factors X_7, X_{11} and X_{12} are coded (ranged from -1.316 to 1.316).

% mole inlet N_2	Best Fit Model	% RMSE
5	$Ma\,\Pr^* = 108.8\times10^{-2} + 0.05\times10^{-2}\,X_{11} - 0.24\times10^{-2}X_7{}^2 - 0.24\times10^{-2}X_{11}{}^2 - 0.11\times10^{-2}\,X_{12}{}^2$	0.13
10	$\mathrm{MaPr}^* = 73.1\times10^{-2} + 0.1\times10^{-2}\,X_{11} + 0.1\times10^{-2}X_{12} + 0.1\times10^{-2}\,X_{12}{}^2 - 0.1\times10^{-2}X_{11}X_{12}$	0.03
15	$Ma\,\Pr^* = (36.9\times10^{-2} + 0.1\times10^{-2}X_{11} + 0.2\times10^{-2}X_{12} + 0.02\times10^{-2}\,X_{12}{}^2$	0.01
20	$Ma\,\Pr^* = (-0.2\times10^{-2} + 0.1\times10^{-2}\,X_{11} + 0.2\times10^{-2}X_{12} - 0.02\times10^{-2}\,X_{12}{}^2$	-0.09

Table 4.16 Best fit models at 4 Nitrogen levels for MaPr* (normalized).

The RMSE indicated a good level of reproduction for the MaPr* response. This was supported by the plot of residuals visualised in Figures 4.9a, 4.9b, 4.9c and 4.9d, in which the residuals for each model were estimated with equation 3.15 for each of the 15 simulation runs outlined in Table 4.15.

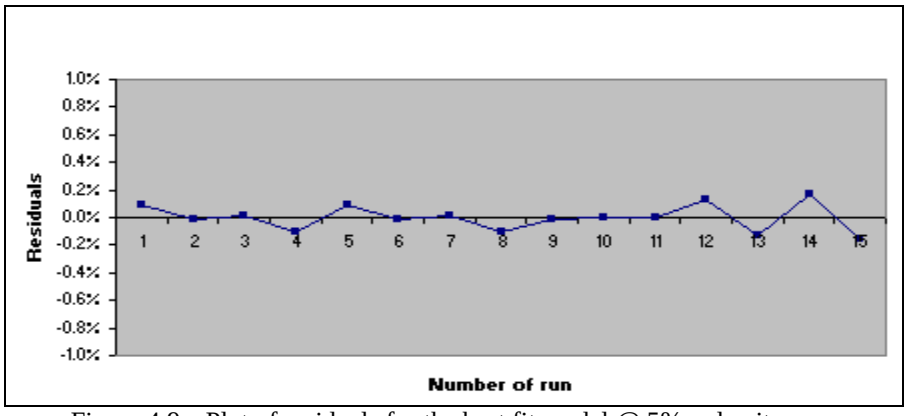

Figure 4.9a Plot of residuals for the best fit model @ 5%mole nitrogen.

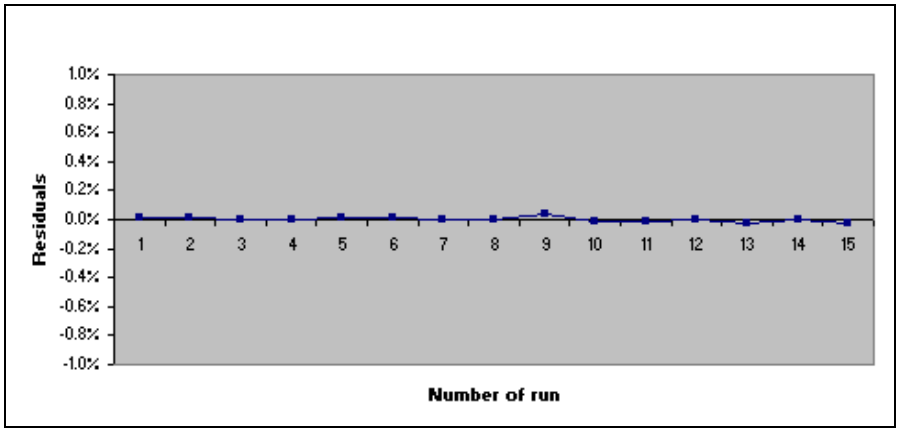

Figure 4.9b Plot of residuals for the best fit model @ 10%mole nitrogen.

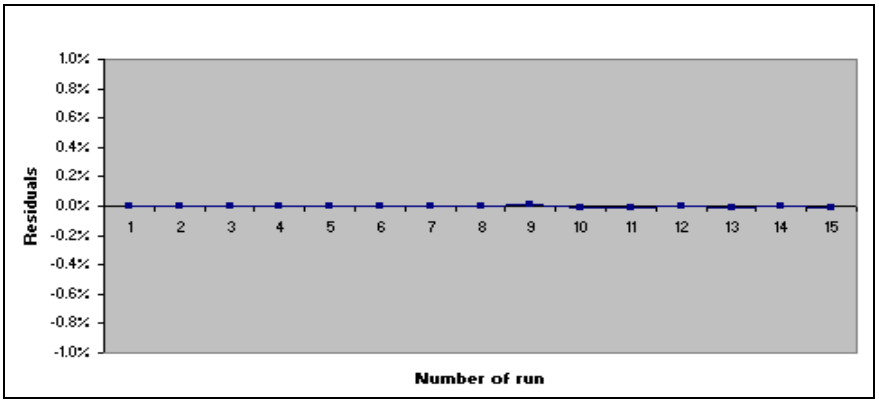

Figure 4.9c Plot of residuals for the best fit model @ 15%mole nitrogen.

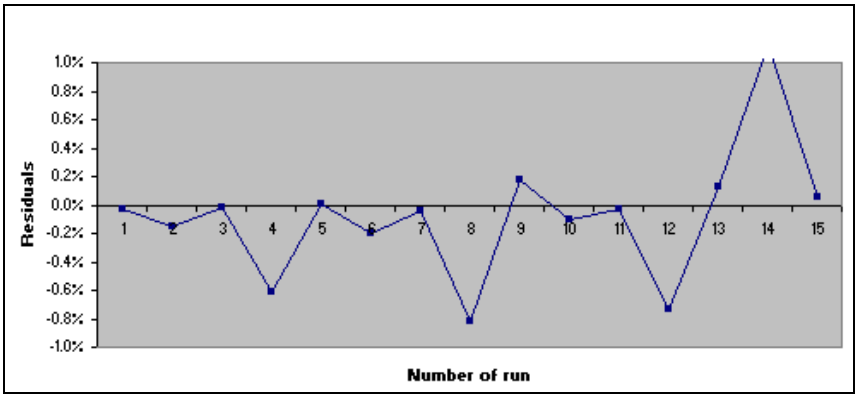

Figure 4.9d Plot of residuals for the best fit model @ 20%mole nitrogen.

The graphs show the residuals with very low values and randomly distributed; therefore, as commented on in section 3.1.2, this suggests that the model fits the data well. The plot of residuals together with the low RMSE confirmed the good agreement of the models to represent the simulation results.

4.3.3 Optimisation stage

The final optimisation stage was applied after finding the best fits.

a. Optimize RSM model

The reduced models obtained and presented in Table 4.16 are non-linear in nature on the variables, and comprise three continuous variables. This class of models or equations is not difficult to optimise, so the NLP solver in Excel® can be considered sufficient to carry out this optimisation. As detailed in section 3.2.2, this solver, based on the generalised reduced gradient (GRG2) non-linear optimisation code, has an issue regarding its tendency to converge on a single optimum point close to the starting position and the software has not certainty in knowing if this is a global optimum point. In order to ensure reliability and robustness in the solutions found, it was suggested to start from different points to find out the best solution. Consequently, the models in Table 4.16 were optimised by the NLP solver in Excel ® to maximise MaPr*, and the starting points were varied for the three factors along the studied ranges for each one separately or in combination respectively. There were no computational difficulties found, as the solver could maximise the MaPr* in seconds; however, the starting point combinations yielded different optimal points, as stated before. It was therefore necessary to select the optimum point of the solutions reached from different sets of starting points in each model. The

selection criterion was also the maximum value of MaPr*. The final optima results for each case were achieved with the coded variables presented in Table 4.17, and Figure 4.10 visualises the MaPr* values for both the base-case and the optimum solution at each nitrogen scenario.

Additionally, as suggested in the approach, a set of confirmatory runs were performed around the maximum found for each case to generate feasible design. The results are exposed as the percentage of difference between the reduced model and the simulation in the last column of Table 4.17.

Inlet N_2	Coded variables			Difference
	X7	X11	X12	Reduced model-Simulation
5% mole	0	0.1	-0.02	0.4%
10% mole	-1.316	0.334	1.316	-0.2%
15% mole	-1.316	1.316	1.316	0.1%
20% mole	-0.002	1.316	1.316	0.01%

Table 4.17 Coded variables for optimal results at each N_2 case.

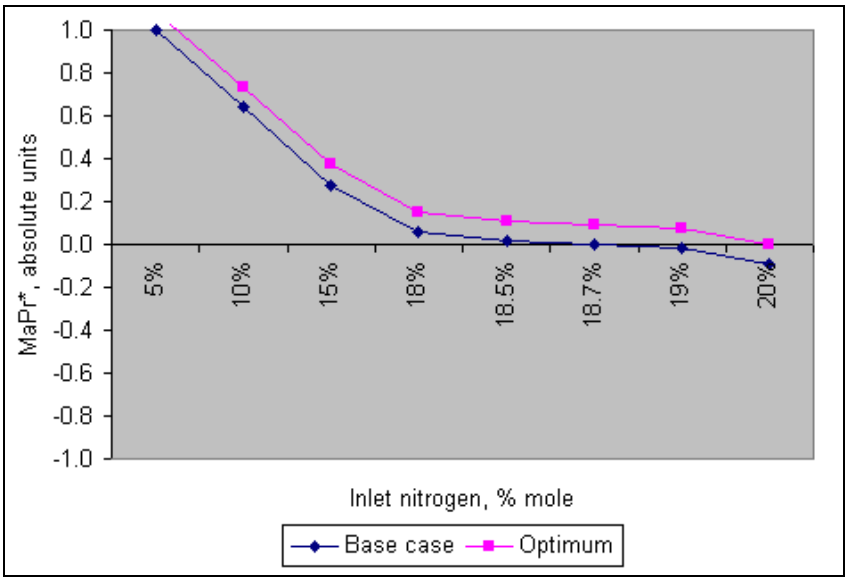

Figure 4.10 MaPr* for optimal results and base cases at each N_2 case.

Table 4.18 shows the actual MaPr* and its improvements with respect to each base-case for the optimal results at each nitrogen scenario. The conditions of each case are also presented as main product compositions, percentages of variation in demethanizer reboiler duty, C_3+ recovery and high-pressure compression power in Tables 4.18a, 4.18b, 4.18c, and 4.18d respectively.

Streams	Residue Gas High Pressure			Residue Gas Low Pressure			C_2+		
Molar Fraction	BC	OC	% Diff.	BC	OC	% Diff.	BC	OC	% Diff.
N_2	0.06	0.06	**0**	0.08	0.08	**0**	0	0	**0**
CO_2	0	0	**0**	0	0	**0**	0	0	**0**
C_1	0.93	0.93	**0**	0.90	0.91	**1**	0.01	0.01	**0**
C_2	0.02	0.01	**-34**	0.01	0	**-67**	0.53	0.53	**0**
C_3	0	0	**0**	0	0	**0**	0.27	0.26	**-3**
NC_4	0	0	**0**	0	0	**0**	0.09	0.08	**-3**
IC_4	0	0	**0**	0	0	**0**	0.04	0.04	**0**
NC_5	0	0	**0**	0	0	**0**	0.03	0.02	**-3**
IC_5	0	0	**0**	0	0	**0**	0.02	0.02	**0**
C_6+	0	0	**0**	0	0	**0**	0.01	0.01	**0**
H_2O	0	0	**0**	0	0	**0**	0	0	**0**
Rate, kg/s	91.931	90.911	**-1.1**	9.7664	9.7533	**0**	47.111	48.142	**+2.1**
T, ºC	43	43	**0**	44	44	**0**	21	21	**0**
P, Kg/cm²	71.4	71.4	**0**	10	10	**0**	25.3	25.3	**0**
Demethanizer reboiler duty, kW							5332	4891	**-8.3**
C_3+ Recovery, %							99.72	99.89	**+0.2**
High pressure compression power, kW							12975	10517	**-18.9**
MaPr*, absolute units							1	1.084	**8.4**

BC=Base Case; OC = Optimum case

Table 4.18a Optimal results vs. base case comparation at 5% inlet N_2.

*Operating data used is based on August 2008 when feed contains 5% mole nitrogen.

Streams	Residue Gas High Pressure			Residue Gas Low Pressure			C_2+		
Molar Fraction	BC	OC	% Diff.	BC	OC	% Diff.	BC	OC	% Diff.
N_2	0.12	0.12	**0**	0.15	0.15	**0**	0	0	**0**
CO_2	0	0	**0**	0	0	**0**	0	0	**0**
C_1	0.86	0.87	**1**	0.83	0.84	**1**	0.01	0.01	**0**
C_2	0.02	0.01	**-34**	0.02	0.01	**-64**	0.53	0.54	**2**
C_3	0	0	**0**	0	0	**0**	0.27	0.27	**0**
NC_4	0	0	**0**	0	0	**0**	0.09	0.09	**0**
IC_4	0	0	**0**	0	0	**0**	0.04	0.04	**0**
NC_5	0	0	**0**	0	0	**0**	0.03	0.02	**-3**
IC_5	0	0	**0**	0	0	**0**	0.02	0.02	**0**
C_6+	0	0	**0**	0	0	**0**	0.01	0.01	**0**
H_2O	0	0	**0**	0	0	**0**	0	0	**0**
Rate, kg/s	95.914	94.408	**-1.5**	10.985	10.858	**-1.1**	46.281	47.831	**+3.3**
T, ºC	43	43	**0**	44	44	**0**	21	21	**0**
P, Kg/cm²	71.4	71.4	**0**	10	10	**0**	25.3	25.3	**0**
Demethanizer reboiler duty, kW							5332	3838	**-28**
C_3+ Recovery, %							99.64	99.89	**+0.2**
High pressure compression power, kW							12652	10959	**-13.4**
MaPr*, absolute units							0.644	0.735	**9.0**

BC=Base Case; OC = Optimum case

Table 4.18b Optimal results vs. base case comparation at 10% inlet N_2.

*Operating data used is based on August 2008 when feed contains 5% mole nitrogen.

Streams	Residue Gas High Pressure			Residue Gas Low Pressure			C_2+		
Molar Fraction	BC	OC	% Diff.	BC	OC	% Diff.	BC	OC	% Diff.
N_2	0.18	0.18	**0**	0.20	0.20	**0**	0	0	**0**
CO_2	0	0	**0**	0	0	**0**	0	0	**0**
C_1	0.80	0.81	**1**	0.77	0.78	**1**	0.01	0.01	**0**
C_2	0.02	0.01	**-34**	0.02	0.01	**-60**	0.52	0.54	**4**
C_3	0	0	**0**	0	0	**0**	0.28	0.26	**-5**
NC_4	0	0	**0**	0	0	**0**	0.09	0.09	**0**
IC_4	0	0	**0**	0	0	**0**	0.04	0.04	**0**
NC_5	0	0	**0**	0	0	**0**	0.03	0.03	**0**
IC_5	0	0	**0**	0	0	**0**	0.02	0.02	**0**
C_6+	0	0	**0**	0	0	**0**	0.01	0.01	**0**
H_2O	0	0	**0**	0	0	**0**	0	0	**0**
Rate, kg/s	99.764	98.05	**-1.7**	12.001	11.816	**-1.5**	45.697	47.514	**+3.3**
T, ºC	43	43	**0**	44	44	**0**	22	22	**0**
P, Kg/cm²	71.4	71.4	**0**	10	10	**0**	25.3	25.3	**0**
Demethanizer reboiler duty, kW							5332	2882	**-46**
C_3+ Recovery, %							99.60	99.87	**+0.3**
High pressure compression power, kW							12350	11472	**-7.1**
MaPr*, absolute units							0.278	0.374	**9.5**

BC=Base Case; OC = Optimum case

Table 4.18c Optimal results vs. base case comparation at 15% inlet N_2.

*Operating data used is based on August 2008 when feed contains 5% mole nitrogen.

Streams	Residue Gas High Pressure			Residue Gas Low Pressure			C_2+		
Molar Fraction	BC	OC	% Diff.	BC	OC	% Diff.	BC	OC	% Diff.
N_2	0.23	0.23	**0**	0.27	0.27	**0**	0	0	**0**
CO_2	0	0	**0**	0	0	**0**	0	0	**0**
C_1	0.74	0.75	**1**	0.71	0.72	**1**	0.01	0.01	**0**
C_2	0.03	0.02	**-42**	0.02	0.01	**-56**	0.53	0.54	**2**
C_3	0	0	**0**	0	0	**0**	0.28	0.27	**-6**
NC_4	0	0	**0**	0	0	**0**	0.09	0.09	**0**
IC_4	0	0	**0**	0	0	**0**	0.04	0.04	**0**
NC_5	0	0	**0**	0	0	**0**	0.03	0.03	**0**
IC_5	0	0	**0**	0	0	**0**	0.02	0.02	**0**
C_6+	0	0	**0**	0	0	**0**	0.01	0.01	**0**
H_2O	0	0	**0**	0	0	**0**	0	0	**0**
Rate, kg/s	103.67	101.86	**-1.7**	12.916	12.685	**-1.7**	45.164	47.203	**+4.5**
T, ºC	43	43	**0**	44	44	**0**	22	22	**0**
P, Kg/cm²	71.4	71.4	**0**	10	10	**0**	25.3	25.3	**0**
Demethanizer reboiler duty, kW							5332	2287	**-57**
C_3+ Recovery, %							99.52	99.85	**+0.3**
High pressure compression power, kW							12070	11977	**-0.8**
MaPr*, absolute units							-0.096	0.002	**9.8**

BC=Base Case; OC = Optimum case

Table 4.18d Optimal results vs. base case comparation at 20% inlet N_2.

*Operating data used is based on August 2008 when feed contains 5% mole nitrogen.

Figure 4.11 shows the optimal results compared with the base case data for the optimised parameters at the 10% mole inlet nitrogen scenario.

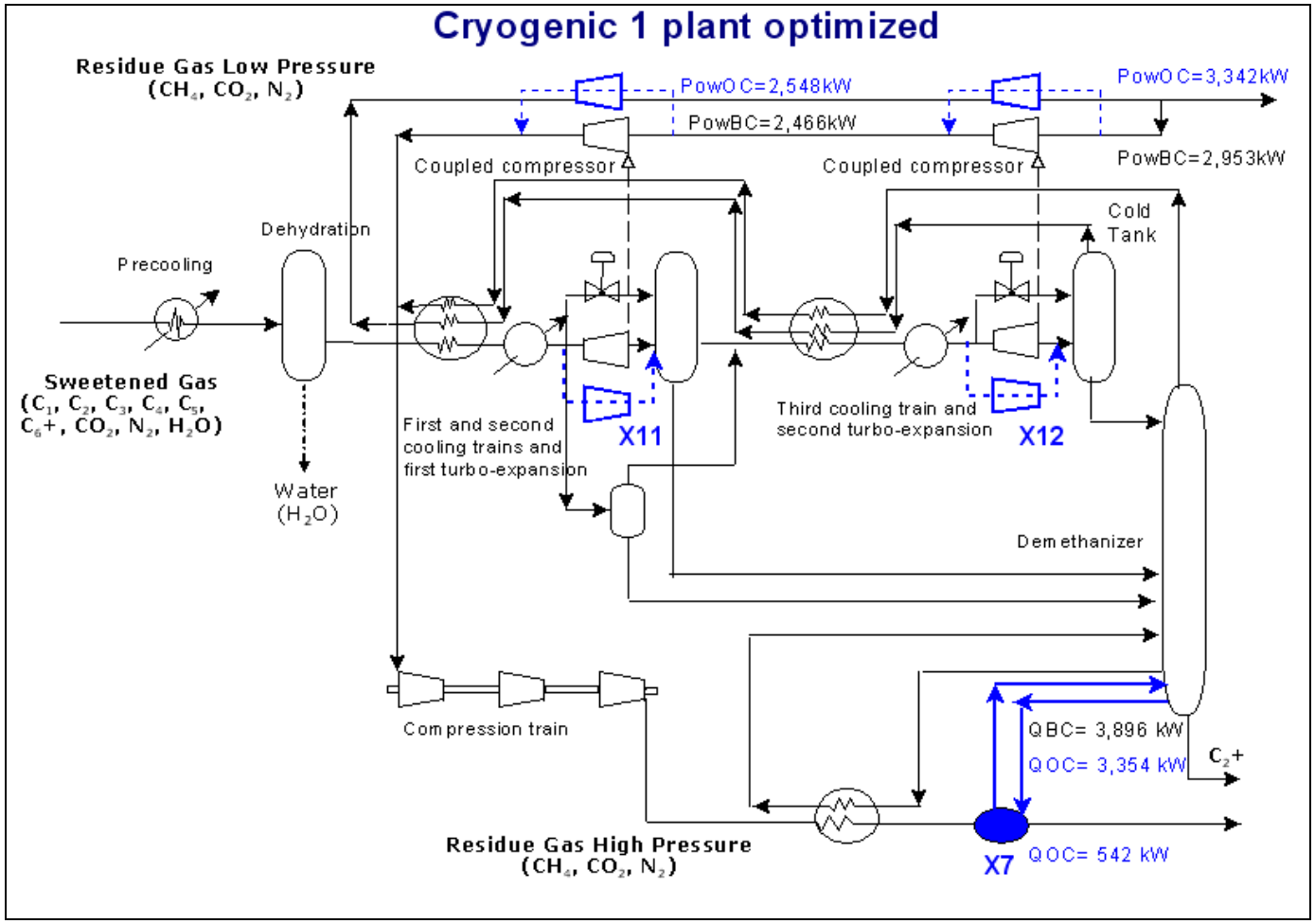

Figure 4.11 Optimal results vs. base case comparation at 10% inlet N_2.

BC=BaseCase; OC= Optimum case.

The results in the previous Tables show clearly a trend to reduce the C_2+ product as the inlet nitrogen is increased, but on the other hand to increase the residue gas streams. As explained in the diagnosis stage for the nitrogen effects on the MaPr response, its properties make this to happen. This is visible in the composition of methane in the residue gas streams and in the flowrates of both, the residue gas and C_2+ for the base-case of the four levels of nitrogen. For the one specific level of nitrogen, comparison between base-case and optimum case exhibits a product composition that does not vary significantly. The noticeable improvements are given in the demethanizer reboiler, the high-pressure compression power and the C_3+ recovery. In general, the following can be observed for these indicators.

Demethanizer reboiler duty: at a fixed nitrogen level when moving from the base-case to the optimum case, a reduction in this duty is observed. This, as said before, seems to be consequence of the heat transferred by the new pumparound from the demethanizer to the high pressure heat exchanger in the optimum case, which reduces the duty needed by the reboiler and produces a better heat distribution along the column, making fractionation easier. This fact yields to a reduced low-pressure steam consumption that affects positively the MaPr response. The difference in reboiler duty from the base-case to the optimum case increases considerably as the inlet nitrogen increases. This is, as explained in the diagnosis stage, because the C_2+ inlet to the plant is reduced, due to the increasing nitrogen content, which results in a decrease in the total duty required by the reboiler.

C_3+ recovery: at a fixed nitrogen level when moving from the base-case to the optimum case, an increase is observed. The settings of the first and second additional turbo-expanders yield an increase in the liquid entering the demethanizer. This effect improves C_3+ recovery in the system at each nitrogen level. On the other hand, when nitrogen is increased in the system, the difference in C_3+ recovery is slightly increased for the higher levels of 15% and 20% of inlet nitrogen. This seems to be the result of increasing liquid separation by the additional turboexpander in paralell with the first turboexpander, which has a full capacity in the corresponding optimal points. Notice that the increasing inlet nitrogen produces a lower total amount of liquid in the system.

High pressure compression power: at a fixed nitrogen level it is observed that when moving from the base-case to the optimum case, the high-pressure compression power

decreases notably. This occurs because the two new additional turbo-expanders in the system, through its coupled compressors, provide more power to the residue gas sent back to the high-pressure compressors requesting less power. The net effect is a reduction in the high-pressure steam required to run the high-pressure compressors. On the other hand, with the increasing nitrogen content it is evident that with a high level of inlet nitrogen for the optimum case, the liquid recovery is increased due to the increased turbo-expander capacity and there is more RG in the vapour phase; this fact produces that the power required for high-pressure compression is higher at the high inlet nitrogen level than at the low level.

*MaPr**: at a fixed nitrogen level, this is increased when moving from the base-case to the optimum case as a net result of the reduction in demethanizer reboiler duty, an increase in C_3+ recovery and a decrease in high-pressure compression power. Nevertheless, it can be observed that when increasing the inlet nitrogen level, this difference is increased slightly, as the reference value is the same; however, at a fixed nitrogen level, both of the MaPr* values for the base-case and for the optimum case are seriously reduced when comparing higher nitrogen levels with lower levels. This was observed in Figure 4.10, and the effect of the inlet nitrogen in the MaPr was detailed in the diagnosis stage in which the main reason for this happening was based on the penalty applied to the residue gas due to the nitrogen content (N_2Pe). Other effects regarding demethanizer reboiler duty, C_3+ recovery and high-pressure compression power were also detailed in the diagnosis stage and addressed in previous paragraphs.

To complete the evaluation stage, it was necessary to consider the capital costs associated with the structural changes proposed by the retrofit. In order to do this, and as the nitrogen content in the inlet gas is a variable factor which is expected to increase from the base-case value (5% mole), a case with 10% mole of inlet nitrogen was selected for this following detailed study. In general, capital investment was estimated for the new additional units considered in the current study as:

1. *Additional pumparound (X_7=PA-03):*

Capital Investment(X_7) =

$$Pump + Piping + Arrangements(HeatExchanger) + Arrangements(Column) \quad (4.10)$$

2. *Additional first turboexpander (X_{11}=-GC-101AD):*

Capital Investment(X_{11}) =

$$Turbine + Compressor + InstallationArrangements \quad (4.11)$$

3. *Additional second turboexpander(X_{12}=GC-102AD):*

Capital Investment(X_{12}) =

$$Turbine + Compressor + InstallationArrangements \quad (4.12)$$

The index used to compare the different schemes and then plot was defined as:

$$CIPA = \left(\frac{CI\langle X_i \rangle}{PA} \right) \bullet 100 \quad (4.13)$$

where CIPA=Index of capital investment over plant assets [%]; CI(X_i)=Capital investment of i [£]; PA=Plant assets [£]; and current plant assets were estimated to have a value of £17,600. Table 4.19 shows the calculation basis for each costing item, based on the previous equations and the database in Timmerhaus et al. (Timmerhaus et al., 2003).

The optimum solution for the 10% inlet nitrogen case comprise factors X_7, X_{11} and X_{12} set at optimal conditions to yield maximum improvement in MaPr. However, when budget restrictions are present, it is necessary to look at different retrofitting options with lower

capital costs. Therefore, the optimum solution can be split into three sets of promising options, as all of them yield to improvements in the process. The increases in MaPr obtained by each one separately will be less than collectively, and so will the capital investment. From this perspective, it is possible to have a spectrum of feasible and reliable investment opportunities at different budget levels.

Item	Features	Sizing and capacities	Capital cost estimated, MM£/Yr
1. Additional pumparound from demethanizer to high pressure heat exchanger (X_7)			
Pump	Centrifugal pump, electric motor included 12-20, API-610 Cast steel casing	Flowrate: 0.187 m^3/s Pressure: 33.742 kg/cm^2	0.015
Pipe	Purchased cost of cast-iron pipe, bell and spigot pipe, 1035-1725 kPa	Diameter: 0.1524 m Length: 30 m	0.0001
Installation arrangement	Demethanizer and heat exchanger arrangements plus installation costs	40% of purchase cost	0.0058
Totals			**0.02**
2. Additional turboexpander in paralell with first turboexpander (X_{11})			
Compressor	Purchased cost of compressors, including drive, gear mounting, base plate, normal 12-28, centrifugal turbine, carbon steel	Power capacity: 2,500 kW	0.172
Turbine	Purchased cost of turbine and internal combustion engine drivers 12-35, steam turbine	Power capacity: 2,500 kW	0.0178
Installation arrangement	Compressor and turbine copling and placement in the system	40% of purchase cost	0.0760
Totals			**0.27**
2. Additional turboexpander in paralell with first turboexpander (X_{11})			
Compressor	Purchased cost of compressors, including drive, gear mounting, base plate, normal 12-28, centrifugal turbine, carbon steel	Power capacity: 2,953 kW	0.204
Turbine	Purchased cost of turbine and internal combustion engine drivers 12-35, steam turbine	Power capacity: 2,953 kW	0.0193
Installation arrangement	Compressor and turbine copling and placement in the system	40% of purchase cost	0.0892
Totals			**0.31**

Table 4.19 Calculation basis for each costing item from Timmerhaus et al. (Timmerhaus et al., 2003).

This portfolio of opportunities was created and is presented in Figure 4.12 as a comparison between the increase in MaPr and the index % capital invested / plant assets. All three promising options are included on a standalone basis, in combinations of two and all the three together, which was the optimum case found. The first promising option, pressure of demethanizer (X_1), which does not need capital investment is also incluced for comparison purposes. Figure 4.13 presents the payback periods estimated with

equation 3.23 for each of the corresponding investments stated in Figure 4.12. This portfolio can be very useful for supporting decision making procedures in practice, as it provides a simple view of the reliable opportunities available to make cost-effective investments in the plant.

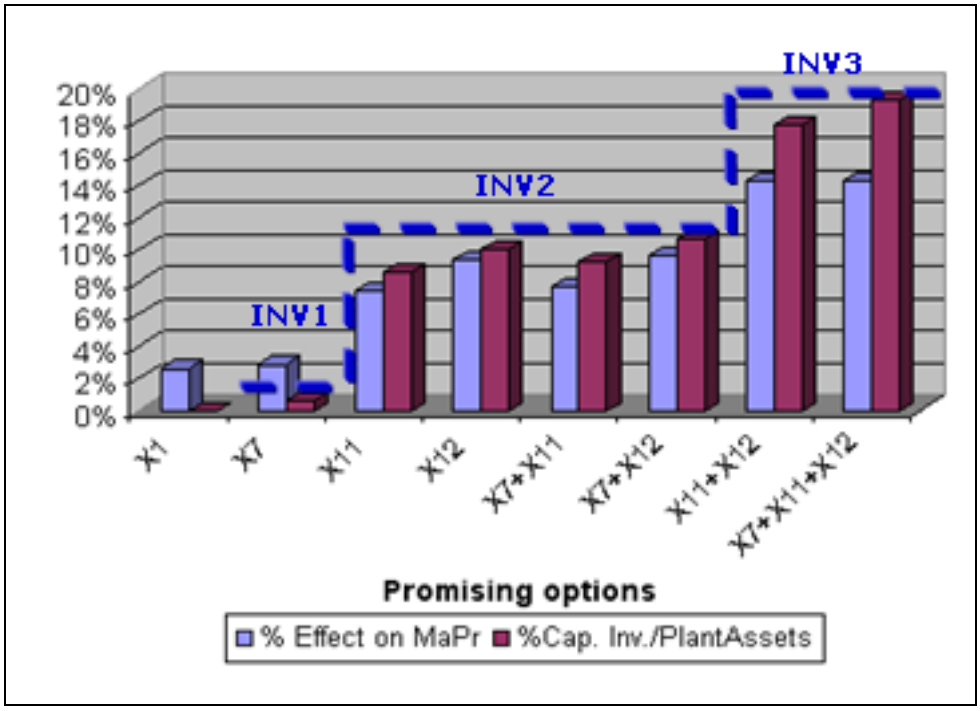

Figure 4.12 MaPr and Capital Costs comparative @10% inlet N_2.

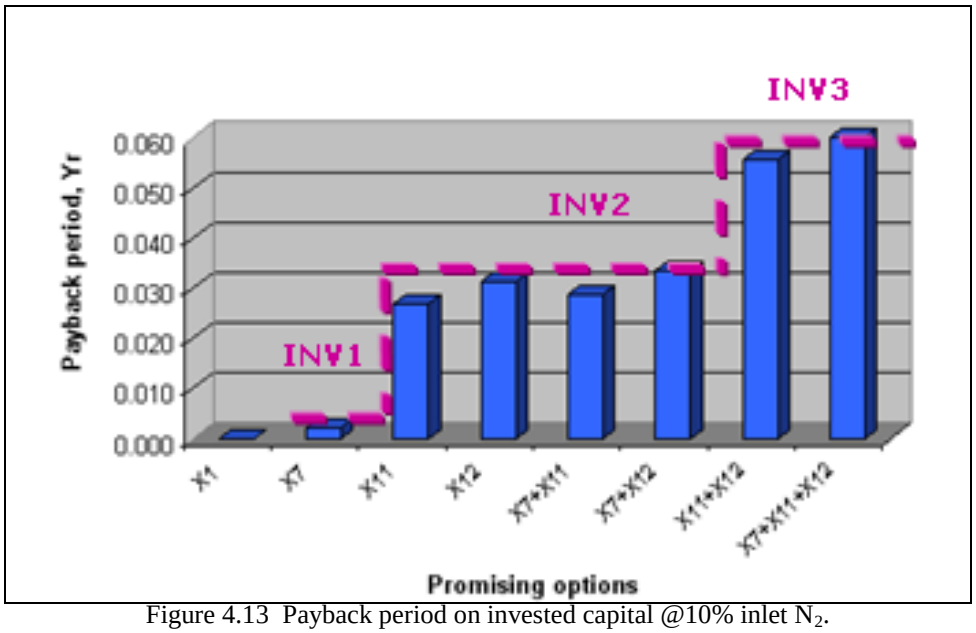

Figure 4.13 Payback period on invested capital @10% inlet N_2.

In Figures 4.12 and 4.13 it can be clearly observed that the first option, pressure in

demethanizer (X_1) does not request investment yielding to 2.6% increase in MaPr. This option is the first suggested to do as the payback period is cero.

Besides this first no-investment option, it can be observed 3 levels of investment according to the capital investment for all the available options; these levels are identified with dashed lines in both graphs. The choice of the investment level mainly depends on the budget availability.

INV1: The first level of investment only includes the first option, the introduction of pumparound on a standalone basis (X_7) which is the least expensive option, with only a 0.7% cap. inv. / plant assets index and it provides the lowest increase in MaPr (2.9%) with respect to the other options. This is due mainly to its contribution towards a lower duty in the demethanizer reboiler. It is seen that because of that, this option has the lowest payback period of 0.002 years. If very limited budget is available for investment this option would be the one to select even when the MaPr increase obtained is not significant, it will improve the heat distribution in the column and operation will benefit.

INV2: The second level of investment comprises the range of 10% cap. inv. / plant assets index with the four options with one additional turbo-expander on a standalone basis or in combination with an additional pumparound. As the payback period for all four options in this set is very close at 0.29 years on average, it is suggested that additionally, the physical feasibility and operational difficulty (control system) must be taken into account to choose the final option.

The first option in this level is the additional turbo-expander in parallel with the first one existing (X_{11}), which achieves a 7.4% increase in MaPr vs. a capital cost index of 8.5%. The increase as detailed above is due mainly to the high-pressure compression power reduction and the higher C_2+ recovery achieved. This is considerably higher than the first option, as is the increase in its capital cost. The payback period is 0.26 years which is the lowest of all the options in this level. As this is only one turbo-expander added in paralell, there is physical feasibility and it would not introduce control difficulty yielding to be the best option to select in this case.

The second option in this level is the additional turbo-expander to the second one existing

(X_{12}). The effect of this in MaPr is similar to the first additional turbo-expander, but in a higher proportion (9.4%) due its larger power capacity. This fact also contributes to its higher capital cost index of 10%. The payback period is 0.30 years which is high with respect to the average of all the options in this level. This is only one turbo-expander added in paralell, there is physical feasibility and it would not introduce major control difficulty but, because of the higher payback period than the previous option, this would be the second option to select in this level.

Following with the standalone scenario are two options combined. The third option in this level is the combination of the two additional items – pumparound and turbo-expander to the first existing option (X_7+X_{11}) – which produces an increase of 7.7% in MaPr and a 9.2% increase in the associated capital cost index. This is as a result of the additive combination of both factors. The payback period is 0.28 years which is slightly lower than the average with respect to all the options in this level. This implies two structural changes in which there is physical feasibility but, it may introduce control difficulty and, because of that and the average payback period, this would be the third option to select in this level.

Next in the ascending sequence is the combination of the additional pumparound and turbo-expander to the second one existing (X_7+X_{12}), which presents an increase of 9.7% in MaPr with a 10.7% increase in the associated capital cost index. The payback period is 0.32 years which is the highest with respect to the average of all the options in this level. This also implies two structural changes in which there is physical feasibility but, it it also may introduce control difficulty and, because of that and that the average payback period is the highest, this would be the last option to select in this level.

INV3: This final level of investment is conformed by the two options – the one that includes the two turbo-expanders with a payback period of 0.055 years and the final optimum solution found, which comprises the three options and a payback period of 0.060 years. This last set has the highest payback periods of all the levels identified.

The first of the third investment level is formed by the additional turbo-expanders to the first one and the second one existing (X_{11}+X_{12}). In summary, this yields a 14.2% increase in MaPr and a 17.7% increase in the capital cost index. The payback period of 0.055 years

is the lowest for the two options in this level which clearly shows that this is the best option to invest in this third level.

The final bar shows the optimum solution found with the three parameters optimised, which has the highest value of 14.24% for all possible options and requires the highest capital cost index at 19.2%. However, its payback period is the highest of all the cases. Therefore, it is highly recommended to leave this option in second place after the previous one in this third investment level.

4.4 Discussion

The Retrofit Design Approach was applied to the first case study, and the following issues addressed on this application:

1. *Global vs. local optimality*: It can be argued at this point that the global optimality of the results found from the study cannot be guaranteed, and alternative solutions that give more cost-effective improvements in the plant may exist.

   To tackle this issue, the local optimal solutions in the worked searching space were found by starting the optimisation from different initial points. Following this, a selection was made from among the local optimal points of the one that yielded t the maximum objective function (pseudo global optimum). Although it is not possible to guarantee globality totally, the screening carried out on the local optimal points highly reduced the risk of not achieving a global optimum solution.

   Besides this, solutions were derived from the most important factors that significantly affect the MaPr response. These were identified through the application of a DOE, which is a systematic tool used to explore the space of the solutions with a high level of statistical confidence. This helped to ensure a high level of confidence in the results achieved.

   To avoid the error of achieving a mathematical optimum (given by the equation) but not a real maximum point (given by the simulation) with the reduced models built, the

optimal solutions were subjected to confirmatory runs and verified to be maximal in the ranges studied.

This confronts the acceptable level of disadvantages mentioned in the literature for the RSM and NLP problems about not relying on the globality of the solutions found. In the present case study, globality in the solutions cannot be fully guaranteed; however, it was proven that the solutions found had high levels of certainty and statistical confidence – enough to be considered pseudo global optimal solutions. These feasible and reliable pseudo optimal solutions meet the expectations required by the users.

2. Solution time: Regarding the required computational time to obtain the final portfolio of cost-effective solutions, it was found that to carry out the whole approach the number of factors is extremely important. As it was mentioned in the chapter 3, this number defines the simulations requested for the design of experiments. For this specific study case, the prelimiar computational time used for the model building and its validation was considerable (600 minutes in average). The evaluation stage took the largest period of time (roughly 1,260 minutes), followed by the diagnosis stage with 960 minutes approximately and finally the optimisation with roughly 681 minutes. Nevertheless, this time could be reduced as experience in retrofit design and in simulation convergence is gained. The relatively low number of simulations was due mainly to the feature mentioned in section 3.1.2 for the CCD designs; construction through a sequential experimentation from a fractional factorial design at two levels by adding some additional points yields this. The optimisation stage, on the contrary, was the shortest in time, as the reduced model could reproduce with low errors the studied response and the time to optimise it took just minutes. This part offsets the long time of previous stages and becomes the promising feature of the proposed approach. To have a complete view, it becomes necessary to carry out a comparison with other conventional methods to solve this problem, including deterministic or stochastic methodologies. Table 4.20 specifies the computational time applied to each one of the stages in the proposed Retrofit Design Approach for the study case I.

Stage	Task	No. of tasks	Time per task	Total time
	Simulations for model building	30	15 minutes	450 minutes
	Simulations for model validation	10	15 minutes	150 minutes
Diagnosis	Simulations in selection of continous variables	50	15 minutes	750 minutes
	Simulations in selection of discrete variables	14	15 minutes	210 minutes
Evaluation	Simulations in the initial screening DoE	64	15 minutes	960 minutes
	ANOVA and evaluation of factor's effects	1	60 minutes	60 minutes
	Additional simulations to initial DoE	14	15 minutes	210 minutes
	Surface model fitting	1	30 minutes	30 minutes
Optimisation	Optimal confirmatory simulations	48	15 minutes	576 minutes
	Complementary simulations to build the portfolio	7	15 minutes	105 minutes
Total of time				**3,501 minutes (59 hours)**

Table 4.20 Computational time of the proposed Retrofit Design Approach for the study case I.

3. *Nitrogen effect*: It was shown that inlet nitrogen to the plant strongly affects its MaPr, which seems to be consistent with what was found by Salas et al. (Salas et al., 2003), where a similar unit was analysed for different levels of inlet nitrogen ranging from 1 to 50 mol %. They stated that high concentrations result in a reduction of the liquid recoveries in the process. In the current case study, this fact is seen to be one of the reasons for the reduction of the estimated MaPr, although the main reason appears to be the penalty for the gross caloric value of the RGHP product. It was found that as the inlet nitrogen increased, the GCV reduced and, consequently, the billing prices were directly affected, which in turn reduced the NPr and MaPr obtained by applying the stated penalty (N_2Pe).

This effect produced the highest value in the RSM results, is an important issue to consider in further studies.

It is worthwhile mentioning that these findings cannot be extrapolated to spatial regions outside the bounds studied. To do so would be extremely unreliable, as the operating conditions may change critically or be unfeasible, or the simulation results may differ significantly from reality.

4.5 Summary

The proposed approach for retrofitting was applied to a natural gas liquids (NGL) recovery unit currently in operation. A retrofit design for the entire plant was performed using RSM, to determine optimal operating conditions and structural changes by setting the objective function to maximise marginal profit. As a result of this, different retrofit options were analysed and a portfolio of schemes generated, based on capital analysis and operating limitations.

The best revamping alternatives arising from retrofit design were an additional pumparound, an additional turbo-expander to the first existing and an additional turbo-expander to the second existing. The largest improvement in MaPr was given by the combined case, which considered all three changes, and the marginal profit was seen to increase by 9 %.

Nevertheless, the best cost-effective alternative depends on the available budget and the intended payback period, and it can be chosen from the final opportunities portfolio. This fact was the principal achievement obtained, to account for a viable investment portfolio that provides the management team with simple but reliable opportunity areas of improvement in the Cryogenic 1 plant.

Additionally, it was demonstrated that the nitrogen inlet composition is a key factor in the benefits estimated and, thus, this is a starting point for the strategy of the centre to look for alternatives to prevent or solve future problems that the rising content of this component

in the feeding stream may cause. Another important issue derived from increasing the nitrogen inlet was the fact that the RGLP sent to internal customers in the gas processing centre will reduce its GCV, which will in turn yield operational adjustments to furnaces, steam generators and electricity turbo-generators.

Therefore, it can be concluded that the Retrofit Design Approach was applied and shown to be a practical and reliable approach to achieve pseudo optimal solutions over a reasonable timescale.

Chapter 5. Case study II

The second industrial case study is the Hydrocarbon Fractionation process, and involves a distillation sequence to achieve the separation of components in the C_2+ coming from the Cryogenic plant of Case Study I, other cryogenic and liquid sweetening plants plus external C_3+ feedings. Similar to the structure of Case Study I, the description of the process is first given with process data, product specifications and economic parameters. This is followed by section to describe simulation model and retrofit objectives. The proposed Retrofit Design Approach is then applied, and finally, results are shown and discussed.

5.1 Hydrocarbon Fractionation (HCF) process

5.1.1 Process description

The case study in this section is the Hydrocarbon Fractionation (HCF) process, which unit is named Fractionator 1. The main purpose of the plant is to separate the hydrocarbon components into the main products: Gas Liquified from Petroleum (LPG), Light Naphtas (C_5+), Heavy Napthas (C_6+), and Ethane (C_2) gas. In total the HCF plant is design to process 105,000 barrels per day. The plant has the flexibility to shut down the section of hydro-cracking, which does not affect normal operation of the plant. Nowadays, this occurs most of the time as the propane is not frequently produced in the plant. The process is mainly divided into: fractionation, gasoline recovery, and refrigeration sections. Figure 5.1 shows the schematic diagram of the HCF process.

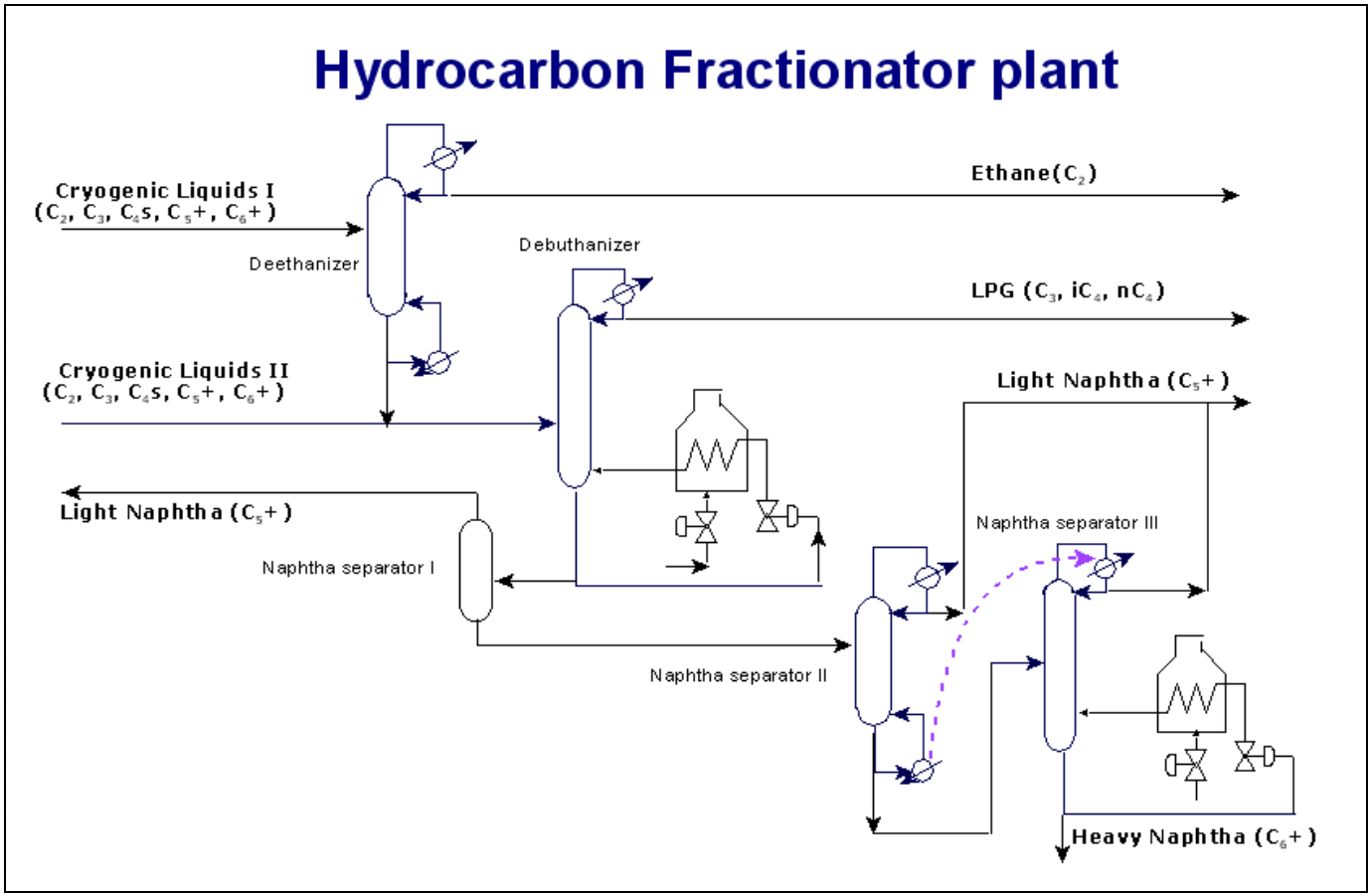

Figure 5.1 Hydrocarbon Fractionation (HCF) general process.

De-ethanizer columns

The C_2+ feed from the Cryogenic and Liquid Sweetener units is paralelly sent to each of the two de-ethanizer columns. The feed is fed to the 6^{th} stage of each column. The function of the de-ethanizer columns is to separate the ethane from the feed stream, for which each one includes of 20 stages. The trays are valve type, from 1 to 5 are made in one step, and from 6 to 20 are made in two steps. The heat required to carry out the separation is provided through two thermosyphon type reboilers which use Low Pressure Steam (LPS) at 4.6 kg/cm^2.

The vapour produced in the top of the columns is partially condensed by propane refrigerant condensers. Ethane product is sent to the compression system to be sold as final product; this is re-injected in the pipe of RGHP due to topological reasons. The bottom product consists of propane and heavier components; these are sent to the de-butanizer column.

De-butanizer column

The bottom liquid from de-ethanizer columns and the C_3+ received from the upstream process (Cryogenic 2 unit) are mixed and fed to the 28^{th} stage of the de-buthanizer. The function of this column is to separate the inlet propane and butane from the gasoline, for which it comprises of 45 trays valve type: from 1 to 27 are made in two steps and from 28 to 45 are made in four steps. The heat required to perform the separation is supplied to the bottom reboiler through a direct fire heater (gas furnace). The vapour, which is rich in propane and butanes, is partially condensated by six cooling water condensers. The distillate is sent as the feed to the de-propanizer column. The bottom product of the de-butanizer consists of mainly pentanes and heavier compounds (C_6+).

De-propanizer column

This column is seldom used to produce coolant propane and because of that, it is not shown in Figure 5.1. However, to avoid operating difficulties and delays during the start-up of this column, it is preferred to keep its reboilers operating with LPS at low capacity.

Naphthas separator columns

The bottom of the de-butanizer is sent to the first naphtha separator, which is a tank that performs an initial split of light naphtha (C_5+), and heavy naphtha (C_6+). This first separator sends the liquid recovered to the 20th stage of the second naphtha separator that is a distillation column to separate the light hydrocarbons from the feed stream. The column comprises 28 trays valve type made in one step. The vapour product from the top is mainly light napthas. The liquid product from the bottom is fed to the 35th stage of the third separator of naphtha. The function of this column is to perform the final reformation of the naphtha and has 40 trays valve type made in a single step. The heat required to perform the separation is provided by a gas furnace as the reboiler. The vapours from the top of the third and the bottom of the second naptha separator are heat-integrated. An additional condenser facilitates the condensation of the top vapours of the third naptha separator. A part of these top condensates is sent back as reflux to the third naptha separator and the other part is sent to be mixed with the top condensates of the second naphta separator. This stream is directly sold as product. The bottoms of this last column, mainly containing heavy naphtha, are pumped to final customers.

5.1.2 Process data and specifications

The HCF plant has five major products. Table 5.1 presents the feed flowrate, composition, operating condition and the required recovery for LPG. Table 5.2 introduces the boiling point of the products at 1 atm of pressure, the separation matrix, and for each column the total number of trays and its diameters (Φ) are also shown. Table 5.3 exhibits the specifications for the main products and specification for C_6+ has not been set. Table A.5 in the Appendix presents the pressures, temperature, and mass flow rate, in normal operating conditions for the major equipment in the plant. The limits for operational parameters in the HCF plant are listed in Table A.6 of the Appendix.

Components	Molar fraction		
	Inlet C_2+ (internal)	Inlet C_3+ (external)	Total Inlet
C_1	0.0157	0.0001	0.0121
C_2	0.3709	0.0098	0.2887
C_3	0.2704	0.5928	0.3442
NC_4	0.1168	0.1983	0.1354
IC_4	0.0532	0.0822	0.0598
NC_5	0.0504	0.0512	0.0506
IC_5	0.0422	0.0429	0.0424
C_6+	0.0800	0.0223	0.0668
Flowrate, kg/s	45.36	13.42	58.78
T, °C	40.8	30	38.3
P, kg/cm^2	23	15.3	21.2
LPG Recovery, %			90.4

Table 5.1 Feed stream and LPG recovery in the HCF plant.

Component	Boiling T at 1 atm, °C	Mass Recovery Fractions				
		De-ethanizer 20 stages $\Phi_{\square}$ = 2.4 □m Φ_2 = 3.3 m	De-buthanizer 45 stages $\Phi_{\square}$ = 3.9 □m Φ_2=4.8 m	De-propanizer 47 stages $\Phi_{\square}$ = 3.5 m Φ_2 =4.5 m	First naptha column 28 stages Φ =1.6 m	Second naptha column 40 stages Φ =2.2 m
Methane	-164					
Ethane	-89	0.99				
Propane	-42	0.01		0.98		
i-Butane	-11.7		0.98	0.02		
n-Butane	-0.5		0.98	0.02		
i-Pentane	28		0.02		0.98	0.01
n-Pentane	36				0.98	0.01
C_6+	69				0.02	0.99

Table 5.2 Boiling points and separation matrix for the HCF plant components.

Product	Parameter	Unit	specification
Ethane (C_2)	H_2S content	ppm	$\leq$ 50
	CO_2 content	% vol	$\leq$ 0.03
	Methane content	% vol	$\leq$ 3.5%
	Ethane content	% vol	$\geq$ 93%
	Propane content	% vol	$\leq$ 4%
Propane (C_3)	Propane content	% vol	$\geq$ 98%
Propane-Butanes (LPG)	Ethane content	% vol	$\leq$ 2.5
	Pentane content	% vol	$\leq$ 2
	Total Sulfur	ppm	$\leq$ 140
Light Naphtha (C_5+)	Butanes content	% vol	$\leq$ 2
	Total Sulfur	ppm	$\leq$ 140

Table 5.3 Product specification in the HCF plant.

5.1.3 Economic considerations

For the annualization of capital cost, 12 % of interest rate and 10 years of project life is used.

NPr, MaPr and MaPr* defined in equations 3.17, 3.18 and 3.19 are used. It is important to note that there is no need for a penalty to be applied in this case. However, different from the case study I, the existing design of heat recovery systems are not highly integrated and hence, revamping of heat recovery is considered. As stated in Section 2.1.2, the heat recovery in the HEN is closed related with any changes of process operating conditions. This interaction in the retrofit design can be investigated by either an iterative or a sequential procedure. In order to obtain optimal retrofit solutions, all the possibilities need to be assessed by considering both process changes and heat recovery. The capital costs need to be considered in the objective function or studied response, thus the Marginal Profit Capital Affected (MPCA) and the MPCA* (MPCA normalised) were then estimated by equations 3.20 and 3.21.

The economic calculation has been carried out in the Excel environment in units of Mexican Pesos (MXN) per day. These were further converted to GBP (£) per year using the exchange rate average of 20 MXN = 1 GBP (£).

The objective function is defined based on the maximization of the annualized MPCA. The number of annual working days for the plant is considered to be 350 per year (30 days of maintenance period for every two years). The available utilities with its operating ranges and costs are showed in Table 5.4, and the unit prices for the raw-material and products are summarized in Table 5.5. These are based on the average of year 2008.

Hot utilities	**Temperature ranges, ℃**	**Cost, £/kW^{-1}.y^{-1}**
Fuel Gas	280	120
High pressure steam	450	379
Medium pressure steam	360	358
Low pressure steam	180	242
Hot water	90	33
Cold utilities		
Cooling water	25-35	25
Propane	-45	472
Power		
Electricity		300

Table 5.4 Available utilities for HCF plant.

Component	**Type**	**Unit Cost**
Cryogenic Liquids Internal (C_2+)	Raw Material Liquid phase	139.9, £/m^3
Cryogenic Liquids External (C_3+)	Raw Material Liquid phase	177.8, £/ m^3
Ethane (C_2)	Product Gas phase	0.109, £/ m^3
LPG (C_3/C_4)	Product Liquid phase	0.3, £/Kg
Light Naphthas (C_5+)	Product Liquid phase	287, £/ m^3
Heavy Naphthas (C_6+)	Product Liquid phase	338.4, £/ m^3

Table 5.5 Raw material and products unit costs for HCF plant.

The capital cost of new units was estimated by equation 3.22. The installation costs associated were calculated as 50% of equipment cost (acquisition plus piping costs) for this case.

For the capital cost of the HEN, following to each one of the proposed retrofit schemes identification, the area cost is updated depending on the situation either with new area or with area added to existing HE. The additional area added to the existing HE were not considered in this case study, due to users' preference on the introduction of new heat exchanger if adding new heat exchanger area is necessary. The capital cost used for comparison was the Annualized Capital Cost for HE (ACC_{HE}), which is derived from equation 3.22 as:

$$ACC_{HE} = CC_{HE} \bullet AF \qquad (5.1)$$

where

ACC_{HE} = Annualized Capital Cost for HE [MM£/Y]; CC_{HE} = Capital Cost of the HE (new HE area cost plus piping cost plus installation cost) [MM£]; AF= Annualization Factor [Y^{-1}].

The installation cost is assumed to be 50% of the HE cost (new HE area plus piping costs).

All the cost information is based on Timmerhaus (Timmerhaus et al., 2003).

The energy savings are quantified from the reduction of energy requirements multiplied by the utility unit cost. The carbon taxation reduction is estimated from equation 3.25 with EPA42 factor = CO_2 emission factor of 117.6471 $lbCO_2/MMBtu$ for furnace combustion, based on EPA-42 factor ((EPA), 2006), and 75% of efficiency for the steam generators becomming:

$$CO_2T = \frac{HUR \bullet EPA42\ factor \bullet 0.75 \bullet SCCO_2}{1.7} \qquad (5.2)$$

where

CO_2T= Annualized benefit from reduction in CO_2 emissions´tax [MM£/Y]; HUR = Hot

Utility Reduction [MMBtu/Y]; EPA42 factor = EPA-42 emissions´factor [MMTon CO_2/MMBtu]; $SCCO_2$ = Estimated Social Cost of CO_2 [$USD/Ton CO_2].
The exchange rate average used was of 1.7 $USD = 1 GBP (£).

The payback period was calculated from equation 3.24.

5.2 Process simulation

5.2.1 Simulation model

The HCF plant has been simulated with Aspen Plus® simulator 2006.5 SM, setting the Peng-Robinson (PR) method for the equation of state for the calculation of thermodynamic properties (AspenTechnology, 2007). The entire flowsheet used standard modules available in the Aspen Plus library.

In an attempt to make the simulation results as reliable as possible, a number or assumptions were made, based on the normal operating strategy of the plant, these are listed as follows:

Modeling Assumptions

1. There is an evidence of hydrate formation in operational data but it has been effectively solved by adding methanol to the system. Thus, hydrate problems in the systems were not considered by assuming zero water content in the inlet C_2+ stream.
2. The capacity of propane cooling used in de-ethanizer column condenser is not restricted.
3. The refrigeration cycle is not represented explicitly in the flowsheet, but the power requirement for the refrigeration cycle is estimated using a Coefficient of Performance (COP) of 1.4 as detailed in chapter 4.
4. The de-propanizer column is not normally operated. However, a reduced and constant amount of LPS is consumed through its reboilers to avoid delays when it is needed to be operated. This is considered in the MaPr.
5. Because of the low feed received in the plant nowadays, the base case only contains one de-ethanizer column in operation.

Calculators

Similarly to case I in chapter 4, the calculator blocks in Aspen estimated NPr, MaPr, and air environmental emissions from correlation factors stated in EPA-42 ((EPA), 2006).

The data of temperature and enthalpy flow rates used to generate the grand compound curves and the HEN analysis were directly extracted from the simulation results data sheets.

5.2.2 Base-case and model validation

The plant processes an average of 45.36 kg/s of C_2+ and 13.42 kg/s of C_3+. The simulation for the base-case was carried out with the average of production data for the period June of 2008 to June of 2009; the main parameters used for the base-case simulation are given in Table 5.6. Table 5.7 presents the conditions and compositions of key process streams from the base-case simulation, including LPG recovery.

Equipment	Input parameters	Value	Output variables	Value
De-ethanizer columns	Top Pressure, Kg/cm²	14.5	Reflux Ratio	1.7
	Number of stages	20	Top Temperature, ºC	-15.4
	Murphree stages efficiency	0.58	Bottom Pressure, Kg/cm²	14.8
	Condenser	Partial	Bottom Temperature, ºC	78.4
De-ethanizer column reboilers			Duty, MW	11.5
De-ethanizer column condensers			Duty, MW	6.7
De-butanizer column	Top Pressure, Kg/cm²	11.2	Reflux Ratio	0.6
	Number of stages	45	Top Temperature, ºC	54.9
	Murphree stages efficiency	0.65	Bottom Pressure, Kg/cm²	11.8
	Condenser	Total	Bottom Temperature, ºC	147.0
De-butanizer column furnace reboiler			Duty, MW	26.7
De-butanizer column condensers			Duty, MW	25.2
De-propanizer column reboilers			Duty, MW	7.0

First Naphtha separator tank	Temperature, ºC	93.3	Vapour fraction	0.51
	Pressure, Kg/cm²	2.8		
First Naphtha separator column	Top Pressure, Kg/cm²	2.3	Reflux Ratio	0.7
	Number of stages	28	Top Temperature, ºC	67.8
	Murphree stages efficiency	0.65	Bottom Pressure, Kg/cm²	2.5
	Condenser	Total	Bottom Temperature, ºC	93.6
Heat integration exchanger			Duty, MW	0.7
First Naphtha separator column Condenser			Duty, MW	0.8
Second Naphtha separator column	Top Pressure, Kg/cm²	3.5	Reflux Ratio	0.4
	Number of stages	40	Top Temperature, ºC	110.0
	Murphree stages efficiency	0.68	Bottom Pressure, Kg/cm²	4.0
	Condenser	Total	Bottom Temperature, ºC	122.3
Second Naphtha separator column Condenser			Duty, MW	3.1
Second Naphta separador column furnace reboiler			Duty, MW	3.9
First Naphtha separator tank Condenser			Duty, MW	2.4
C_6+ Cooler			Duty, MW	0.06
C_5+ Cooler			Duty, MW	1.8
De-ethanizer Reboiler pump			Duty, MW	0.3
Second Naphthas column Reboiler pump			Duty, MW	0.01
Ethane compressors			Duty, MW	1.5

Table 5.6 Main parameters and variables in the HCF base-case simulation.

The largest energy consumers are the reboilers of the de-butanizer column and the de-ethanizer column respectively, as given in Table 5.6. The former requires direct heating from flue gas and the latter Low Pressure Steam (LPS @ P=4.5 kg/cm^2). The steam required in the plant can be described as follows: High Pressure Steam (HPS @ P=100 kg/cm^2) is used in the expander to drive compressors, and then it is transformed into Low Pressure Steam (LPS @ P=4.5 kg/cm^2) which is used in the reboilers of de-ethanizer and de-propanizer. Medium Pressure Steam (MPS @ P=45 kg/cm^2) is imported to drive refrigeration compressors. Intermediate Pressure Steam (IPS @ P=24 kg/cm^2) is also imported to be used for pumps, and then this used LPS is utilized in the reboiler of the de-ethanizer. Additional LPS is used for the remaining heating duties for the de-ethanizer and de-propanizer. In the HCF plant, the less energy consumption implies a reduction in the amount of steam imported (LPS, IPS, MPS or HPS) and as a consequence, the better MPCA obtained.

Parameter	Ethane (C_2)			LPG			Light Naphtha (C_5+)			Heavy Naphtha (C_6+)		
Molar Fraction	**OD**	**SM**	**% Diff.**	**OD**	**SM**	**% Diff.**	**OD**	**SM**	**% Diff.**	**OD**	**SM**	**% Diff.**
C_1	**0.0477**	**0.0478**	**+0.2**	**0**	**0**	**0**	**0**	**0**	**0**	**N/A**	**0**	**N/A**
C_2	**0.9330**	**0.9329**	**-0.01**	**0.0135**	**0.0129**	**-4**	**0**	**0**	**0**	**N/A**	**0**	**N/A**
C_3	**0.0193**	**0.0193**	**0**	**0.6228**	**0.6265**	**+0.6**	**0**	**0**	**0**	**N/A**	**0**	**N/A**
NC_4	**0**	**0**	**0**	**0.2519**	**0.2484**	**-1**	**0.0092**	**0.0095**	**+3**	**N/A**	**0**	**N/A**
IC_4	**0**	**0**	**0**	**0.1118**	**0.1122**	**+0.4**	**0.0003**	**0.0003**	**+3**	**N/A**	**0**	**N/A**
NC_5	**0**	**0**	**0**	**0**	**0**	**0**	**0.2727**	**0.2736**	**+0.3**	**N/A**	**0.0887**	**N/A**
IC_5	**0**	**0**	**0**	**0**	**0**	**0**	**0.2001**	**0.2042**	**+2**	**N/A**	**0.0452**	**N/A**
C_6+	**0**	**0**	**0**	**0**	**0**	**0**	**0.5177**	**0.5124**	**-1**	**N/A**	**0.8661**	**N/A**
Flowrate, kg/s	**10.23**	**10.23**	**0**	**29.19**	**29.14**	**-0.2**	**18.88**	**18.90**	**0.1**	**0.51**	**0.51**	**0**
T, ºC	**-15.4**	**-15.4**	**0**	**30.7**	**30.7**	**0**	**38**	**38**	**0**	**40**	**40**	**0**
P, Kg/cm²	**14.5**	**14.5**	**0**	**7.2**	**7.2**	**0**	**8.6**	**8.6**	**0**	**2.8**	**2.8**	**0**
LPG Recovery (mass), %							**OD = 90.4**			**SM = 90.5**		

OD=Operating Data; SM = Simulation results

Table 5.7 Base case simulation: operating data vs. simulation results for HCF plant.
Operating data used is based on average June, 2008 – June, 2009.

From this Table 5.7, simulation results showed a good level of agreement with real operating data.

Table 5.8 provides an insight of the environmental indexes that is estimated from the model. The ranges that are suggested by the European Integrated Pollution Prevention and Control Bureau ((EIPPCB), 2003) for these indexes and the limits regulated by the Mexican Law (MexicanGovernment, 2007) are also presented as a reference.

Parameter	**EPA42** emission factor	**EIPPCB**	**MX Law[1]**	**HCF unit simulation**
Air emissions				
SO_2 (Ton SO_2 / MM Ton HC)	0.0006	30-6,000	50	0
NOx (Ton NOx / MMTon HC processed)	0.09804	60-500	190	36.7
CO_2 (Ton CO_2 / Ton HC processed)	117.6471	0.02-0.82	N/A	0.044
VOC (Ton VOCs / MM Ton HC processed)	0.0054	50-6,000	N/A	2,185
Water discharges				
T range (*C)	Direct from laboratory	10-35	40	N/A
Oil (mg/l)	Direct from laboratory	0.05-9.8	15	N/A
BOD5 (mg/l)	Direct from laboratory	2-50	30	N/A
Suspended Solids (mg/l)	Direct from laboratory	2-80	40	N/A
Total N (mg/l)	Direct from laboratory	1.5-100	15	N/A
Lead (mg/l)	Direct from laboratory	0.2-0.5	0.2	N/A
Waste / energy				
Ton Waste Generated / MTon HC processed	Direct data	133 - 4,200	N/A	N/A
Specific Energy Consumption, GJ / Ton HC processed	Eq. 4.8	1-4	N/A	1.713

1 NOM-001-SEMARNAT-1996

Table 5.8 Environmental indexes estimated for the HCF plant (June08-June09).

5.3 Application of the proposed Retrofit Design Approach

As previously explained, the methodology proposed to address the plant retrofit design is based on sequential approach between two levels of analysis for revamping of heat recovery. The first considers process improvements which either directly increase the profit or that reduce the energy targets. Once the process conditions have been fixed from this first optimum scenario, the HEN retrofit is developed in the second level. Therefore, the proposed Retrofit Design Approach was applied at these two levels as described below.

5.3.1 Diagnosis stage

The diagnosis stage was first applied to identify the promising continuous or discrete variables to obtain a cost-effective improvement in the process.

Selection of key design variables: The independent variables in the plant comprised the initial list of variables to explore. The impact of the listed variables was assessed by the sensitivity analysis described in Section 3.2.2. Two responses were selected to be studied, MPCA and energy target. The variables were ranged from the minimum to the maximum of operating range referred in the Table A.6 of the Appendix. Three criteria defined in Section 3.2.2 were applied to this study to select the promising variables: 1) a minimum increase in 5% in the MPCA when compared with the base case, or 2) a combination of a mimimum of 1% increase in the MPCA (compared with base case) and of a minimum of 3% of reduction in energy targets, or 3) no increase of MPCA but with a minimum decrease of 5% in the energy targets.

Energy targets: The process streams data are listed in Table 5.9, extracted from the Aspen Plus simulator report sheet and these data were worked in Sprint® version 2.4.001 where energy targets, Composite Curve (CC) and Grand Composite Curve (GCC) were calculated for a ΔT_{min} of 10 ºC. Minimum hot utility requirement is 42.570 MW and minimum cold utility requirement is 33.489 MW.

The corresponding CC and GCC are shown in Figures 5.2 and 5.3 respectively. The plus-minus principle was applied by manipulating the controllable variables in order to

improve heat recovery. The summary of this analysis is presented in Table 5.10 for the internal column pressures as these were suggested by the users' procedures to independently control.

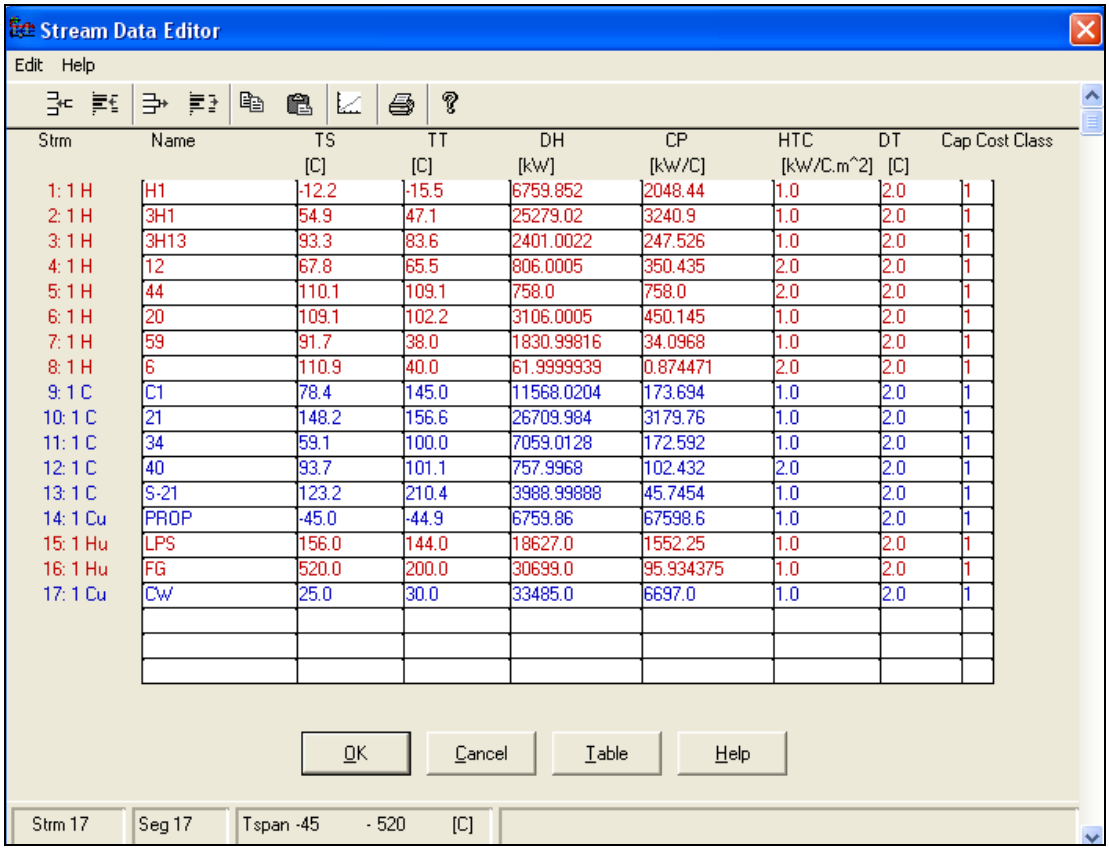

Strm	Name	TS [C]	TT [C]	DH [kW]	CP [kW/C]	HTC [kW/C.m^2]	DT [C]	Cap Cost Class
1: 1 H	H1	-12.2	-15.5	6759.852	2048.44	1.0	2.0	1
2: 1 H	3H1	54.9	47.1	25279.02	3240.9	1.0	2.0	1
3: 1 H	3H13	93.3	83.6	2401.0022	247.526	1.0	2.0	1
4: 1 H	12	67.8	65.5	806.0005	350.435	2.0	2.0	1
5: 1 H	44	110.1	109.1	758.0	758.0	2.0	2.0	1
6: 1 H	20	109.1	102.2	3106.0005	450.145	1.0	2.0	1
7: 1 H	59	91.7	38.0	1830.99816	34.0968	1.0	2.0	1
8: 1 H	6	110.9	40.0	61.9999939	0.874471	2.0	2.0	1
9: 1 C	C1	78.4	145.0	11568.0204	173.694	1.0	2.0	1
10: 1 C	21	148.2	156.6	26709.984	3179.76	1.0	2.0	1
11: 1 C	34	59.1	100.0	7059.0128	172.592	1.0	2.0	1
12: 1 C	40	93.7	101.1	757.9968	102.432	2.0	2.0	1
13: 1 C	S-21	123.2	210.4	3988.99888	45.7454	1.0	2.0	1
14: 1 Cu	PROP	-45.0	-44.9	6759.86	67598.6	1.0	2.0	1
15: 1 Hu	LPS	156.0	144.0	18627.0	1552.25	1.0	2.0	1
16: 1 Hu	FG	520.0	200.0	30699.0	95.934375	1.0	2.0	1
17: 1 Cu	CW	25.0	30.0	33485.0	6697.0	1.0	2.0	1

Table 5.9 HCF process streams and utilities at normal operating conditions.

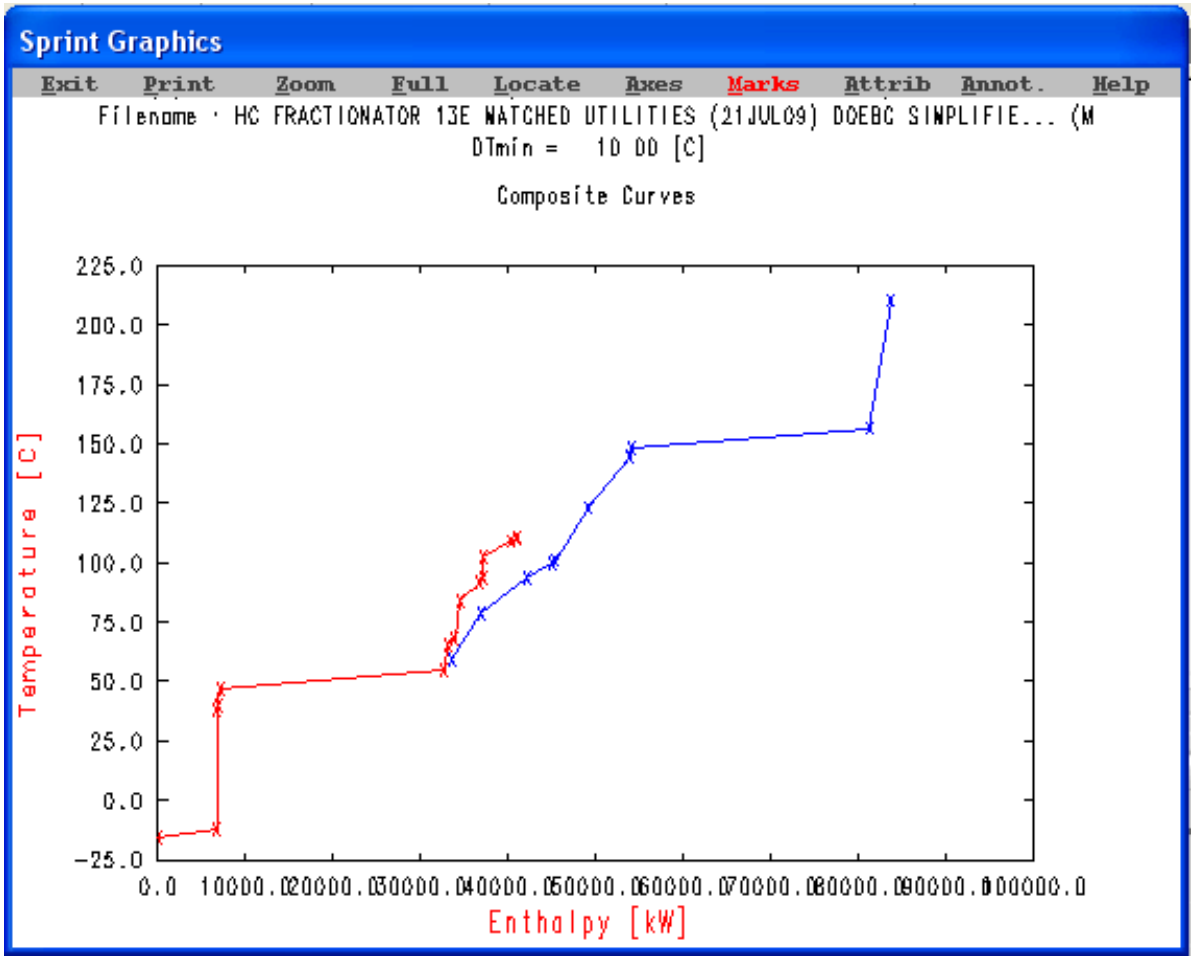

Figure 5.2 Composite Curves for HCF process.

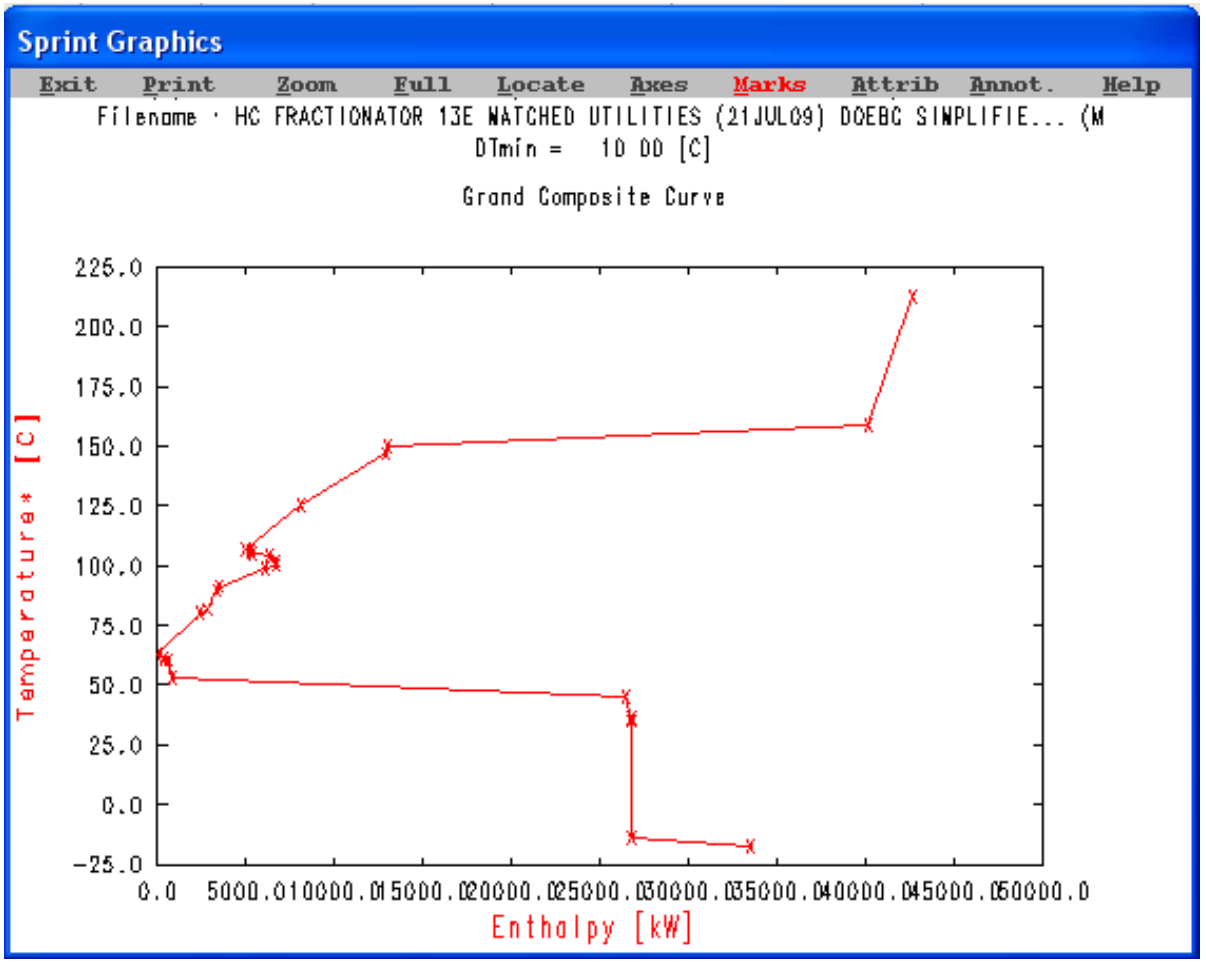

Figure 5.3 Grand Composite Curve for HCF process.

Type	Stream	Associated Equipment	Heat duty, MW	Controlable parameter	+/- Principle suggests
Below Pinch Streams					
Hot	H1 Top vapour	De-ethanizer column	6.759	Pressure	Decrease heat load
Hot	3H1 Top vapour	De-buthanizer column	25.279	Pressure	Decrease heat load
Above Pinch Streams					
Hot	3H13 Vapour	1st naphtha Separator Tank Pressure	2.401	Pressure not independent	Increase heat load
Hot	12 Top vapour	First naphtha separator column	0.806	Pressure	Increase heat load
Hot	44 Top vapour	Second naphtha separator column	0.758	Pressure	Increase heat load
Hot	20 Vapour	2nd naphtha column condenser-1st naphtha column reboiler	3.106	Pressure	Increase heat load
Hot	59 C_5+ product	1st and 2nd naphtha separator columns	1.831	Pressure	Increase heat load
Hot	6 C_6+ product	Second naphtha separator column	0.0619	Pressure	Increase heat load
Cold	C1 Liquid bottoms	De-ethanizer column	11.568	Pressure	Decrease heat load
Cold	21 Liquid bottoms	De-buthanizer column	26.709	Pressure	Decrease heat load
Cold	40 Liquid bottoms	First naphtha separator column	0.758	Pressure	Decrease heat load
Cold	S21 Liquid bottoms	Second naphtha separator column	3.988	Pressure	Decrease heat load

Table 5.10 Process streams and equipment above and below pinch point in the HCF plant.

Figures: 5.4, 5.6, 5.9, and 5.7 show impacts of column pressures on energy targets.

$$\frac{(HotUtility\,T\arg et_{Response} - HotUtility\,T\arg et_{BaseCase})}{HotUtility\,T\arg et_{BaseCase}}$$

$$\frac{(ColdUtilityTarget_{Response} - ColdUtilityTarget_{BaseCase})}{ColdUtilityTarget_{BaseCase}}$$

It is important to study operational issues associated with those process changes.

Due to operational and safety issues, the pressures could only be ranged in the normal operating limits respectively which are referred in the Table A.6 of the Appendix.

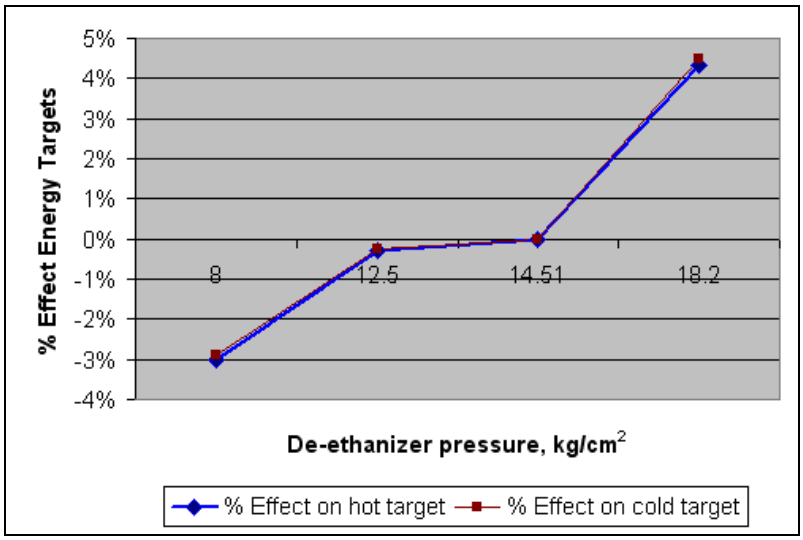

Figure 5.4 Effect of de-ethanizer pressure in hot and cold targets for the HCF process.

Figure 5.4 supports the plus/minus principle application to the hot (top) and cold (bottom) streams on this column. It is clearly seen that the lower the pressure in de-ethanizer column the better. As the cold stream is above the pinch, the principle suggested to reduce its heat load, which is done by decreasing the column pressure. This result is explained by the increasing relative volatility (α) for the light (C_2) and heavy (C_3) components in this column while pressure is reduced, yielding this to an easier separation and thus, requiring less duty.

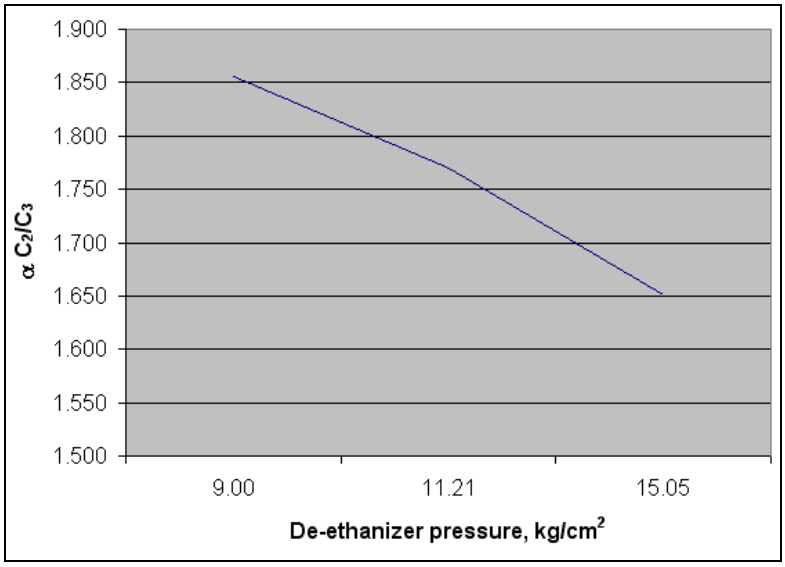

Figure 5.5 Effect of de-ethanizer pressure in $\alpha C_2/C_3$.

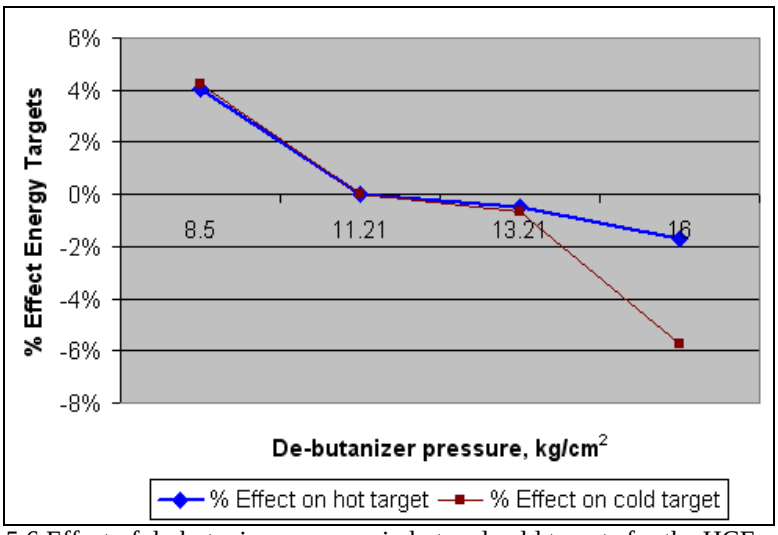

Figure 5.6 Effect of de-butanizer pressure in hot and cold targets for the HCF process.

The operating pressure for the de-butanizer column, on the other hand, has a negative effect on the targets when it is increased, thus the higher the better on hot and cold targets. The plus/minus principle had stated that for the hot stream 3H1 –vapours from top of de-butanizer column- which is below the pinch (25.2 MW), the pressure should be increased and, on the other hand, for the cold stream C1 –liquids from bottom of de-butanizer column- which is above the pinch (26.7 MW) the pressure should be reduced in this column. To understand the negative effect on Figure 5.6, the relative volatilities of the nC_4/iC_5 are visualized in Figure 5.7 presenting an improvement with the lower pressures. Therefore, it cannot explain the stated negative effect.

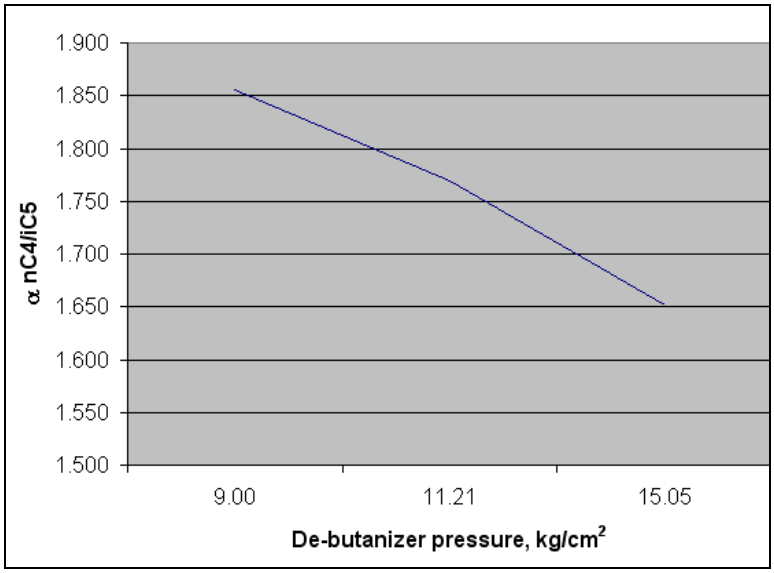

Figure 5.7 Effect of de-butanizer pressure in α nC_4/iC_5.

Besides that, it is generally seen that two columns in series have similar trends for the pressure effects. Nevertheless the case of the de-ethanizer and de-butanizer has shown to have contrary effects on the energy targets when the internal pressure is increased. As found, the relative volatilities do not explain this fact therefore this result seems to be driven by an external factor. In order to find out what is occurring, Figure 5.8 exhibits the vapour fraction behaviour of the first separator tank of naphtha which is located just following the de-butanizer column. Finally the effect found for the energy targets in Figure 5.6 appears to be explained by this fact.

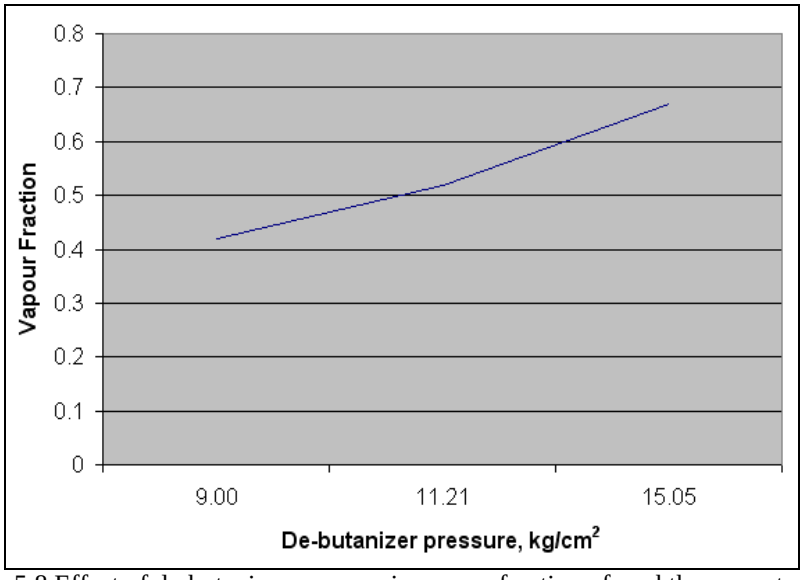

Figure 5.8 Effect of de-butanizer pressure in vapour fraction of naphtha separator tank.

The effect of this vapour fraction can be described as follows: the rising de-butanizer pressure increases the temperature of the liquid at the bottom outlet, when this stream is

introduced to the naphtha separator tank, a higher vaporization fraction is produced inside the tank; as a consequence of this the vapour stream (3H13) at the top outlet increases its flowrate and thus its heat load, favouring the suggestion of the minus/plus principle in Table 5.10 for this stream. The liquid flowrate at the outlet of this tank is thus reduced and so do the duties needed to separate this stream into C_5+ and C_6+. This fact mainly benefits to the suggested reduction of heat load for stream S21 – liquid stream from the bottom of the second naphtha separator column- improving the energy targets.

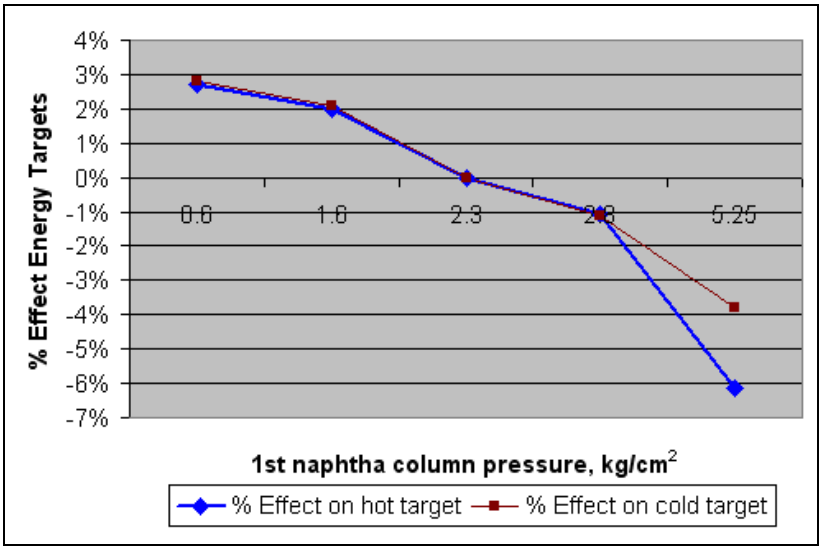

Figure 5.9 Effect of first naphtha column pressure in hot and cold targets for the HCF process.

The pressure of the first naphtha separator column has negative values of effect on targets when it is increased from the normal operating pressure, thus the higher its pressure, the better effect on energy targets. This result agrees with the suggestion done for the hot stream 12 – top vapours of first naphtha separator column – which is above pinch, to increase its heat load.

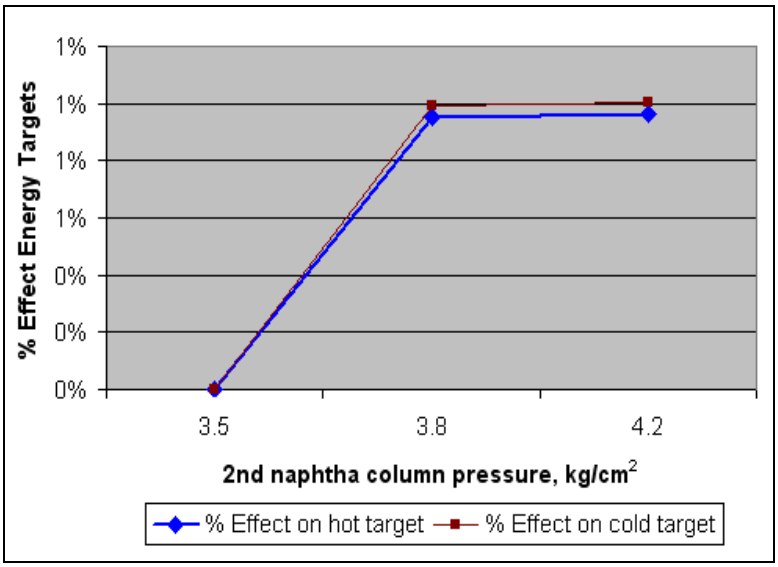

Figure 5.10 Effect of second naphtha column pressure in hot and cold targets for the HCF process.

Increasing operating pressure of the second haphtha separator column can slightly increase energy targets.

By following the criteria for the selection of the potential cost-effective continuous variables, improvement has been observed for three variables as detailed in Table 5.11.

Unit	Variable	Disturbance Range	Best setting	Variation MPCA, %	LPG recovery, %	Hot target, %	Cold target, %
De-ethanizer column	Stage 1 Pressure, Kg/cm²	8 to 18.2	8	1.6	0.01	-3	-3
De-butanizer column	Stage 1 Pressure, Kg/cm²	8.5 to 16	16	1.8	0.01	-2	-6
1st naphtha column	Stage 1 Pressure, Kg/cm²	3.5 to 4.2	3.5	0.2	0.00	-4	-6

Table 5.11 Promising continuous factors in the HCF plant.

Conceptual understanding based on Process Integration: The process integration concepts were applied to explore structural alternatives to improve the HCF plant performance, including:

1. Column feed location
2. Thermal condition of column feed
3. The number of column stages and their efficiency

4. Distillation sequencing arrangements

In the same manner that for the continuous variables, the sensitivity analysis was carried out to select a set of options that allow promising and feasible changes for the case study:

1. Column feed location. Four columns in the system were explored in this case. The current position of the feeding stage for each column was varied by 3 stages above and 3 stages below. This number was chosen by taking into account the total number of stages for all the columns, 3 trays were considered to be a reasonable number for this purpose. This was analyzed through the composition profile of each column, with which internal mixing effects can be examined. An internal mixing effect can be explained as a re-mixing effect along the column structure, which indicates ineffective use of energy for the separation. Figure 5.11, presents the composition profiles of de-ethanizer column with the feeding stage position variations above and below of the base case position (Feed stage 7).

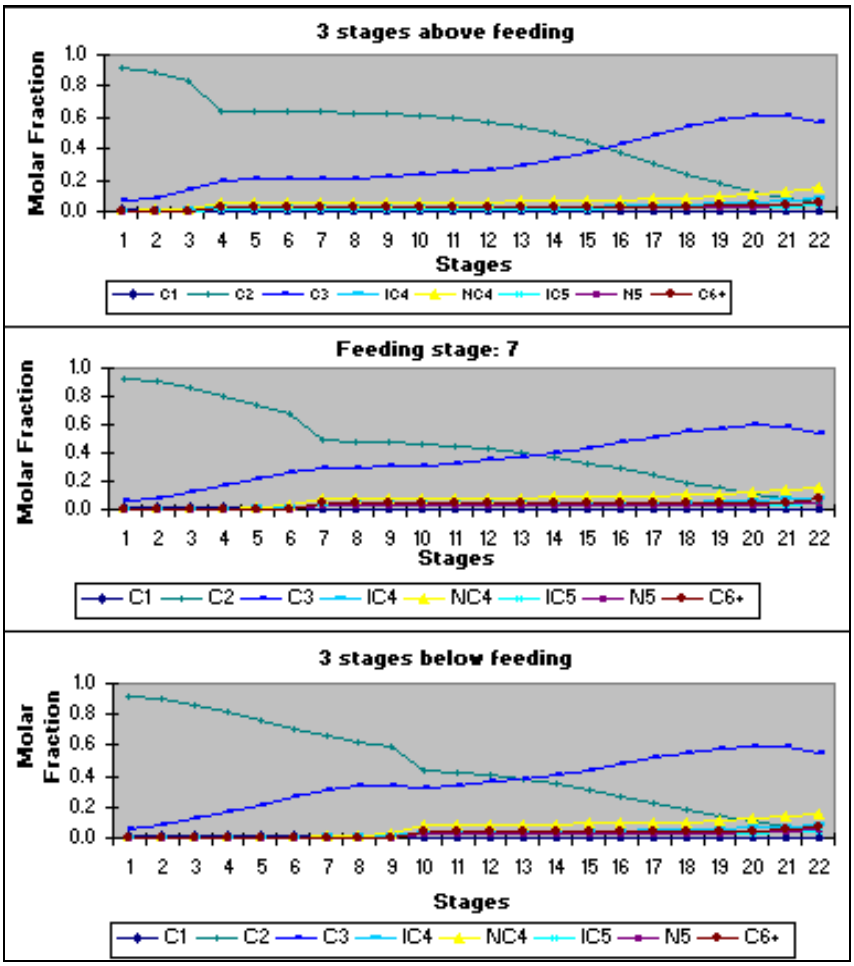

Figure 5.11 Effect of feeding stage to de-ethanizer on its composition profile.

The composition profiles do not show any evidence of significant improvement in the de-ethanizer column, therefore it was concluded that the change of feeding stage position for this column can be rejected as a promising variable.

In a similar manner the de-butanizer, the first and the second naphtha columns were assessed and no evidence of significant improvements by changing the feeding stage position for these columns was found. Therefore, these options were not considered in the list of promising variables.

2. Thermal conditions of column feed. The feed condition was considered as a structural option because in case of this results in a promising variable, the energy associated will need to change. Hence, heating or cooling for the feed will need to be provided and this will imply a structural change. The effect of this action was analyzed with the inlet Vapour Fraction (VF) in the composition profile of each on of the four columns. Figure 5.12 visualizes the composition profile of de-ethanizer column with the variation of VF. The base case for this column has a saturated liquid feed with VF at 0 value, it was varied from VF <0(subcooled liquid), 0.16 (liquid-vapour), 1(saturated vapour), and to VF>1 values (superheated vapour).

As the VF for the inlet stream is increased in de-ethanizer column, it is observed a reduction in the ethane composition along the column, and even a reduced purity in the top stage. Moreover, propane increases its composition along the column becoming this higher than the ethane, which reduces LPG recovery. The rest of component profiles do not seem to have variations. For the purpose of this study it is concluded that changing inlet condition for de-ethanizer is not a promising variable.

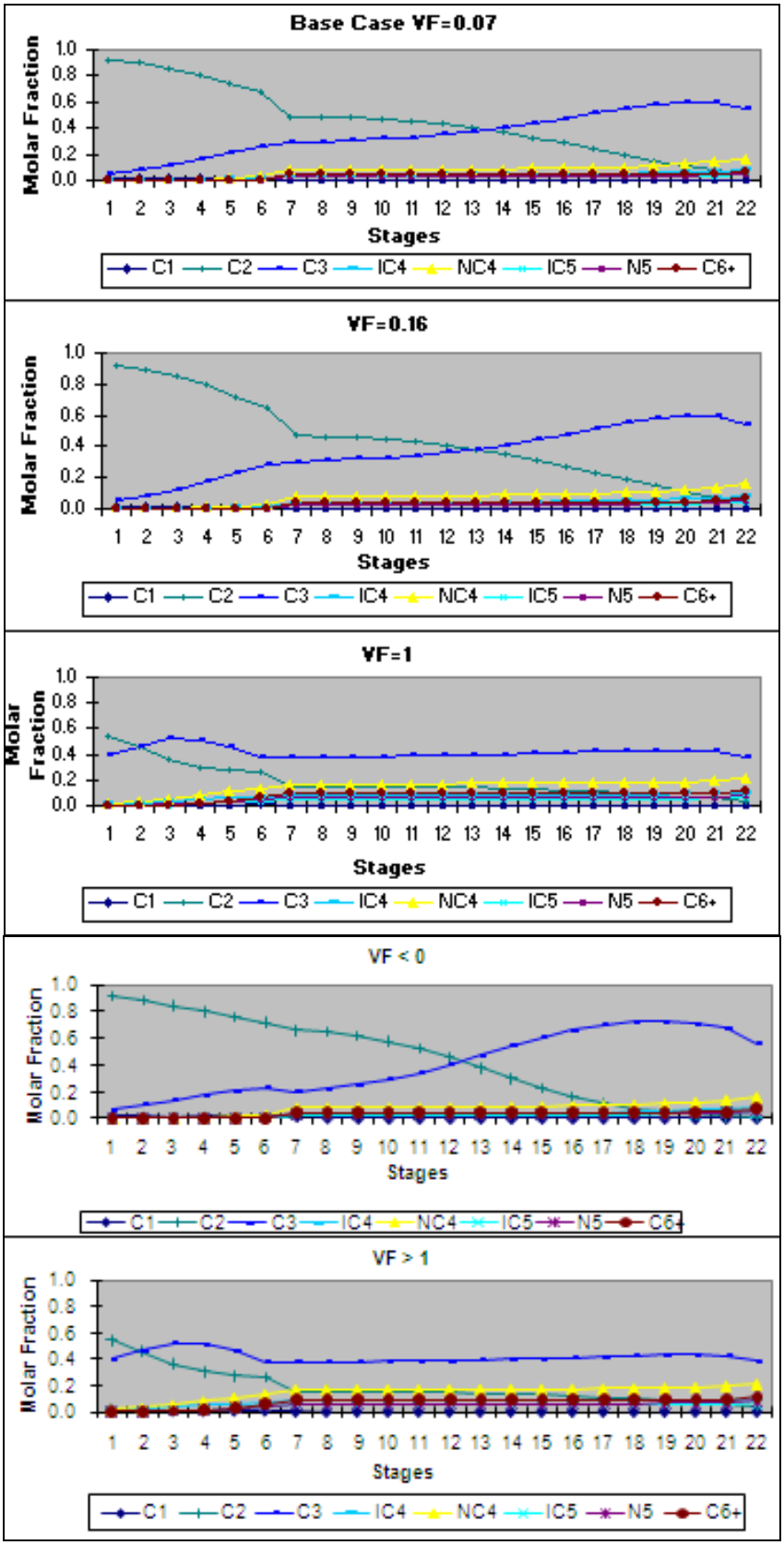

Figure 5.12 Effect of feed condition to de-ethanizer column on its composition profile.

For the de-butanizer column the base case has a value of VF of 0.01, and it was changed between 0.25 and 1. No improvements were observed.

The first naphtha separator column has a base case with a VF value of 0.03 and it was changed between 0.25 and 1. There was no evidence of improvement for the separation of light naphtha (iC_5 and nC_5) and heavy naphtha (C6+) in this column. Thus, this variable is not considered in the evaluation stage.
The second naphtha separator column has a base case with a VF value of 0 and it was changed between 0.25 and 1. No significant improvement exists for the separation of light and heavy naphthas either. Therefore this variable, similarly to the previous columns, is not considered in the evaluation stage.

In summary, for all the columns with respect to the inlet condition as VF, the MPCA response did not show an improvement, and change of thermal feed condition implies structural modification of heat recovery systems. Consequently, this was not considered in the following evaluation stage.

3. The number of column stages and their efficiency. Two options were carried out at this step: an increase in the number of current stages and an upgrade of column internals with high efficiency. It was selected to add 5 stages to all the columns. For the efficiency, an increase of 20% was set and fixed for all the columns which is based on efficiency offered by industry available in the current market (Koch-Glitsch, 2010). If this factor has a considerable impact during the evaluation, the different number of trays will be tested and the more appropriate number of stage will be selected. Table 5.12 shows the results for the impact of number of stages and their efficiency on MPCA.

The changes given by the number of stages and their efficiency in the de-butanizer, the first and the second naphtha columns were of a very low order so these were considered negligible. From the table, the only promising variables considered are the number of stages in de-ethanizer column and the stage efficiency of de-ethanizer column.

Description	Range	Best setting	Variation MPCA, %	LPG recovery, %	Variation Duty Hot, %	Variation Duty Cold, %
Number of stages in de-ethanizer column	20 to 25	25	1.3	0.00	-9.3	-16
Number of stages in de-butanizer column	45 to 50	45	-0.02	0.02	0.0	0.01
Number of stages in 1st naphtha column column	28 to 33	28	0.0	0.00	0.0	0.0
Number of stages in 2nd naphtha column	40 to 45	40	0.0	0.00	0.0	0.0
Efficiency in de-ethanizer column stages	0.58 to 0.78	0.78	1.8	0.01	-11.6	-20
Efficiency in de-butanizer column stages	0.65 to 0.85	0.65	0.0	0.00	0.0	0.0
Efficiency in 1st naphtha column stages	0.65 to 0.85	0.65	0.0	0.00	0.0	0.0
Efficiency in 2nd naphtha column stages	0.68 to 0.88	0.68	0.0	0.00	0.0	0.0

Table 5.12 Effect of column stages and their efficiency in the MPCA for the HCF plant.

4. Distillation sequencing arrangements. A series of feasible distillation arrangements were screened and simulated. Because of high purchase cost of a new column, the retrofit design was focused on searching for arrangements that could re-use the existing columns in the plant. In order to achieve this, it was needed to take into account both, the size of the columns in the plant presented in Table 5.2, and the distillation sequencing arrangements presented in Figure 2.3 in the section 2.1.1. Following to these two considerations, the set of possible arrangements was listed:

1. A sloppy arrangement with columns: de-ethanizer and de-butanizer.
2. A sloppy arrangement with columns: de-ethanizer and de-propanizer.
3. A sloppy arrangement with columns: de-ethanizer and 2nd naphtha.
4. A sloppy arrangement with columns: de-ethanizer, 1st naphtha, and 2nd naphtha.
5. A sloppy arrangement with columns: de-ethanizer, 1st naphtha, and de-butanizer.
6. A sloppy arrangement with columns: de-ethanizer, 1st naphtha, and de-propanizer.
7. A prefractionator arrangement between de-ethanizer and de-butanizer columns.

8. A prefractionator arrangement between de-ethanizer and de-propanizer columns.
9. A prefractionator arrangement between de-ethanizer and 2nd naphtha columns
10. A prefractionator arrangement in 1st naphtha column and de-butanizer.
11. A prefractionator arrangement in 1st naphtha column and de-propanizer.
12. A prefractionator arrangement in 1st naphtha and 2nd naphtha columns.

From Tables 5.1 and 5.2, the inlet stream can be roughly divided in three groups: around 30% is the lightest components (methane and ethane), a nearly 54% of components with medium boiling points (propane and butanes), and about 16% of the heaviest consisted of pentanes (nC_5, iC_5) and C_6+.

It is preferred to minimise any structural changes in the basic sequence of the columns. Under this perspective, options 3, 4, 5, 6, 9, 10 and 11 are excluded.

It was mentioned earlier that the production of propane is seldom occurred, and therefore, options number 2 and 8 are also not favoured. The main reason is that these options will imply the use of the de-butanizer column in propane production when it is needed. The structure for the production of propane is already set in the de-propanizer column and will change the basic sequence of the columns. Moreover, by inspecting the location in the plant of these two columns, it is found that these columns have the longer distances, making it much more difficult to arrange for interconnections.

Prefactionator is favoured when intermediate product comprises a large fraction of the feed (e.g. more than 50%). However, midddle boiling point components (nC5) for this case is about 26% of feed, and therefore, option 12 is not selected.

It is imperative to note that the side-stream columns were not considered in this case study by following heuristics mentioned in section 2.1.1 for sequencing of complex columns with a pure sidestream product coming from an inlet stream of 3 components. If this were the case, from Table 5.2 methane and ethane can conform a 1st group (A), propane, iso and normal butane the 2nd group (B) and naphtas the 3rd group (C). If the compositions in Table 5.1 are analysed, it is clear that the B component composition is bigger than 50% but for the components A and C compositions, these are not less than 5%

each one hence, this conditions did not suggest to apply the side-stream arrangement in this case.

After screening of available options, two feasible arrangements were selected for further analysis: the sloppy arrangement for de-ethanizer and de-butanizer, and the prefractionator arrangement in de-ethanizer and de-butanizer. These are diagrammed in Figures 5.13, and 5.15 respectively.

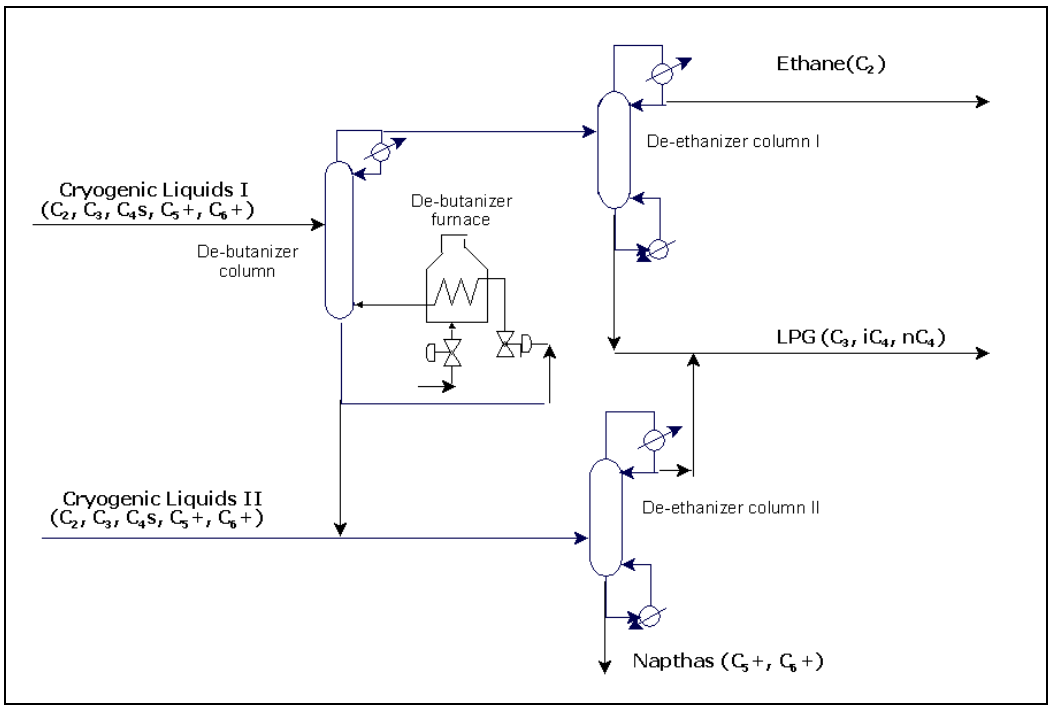

Figure 5.13 The sloppy arrangement for de-ethanizers and de-butanizer columns.

In the sloppy arrangement, to obtain the best match with the feed stages in terms of composition and temperature, and to minimize the mixing effects inside the columns, the feed stage were varied. The trends were found to be similar to the option of column feed location (i.e. Figure 5.11). No change is made for the feed stage for both columns as no significant improvement has been found. The composition profiles for the columns involved in this sloppy arrangement are shown in Figure 5.14. The hydraulic of the three columns seems to be reasonable without any hydraulic problems (e.g. flooding or entrainment). The energy consumption for this arrangement is increased when compared with base case. The increase is originated by the operation of two de-ethanizer columns instead of one de-ethanizer column in operation such as in base case, which yields to a reduced utilization of the capacity of these two columns with less flowrates through each

one. An additional reason is due to one of the two de-ethanizer columns, which is processing more heavy components than in the base case. Because of these reasons, the sloppy distillation arrangement applied to this case seems to be inefficient. Table 5.13 presents a summary of the results for this case. As mentioned, there is an increase in duty of 7.6% which reduces the MPCA in 10.6% despite a slight increase in LPG of 0.07%. Moreover, the presence of butanes content in the C_5+ product in 2.2% volume (bigger than the maximum available of 2% volume) is the major disadvantage of this distillation arrangement as this product will not be possible to sell under this composition.

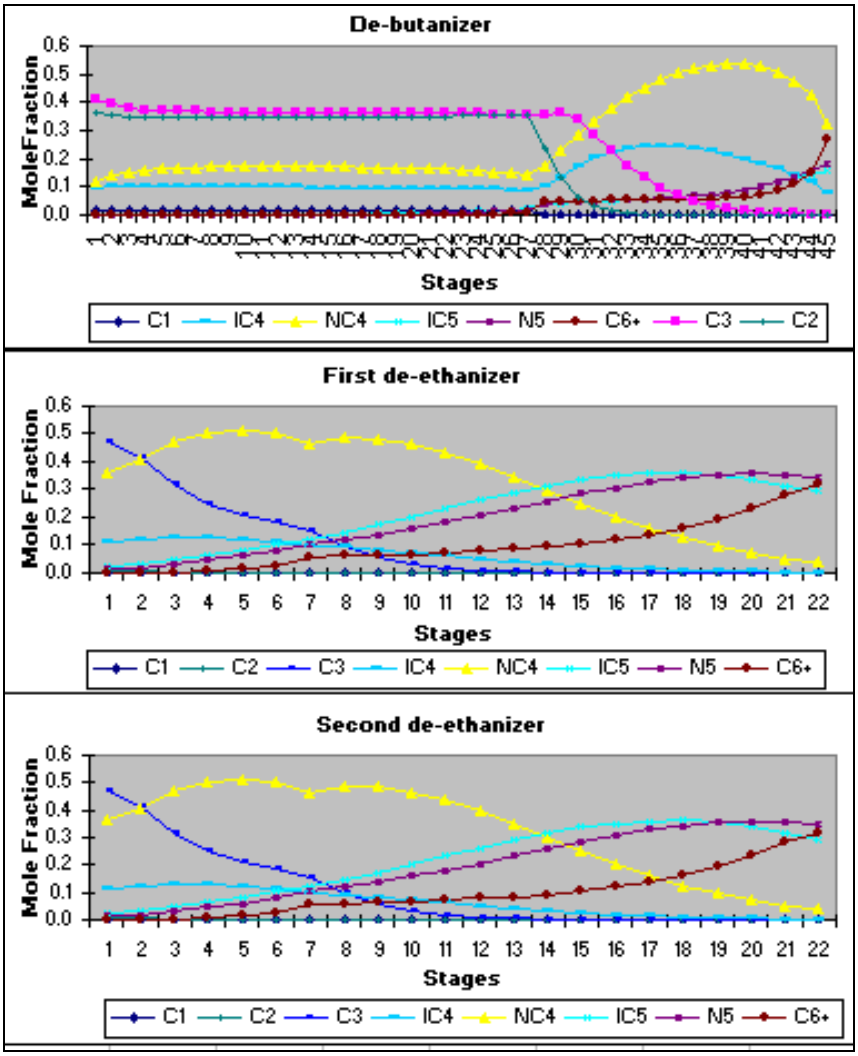

Figure 5.14 Composition profiles for de-ethanizer and de-butanizer in the sloppy arrangement.

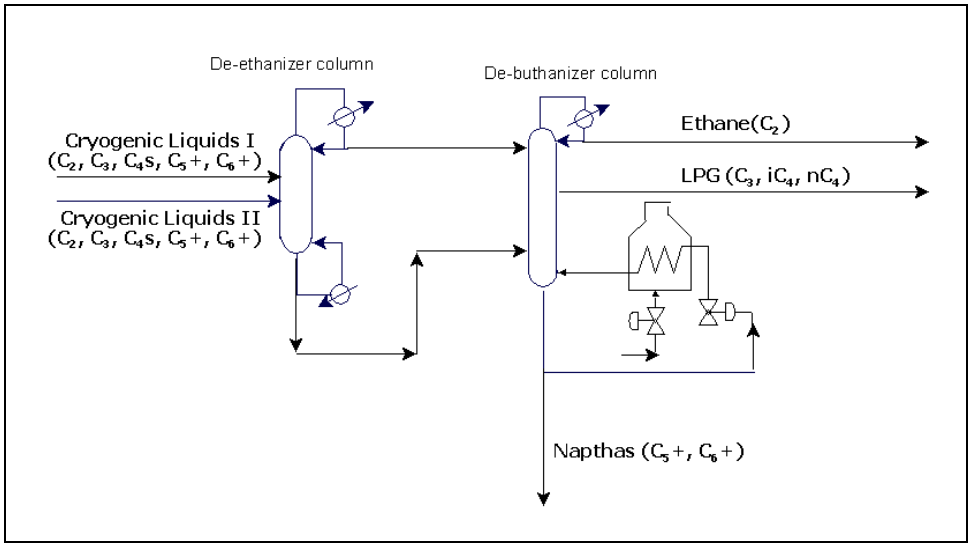

Figure 5.15 The prefractionator arrangement in de-ethanizer and de-butanizer columns.

In the prefractionator arrangement similar to the previous arrangement, stages for feed stage and the middle product stream were varied. No promising changes were found in the de-ethanizer column. In the debutanizer, the position of the feed stages coming from de-ethanizer, and the stages for the middle product extraction presented a significant repercussion in the mixing effects of the components. The final positions in de-butanizer were: feed stage number 30 for the stream coming from the bottom of de-ethanizer, feed stage number 5 for the stream coming from top of de-ethanizer, product stage number 16 for the C_3 extraction and product stage number 34 for the C_4s extraction. The composition profiles for the columns involved in the prefractionator arrangement are shown in Figure 5.16. No hydraulic problem (flooding or entrainment) was found in this arrangement, and its duty consumption is highly reduced when compared with the base case. The decrease is originated in the de-butanizer due to considerable reduction in the mixing effects inside this column which reduces the duty needed to perform the separation. Besides this and different from the sloppy case, the prefractionator operates with just one de-ethanizer column at full capacity and the de-butanizer column in sequence. This leads to more efficient use of energy in the system. Table 5.13 presents a summary of the results achieved for this case. There is an important reduction in duty of 43.6% as previously stated, which increases the MPCA in 27% despite a slight decrease in LPG of 1%. However, this table presents a significant drawback of the prefractionator arrangement which is the presence of butanes content in the C5+ product in 4.5% volume (bigger than the maximum available of 2% volume) as it will not be possible to sell this final product with this composition. It is important to remark that after several attempts in the de-butanizer by increasing the reflux ratio, increasing the reboiler duty, varying the feeds

and LPG product flowrates to reduce this butanes content in the C5+ product, it was not possible to be achieved. Although the prefractionator arrangement can be potentially energy efficient, this arrangement has not been considered, due to off-specification of one of final products. Nevertheless, it will depend on the economic trade-off, if the C_5+ product sales are much less than the energy saving that can be achieved, and this can offset the penalty by the out of specification product, the prefractionator arrangement may be considered a promising option.

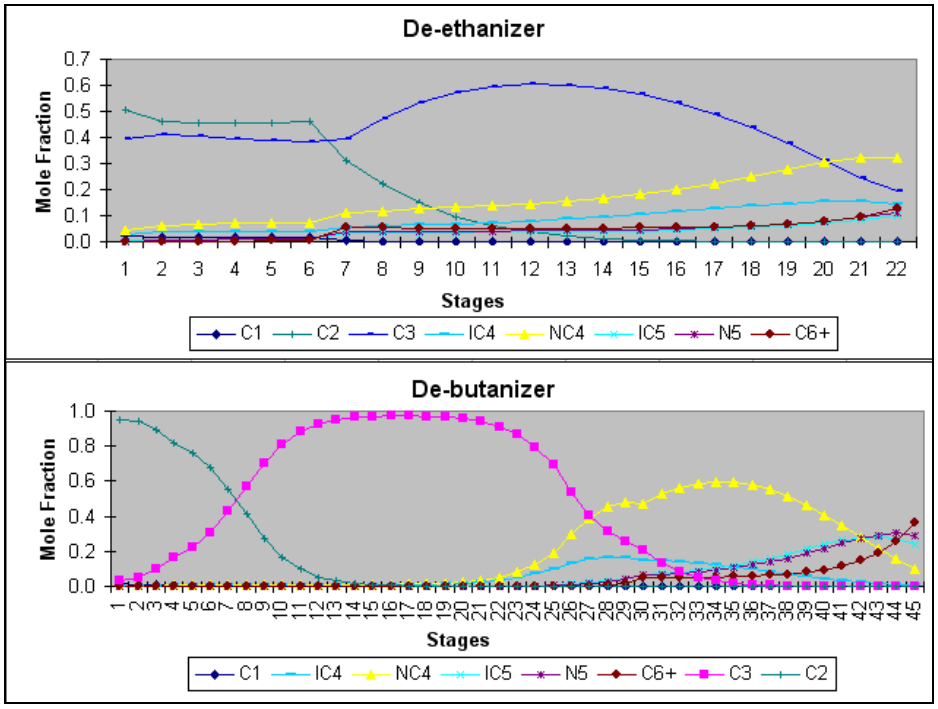

Figure 5.16 Composition profiles for de-ethanizer and de-butanizer in the prefractionator arrangement.

Distillation Arrangement	Failures	Variation MPCA, %	LPG recovery, %	Variation Duty, %
Base Case	None	0%	0%	0%
Sloppy 2 de-ethanizers and de-butanizer	Butanes content in C_5+ : 2.2% > 2% Maximum specified	-10.6	0.07%	7.6%
Prefractionator de-ethanizer and de-butanizer	Butanes content in C_5+ : 4.5% > 2% Maximum specified	27%	-1%	-43.6%

Table 5.13 Feasible distillation arrangements simulation results in the HCF plant.

Following this pre-screening SA, the potential structural factors towards increasing MPCA response were selected. These are summarized in Table 5.14.

Factor	Description
CONTINUOUS (OPERATIONAL VARIABLES)	
X_1	Column pressure of de-ethanizer
X_2	Column pressure of de-butanizer
X_3	Column pressure of first naphtha column
DISCRETE (STRUCTURAL CHANGES)	
X_4	Increase the number of stages (NT) in the de-ethanizer column
X_5	Increase the efficiency of the current stages (Eff) in the de-ethanizer column

Table 5.14 Feasible factors for the HCF plant.

5.3.2 Evaluation stage

Promising variables showed in Table 5.14 were assessed to understand its detailed impact on the response. The initial size of the problem is five factors, with at least two possible levels for each factor. In the diagnosis stage, there were no geometrical restrictions in the outputs for the searching space (geometrical form). As stated in Section 3.2.2 a first screening DOE was applied to identify the most important factors, after which it would be possible to fit a reduced model based on these. Details of the first part of the evaluation stage are described below, where the screening DOE was applied.

Preliminary screening: For this case, as the number of factors is five, which is not high, the first screening DOE was a full factorial design (Full FD) at two levels to minimise the confounding pattern. Matlab® was able to automatically find and generate a Full FD on two levels based on five factors, and the maximum number of runs (2^k) by using the function "ff2n". For this design the resolution level was V which confounding level, as explained in section 3.2.2, facilitates the analysis. The number of simulations achieved by the generated design was thirty-two. The complete data sheet given by Matlab®, including the confounding level, is shown in Table A.7 from the Appendix The generators were: 'X_1', 'X_2', 'X_3', 'X_4', and 'X_5', while the screening two-level Full FD obtained is visualised in Table A.8 from the Appendix in coded variables (levels for each factor) dictated by the design. Its corresponding natural variables (i.e. real value for each factor), according to the considerations made in the diagnosis stage, are presented in Table 5.15. Therefore, Table A.8 from the Appendix and Table 5.15 present the settings of each run. As assumed in section 3.1.2, interactions between three or more factors had a lower effect on the MaPr response, so these were not taken into consideration.

Factor	Units	Level (-1)	Level (+1)
X_1	Kg/cm^2	8	18.2
X_2	Kg/cm^2	8.5	16
X_3	Kg/cm^2	3.5	4.2
X_4	Number	20	30
X_5	%	58	78

Table 5.15 Natural variables for the 5 factors at 2 levels used in Full FD.

Thirty-two simulations set in this first screening design were run and the ANOVA for the simulation responses carried out in the statistic toolbox of Matlab 7.0.1. Table 5.16 presents the results for the main factors, as detailed in section 3.1.5, from which the last column shows the p-values for each factor (Prob>F). Factors X_2 and X_5 were observed to have a p-value < 0.005; therefore, as stated in Chapter 3, these are statistically significant as well as being the most important factors. On the other hand, factor X_1 is in the limit of p-value and was also defined as most important factor.

Factor	Sum of Squares	F test value	Prob>F p-value
X_1	1.05254	95.59	0
X_2	1.06116	96.38	0
X_3	0.05351	4.86	0.0365
X_4	0.10322	9.37	0.0051
X_5	0.31508	28.62	0
Error	0.28628		
Total	2.89115		

Table 5.16 ANOVA results for main factors HCF.

Table 5.17 shows the ANOVA results for the second-order interactions in which it is visualised that all the second order interactions yielded p-values larger than 0.005 hence, these interactions are not significantly important.

Interaction	Sum of Squares	F test value	Prob>F p-value
X_1 X_2	0.01204	1.98	0.1787
X_1 X_3	0.01291	2.12	0.1646
X_1 X_4	0.05706	9.38	0.0074
X_1 X_5	0.023	3.78	0.0697
X_2 X_3	0.02101	3.45	0.0817
X_2 X_4	0.00001	0	0.9769
X_2 X_5	0.01192	1.96	0.1807
X_3 X_4	0.00024	0.04	0.8462
X_3 X_5	0.01464	2.41	0.1405
X_4 X_5	0.03611	5.94	0.0269
Error	0.09736		
Total	2.89115		

Table 5.17 ANOVA results for 2nd order interactions.

In can be observed from Table 5.16 that the p-values of X_1, X_2 and X_5 laid in the case mentioned for ANOVA in Chapter 3 being set at zero value. Consequently, to properly rank them in their order of importance, and to verify the results provided by the ANOVA, the effect of each of the factors as a main or second-order interaction was estimated by equation 3.16. Once this was done, it was possible to rank the order of importance of the most important factors. Table 5.18 presents both the p-value for the most important factors and the effect of the factor for comparison purposes.

Factor	**Description**	**Prob>F p-value**	**Factor's Effect, Absolute units**
X_2	Column pressure of de-butanizer	0	0.364
X_1	Column pressure of de-ethanizer	0	-0.363
X_5	Efficiency of stages in de-ethanizer	0	0.198
X_4	Number of stages in de-ethanizer	0.0051	0.104
X_3	Column pressure of first naphtha column	0.0365	0.082

Table 5.18 Results of the analysis of variance for HCF screening of factors.

Figure 5.17 plots the effect of all the main factors and second-order interactions on MPCA estimated with equation 3.16 respectively on the y-axis of each of the main factors and interactions on the x-axis. It can be seen that factors X_2 (column pressure of

de-butanizer), X_1 (column pressure of de-ethanizer), and factor X_5 (efficiency of stages in de-ethanizer column) fall outside the limit established by the dashed line in the value of ± 0.1 for the effect on MPCA, and factor X_4 falls on it. Therefore, this proves what ANOVA found, namely that these factors are really the most important factors for the response MPCA, while the remaining main factors do not produce any significant effect on MPCA.

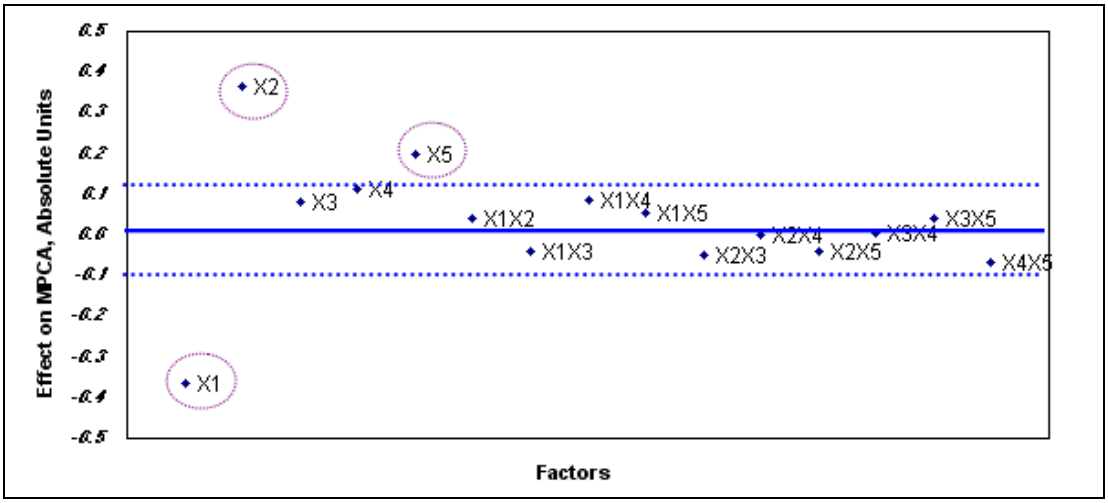

Figure 5.17 Effect of factors on MPCA response for HCF plant.

The Retrofit Design Approach continues with the second part of the evaluation stage, in which RSM was applied based on the previously identified most important factors to obtain a reduced model.

Application of RSM: As proposed by the approach (section 3.2.2) a Central Composite Design (CCD) was built for the three most important factors found. This is shown in Table 5.19 with the star points placed at the α values calculated as referred to in Chapter 3:

$$\alpha = \pm\left(NumberOfFactors\right)^{1/4} = \pm(3)^{1/4} = \pm 1.316$$

The major considerations made in the RSM for the CCD limits were:

- Factor X_2: The maximum limit showed in Table A.6 of the Appendix was set as the coded level +1.316, and the minimum limit was set as the coded level -1.316. The rest of levels in the design were kept as in the screening DOE.

- Factor X_1: The maximum limit showed in Table A.6 of the Appendix was set as the coded level +1.316, and the minimum limit was set for the coded level -1.316. The rest of levels in the design were kept as in the screening DOE.
- Factor X_5: The maximum value offered in the market for this class of column (85%) was set as the coded level of +1.316. For the coded level of -1.316, the current efficiency was taken (58%). The complementary levels in the design were ranged between these two limits.

Table 5.19 lists both the coded variables (i.e. levels for each factor) dictated by the design and its corresponding natural variables (i.e. real value for the factor) at each run.

Number of simulation	Coded Variables			Natural Variables		
	X_1 absolute units	X_2 absolute units	X_5 absolute units	X_1 kg/cm^2	X_2 Kg/cm^2	X_5 Fraction
1	-1	-1	-1	8	9	0.65
2	-1	-1	1	8	9	0.78
3	-1	1	-1	8	15.0	0.65
4	-1	1	1	8	15.0	0.78
5	1	-1	-1	18.2	9	0.65
6	1	-1	1	18.2	9	0.78
7	1	1	-1	18.2	15.0	0.65
8	1	1	1	18.2	15.0	0.78
9	1.316	0	0	19.4	11.2	0.72
10	-1.316	0	0	5.9	11.2	0.72
11	0	1.316	0	14.5	16.3	0.72
12	0	-1.316	0	14.5	8.3	0.72
13	0	0	1.316	14.5	11.2	0.85
14	0	0	-1.316	14.5	11.2	0.58
15	0	0	0	14.5	11.2	0.72

Table 5.19 CCD applied to HCF.

Fifteen simulations were run following this CCD circumscribed design. The MPCA responses were obtained and the linear least squares (LLS) method carried out in Matlab for fitting the corresponding model. The best fit model with a RMSE of 0.93% is shown in the form MPCA as a function of factors X_2, X_1 and X_5, which are coded (ranged from 0 to 1.316) as follows:

$$MPCA = 0.93 + 0.05\,X_1 - 0.01X_2 - 0.07X_5 - 0.03\,X_1^{\,2} - 0.04X_2^{\,2} + 0.03X_5^{\,2} \qquad (5.3)$$

The RMSE indicated an acceptable level of reproduction for the MPCA response. This was verified with the residual plot presented in Figure 5.18.

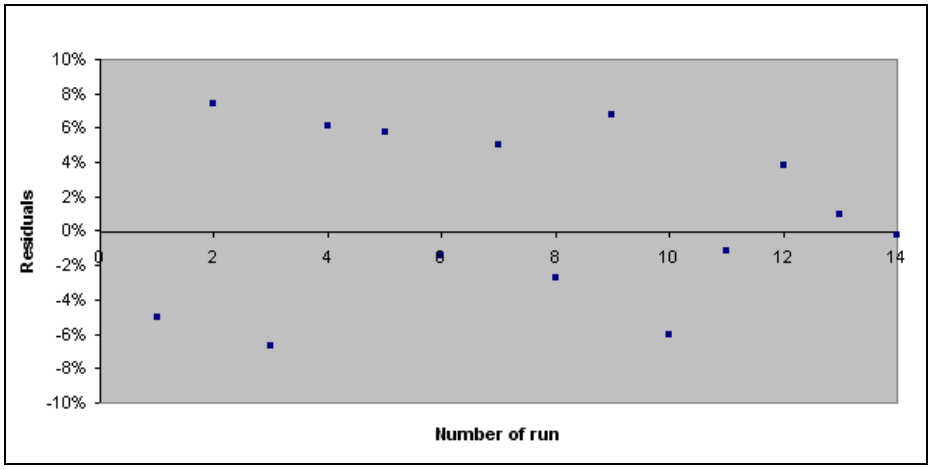

Figure 5.18 Plot of residuals for the best fit model in HCF plant.

This plot shows that the residuals for the model in all the 14 runs requested by the CCD are randomly distributed and have values of less than 8%; as commented in section 3.1.4, this verifies the reliability of the response surface model to predict the simulation response MPCA.

5.3.3 Optimisation stage

1. Optimize RSM model: To avoid operational problems (ethane compressors'surge and columns' flooding), the optimisation was carried out within normal operating limits (i.e. +1 and -1 levels) for the factors X_1 and X_2. The factor X_5 was also set in the +1 and -1 range to take into account the difficulties in achieving the efficiency that suppliers offer to work under current conditions. It was possible to maximize the best fit model based on a NLP optimisation. This was directly done by varying the three variables simultaneously and using the solver in Excel®. As detailed in section 3.2.2, to ensure reliability and robustness in the solutions found, and thus globality, it was started from different points for the three factors to start from -1, 0, and +1 in combinations respectively. Similar to the previous case I, there were no computational difficulties found, as the solver could maximise the MPCA in seconds; however, the starting point combinations yielded

different maximal points. Thus, it was necessary to select the optimum point of the solutions reached from different sets of starting points. The selection criterion was also the maximum value of MPCA. The final optimum result was achieved with the coded and corresponding natural variables presented in Table 5.20. Additionally, as suggested in the approach, and as the fit model RMSE was not too low, a set of confirmatory runs were performed around the maximum found with the reduced model optimized to generate feasible design (i.e. that the maximum found was a real maximum). The results are exposed as the percentage of difference between the reduced model and the simulation in the last column of Table 5.20.

Coded variables			**Natural variables**			**Difference**
X_1	X_2	X_5	X_1 kg/cm^2	X_2 Kg/cm^2	X_5 Fraction	**Reduced model-Simulation**
-1	1	1	8	15	0.78	0.062%

Table 5.20 Coded and natural variables for optimal results.

The conditions of the optimum case are presented in Table 5.21 as main product compositions, total hot and cold utility requirements, improvements in LPG recovery and in MPCA* (normalised MPCA). Figure 5.19 schematizes the flowsheet of the plant with the base case and the optimum case data.

For the MPCA*, the results show that there is an increase of 4.7% in the optimum case, and this increase reached was mainly due to: the total hot utility consumption (with a reduction in 4.4%), the cold utility consumption (with a reduction in -1.8%) and the LPG recovery (with an increase in 1%). In general, as stated in the diagnosis stage, the followings can be observed for these indicators.

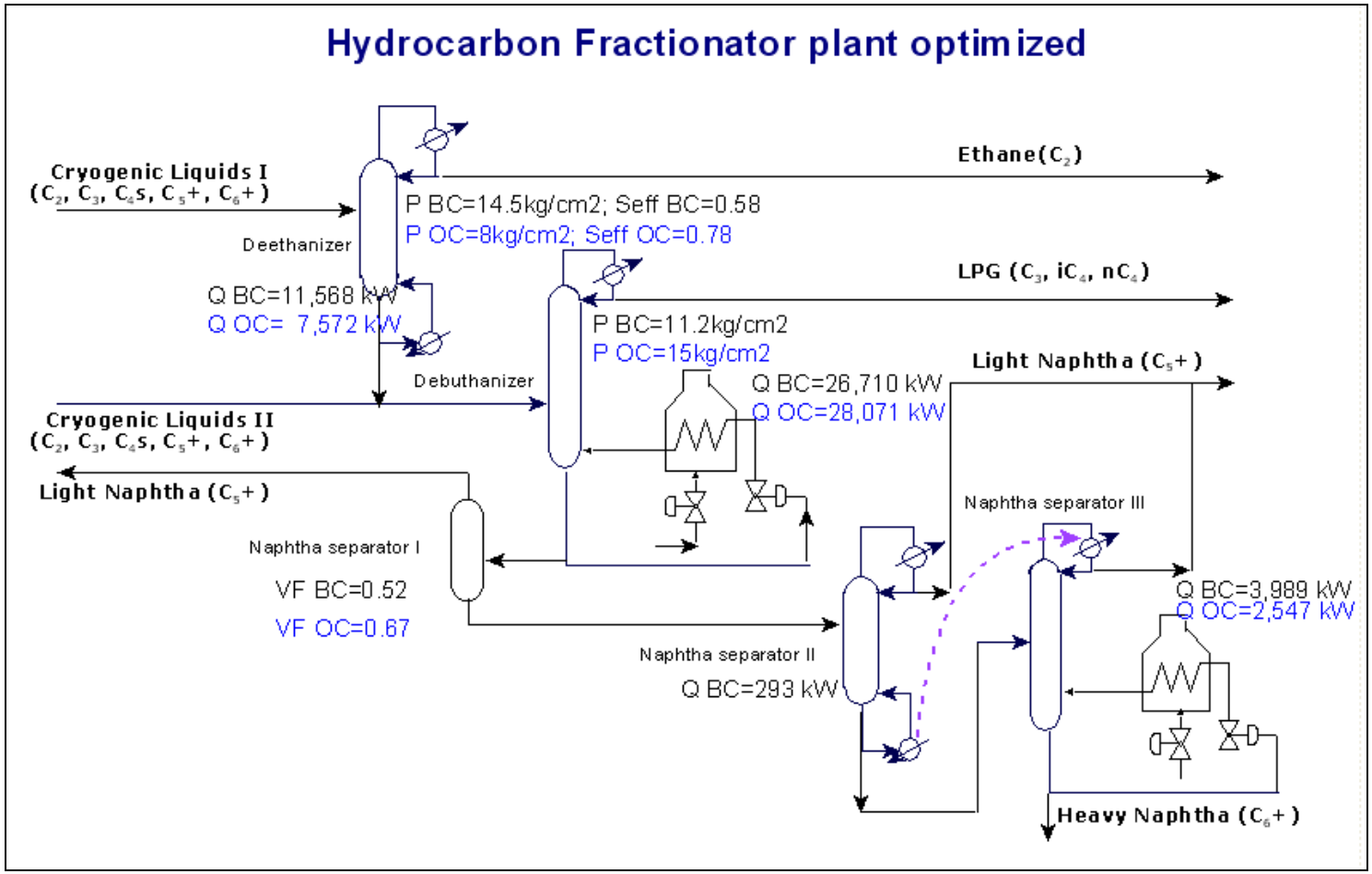

BC=Base Case; OC = Optimum case.

Figure 5.19 Optimal results vs. base case comparation for HCF.

Streams	Ethane gas			LPG			C_5+		
Molar Fraction	BC	OC	% Diff.	BC	OC	% Diff.	BC	OC	% Diff.
C_1	0.0478	0.0543	**13**	0	0	**0**	0	0	**0**
C_2	0.9329	0.9386	**0.61**	0.0129	0.0083	**-36**	0	0	**0**
C_3	0.0193	0.0071	**-63**	0.6265	0.6313	**0.8**	0	0	**0**
NC_4	0	0	**0**	0.2484	0.2482	**-0.1**	0.0095	0.0090	**-5**
IC_4	0	0	**0**	0.1122	0.1122	**0**	0.0003	0.0003	**0**
NC_5	0	0	**0**	0	0	**0**	0.2736	0.2727	**-3**
IC_5	0	0	**0**	0	0	**0**	0.2042	0.2053	**1**
C_6+	0	0	**0**	0	0	**0**	0.5124	0.5127	**0.1**
Rate, kg/s	10.23	10.23	**0**	29.15	29.15	**0**	18.89	18.89	**0**
T, ºC	-15.4	-33.3	**117**	30.7	30.7	**0**	38	38	**0**
P, Kg/cm²	14.5	8	**-45**	7.2	7.2	**0**	8.6	8.6	**0**
Total hot utility, kW							40.6	38.9	**-4.4**
Total cold utility, kW							39.0	38.3	**-1.8**
LPG Recovery, %							90.5	91.5	**1**
MPCA, absolute units							1	1.047	**4.7**

BC=Base Case; OC = Optimum case

Table 5.21 Optimal results vs. base case comparation for HCF.

Total hot utility consumption: When moving from the base-case to the optimum-case, a reduction for hot utility requirement is observed. This is mainly due to a decrease in the reboiler duty of the de-ethanizer. It has been explained in Figures 5.4 and 5.5 that the low pressure set in this column for the optimum case increases relative volatility (α) for the light (C_2) and heavy (C_3) components, which allows an easier separation and, thus, requires less duty. This separation is facilitated with the higher efficiency of the trays for the optimum case. Finally, as it was explained in Figures 5.6, 5.7 and 5.8, the high pressure in the de-butanizer column results in a reduction in liquid towards the first and second naphtha columns yielding to a reduction in the energy consumption in those columns.

Total cold utility consumption: This indicator is reduced for the optimum-case. This is basically a result of the same reasons for the hot utility reduction. An easy separation in the de-ethanizer reduces the energy needed to carry out the separation, and the reduction of liquid to be fractionated in the naphthas' columns also yields to a reduction in energy needed to achieve the separation.

LPG recovery: This increase is mainly due to the higher trays' efficiency in the de-ethanizer column, which facilitates the separation of the components inside the column resulting in a richer in ethane product from the top.

2. Optimising the HEN: as referred in the description of this case study, this process only contains one heat integrated arrangement, which is the heat recovery between the reboiler of the first naphtha column and a first condenser of the second naphtha column. On the other hand, the system has a considerable number of heat sinks and sources and therefore, HEN retrofit must be addressed.

It was stated in Section 5.1.1 that the de-propanizer column seldom operates to produce coolant propane, and for that reason it was not taken into account in the previous sections. However, it was also mentioned that its reboilers operate with LPS at reduced capacity. This implies that the operation of those reboilers affects the MPCA and because of that, those were considered in the HEN to be retrofit.

Operating conditions are not the same with base case after adopting optimal solutions found in the previous step, thus new ET, CC, GCC and pinch point need to be found.

The energy targets, CC and GCC have been worked in SPRINT® for the optimum scheme presented in Tables 5.20 and 5.21 with a ΔTmin of 10 ºC. Figures 5.20 and 5.21 show the currents GCC, and HEN structure; the HEN data report for the starting scheme is given in Table 5.22, and the utility targets are hot utility target of 37,054 kW and cold utility target of 27,152 kW.

Note that these are significatively lower than the targets of the base case in about 12% for the hot target and 18% for the cold target (i.e. hot utility of 42MW and cold utility of 33MW respectively in the base case). The pinch point for this optimized scheme is located at 65.10 ºC slightly higher than the base case of 62.8 ºC.

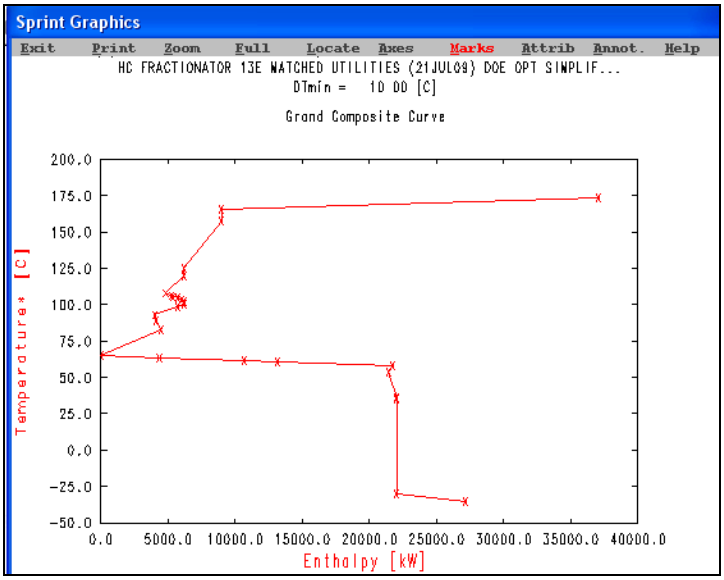

Figure 5.20 Current GCC for HCF plant at optimized scheme.

The energy recovery estimated with this data from the CC at ΔTmin of 10 ºC was found to be 6.9 MW. An interesting point because it implies a big energy saving potential, is that the total hot utility used estimated is 45.383 MW, which is about 22% more than the hot utility target and the cold utility used has a duty of 35.481 MW that is about 30% more than the respective target.

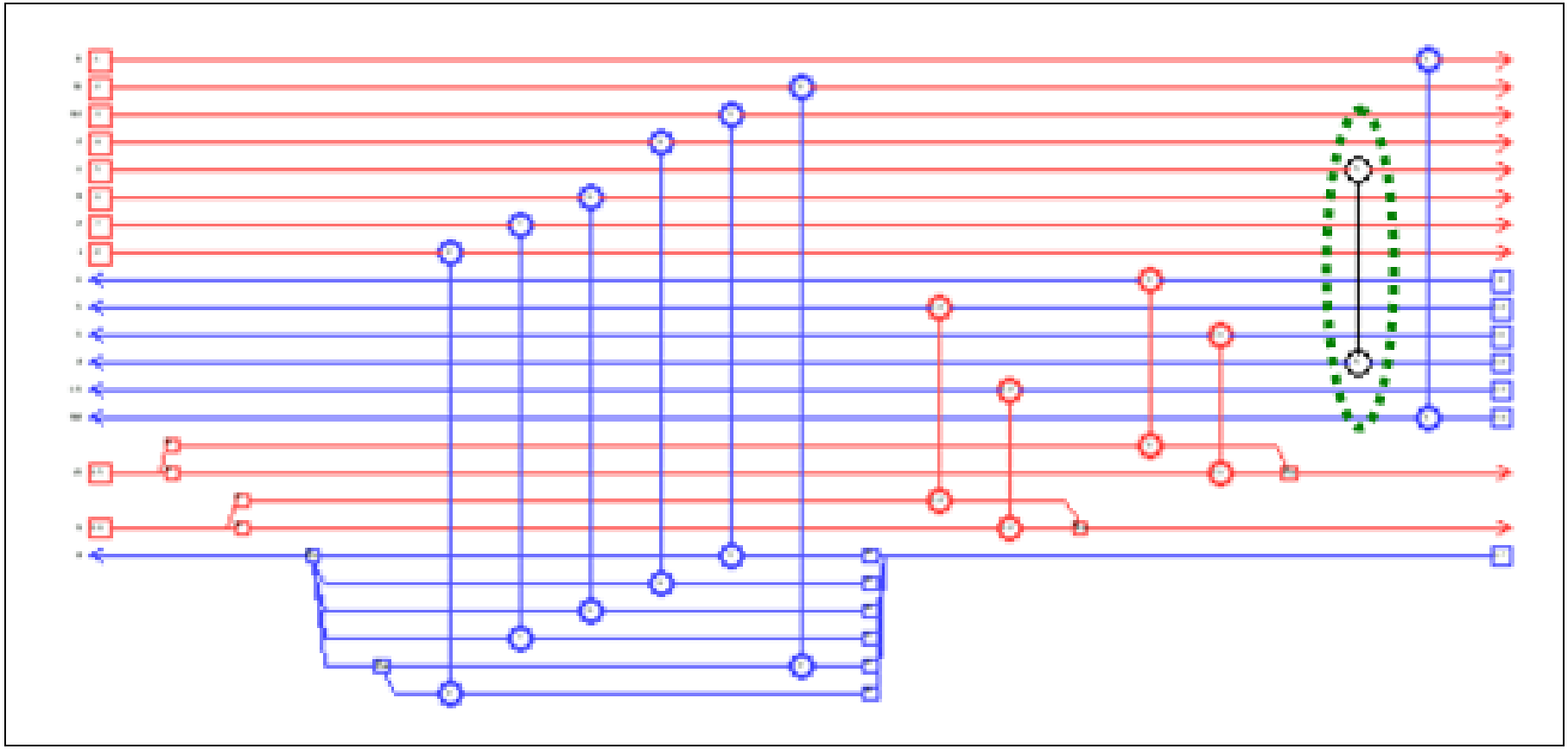

Figure 5.21 Existing HEN for HCF plant at optimized scheme (topology).

Number of Heat Exchanger	Used area from SPRINT®, m^2	Heat transfer coefficient from SPRINT®, kW/($^oC.m^2$)	Duty, MW
1	738	0.5	5.145
2	1,251	0.5	22.610
3	104	0.5	3.121
4	12	0.7	0.329
5	21	1	0.293
6	62	0.5	2.421
7	116	0.5	1.793
8	2	0.7	0.062
9	243	0.5	7.572
10	497	0.5	28.070
11	210	0.5	6.945
12	21	0.5	2.800
Total	**3,277**		**81.161**

Table 5.22 Existing HEN for HCF plant at optimized scheme (report data).

In Figure 5.21, the heat exchanger with a dashed circle is the existing one, which corresponds to the number five in Table 5.22, and it transfers 0.293 MW of process-to-process heat. If this data is compared with the energy recovery potential for the sytem (i.e. 6.904 MW), about 4% of its available energy recovery is only utilised. Hence, there is large heat integration potential in this plant. This fact strongly recommends carrying out a HEN retrofit in this plant to improve its energy recovery.

The cross pinch report is presented in Table 5.23 from SPRINT® and this shows that five exchangers transfer heat across the pinch in total of 7.371 MW.

Number of Heat Exchanger	Duty, MW
3	3.121
6	2.421
7	0.701
8	0.035
9	0.989
11	0.102
Total	**7.371**

Table 5.23 Cross pinch report for existing HEN in HCF plant at optimized scheme.

Following to the identification of the current HEN performance under the optimal conditions, the next step was to search the possible cost-effective options to be considered for the retrofit.

First at all, the GCC showed a big energy saving potential due to a small energy recovery, and to an over-consumption of hot and cold utilities of about 22% in hot utility energy used and of about 30% in cold utiility more than the respective target. As a consequence of that, the preliminar exploration of heat recovery systems was considered at this point looking for potential options to yield to improvements in the HCF; two possibilities were analysed below.

Heat pumping. Possibility to include a heat pump in the distillation columns is considered. The heat pump can be used in a distillation column to receive heat from a low temperature stream, raise it with an auxiliary device to a higher temperature stream which can then provide heat to the process. Two main considerations have been stated by Smith (Smith, 2005) for the heat pump device: the first is that the integration of the heat pump across the pinch is the most appropriate manner to yield a saving as this pumps heat from the heat source to the heat sink, and the second is that the temperature lift should be less than 25 ºC. The pinch point for the base case was found to be 62.8 ºC, by inspecting the temperature profiles of all the columns in the system, the only column that operates across this pinch point is the de-butanizer column, therefore that was considered for the heat pump. The temperature lift in de-butanizer column is about 102ºC which is bigger than the 25ºC suggested. Nevertheless this fact, the simulation was set to test this option and its results are given in Table 5.24. The heat pumping illustrated in Figure 5.22 is not considered for further study, due to negative impact on MPCA.

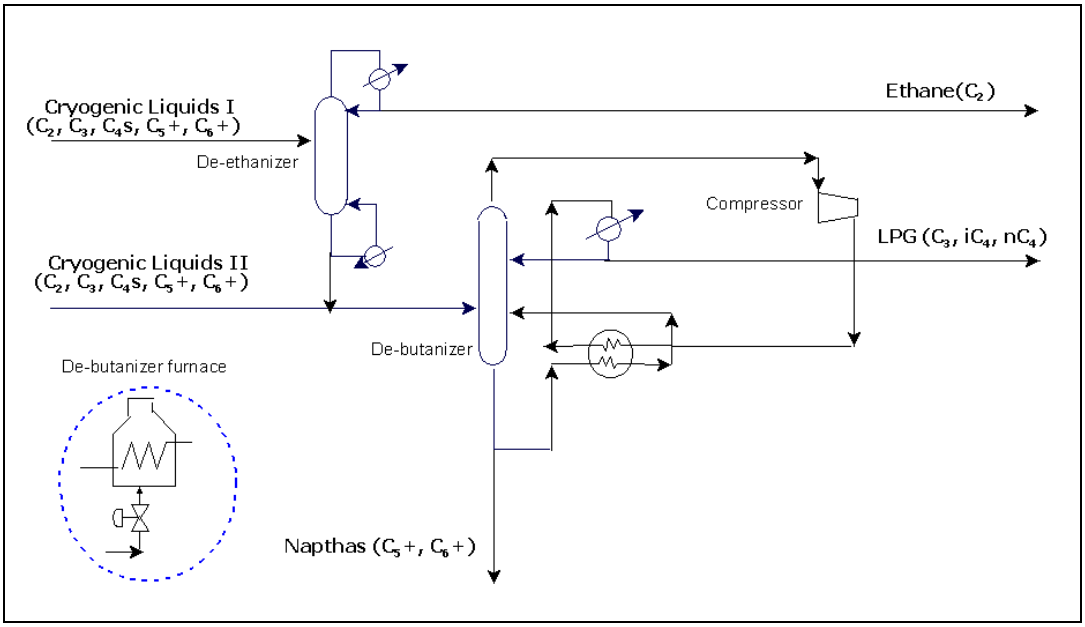

Figure 5.22 Heat pump in de-butanizer.

Description	Units	Values
Temperature of the top vapours of de-butanizer	ºC	55
Power requested by compressor	MW	38.2
De-butanizer reboiler duty	MW	26.7
Temperature of the bottom liquids of de-butanizer	ºC	157
De-butanizer condensers duty	MW	35.5
Variation in MPCA	**%**	**-108**

Table 5.24 Heat pump device in the column de-butanizer.

Waste energy recovery. The option regarding the possibility of using the energy contained in the tail gas of the furnace reboiler of de-butanizer column was explored.

The option for the de-butanizer column is schematized in Figure 5.23. The heat available for recovery in the tail gas of the de-butanizer furnace at current conditions was estimated able to produce 0.007 kg/s of low pressure steam (LPS) at 4.5 kg/cm2 and 155ºC, which can be used either heating up a cold stream or generating electricity. Savings from the first case is 16 kW which is estimated as 3,872 £·yr^{-1} while additional piping and heat exchanger are needed. On the other hand, the electricity to be generated is about 16 kW which is estimated as 4,800 £.yr-^{1}. In consideration of generating this electricity, an additional heat exchanger on the tail gas, a steam turbine to generate electricity and piping are needed. Table 5.25 shows the capital cost estimated by equation (5.2) and the costs comprised in Timmerhaus et al. (Timmerhaus et al., 2003) of the equipment referred.

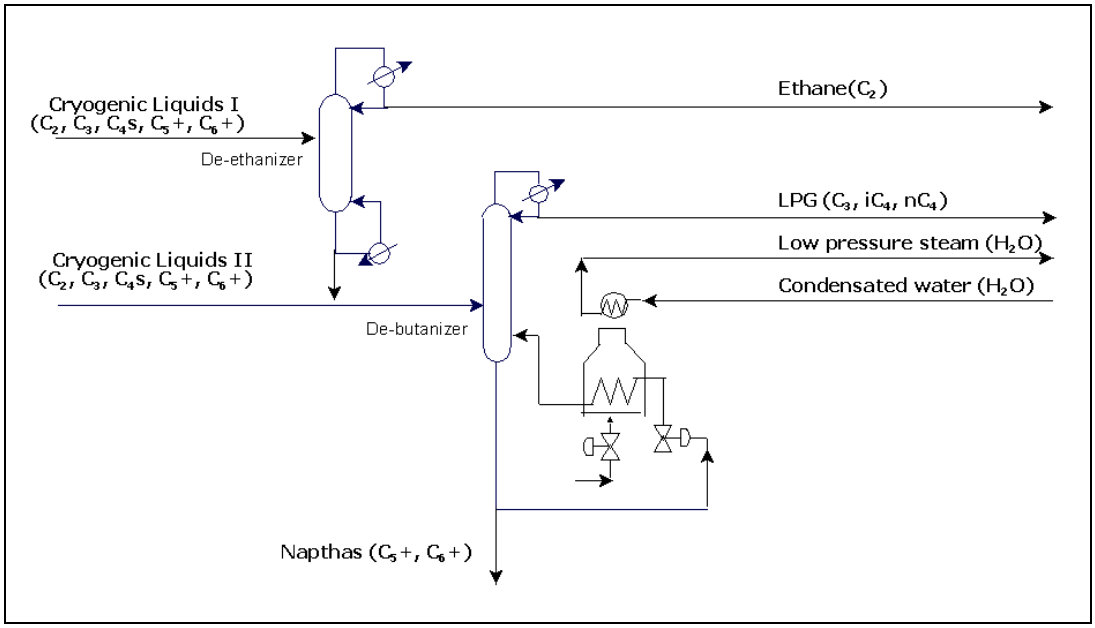

Figure 5.23 The tail gas recovery arrangement in de-butanizer furnace.

Item	Features	Sizing and capacities	Capital cost estimated, MM£/Yr
1. Cold stream heating up.			
Heat exchanger in tail gas	Purchased cost of fixed-tube-sheet heat exchangers with 0.019-m (3/4-in.) OD x 0.0254-m (1-in.) square pitch and 4.88-m or 6.10-m (16- or 20-ft) bundles and carbon-steel shell operating at 1035 kPa (150 psia)	Surface area: $10m^2$	0.00125
Heat exchanger in heating point	Purchased cost of fixed-tube-sheet heat exchangers with 0.019-m (3/4-in.) OD x 0.0254-m (1-in.) square pitch and 4.88-m or 6.10-m (16- or 20-ft) bundles and carbon-steel shell operating at 1035 kPa (150 psia)	Surface area: 10 m^2	0.00125
Pipe	Purchased cost of cast-iron pipe, bell and spigot pipe, 1035-1725 kPa	Diameter: 0.1524 m Length: 40 m	0.0004
Installation arrangement	Heat exchangers arrangements plus installation costs	40% of purchase cost	0.0012
Totals			**0.0041**
2. Electricity generation.			
Heat exchanger in tail gas	Purchased cost of fixed-tube-sheet heat exchangers with 0.019-m (3/4-in.) OD x 0.0254-m (1-in.) square pitch and 4.88-m or 6.10-m (16- or 20-ft) bundles and carbon-steel shell operating at 1035 kPa (150 psia)	Surface area: 10 m^2	0.00125
Electricity generator	Purchased cost of variable-speed drives, includes handwheel control with a built-in indicator and TEFC motor 1.5/1 Speed variation	Power capacity: 25 kW	0.0014
Turbine	Purchased cost of turbine and internal combustion engine drivers 12-35, steam turbine	Power capacity: 25 kW	0.0012
Pipe	Purchased cost of cast-iron pipe, bell and spigot pipe, 1035-1725 kPa	Diameter: 0.1524 m Length: 10 m	0.00010
Installation arrangement	Heat exchanger, electricity generator and turbine arrangements plus installation costs	40% of purchase cost	0.0015
Totals			**0.0055**

Table 5.25 Calculation basis for each costing item in tail gas heat recovery (Timmerhaus et al., 2003).

Overall results are shown in Table 5.26 for the two possibilities mentioned to use the LPS that can be generated from the energy recovered in the tail gas.

Option	Sales, MM£/Yr	Capital Costs, MM£/Yr	Net income, MM£/Yr
Heating a cold stream	0.0038	0.0041	-0.0003
Electricity generation	0.0048	0.0055	-0.0007

Table 5.26 Net income apprasing for two available options (Timmerhaus et al., 2003).

Therefore, these options are not considered in the evaluation stage.

HEN retrofit. Following to this the HEN was analysed for retrofit. In chapter 2 it was also exposed that there are two alternative ways to perform a retrofit design: -"retrofit by inspection" or- "retrofit by automated design". Both alternatives were explored in this study at minimising total cost with ΔT min of 10 ºC.

1. Retrofit by inspection: HEs 3, 6, 7, 8, 9 and 11 that have heat transfer across the pinch were examined.

Structural changes: The sequence to test each change in the HEN was set favouring the re-using of the existing equipment, in this manner the order of priority to remove existing cross-pinch exchangers was by re-sequencing, by re-piping, and in the final place by adding a new match. The introduction of new utility paths and splitting streams were also explored. Finally the HEs' duty was also let to be re-distributed. Additionally, the practical constraints were set as:

Maximum number of re-sequencing: 2
Maximum number of re-piping: 4
Maximum number for splitting streams: 2
Maximum number of new match: 2

The retrofit design by inspection was carried out based on the highest cost-benefit provided by each movement. The changes were done one by one sequentially in the SPRINT® software. It was started with the HE number 9, which has the highest duty consumption across the pinch (7.5 MW). There are no possibilities to resequence it as no additional HEs are set on its hot and cold streams. Next it was searched for repiping, and here, stream splitting similarly to the introduction of new utility matches were also explored. This procedure was applied to the HEs 11, 3, 6, and 7 subsequently (i.e. in the order of duty). Finally the addition of a new match was studied in the current HEN. Subsequent combinations of promising options in search of the best choices were made. Once the promising schemes were selected, a final NLP optimisation was performed in

the software to adjust its duty for improving the energy recovery (i.e. distributing flowrates and duties).

Two final promising retrofit options obtained by inspection are both repiping, and its topology is shown in Figures 5.24 and 5.25.

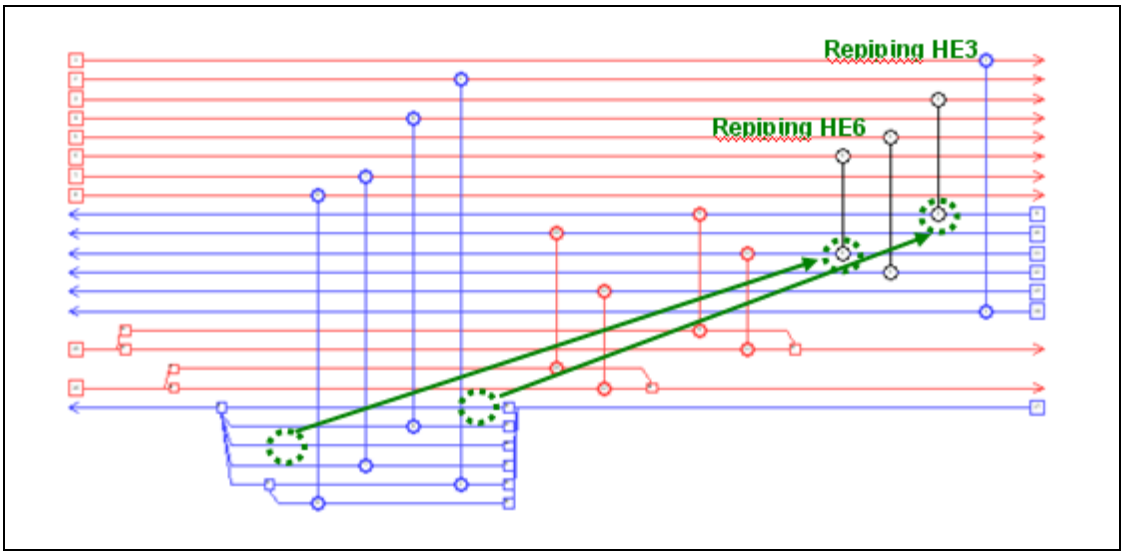

Figure 5.24 Modified HEN option1 for HCF plant at optimized scheme (topology).

Figure 5.24 shows the first option which includes: 1) the HE number 3 -the condenser of the first separator naphtha tank- repiped from a cooling water stream to pre-heat the bottoms of de-ethanizer column; and 2) the HE number 6 –the second condenser of the second naphtha column- repiped from a cooling water stream to pre-heat the bottoms of the de-propanizer column.

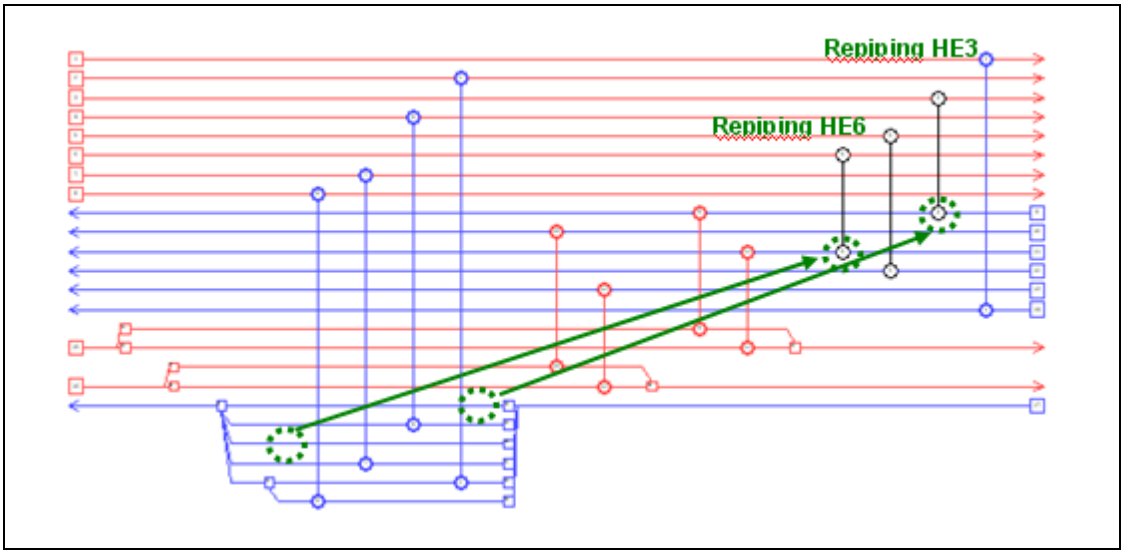

Figure 5.25 Modified HEN option 2 for HCF plant at optimized scheme (topology).

Paralelly, by studying the plot plan it was identified that the HE number 3 can be repiped to pre-heat the bottoms of de-propanizer column instead of pre-heating the bottoms of the de-ethanizer with similar energy savings. This second option however has lower piping costs than the first one as the distance between HE number 3 and the de-propanizer is closer than with the de-ethanizer. Figure 5.25 presents the stated second option which comprises: 1) the HE number 3 -the condenser of the first separator naphtha tank- repiped from a cooling water stream to pre-heat the bottoms of de-propanizer column; and 2) the HE number 6 –the second condenser of the second naphtha column- repiped from a cooling water stream to pre-heat the bottoms of the de-propanizer column.

Table 5.27 shows the capital cost estimated by equation (5.3) and the costs in Timmerhaus et al. (Timmerhaus et al., 2003) of the two best retrofit options obtained by inspection. As stated in the section 5.1.3, the piping and arrangement costs associated were calculated as 50% of the HE capital cost.

Item	Features	Sizing and capacities	Capital cost estimated, MM£/Yr
1. HEN retrofit design by inspection option 1.			
Heat exchanger 3 additional area	Purchased cost of fixed-tube-sheet heat exchangers with 0.019-m (3/4-in.) OD x 0.0254-m (1-in.) square pitch and 4.88-m or 6.10-m (16- or 20-ft) bundles and carbon-steel shell operating at 1035 kPa (150 psia)	Surface area: 78m^2	0.038
Heat exchanger 6 additional area	Purchased cost of fixed-tube-sheet heat exchangers with 0.019-m (3/4-in.) OD x 0.0254-m (1-in.) square pitch and 4.88-m or 6.10-m (16- or 20-ft) bundles and carbon-steel shell operating at 1035 kPa (150 psia)	Surface area: 74 m^2	0.036
Pipe	Purchased cost of cast-iron pipe, bell and spigot pipe, 1035-1725 kPa	Diameter: 0.33 m Length: 60 m	0.173
Installation arrangement	Heat exchangers arrangements plus installation costs	50% of purchase cost	0.124
Totals			**0.371**
2. HEN retrofit design by inspection option 2.			
Heat exchanger 3 additional area	Purchased cost of fixed-tube-sheet heat exchangers with 0.019-m (3/4-in.) OD x 0.0254-m (1-in.) square pitch and 4.88-m or 6.10-m (16- or 20-ft) bundles and carbon-steel shell operating at 1035 kPa (150 psia)	Surface area: 112m^2	0.048
Heat exchanger 6 additional area	Purchased cost of fixed-tube-sheet heat exchangers with 0.019-m (3/4-in.) OD x 0.0254-m (1-in.) square pitch and 4.88-m or 6.10-m (16- or 20-ft) bundles and carbon-steel shell operating at 1035 kPa (150 psia)	Surface area: 180 m^2	0.067
Pipe	Purchased cost of cast-iron pipe, bell and spigot pipe, 1035-1725 kPa	Diameter: 0.33 m Length: 90 m	0.260
Installation arrangement	Heat exchangers arrangements plus installation costs	50% of purchase cost	0.188
Totals			**0.563**

Table 5.27 Calculation basis for each HEN best retrofit design option (Timmerhaus et al., 2003).

Table 5.28 presents the results for these two HEN retrofit best options achieved by inspection; the initial HEN is also included for comparison purposes.

Concept	Current HEN no retrofit design	HEN Retrofit design by inspection 1	HEN Retrofit design by inspection 2
New Area, m^2	0	152	291
Number of matches eliminated	0	0	0
Number of re-sequencings	0	0	0
Number of re-pipings	0	2	2
Number of new matches	0	0	0
ACC, MM£/Yr	0.234	0.605	0.797
Energy Reductions, MM£/Yr	0.6	1.6	1.6
% improvement MPCA	4.7	13.4	12.9
Payback period, Yr	0.438	0.377	0.497
Potential CO_2 Tax Reductions, MM£/Yr	0.4	1.1	1.1

Table 5.28 HEN retrofit design by inspection for HCF plant at optimized condition.

The previous results reveal that the performance of the current HEN at optimal conditions has been significatively improved from base case to 4.7%; from there, the modified HEN 1 achieved the highest improvement of 13.4% followed by the modified HEN 2 with 12.9%. The main reason is the reduction in LPS consumption due to two repiped HE.

2.Retrofit by automated design: SA was selected in this part to find optimal solutions within a reasonable solving time. It was performed within the SPRINT® with SA parameters given in Tables 5.29 and 5.30.

Annealing parameters	Set value
Random number generator seed	1
Initial annealing “temperature”	100,000,000
Final annealing “temperature”	$1.00000x10^{-05}$
Markov chain length	30
Maximum iteration	25,000
Maximum consecutive failed chains	10
Maximum unsuccessfull moves	300
Cooling parameter	0.01
Move acceptance criteria	Metropolis

Table 5.29 Parameters used in the annealing algorithm.

Heat exchanger changes		Bypass changes	
Add heat exchanger	0.01	Add bypass	0.34
Delete heat exchanger	0.01	Add split	0.35
Delete heat spare exchanger	0.01	Delete bypass	0.2
Modify heat duty	0.5	Modify bypass	0.1
Reconfigure heat exchanger	0.47	Delete spare mixer	0.01
Change class		**Heat exchanger reconfiguration**	
Heat exchanger change	0.33	Resequence heat exchanger	0.5
Bypass change	0.33	Repipe heat exchanger	0.5
Utility temperature change	0.34		

Table 5.30 Structural changes probabilities set in the Move Probabilities editor.

The annealing history was observed and the results for each one of three classes of changes were saved, then the best option was selected.

The optimum solution gained by the SA based design, which meets all the constraints, is shown in Figure 5.26 below.

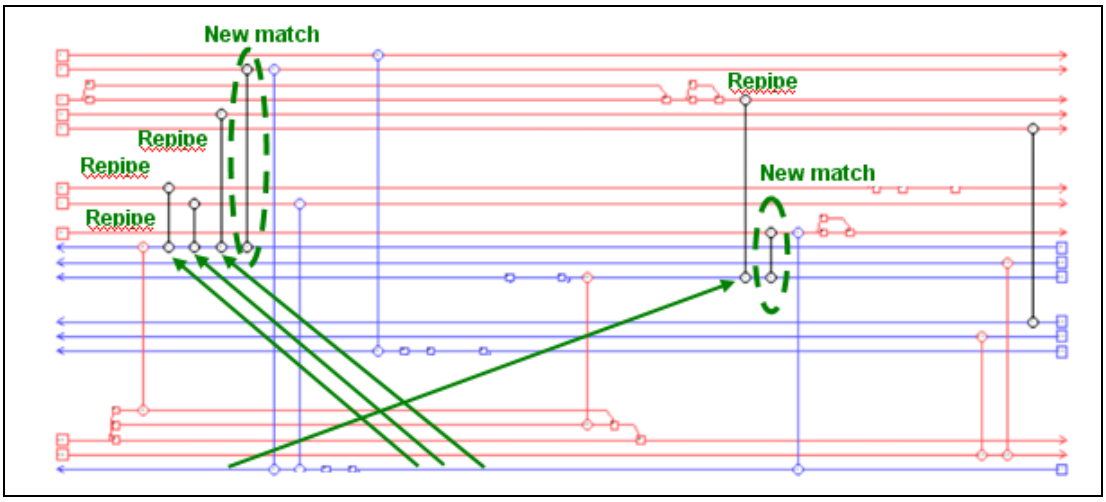

Figure 5.26 Modified HEN in SA retrofit design for the HCF plant at optimal conditions.

Figure 5.26 presents the best retrofit design obtained by SA which comprises:

1) The HE number 3 -the condenser of the first separator naphtha tank- was repiped from a cooling water stream to pre-heat the bottoms of de-propanizer column.

2) The HE number 4 –the condenser of first naphtha column- was repiped from a cooling water stream to pre-heat the bottoms of de-ethanizer column.

3) The HE number 6 -the second condenser of second naphtha column- was repiped from a cooling water stream to pre-heat the bottoms of de-ethanizer column.

4) The HE number 7 –the condenser of light naphtha product- was repiped from a cooling water stream to pre-heat the bottoms of de-ethanizer column.

5) A new HE 13 to match the condenser of the heavy naphtha product and the bottoms of de-propanizer column.

6) A new HE 14 to match the top vapours of de-butanizer column with the bottoms of de-ethanizer column.

Table 5.31 shows the capital cost (Timmerhaus et al., 2003) of this SA retrofit design obtained.

Item	Features	Sizing and capacities	Capital cost estimated, MM£/Yr
Heat exchanger 3 additional area	Purchased cost of fixed-tube-sheet heat exchangers with 0.019-m (3/4-in.) OD x 0.0254-m (1-in.) square pitch and 4.88-m or 6.10-m (16- or 20-ft) bundles and carbon-steel shell operating at 1035 kPa (150 psia)	Surface area: 216m^2	0.104
Heat exchanger 6 additional area	Purchased cost of fixed-tube-sheet heat exchangers with 0.019-m (3/4-in.) OD x 0.0254-m (1-in.) square pitch and 4.88-m or 6.10-m (16- or 20-ft) bundles and carbon-steel shell operating at 1035 kPa (150 psia)	Surface area: 46m^2	0.022
New heat exchanger 13 area	Purchased cost of fixed-tube-sheet heat exchangers with 0.019-m (3/4-in.) OD x 0.0254-m (1-in.) square pitch and 4.88-m or 6.10-m (16- or 20-ft) bundles and carbon-steel shell operating at 1035 kPa (150 psia)	Surface area: 369 m^2	0.178
New heat exchanger 14 area	Purchased cost of fixed-tube-sheet heat exchangers with 0.019-m (3/4-in.) OD x 0.0254-m (1-in.) square pitch and 4.88-m or 6.10-m (16- or 20-ft) bundles and carbon-steel shell operating at 1035 kPa (150 psia)	Surface area: 63 m^2	0.030
Pipe	Purchased cost of cast-iron pipe, bell and spigot pipe, 1035-1725 kPa	Diameter: 0.33 m Length: 180 m	0.519
Installation arrangement	Heat exchangers arrangements plus installation costs	50% of purchase cost	0.427
Totals			**1.281**

Table 5.31 Calculation basis for each HEN best retrofit design option (Timmerhaus et al., 2003).

The final results for the SA retrofit design are summarised in Table 5.32. In this Table the initial HEN with the optimized condition and the best retrofit obtained by inspection are also presented for comparison purposes.

Concept	Current HEN no retrofit design	HEN Retrofit design by SA	HEN Retrofit design by inspection 1
New Area, m^2	0	693	152
Number of matches eliminated	0	0	0
Number of re-sequencings	0	0	0
Number of re-pipings	0	4	2
Number of new matches	0	2	0
ACC, MM£/Yr	0.234	1.514	0.605
Energy Reductions, MM£/Yr	0.6	2.1	1.6
% improvement MPCA	4.7	17.3	13.4
Payback period, Yr	0.438	0.731	0.377
Potential CO_2 Tax Reductions, MM£/Yr	0.4	1.4	1.1

Table 5.32 HEN retrofit by SA best option for HCF at optimal conditions.

It is clear from this table that the performance of the modified HEN has been considerably improved by the SA optimisation. A comparison between the retrofit designs obtained by SA and by inspection clearly shows that the former has given better improvement in MPCA. This improvement is basically due to an increased energy recovered in the system by better heat integration and this also leads to significant reduction in CO_2 taxes. However, there is a considerable capital investment to do, as more structural changes are requested. Practical difficulties assocatied with implementation is implied to carry on the 4 repipings and the 2 new matches suggested by the SA design in the current HEN, compared to 2 repiping from the design by inspection. It can be concluded that the 3 options presented in Table 5.32 provide a meaningful base to do investment decision-making as these provide a view of the improvements, difficulty and payback period of the designs proposed. Nevertheless, the final decision will depend on the budget and priorities of the final users (i.e. shareholders).

Complementary HENs optimisation: In generating a portfolio of retrofit designs at

various capital investment levels, it was decided to conduct an additional HEN retrofit study. The previous retrofit designs were carried out based on optimal values for three most important factors. Two of them are column pressures of de-ethanizer and de-butanizer and do not imply a major change in the columns. The third factor is the stages' efficiency of de-ethanizer that requires a major internal change in the column (i.e. renewing all the current trays). Therefore, there are two capital investment levels related to these factors: no investment for the case with the change of two columns pressure and an investment for the case with the changes of two columns pressures and tray upgrading. The previous HEN retrofit designs dealt with the capital investment level (i.e. 3 parameteres optimized) and will be referred as Case A in the rest of the thesis. An additional HEN retrofit study was carried out with the no investment option, which only starts with column pressure adjustment (Case B). The same HEN optimisation procedure was executed on this case and it is described as follows.

The energy targeting and the energy recovery study were worked in SPRINT® for the Case B with a ΔTmin of 10 ºC. The simulation results were taken directly from Aspen Plus®. The HEN to be optimised was set, the cross pinch report showed the HEs which had heat transfer across the pinch. Next, the retrofit designs were addressed by inspection and by SA. The same considerations applied to Case A were made. Two final best promising retrofit options were obtained, one by inspection and one by SA, respectively.

Retrofit designs obtained by both methodologies were similar to those achieved in case A.

For retrofit by inspection the best design includes:

1) The HE number 3 -the condenser of the first separator naphtha tank- repiped from a cooling water stream to pre-heat the bottoms of de-ethanizer column.

2) The HE number 6 –the second condenser of the second naphtha column- repiped from a cooling water stream to pre-heat the bottoms of the de-propanizer column.

For retrofit by SA the best design achieved comprises:

1) The HE number 3 -the condenser of the first separator naphtha tank- was repiped from a cooling water stream to pre-heat the bottoms of de-propanizer column.

2) The HE number 4 –the condenser of first naphtha column- was repiped from a cooling water stream to pre-heat the bottoms of de-ethanizer column.

3) The HE number 6 -the second condenser of second naphtha column- was repiped from a cooling water stream to pre-heat the bottoms of de-ethanizer column.

4) The HE number 7 –the condenser of light naphtha product- was repiped from a cooling water stream to pre-heat the bottoms of de-ethanizer column.

5) A new HE 13 to match the condenser of the heavy naphtha product and the bottoms of de-propanizer column.

6) A new HE 14 to match the top vapours of de-butanizer column with the bottoms of de-ethanizer column.

Finally, the Table 5.33 presents the results for the HEN retrofit designs achieved by inspection and by SA of the cases A and B for comparison purposes.

Concept	**Case A**	**Case A HEN Retrofit by inspection**	**Case A HEN Retrofit by SA**	**Case B**	**Case B HEN Retrofit by inspection**	**Case B HEN Retrofit by SA**
New Area, m^2	0	152	693	0	161	713
Number of matches eliminated	0	0	0	0	0	0
Number of re-sequencings	0	0	0	0	0	0
Number of re-pipings	0	2	4	0	2	4
Number of new matches	0	0	2	0	0	2
ACC, MM£/Yr	0.234	0.605	1.514	0	0.371	1.281
Energy Reductions, MM£/Yr	0.6	1.6	2.1	0.5	1.5	2.0
% improvement MPCA	4.7	13.4	17.3	3.9	12.1	16.7
Payback period, Yr	0.438	0.377	0.731	0	0.256	0.641
Potential CO_2 Tax, MM£/Yr	0.4	1.1	1.4	0.4	1.0	1.4

Table 5.33 Best retrofit designs by inspection and by SA for Cases A and B.

Table 5.33 reveals that for the two specific cases A and B, in which the only difference is the efficiency of the trays, the performance yielded to a slight improvement in the MPCA (i.e. 0.8%). As explained in Table 5.18, this is the result of an easier separation and reduction of energy needed in the reboiler of the de-ethanizer due to greater efficiency in the trays of the column. The HEN retrofit designs achieved in the two cases were similar, with new area requested for Case B slightly bigger than in Case A. This fact is due to similar conditions held in the HCF process as the efficiency of the trays only affected the

first column of the system, the de-ethanizer, and the rest of the process remained the same. For the capital costs estimation, it is clear that in the Case B again, the only difference with respect to the Case A is costs for column upgrading and the used area slightly increased. Therefore, although the improvements in the MPA of case B are slighly reduced in comparison with Case A, the payback periods for the retrofit designs of case B are also decreased.

Again, the final decision may depend on additional factors; however, the data presented in the Table 5.33 provide the feasible options which comprise a portfolio based on the Retrofit Design Approach developed. It has resulted in a series of promising and reliable options for structural changes, leading to the improvement of the performance of the HCF process.

Final portfolio of retrofit designs:

To conclude with the Retrofit Design Approach application to this case study, the promising sets of retrofit designs options are plotted in Figures 5.27 and 5.28. These present the MPCA improvement and the CO_2 tax reduction against the capital cost. The comments on each one has already been detailed in the previous section and there is only presented a brief final description.

For clarification, identified solutions are marked in Figures 5.27 and 5.28 with the following labels:
A = Case A; A1= Case A, HEN retrofit by inspection; A2= Case A, HEN retrofit by SA.
B = Case B; B1= Case B, HEN retrofit by inspection; B2= Case B, HEN retrofit by SA.

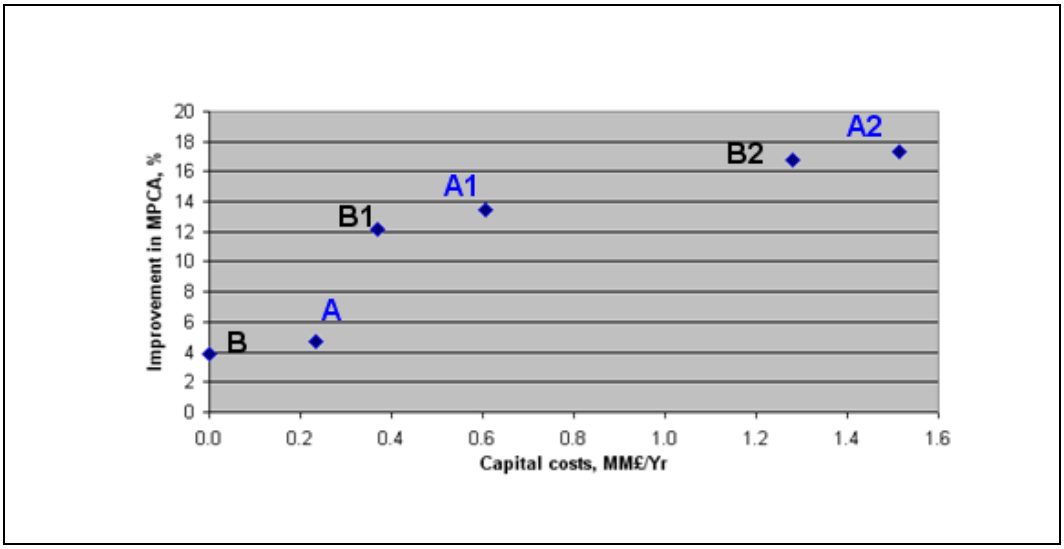

Figure 5.27 Retrofit designs portfolio for improvements in MPCA.

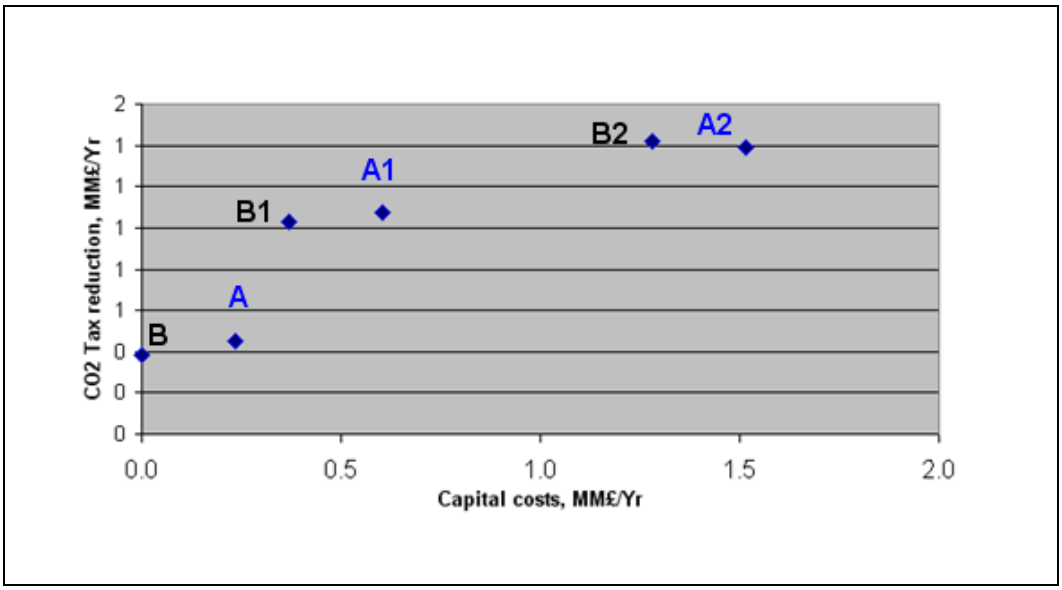

Figure 5.28 Retrofit designs portfolio for reduction in CO_2 tax.

The Figure 5.27 exposes that in general, as the capital cost increases the improvement in the MPCA trends to increase. Figure 5.28 visualizes the same trend for the CO_2 tax reduction while increasing capital costs. These effects are proportional to the energy savings obtained from the energy recovery in the system with the HEN retrofit designs. This was clear from Table 5.33. Case A shows a higher capital cost than case B in all the retrofit designs obtained.

It is important to note that, as for Case B, it is not always needed a capital investment to achieve an improvement in the MPCA, however this is relatively low in comparison with the rest of the cases.

5.4 Discussion

The proposed Retrofit Design Approach has been applied to the HCF process. Retrofit design analysis of the entire plant has been performed based on simulations and RSM to determine optimal operating conditions and structural changes by setting the objective function as maximizing MPCA. Final HEN optimisation was carried out to further achieve significative increases in MPCA. Some of the designs identified did not demand a large capital investement.

With respect to the required computational time to obtain the final portfolio of cost-effective solutions, it was found that for this specific study case, the prelimiar computational time used for the model building and its validation was considerable (750 minutes in average). The diagnosis stage took the largest period of time (roughly 1,080 minutes), followed by the evaluation stage with 1,030 minutes approximately and finally the optimisation with roughly 735 minutes. Table 5.34 specifies the computational time applied to each one of the stages in the proposed Retrofit Design Approach for the study case II.

Stage	Task	No. of tasks	Time per task	Total time
	Simulations for model building	30	20 minutes	600 minutes
	Simulations for model validation	10	15 minutes	150 minutes
Diagnosis	Simulations in selection of continous variables	24	15 minutes	360 minutes
	Simulations in selection of discrete variables	36	20 minutes	720 minutes
Evaluation	Simulations in the initial screening DoE	32	20 minutes	640 minutes
	ANOVA and evaluation of factor's effects	1	60 minutes	60 minutes
	Additional simulations to initial DoE	15	20 minutes	300 minutes
	Surface model	1	30 minutes	30 minutes

	fitting			
Optimisation	Optimal confirmatory simulations	9	20 minutes	180 minutes
	HEN retrofit by inspection in Sprint®	10	10 minutes	100 minutes
	HEN retrofit by SA in Sprint®	20	10 minutes	200 minutes
	HEN retrofit by inspection simulations	8	15 minutes	120 minutes
	HEN retrofit by SA simulations	3	15 minutes	45 minutes
	Complementary simulations to build the portfolio	6	15 minutes	90 minutes
Total of time				**3,595 minutes (60 hours)**

Table 5.34 Computational time of the proposed Retrofit Design Approach for the study case II.

The promising sets of retrofit design options were presented in the final investments portfolio. A wide range of cost-effective and reliable schemes were covered. The final designs provide a supportive basis for decision-making process for management.

The operative factors that were most significant for improvements in the MPCA were the pressure of the de-ethanizer, pressure of the de-butanizer and the trays' efficiency in the de-ethanizer column. In general, the most profitable structural changes were achieved after the HEN retrofit. The effect on the retrofit designs was studied in both, the energy recovery and the CO_2 tax reductions.

Finally, it can be said that the best cost-effective solution will strongly depend on the available capital, the intended payback period, the installation feasibility and the company policy among other factors.

5.5 Summary

A simulation-RSM based retrofit design framework has been proposed. The novel approach has been developed to address highly complex design problems. It is not based on dividing the problem into parts to study, analyze and solve it. On the other hand, it addresses the problem as a whole system. The final result integrates all the opportunities

identified in the approach to yield a suitable retrofit options portfolio.

This chapter has presented an industrial case study for the application of Retrofit Design Approach proposed. Although the approach has proven to be practical, based on commercial simulator, and statistic analyzer, it is needed the knowledge of the process integration concepts in order to benefit from the structural changes suggested. A number of simulations have been performed in the Retrofit Design Approach. As the current approach has not been automated, this requires considerable computational time to achieve the final results. The principal challenge of the methodology is to consider implicitly the energy improvements and the costs of capital from the initial diagnosis phase in the response MPCA in order to target to a higher potential for utilities reduction.

Chapter 6. Conclusions and future work

6.1 Summary

Retrofit design approaches have developed dramatically over the past three decades, to the extent where they have incorporated both mathematical and the conceptual approaches in order to find more reliable and global optimal solutions in reasonable periods of time. Pinch technology is the leader in the conceptual approach (i.e. the graphical approach), and continues to be used because it has been proven to be efficient and effective through the three decades. On the mathematical side, simulation and optimisation have been at the forefront. Simulation leads to an almost exact description of the process; sensitivities of operating parameters allow us to assess its controlling effect on process performance without the costs of expensive trials. Nowadays, mathematical formulae involved in the optimisation process have increased the power to cover the searching space and the major advantage in reaching global optimal points with the large number of mathematical programming tools available for deterministic and stochastic optimisation. The alternative experimental optimisation is also available and was presented along this research as practical and reliable tool. Nevertheless, the main disadvantage is in relation to the large computational burden that makes the process highly time-consuming. Furthermore, the more automated these tools become, the more they stand out of the user interaction during the whole process. This interaction is still essential to facilitate the feasibility of the promising solutions by considering and testing factors previously out of the scope of practicability. This is the reason why conceptual and mathematical approaches tend to be used together nowadays.

More powerful design concepts can be utilised with process simulation and optimisation, and alternative design concepts can be evaluated easily and the best option selected. Nevertheless, basic knowledge of process integration needs to be considered in the algorithms to assure reliable and cost-effective pathways, as multiple trade-offs need to be undertaken between improvements achieved and costs involved in the promising changes. In this manner, process design becomes less dependent on the experience of a few important individuals, which makes it far more systematic.

The approach selected depends ultimately on the features of the problem, the resources available, and the user requeriments; thus, there is no unique methodology that fits all the problems. In this case, a systematic manner is necessary to validate certainty. The estimation of factor effects as main or as an interaction between two or more factors is necessary to lead to a deeper understanding of the process and its changes. An important consideration to take into account is the delivery of the methodology to the final users, which should be comprehensible and practical. The tools integration feature of the proposed approach supports this delivery among different software with similar function. Therefore, it becomes necessary to contribute to the development of a systematic approach that can be used to obtain practical and realistic solutions when optimising complex operational plants, which are easy to modify by users and offer an understandable opportunities portfolio.

In this research, a Retrofit Design Approach simulation-based was proposed and the retrofit design guidelines developed to be applied in production processes. The classical methods of experimental design, process simulations of the plants and process integration concepts were used along with RSM methodology leading to general design guidelines for improving profitability. These guidelines were tested to develop a portfolio of retrofit design opportunities.

The approach can be used to evaluate and improve existing processes; it was tested at two currently operating gas processing plants:

In the case of study I, the natural gas liquid recovery unit which principal purpose is to separate sweetened natural gas into useful saleable productswas chosen to be studied. The simulation model was built under certain assumptions and a validation process was run to show an acceptable level of real data reproduction. Following this, process integration concept-guided sensitivity analysis was performed. The operative ranges for the controllable variables in the plant were explored to find promising factors that strongly impact the MaPr response. The most important factors found given by the ANOVA were the nitrogen composition in the feed, and the operating pressure of demethanizer column for the continuous variables. For the discrete factors: an additional pumparound from the demethanizer to a heat exchanger and the power generation capacity of first and second turboexpanders. The nitrogen composition and demethanizer pressure were fixed for

simplicity reasons, and taking advantage of not presenting important interactions (independent factors). The RSM was then applied for the structural changes. As the discrete factors do not exist for the current plant, the low level was set as cero and then the increasing levels for the response surface were set on the continuous range (percentage of pump capacity and of power generation capacity). A best fit model was obtained for each nitrogen level fixed with a very low RMSE, which indicated a good level of reproduction for the profit response. Moreover, it was supported by the respective randomly distributed residuals plot. An optimisation stage based on the fit model for the plant was performed. The objective function was the maximisation of the MaPr. There were presented improvements in the MaPr for the four nitrogen levels studied. The specific reasons were a reduction in reboiler duty for the demethanizer column, an increase in C3+ recovery and a reduction in NG compression power. From all four scenarios, it can be seen that the most profitable scenario to be applied depends strongly on the inlet nitrogen. Additionally, as nitrogen content in the inlet gas is highly likely to be increased, a carefully selected scenario must be applied. There was presented a final portfolio under comparative plots with increase in MaPr vs. capital costs and the payback period on invested capital.

An important variant was that during this first NGL process the approach did not explore the HEN retrofit, while in the second HCF plant the approach was proven and completed with the HEN retrofit, which yielded higher benefits. However, it was still possible to find profitable improvements in the NGL plant, as the final graphs showed. Furthermore, it was possible to gain considerable increases in MaPr by through relatively inexpensive changes in the plant. This is a flexibility feature that the Retrofit Design Approach has proven to have.

In the second case study, the HCF process provided a more complete example for Retrofit Design Approach application. Similar to the first case, the simulation model was the base of the study, some assumptions were made and the validation results presented a good level of process reproduction. These process integration concepts were applied and acted as the guide for the sensitivity analysis performed. In addition to the first case, one of the tools to develop in this analysis was set in the process energy targets and opportunities made available for its reduction. The MPCA was used as the studied response in this study case. This indicator comprised the capital cost incurred in the structural changes referred to, in addition to the MaPr led by the changes. With the purpose of finding

promising factors that strongly impact the MaPr in the first instance, the operative ranges for the controllable variables were covered. In the second instance, a wide range of structural arrangements for the distillation columns were tested (i.e. sloppy, and prefractionator arrangements). The final factors to be analysed by RSM were selected – a total of three continuous and two discrete factors – based on the MPCA variation of those which yielded the highest improvements. Once this selection was done, the RSM was performed to find the most important factors. The ANOVA showed that the operating pressure of de-ethanizer column, the operating pressure of de-butanizer column for the continuous variables and the efficiency of the stages in de-ethanizer column as the discrete factors were the most important. The RSM was executed for the three most important factors found and a best fit model could be obtained with low RMSE, which suggested a good level of reproduction for the MPCA response. The residuals plot evidenced a randomly distributed trend that supported a good fit model. The optimisation stage was developed under two levels, the first based on the model fit for the plant, whereby the MPCA response was maximised by varying the three most important factors. The optimum values were found and the improvement in the MPCA was given due to a reduction in the total duty requested by the plant – de-ethanizer and de-butanizer columns mainly. Additionally, the second level in the optimisation stage was the HEN optimisation complemented with the feasible options to recover the energy wasted in the biggest furnace of the plant and an alternative electricity generation scheme. This was performed after the optimum parameters were set at the best levels found. In fact, two main schemes were set – the first was by setting the three parameters and the second by setting only the two continuous parameters (operating pressures), which did not require capital investment.

The HEN optimisation was executed in two ways for each scheme, by inspection and by SA. Promising and feasible moves were detected by violations to the pinch. A wide range of retrofit alternatives could be generated based on the HEN optimisation either by inspection or by SA. These promising proposals were complemented with CO2 tax estimations derived from the energy reduction achieved for each one. The final portfolio was shown by comparative plots with increase in MaPr and reduction in CO2 emissions vs. capital costs. Complementary tables were also presented to show the payback period on the invested capital and the general description of the retrofit designs such as the number of re-pipings and the new area needed.

The proposed Retrofit Design Approach to tackle the retrofit problem in the industry presents the principal advantages of handling a large production plant, pseudo optimal solutions are achieved with a simplified model obtained by RSM and the effects of the most important factors towards the studied response can be quantified, which helps in understanding the process. The RSM cannot solve the MINLP problem regarding the initial options in the superstructure; however, a reasonable set of initial options based on process integration tools can be obtained and are considered satisfactory for the user. The achievements gained in the approach are integrated into a suitable retrofits options portfolio. Neverhteless, an important limitation of the Retrofit Design Approach is the time required to perform the approach, which is high during the first and second steps due to the large number of simulations generated. However, this is offset by a considerable reduction of the optimisation time of the model derived from RSM. Another limitation is that the approach has not been automated, which results in high time consumption to manually execute all the runs and analyses in different software. HEN retrofit also takes up a great deal of time depending on the optimal process structure found. Nevertheless, besides the limitations found, Retrofit Design Approach can be considered a suitable approach to address the retrofit problem under the industrial scope.

Because the available budget and intended payback period dictate the best cost-effective alternative, the final opportunities portfolio generated is useful for providing viable investment options. Retrofit Design Approach has been shown to be a practical and reliable approach to achieve pseudo optimal solutions over a reasonable timescale; knowledge of the process integration concepts plays an important roll in order to capitalise on the structural changes suggested. The main challenge of the methodology is to consider implicitly energy improvements, since the first diagnosis stage together with energy targeting differences assure targeting a higher potential for utilities reduction, and consider the capital cost that would be requested to warranty targeting a real optimum.

It was noticeable that, in some cases, the cost-effective retrofit did not require structural modifications to lead to an acceptable benefit. This is one of the most important advantages that the final portfolio provides. Although the Retrofit Design Approach was tested in two complex plants, it is imperative to continue testing it in more plants to assure

robustness in the final results obtained. At this stage of application, the Retrofit Design Approach results seem to agree very well and to be reasonably feasible. The approach can be used as a tool for supporting decision making, as the results are supported by simulations that can represent the real process at a good level and the background of the improvements is sustained by process integration knowledge. Moreover, the stochastic optimisation of the HEN for retrofit strengthens the globality of the solutions found.
The major contribution of the research carried out in this work to the knowledge is: to provide a direct response of the industrial needs to carry out practical retrofit design of complex operating units and to generate reliable options that can be used as a decision-support tool by the management. As found along the content of this thesis, it simplifies the application of academic developments in the industry.

The original contributions to the knowledge are firstly, to combine two design methods, process simulation and response surface methodology, which are rarely used together in the field of chemical engineering for the execution of retrofit studies in the context of process integration. Secondly, the substitution in the RSM of the optimal search method based on ascending or descending slopes, with stepsizes manually set and the repetitive evaluation of the model obtained by direct optimisation of this model, using a numerical optimisation algorithm either linear or nonlinear. This speeds up the rate of solution and helps to improve the globality of solutions found.

6.2 Future work

As needs nowadays are focused increasingly on retrofit designs to reduce energy consumption, and process modelling and optimisation become more widely used, the Retrofit Design Approach proposed will indeed need to be completed in order to reduce its limitations. The main work to carry out in this instance will include the following:

Improving its systematicity, for which is suggested to explore processes that include other process integration variants apart from distillation columns and HENs such as refrigeration, reaction or water systems, which increase the cover of the integrated tools and lead to a more systematic methodology.

Testing the reproducibility level with the same production processes and assumptions made, by different users working independently.

To reduce computation time, it is strongly requested to automate the software involved, firstly by the use of interface links to migrate the information in a faster manner from one piece of software to another, as shown in Table 6.1, and secondly by contemplating a way to automatically execute the structural changes requested in the simulation software, as the current models are code protected and cannot be internally manipulated. In order to do this, it will necessary to migrate in some way the models to a more open environment (i.e. Matlab®).

From software	Information flow	To software
Aspen Plus	Streams report	Sprint
Sprint / User	+ / - Principle proposals	Aspen Plus
Aspen Plus	Sensitivity analysis results	Matlab
Matlab	DoE	Aspen Plus
Aspen Plus	Factor effect	Matlab
Matlab	ANOVA, most important factors, and proposed RSM design	Excel
Excel	Optimized model	Aspen Plus
Sprint	Optimized HEN	Aspen Plus

Table 6.1 Information flow between Retrofit Design Approach software.

To enhance robustness, further optimal designs for experiments may be explored, along with the measurement of how sensitive these particular method solutions are to modifications in their assumptions (robustness affected).

Multi-responses optimisation must be further performed by studying some of the environmental impacts not directly related to the energy used, such as water contaminants and fugitive emissions, as additional responses. To do this, maintenance activities might be included by correlating a model with operational performance.

Globality may be tested by a comparison of its results with other optimisation tools solutions such as pure stochastic or NLP, as well as solution time, to reach the optimal results.

To generate a wider spectrum of probable initial options to address the MINLP problem combinatorial tools such as process graph or P-graph can be applied at the initial stage of the approach.

There is no limitation for the proposed approach to be applied to the grassrooth design. For this specific design the structural changes would migrate from the integer to the continuous domain. This will avoid the infeasibility mentioned for the approach for the integer values.

Further complementary work may focus on estimating the risks implicit in the successful completion probability and the capital expenditure to help the decision makers with routine regulatory decisions.

The support of management and all others concerned in the company will continue to be an essential element in the successful adoption of feasible designs.

Currently, the Retrofit Design Approach has not yet been implemented in the plant, but the intention is to incorporate it as a practice to identify and evaluate the proposed retrofit designs and finally generate the final portfolio to be used in the decision making process.

References

(EIPPCB), E. I. P. P. A. C. B. (2003) Best Available Techniques for Mineral Oil and Gas Refineries (BREF).

(EPA), U. S. E. P. A. (2006) AP42_NATGAS_COMBUSTION(EPA-R09-OAR-2006-0635-0013).

ANNAKOU, O. & MIZSEY, P. (1996) Rigorous Comparative Study of Energy-Integrated Distillation Schemes. *Ind. Eng. Chem. Res. ,* 35**,** 1877-1885.

ASPENTECHNOLOGY, I. (2007) Aspen Plus v21.0 User Guide.

ATHIER, G., FLOQUET, P., PIBOULEAU, L. & DOMENECH, S. (1996) Optimization of HEN by coupled Simulated Annealing and NLP procedures. *Computers chem. Engng,* 20**,** S13-SI8.

ATHIER, G., FLOQUET, P., PIBOULEAU, L. & DOMENECH, S. (1998) A Mixed Method For Retrofiting Heat-Exchanger Networks. *Computers them. Engng,* 22 S505-S511.

AUDUN ASPELUND, D. O. B., TRULS GUNDERSEN (2007) An Extended Pinch Analysis and Design procedure utilizing

pressure based exergy for subambient cooling. *Applied Thermal Engineering,* 27**,** 2633–2649.

BHAW, N. & ZHELEV, T. K. (2000) Combined water–oxygen pinch analysis for better wastewater treatment management. *Waste Management,* 20**,** 665-670.

BOX, G. E. P., AND WILSON, K.B. (1951) On the Experimental Attainment of Optimum Conditions. *Journal of the Royal Statistical Society,* Series B 1-45.

BOX, G. E. P. & DRAPER, N. R. (1987) Empirical Model-Building and Response Surfaces.

CERVANTES, M. J. & ENGSTROM, T. F. (2004) Factorial Design Applied to CFD. *Journal of Fluids Engineering,* 126**,** 791-798.

DAVIM, J. P. & CARDOSO, R. (2005) Thermo-mechanical model to predict the tribological behaviour of the composite PEEK-CF30/steel pair in dry sliding using multiple regression analysis. *Industrial Lubrication and Tribology,* 57**,** 181–186.

DAVIS, E. & IERAPETRITOU, M. (2008) A Kriging-Based Approach to MINLP Containing Black-Box Models and Noise. *Ind. Eng. Chem. Res. ,* 47**,** 6101–6125.

DOLAN, W. B., CUMMINGS, P. T. & VAN, M. D. L. (1989) Process optimization via simulated annealing: application to network design. *AIChE Journal,* 35**,** 725–736.

DOLAN, W. B., CUMMINGS, P. T. & VAN, M. D. L. (1990) Algorithmic efficiency of simulated annealing for heat exchanger network design. *Comput. Chem. Eng.,* 14 1039–1050.

DURAN, M. A. & GROSSMANN, I. E. (1986) An Outer-Approximation Algorithm for a Class of Mixed-integer Nonlinear Programs. *Math. Program.,* 36**,** 307–339.

E. S. FRAGA, R. P., AND G. W. A. ROWE (October 2001) A visual representation of process heat exchange as a basis for user interaction and stochastic optimization. *Trans IChemE,* 79**,** 765-776.

EDGAR, T. F., HIMMELBLAU, D. M. & LASDON, L. S. (2001) Optimisation of chemical processes

EL-HALWAGI, M. & MANOUSIOUTHAKIS, V. (1989) Synthesis of Mass Exchange Networks. *AIChE Journal,* 35**,** 1233-1244.

ERIK BEK-PEDERSEN, R. G. (2004) Design and synthesis of distillation systems using a driving-force-based approach. *Chemical Engineering and Processing***,** 251–262.

FAN, S.-K. S. (2003) Implementation of ridge analysis on quadratic response surfaces. *Journal of Statistical Computation and Simulation,* 73**,** 675–684.

FLETCHER, R. & LEYFFER, S. (1994) Solving Mixed Integer Programs by Outer Approximation. *Math. Program.,* 66.

FLOUDAS, C. A. (2000) Deterministic Global Optimization: Theory, Methods and Applications. *Nonconvex Optimization And Its Applications series, Kluwer Academic Publishers, Boston MA,* 37.

FRAGA, E. S., PATEL, R. & ROWE, G. W. A. (2001) A visual representation of process heat exchange as a basis for user interaction and stochastic optimization. *Trans IChemE,* 79 October 765-776.

FRIEDLER, F. (2010) Process integration, modelling and optimisation for energy saving and pollution reduction. *Applied Thermal Engineering,* 30**,** 2270-2280.

FRONTLINESYSTEMS (2003) XL2000: Solver Uses Generalized Reduced Gradient Algorithm. *Support Microsoft Website*.

GAIA FRANCESCHINI, S. M. (2008) Model-based design of experiments for parameter precision: State of the art. *Chemical Engineering Science,* 63**,** 4846-4872.

GEOFFRION, A. M. (1972) A Generalized Benders Decomposition. *J. Optim. Theory Appl.,* 10**,** 237–260.

GROSS, B. & ROOSEN, P. (1998) Total Process Optimisation in Chemical Engineering with Evolutionary Algorithms. *Computers and Chemical Engineering,* 22**,** 229-236.

HANAGANDI, V. & NIKOLAU, M. (1998) A Hybrid Approach to Global Optimisation Using a Clustering Algorithm in a Genetic Search Framework. *Computers and Chemical Engineering,* 22**,** 1913-1925.

HEKKERT, M. P., HENDRIKSA, F. H. J. F., FAAIJB, A. P. C. & NEELISB, M. L. (2005) Natural gas as an alternative to crude oil in automotive fuel chains well-to-wheel analysis and transition strategy development *Energy Policy* 579-594.

HELM, D. (2009) EU Climate-Change policy -a critique. *Smith school working paper series,* October.

HEPBURN, C. (2006) Regulation by prices, quantities or both: a review of instrument choice. *Oxford review of economic policy,* 22**,** 226-247.

HOLLAND, J. H. (1975) *Adaptation in natural and artificial systems,* The University of Michigan Press.

ILZARBE, L., TANCO, M., ALVAREZ, M. J. & VILES, E. (2008) Practical Applications of Design of Experiments in theField of Engineering:A Bibliographical Review. *Qual. Reliab. Engng. Int.* , 24**,** 417–428.

IPCC (1988) Intergovernmental Panel on Climate Change (IPCC).

IRIZARRY, M. D. L. A., WILSON, J. M. & TREVINIO, J. (2001a) A flexible simulation tool for manufacturing cell-design 2: response surface analysis and case study. *IIE Transactions,* 33**,** 837-846.

IRIZARRY, M. D. L. A., WILSON, J. M. & TREVINIO, J. (2001b) A flexible simulation tool for manufacturing cell design 1: Model structure, operation and case study. *IIE Transactions,* 33**,** 827-836.

JANG, W.-H., HAHN, J. & HALL, K. R. (2005) Genetic/quadratic search algorithm for plant economic optimisations using a process simulator. *Computers and Chemical Engineering,* 30**,** 285-294.

JANG W. , J. H., AND KENNETH R. HALL (2005) Genetic/quadratic search algorithm for plant economic optimizations using a process simulator. *Computers and Chemical Engineering,* 30**,** 285-294.

JIA, X., ZHANG, T., WANG, F. & HAN, F. (2006) Multi-objective modeling and optimisation for cleaner production processes. *Journal of Cleaner Production,* 14**,** 146-151.

JOHN D. WILKINSON, H. M. H., KYLE T. CUELLAR, RICHARD N. PITMAN (1998) Next Generation Processes for NGL / LPG Recovery.

KABIR, C. S., CHAWATHE, A., JENKINS, S. D., OLAYOMI, A. J., AIGBE, C. & FAPARUSI, D. B. (2002) Developing New Fields Using Probabilistic Reservoir Forecasting. *SPE Annual Technical Conference and Exhibition proceedings,* Paper Number 77564-MS DOI.

KANTER, J. (2009) Carbon Emissions: To Trade or Tax? *The NewYork Times*.

KARUPPIAH, R. & GROSSMANN, I. E. (2008) Global Optimisation of Multiscenario Mixed Integer Nonlinear Programming Models arising in the Synthesis of Integrated Water Networks under Uncertainty. *Computers and Chemical Engineering,* 32**,** 145-160.

KEFENG WANG, Y. Q., YI YUAN, PINGJING YAO (1998) Synthesis and optimisation of heat integrated distillation systems using an improved genetic algorithm. *Computers and Chemical Engineering,* 23**,** 125-136.

KHALIFA, M. & EMTIR, M. (2009) Rigorous optimization of heat-integrated and Petlyuk column distillation configurations based on feed conditions. *Clean Techn Environ Policy,* 11**,** 107–113.

KIN-LUNG MAA, C.-W. H., AND TERRENCE F. YEEB (2000) Constant approach temperature model for HEN retrofit. *Applied Thermal Engineering,* 20**,** 1505-1533.

KINI, S. D. (2004) An approach to integrating numerical and response surface models for robust design of production systems.

KIRKPATRICK, S., GELATT, C. D. & VECCHI, M. P. (1983) Optimization by Simulated Annealing. *Science,* New Series 220**,** 671–680.

KLEIJNEN, J. P. C. (2008) Response surface methodology for constrained simulation optimization: An overview. *Simulation Modelling Practice and Theory,* 16 50–64.

KLEIJNEN, J. P. C., HERTOG, D. D. & ANGU¨N, E. (2004) Response surface methodology's steepest ascent and step size revisited. *European Journal of Operational Research,* 159 121–131.

KLEIN, R. J. T. & PARRY, M. L. (2007) Inter-relationships between adaptation and mitigation. In: Climate Change 2007: Impacts, Adaptation and Vulnerability. Contribution of Working Group II to the Fourth Assessment Report of the Intergovernmental Panel on Climate Change. *Cambridge University Press, Cambridge, U.K., and New York, N.Y., U.S.A. Retrieved 2009-05-20.***,** 745-777.

KOCH-GLITSCH (2010) ULTRA-FRAC® high performance trays.

LAURA ILZARBE, M. J. A., ELISABETH VILES AND MARTıN TANCO (2008) Practical Applications of Design of Experiments in theField of Engineering:A Bibliographical Review. *Qual. Reliab. Engng. Int.* , 24**,** 417–428.

LAZZARETTO, A. & TOFFOLO, A. (2004) Energy, economy and environmental as objectives in multi-criterion optimisation of thermal systems design. *Energy,* 29**,** 1139-1157.

LEBOREIRO, J. & ACEVEDO, J. (2004) Processes Synthesis and Design of Distillation Sequences Using Modular Simulators: A Genetic Algorithm Framework. *Computers and Chemical Engineering,* 28.

LEE, S. & GROSSMANN, I. E. (2003) Global optimisation of nonlinear generalized disjunctive programming with bilinear equality constraints: applications to process networks. *Computers and Chemical Engineering,* 27**,** 1557-1575.

LI, P., LO¨WE, K., ARELLANO-GARCIA, H. & WOZNY, G. (2000) Integration of Simulated Annealing to a Simulation Tool for Dynamic Optimisation of Chemical Processes. *Chemical Engineering and Processing,* 39**,** 357-363.

LIAUA, L. C., YANG, T. C.-K. & TSAI, M.-T. (2004) Expert system of a crude oil distillation unit for process optimization using neural networks. *Expert Systems with Applications,* 26**,** 247–255.

LINNHOFF, B. & AHMAD, S. (1990) Cost optimum heat exchanger networks -1: Minimum energy and capital using simple models for capital cost. *Comput. them. Engng. ,* 14**,** 729-750

LINNHOFF, B. & HINDMARSH, E. (1983) The Pinch design Method for Heat Exchange Networks. *Chemical Engineering Science,* 38**,** 745-763.

LINNHOFF, B., MASONS, D. R. & WARDLE, I. (1979) Understanding Heat Exchanger Networks. *Computers & Chemical Engineering,* 3**,** 295-302.

LINNHOFF, B. & VREDEVELD, D. (1984) Pinch technology has come of age. *Chemical Engineering Progress,* 80**,** 33-40.

LIU, H. N. A. F. (2001) Refinery hydrogen management for clean fuels production. *Advances in Environmental Research,* 6**,** 81-98.

M. GADALLA, M. J. A. R. S. (2003) Shortcut Models for Retrofit Design of Distillation Columns. *Trans IChemE,,* 81**,** 971-986.

M. S. DIAZ, A. S., J. A. BANDONI, AND E. A. BRIGNOLE (1997) Automatic Design and Optimisation of Natural Gas Plants. *Ind. Eng. Chem. Res. ,* 36**,** 2715-2724.

M. TANCO, E. V., L. ILZARBE AND M. J. ALVAREZ (2009) Implementation of Design of Experiments projects in industry. *Appl. Stochastic Models Bus. Ind.,* 25**,** 478–505.

MAHMOUD, A., SHUHAIMI, M. & ABDELSAMED, M. (2009) A combinedprocessintegrationandfuelswitchingstrategyforemissions reductioninchemicalprocessplants. *Energy,* 34**,** 190–195.

MEHDI MEHRPOOYA, F. G., ALI VATANI (2006) An Optimisation of Capital and Operating Alternatives in a NGL Recovery Unit. *Chem. Eng. Technol. ,* 29**,** 1469–1480.

MEXICANGOVERNMENT (2007) Diario Oficial de la Federacion (DOF). *Official Journal of the Federation* NOM-001-SEMARNAT-1996.

MIZSEY, P., HAU, N. T., BENKO, N., KALMAR, I. & FONYO, Z. (1998) Process control for energy integrated distillation schemes. *Computers chsm. Engng* 22**,** S427-S434.

MIZSEY P., N. T. H., N. BENKO, I. KALMAR AND Z. FONYO (1998) Process control for energy integrated distillation schemes. *Computers chsm. Engng* 22**,** S427-S434.

MONTGOMERY, D. C. (1997) Design and analysis of experiments.

MONTGOMERY, D. C. (2005) Design and analysis of experiments.

MUBARAK EBRAHIM, A.-K. (2000) Pinch technology: an e • cient tool for chemical-plant energy and capital-cost saving. *Applied Energy,* 65 45-49.

MYERS RH, M. D., VINING GG, BORROR CM, KOWALSKI SM (2004) Response surface methodology: A retrospective and literature survey. *Journal of Quality Technology,* 36**,** 53–78.

MYERS, R. H. & MONTGOMERY, D. C. (2002) Response Surface Methodology: Process and Product Optimization Using Designed Experiments. 522–528.

MYERS, R. H., MONTGOMERY, D. C., VINING, G. G. & BORROR, C. M. (2004a) Response surface methodology: A retrospective and literature survey. *Journal of Quality Technology,* 36**,** 53–78.

MYERS, R. H., MONTGOMERY, D. C., VINING, G. G. & BORROR, C. M. (2004b) Response surface methodology: A retrospective and literature survey. *Journal of Quality Technology,* 36**,** 53–78.

NDK. ASANTE & ZHU, X. (1997) An automated and interactive approach for heat exchanger network retrofit. *Trans IChemE,* 75**,** 349-360.

NIELSEN, J. S., HANSEN, M. W. & JOERGENSEN, S. B. (1996) Heat exchanger network modelling framework for optimal design and retrofiting. *Comp. Chem. Engng. ,* 20**,** S249-S254.

NORDMAN, R. & BERNTSSON, T. (2009a) Use of advanced composite curves for assessing cost-effective HEN retrofit -1: Theory and concepts. *Applied Thermal Engineering,* 29**,** 275–281.

NORDMAN, R. & BERNTSSON, T. (2009b) Use of advanced composite curves for assessing cost-effective HEN retrofit -2: Case studies. *Applied Thermal Engineering,* 29**,** 282–289.

NTLHAKANA, L. & ZHELEV, T. (1999) Energy-environment closed loop through oxygen pinch. *Computers & Chemical Engineering* 23**,** S79-S83.

OSMAN, A., MUTALIB, M. I. A., SHUHAIMI, M. & AMMINUDIN, K. A. (2009) Paths combination for HENs retrofit. *Applied Thermal Engineering,* 29**,** 3103–3109.

PETER MIZSEY, N. T. H., N. BENKO, I. KALMAR AND Z. FONYO (1998) Process control for energy integrated distillation schemes. *Computers chsm. Engng* 22**,** S427-S434.

PINTARIC, Z. N. & KRAVANJA, Z. (2000) The two-level strategy for MINLP synthesis of process flowsheets under uncertainty. *Computers and Chemical Engineering,* 24**,** 195-201.

PINTARIC, Z. N. & KRAVANJA, Z. (2004) A strategy for MINLP synthesis of flexible and operable processes. *Computers and Chemical Engineering,* 28**,** 1105-1119.

PINTARIC, Z. N. & KRAVANJA, Z. (2006) Selection of the Economic Objective Function for the Optimisation of Process Flow Sheets. *Ind. Eng. Chem. Res.,* 45**,** 4222-4232.

PONCE-ORTEGA, J. M., A. JIMÉNEZ-GUTIÉRREZ, AND I.E. GROSSMANN (2008) Optimal synthesis of heat exchanger networks involving isothermal process streams. *Computers & Chemical Engineering,* 32**,** 1918-1942

RAHUL ANANTHARAMAN, O. S. A., TRULS GUNDERSEN (2006) Energy Level Composite Curves—a new graphical methodology for the integration of energy intensive processes. *Applied Thermal Engineering,* 26**,** 1378–1384.

REV, E., EMTIR, M., SZITKAI, Z., MIZSEY, P. & FONYO, Z. (2001) Energy savings of integrated and coupled distillation systems. *Computers and Chemical Engineering,* 25**,** 119–140.

ROSEN, S. L., HARMONOSKY, C. M. & TRABAND, M. T. (2008) Optimization of systems with multiple performance measures via simulation: Survey and recommendations. *Computers & Industrial Engineering***,** 327–339.

S. DIAZ, A. S., A. BANDONI AND E. A. BRIGNOLE (1996) A study on the capital and operating alternatives in an Ethane extraction plant. *Computers chem. Engng,* 20**,** S1499-SI504.

SALAS, P., E.RODRIGUEZ & BURGOS, E. (2003) Study evaluates the impact of nitrogen on gas processing efficiency. *Oil & Gas Journal,* 101**,** 50.

SCHONNING, A., NAYFEH, J. & ZARDA, R. (2005) An integrated design and optimization environment for industrial large scaled systems. *Research in Engineering Design,* 16**,** 86–95.
SHAH, P. B. & KOKOSSIS, A. C. (2002) New Synthesis Framework for the Optimization of Complex Distillation Systems. *AIChE Journal,* 48**,** 527-550.
SHANG, J. S. & TADIKAMALLA, P. R. (1998) Multicriteria design and control of a cellular manufacturing system through simulation and optimization. *International journal of production research,* 36**,** 1515-1528.
SMITH, R. (2005) Chemical process design and integration.
TANCO, M., VILES, E. & ALVAREZ, M. J. (2009) Barriers faced by engineers when applying design of experiments. *The TQM Journal,* 21 565-575.
TANCO, M., VILES, E., ILZARBE, L. & ALVAREZ, M. J. (2008) How is Experimentation Carried Out by Companies? A Survey of ThreeEuropean Regions. *Qual. Reliab. Engng. Int.,* 24**,** 973–981.
TANTIMURATHA, L., KOKOSSIS, A. C. & MUELLER, F. U. (2000) The heat exchanger network design as a paradigm of technology integration. *Applied Thermal Engineering,* 20 1589-1605.
TAWARMALANI, M. & SAHINIDIS, N. V. (2002) Convexification and Global Optimization in Continuous and Mixed-Integer Nonlinear Programming: Theory, Algorithms, Software, and Applications. *Nonconvex Optimization And Its Applications series, Kluwer Academic Publishers, Boston MA.,* 65.
TAYAL & C., M. (1999) Optimal Design of Heat Exchangers: A Genetic Algorithm Framework. *Industrial and Engineering Chemistry Research,* 38**,** 456-467.
THEMATHWORKSINC. (2004) Matlab statistics toolbox. *Matlab version 7.0.1 User manual*.
TIMMERHAUS, K., PETERS, M. S. & WEST, R. E. (2003) Plant Design and Economics for Chemical Engineers. *McGraw-Hill Higher Education 5/e*.
TOFFOLO, A. & LAZZARETTO, A. (2002) Evolutionary algorithms for multi-objective energetic and economic optimisation in thermal system design. *Energy,* 27**,** 549-567.
TONG, K. W., KWONG, C. K. & YU, K. M. (2004) Intelligent process design system for the transfer moulding of electronic packages. *Int. J. Prod. Res.,* 42**,** 1911–1931.
U.S.COMMERCEDEPARTMENT (2006) NIST/SEMATECH e-Handbook of Statistical Methods.
UNO, T. U. N. O. (1987) Montreal Protocol
UNO, T. U. N. O. (1999) Agenda 21.
WANG, J. & SMITH, R. (2005) Synthesis and Optimization of Low-Temperature Gas Separation Processes. *Ind. Eng. Chem. Res.,* 44**,** 2856-2870.
WANG, Y. P. & SMITH, R. (1994) Wastewater minimisation. *Chemical Engineering Science,* 49**,** 981-1006.
WAREN, A. & LASDON, L. (1995) The Generalized Reduced Gradient (GRG2) nonlinear optimization code.
WATSON, D. F. A. J. (1995) The simplex method with bounds on the variables, and the branch-and-bound method. *Frontline Systems, Inc.* .
WESTERBERG, A. W. & GROSSMANN, I. E. (2000) Research Challenges in Process Systems Engineering. *AIChE Journal,* 46**,** 1700-3.
WESTERLUND, T. & PETERSSON, F. (1995) A Cutting Plane Method for Solving Convex MINLP Problems. *Computers Chem. Eng.,* 19**,** 131–136.
YANG, T. & TSENG, L. (2002) Solving a Multi-Objective Simulation Model Using a Hybrid Response Surface Method and Lexicographical Goal Programming

Approach-A Case Study on Integrated Circuit Ink-Marking Machines. *The Journal of the Operational Research Society,* 53**,** 211-221.

YU, H., FANG, H., YAO, P. & YUAN, Y. (2000) A combined genetic algorithm:simulated annealing algorithm for large scale system energy integration. *Computers and Chemical Engineering,* 24**,** 2023–2035.

ZHELEV, T. (2007) The conceptual design approach—A process integration approach on the move. *Resources, Conservation and Recycling,* 50**,** 143–157.

Appendixes

Table A.1: Normal operating condition values in the Cryogenic 1 plant.

Equipment	Temperature	Pressure	Flowrate
First cooler	**34-37 ºC**	**63-64.5 Kg/cm²**	**500-600MMPCD**
First separation tank	**34-37 ºC**	**60-65 Kg/cm²**	**500-600MMPCD**
First furnace	**290-300 ºC**	**1-1.9 Kg/cm²**	**0.3-0.49 MMPCD**
Heat exchanger 1: process/process	**5-7 ºC**	**Differential: 0.9-0.79 Kg/cm²**	**200-300MMPCD**
Heat exchanger 2: process/process	**10-19 ºC**	**Differential: 0.9-0.79 Kg/cm²**	**300-500MMPCD**
Heat exchanger 3: process/process	**-16- -20 ºC**	**Differential: 0.9-0.79 Kg/cm²**	**200-300MMPCD**
Heat exchanger 4: process/process	**-16- -18 ºC**	**Differential: 0.9-0.79 Kg/cm²**	**300-500MMPCD**
First chiller	**-6- -10 ºC**	**Differential: 0.9-0.79 Kg/cm²**	**200-300MMPCD**
Second chiller	**-6- -10 ºC**	**Differential: 0.9-0.79 Kg/cm²**	**300-500MMPCD**
Second separation tank	**-16- -20 ºC**	**56-61 Kg/cm²**	**500-600MMPCD**
Third chiller	**-16- -20 ºC**	**Differential: 0.9-0.79 Kg/cm²**	**200-300MMPCD**
Fourth chiller	**-36- -40 ºC**	**Differential: 0.9-0.79 Kg/cm²**	**300-500MMPCD**
Heat exchanger 5: process/process	**-36- -40 ºC**	**Differential: 0.9-0.79 Kg/cm²**	**200-300MMPCD**
Heat exchanger 6: process/process	**-46- -50 ºC**	**Differential: 0.9-0.79 Kg/cm²**	**300-500MMPCD**
Third separation tank	**-19- -22 ºC**	**33-38 Kg/cm²**	**40-50 MMPCD**
Fourth separation tank	**-45- -35 ºC**	**34-39 Kg/cm²**	**450-550MMPCD**
1st turboexpander discharge	**-58- -54ºC / 54-60ºC**	**34-39 Kg/cm²**	**450-550MMPCD**
Fifth separation tank	**-70 - -60 ºC**	**30-35 Kg/cm²**	**450-550MMPCD**
Heat exchanger 7: process/process	**-69 - -75ºC**	**Differential: 0.9-0.79 Kg/cm²**	**110-130 MMPCD**
Heat exchanger 8: process/process	**-65- -70 ºC**	**Differential: 0.9-0.79 Kg/cm²**	**250-310 MMPCD**
Sixt separation tank	**-72- -66 ºC**	**29-34 Kg/cm²**	**400-500 MMPCD**
2nd Turboexpander	**-90- -95ºC / 42-45ºC**	**13-18 Kg/cm²**	**400-500 MMPCD**
Seventh separation tank	**-100-110 ºC**	**13-18 Kg/cm²**	**400-500 MMPCD**

Demethanizer column	**-80- -90 ºC**	**24-25 Kg/cm²**	**200-300 MMPCD**
High Pressure Compressors Discharge	**90-120 ºC**	**60-65 Kg/cm²**	**400-500 MMPCD**

Table A.2: Maximum and minimum Cryogenic 1 operational parameters.

Service	Minimum Limit	Low Limit	Normal Range	High Limit	Maximum Limit
Inlet stream	61.0Kg/cm²	62.0Kg/cm²	63-64.5 Kg/cm²	68.0Kg/cm²	69.0Kg/cm²
Discharge 1st turbo-expander	34.0Kg/cm²	35.0Kg/cm²	38-39 Kg/cm²	40.0Kg/cm²	41.0Kg/cm²
Discharge 2nd turbo-expander	16.0Kg/cm²	17.0Kg/cm²	18-19 Kg/cm²	20.0Kg/cm²	21.0Kg/cm²
C_2+ external product	20.0Kg/cm²	22.0Kg/cm²	30-35.9 Kg/cm²	36.0Kg/cm²	38.0Kg/cm²
Demethanizer column operating pressure	22.5 Kg/cm²	23.0Kg/cm²	24-25 Kg/cm²	26.0Kg/cm²	26.5 Kg/cm²
RGHP	54.0Kg/cm²	55.0Kg/cm²	56-62.9 Kg/cm²	63.0Kg/cm²	64.0Kg/cm²
Suction compressor 2nd turbo-expander	13.0Kg/cm²	14.0Kg/cm²	15-16.9 Kg/cm²	17.0Kg/cm²	18.0Kg/cm²
Suction high pressure compressors	18.0Kg/cm²	19.0Kg/cm²	20-21 Kg/cm²	22.0Kg/cm²	23.0Kg/cm²
RGLP	8.5 Kg/cm²	8.8 Kg/cm²	9-10.5 Kg/cm²	11 Kg/cm²	11.5Kg/cm²
Discharge 1st turbo-expander	- 64 ºC	- 61 ºC	-58- -54ºc	- 55 ºC	- 52 ºC
Discharge 2nd turbo-expander	-103 ºC	- 100 ºC	-90- -95ºC	- 84 ºC	- 81 ºC
Top demethanizer	- 94 ºC	- 91 ºC	-80- -90 ºC	-76 ºC	- 73 ºC
Bottom demethanizer	28ºC	30ºC	32-37 ºC	38ºC	40ºC

Table A.3: Matlab Fractional Factorial Design for Cryogenic 1 factor screening.

```
>> generators = fracfactgen ('a b c d e f g h i j k l', 6,4)

generators =

    'a'
    'b'
    'c'
    'd'
    'e'
    'f'
    'abcdef'
    'cdef'
    'bdef'
    'adef'
    'bcef'
    'acef'

>> [dfF, confounding ] = fracfact (generators)

confounding =

    'Term'       'Generator'    'Confounding'
    'X1'         'a'            'X1'
    'X2'         'b'            'X2'
    'X3'         'c'            'X3'
    'X4'         'd'            'X4'
    'X5'         'e'            'X5'
    'X6'         'f'           'X6'
    'X7'         'abcdef'       'X7'
    'X8'         'cdef'         'X8'
    'X9'         'bdef'         'X9'
    'X10'        'adef'         'X10'
    'X11'        'bcef'         'X11'
    'X12'        'acef'         'X12'
    'X1*X2'      'ab'                [1x32 char]
    'X1*X3'      'ac'                [1x22 char]
    'X1*X4'      'ad'                [1x23 char]
    'X1*X5'      'ae'           'X1*X5'
    'X1*X6'      'af'           'X1*X6'
    'X1*X7'      'bcdef'             [1x30 char]
    'X1*X8'      'acdef'             [1x31 char]
    'X1*X9'      'abdef'             [1x22 char]
    'X1*X10'     'def'               [1x22 char]
    'X1*X11'     'abcef'             [1x23 char]
    'X1*X12'     'cef'               [1x23 char]
    'X2*X3'      'bc'                [1x22 char]
    'X2*X4'      'bd'                [1x23 char]
    'X2*X5'      'be'           'X2*X5'
    'X2*X6'      'bf'           'X2*X6'
```

'X2*X7'	'acdef'	[1x31 char]
'X2*X8'	'bcdef'	[1x30 char]
'X2*X9'	'def'	[1x22 char]
'X2*X10'	'abdef'	[1x22 char]
'X2*X11'	'cef'	[1x23 char]
'X2*X12'	'abcef'	[1x23 char]
'X3*X4'	'cd'	[1x24 char]
'X3*X5'	'ce'	'X3*X5'
'X3*X6'	'cf'	'X3*X6'
'X3*X7'	'abdef'	[1x22 char]
'X3*X8'	'def'	[1x22 char]
'X3*X9'	'bcdef'	[1x30 char]
'X3*X10'	'acdef'	[1x31 char]
'X3*X11'	'bef'	'X3*X11 + X4*X9'
'X3*X12'	'aef'	'X3*X12 + X4*X10'
'X4*X5'	'de'	'X4*X5'
'X4*X6'	'df'	'X4*X6'
'X4*X7'	'abcef'	[1x23 char]
'X4*X8'	'cef'	[1x23 char]
'X4*X9'	'bef'	'X3*X11 + X4*X9'
'X4*X10'	'aef'	'X3*X12 + X4*X10'
'X4*X11'	'bcdef'	[1x30 char]
'X4*X12'	'acdef'	[1x31 char]
'X5*X6'	'ef'	'X5*X6'
'X5*X7'	'abcdf'	'X5*X7'
'X5*X8'	'cdf'	'X5*X8'
'X5*X9'	'bdf'	'X5*X9'
'X5*X10'	'adf'	'X5*X10'
'X5*X11'	'bcf'	'X5*X11'
'X5*X12'	'acf'	'X5*X12'
'X6*X7'	'abcde'	'X6*X7'
'X6*X8'	'cde'	'X6*X8'
'X6*X9'	'bde'	'X6*X9'
'X6*X10'	'ade'	'X6*X10'
'X6*X11'	'bce'	'X6*X11'
'X6*X12'	'ace'	'X6*X12'
'X7*X8'	'ab'	[1x32 char]
'X7*X9'	'ac'	[1x22 char]
'X7*X10'	'bc'	[1x22 char]
'X7*X11'	'ad'	[1x23 char]
'X7*X12'	'bd'	[1x23 char]
'X8*X9'	'bc'	[1x22 char]
'X8*X10'	'ac'	[1x22 char]
'X8*X11'	'bd'	[1x23 char]
'X8*X12'	'ad'	[1x23 char]
'X9*X10'	'ab'	[1x32 char]
'X9*X11'	'cd'	[1x24 char]
'X9*X12'	'abcd'	'X9*X12 + X10*X11'
'X10*X11'	'abcd'	'X9*X12 + X10*X11'
'X10*X12'	'cd'	[1x24 char]
'X11*X12'	'ab'	[1x32 char]

Table A.4 The two-level FFD for Cryogenic 1

Number of simulation	X_1	X_2	X_3	X_4	X_5	X_6	X_7	X_8	X_9	X_{10}	X_{11}	X_{12}
1	-1	-1	-1	-1	-1	-1	-1	-1	1	1	1	1
2	1	-1	-1	-1	-1	-1	-1	1	1	1	-1	-1
3	-1	1	-1	-1	-1	-1	-1	1	-1	-1	-1	1
4	1	1	-1	-1	-1	-1	-1	-1	-1	-1	1	-1
5	-1	-1	1	-1	-1	-1	-1	1	-1	-1	1	-1
6	1	-1	1	-1	-1	-1	-1	-1	-1	-1	-1	1
7	-1	1	1	-1	-1	-1	-1	-1	1	1	-1	-1
8	1	1	1	-1	-1	-1	-1	1	1	1	1	1
9	-1	-1	-1	1	-1	-1	1	-1	-1	-1	1	1
10	1	-1	-1	1	-1	-1	1	1	-1	-1	-1	-1
11	-1	1	-1	1	-1	-1	1	1	1	1	-1	1
12	1	1	-1	1	-1	-1	1	-1	1	1	1	-1
13	-1	-1	1	1	-1	-1	1	1	1	1	1	-1
14	1	-1	1	1	-1	-1	1	-1	1	1	-1	1
15	-1	1	1	1	-1	-1	1	-1	-1	-1	-1	-1
16	1	1	1	1	-1	-1	1	1	-1	-1	1	1
17	-1	-1	-1	-1	1	-1	1	-1	-1	1	-1	-1
18	1	-1	-1	-1	1	-1	1	1	-1	1	1	1
19	-1	1	-1	-1	1	-1	1	1	1	-1	1	-1
20	1	1	-1	-1	1	-1	1	-1	1	-1	-1	1
21	-1	-1	1	-1	1	-1	1	1	1	-1	-1	1
22	1	-1	1	-1	1	-1	1	-1	1	-1	1	-1
23	-1	1	1	-1	1	-1	1	-1	-1	1	1	1
24	1	1	1	-1	1	-1	1	1	-1	1	-1	-1
25	-1	-1	-1	1	1	-1	-1	-1	1	-1	-1	-1
26	1	-1	-1	1	1	-1	-1	1	1	-1	1	1
27	-1	1	-1	1	1	-1	-1	1	-1	1	1	-1
28	1	1	-1	1	1	-1	-1	-1	-1	1	-1	1
29	-1	-1	1	1	1	-1	-1	1	-1	1	-1	1
30	1	-1	1	1	1	-1	-1	-1	-1	1	1	-1
31	-1	1	1	1	1	-1	-1	-1	1	-1	1	1
32	1	1	1	1	1	-1	-1	1	1	-1	-1	-1

Number of simulation	X_1	X_2	X_3	X_4	X_5	X_6	X_7	X_8	X_9	X_{10}	X_{11}	X_{12}
33	-1	-1	-1	-1	-1	1	1	-1	1	-1	-1	-1
34	1	-1	-1	-1	-1	1	1	1	1	-1	1	1
35	-1	1	-1	-1	-1	1	1	1	-1	1	1	-1
36	1	1	-1	-1	-1	1	1	-1	-1	1	-1	1
37	-1	-1	1	-1	-1	1	1	1	-1	1	-1	1
38	1	-1	1	-1	-1	1	1	-1	-1	1	1	-1
39	-1	1	1	-1	-1	1	1	-1	1	-1	1	1
40	1	1	1	-1	-1	1	1	1	1	-1	-1	-1
41	-1	-1	-1	1	-1	1	-1	-1	-1	1	-1	-1
42	1	-1	-1	1	-1	1	-1	1	-1	1	1	1
43	-1	1	-1	1	-1	1	-1	1	1	-1	1	-1
44	1	1	-1	1	-1	1	-1	-1	1	-1	-1	1
45	-1	-1	1	1	-1	1	-1	1	1	-1	-1	1
46	1	-1	1	1	-1	1	-1	-1	1	-1	1	-1
47	-1	1	1	1	-1	1	-1	-1	-1	1	1	1
48	1	1	1	1	-1	1	-1	1	-1	1	-1	-1
49	-1	-1	-1	-1	1	1	-1	-1	-1	-1	1	1
50	1	-1	-1	-1	1	1	-1	1	-1	-1	-1	-1
51	-1	1	-1	-1	1	1	-1	1	1	1	-1	1
52	1	1	-1	-1	1	1	-1	-1	1	1	1	-1
53	-1	-1	1	-1	1	1	-1	1	1	1	1	-1
54	1	-1	1	-1	1	1	-1	-1	1	1	-1	1
55	-1	1	1	-1	1	1	-1	-1	-1	-1	-1	-1
56	1	1	1	-1	1	1	-1	1	-1	-1	1	1
57	-1	-1	-1	1	1	1	1	-1	1	1	1	1
58	1	-1	-1	1	1	1	1	1	1	1	-1	-1
59	-1	1	-1	1	1	1	1	1	-1	-1	-1	1
60	1	1	-1	1	1	1	1	-1	-1	-1	1	-1
61	-1	-1	1	1	1	1	1	1	-1	-1	1	-1
62	1	-1	1	1	1	1	1	-1	-1	-1	-1	1
63	-1	1	1	1	1	1	1	-1	1	1	-1	-1
64	1	1	1	1	1	1	1	1	1	1	1	1
Center	0	0	0	0	0	0	0	0	0	0	0	0

Table A.5 Normal operating condition values in the HCF plant

Description	Temperature	Pressure	Flowrate
De-ethanizer columns	Top -13- -16 ºC	14-15 Kg/cm²	70,000-104,000 BPD
De-butanizer column	Top 60-65 ºC	10 - 12.2 Kg/cm²	50,000-90,000 BPD
First Furnace	158- 166 ºC	0.95-1.25 Kg/cm²	2-4 MMPCD
De-propanizer column	Top 58- 68 ºC	14 - 17 Kg/cm²	20,000-60,000 BPD
First Naphthas separator	90- 96 ºC	2.3 - 3.5 Kg/cm²	20,000-40,000 BPD
Naphtha separator column	Top 60 -80 ºC	1.6 - 2.6 Kg/cm²	10,000-20,000 BPD
Naphtha separator column	Top 100- 120 ºC	3.5 - 4.2 Kg/cm²	9,000-19,000 BPD
Second Furnace	180- 200 ºC	0.60-0.80 Kg/cm²	1-2 MMPCD

Table A.6 Maximal and minimal HCF operational parameters.

Service	Minimum Limit	Low Limit	Normal Range	High Limit	Maximum Limit
Inlet C2+	18 Kg/cm²	20Kg/cm²	22-24 Kg/cm²	26Kg/cm²	28Kg/cm²
Inlet C3+	10Kg/cm²	12Kg/cm²	14-16 Kg/cm²	18.0Kg/cm²	20.0Kg/cm²
Balance tank 1	14.5Kg/cm²	18.0Kg/cm²	19-24 Kg/cm²	25.0Kg/cm²	27.0Kg/cm²
De-ethanizer columns	5.9Kg/cm²	6.5Kg/cm²	8.0-18.2 Kg/cm²	18.5Kg/cm²	19.4Kg/cm²
	38ºC	48 ºC	Top -13 - -16 ºC	65 ºC	78ºC
Balance tank 2	12.0Kg/cm²	13.0Kg/cm²	14-15 Kg/cm²	16.0Kg/cm²	16.5 Kg/cm²
De-butanizer	8.3Kg/cm²	8.4Kg/cm²	8.5-16.05 Kg/cm²	16.5Kg/cm²	16.8Kg/cm²
	55ºC	59 ºC	Top 60-65 ºC	75 ºC	85ºC
De-butanizer furnace	0.21Kg/cm²	0.85Kg/cm²	0.95-1.25 Kg/cm²	1.25Kg/cm²	2.0Kg/cm²
Balance tank 3	8.0Kg/cm²	9.0Kg/cm²	10-12.2 Kg/cm²	13.0Kg/cm²	14.0Kg/cm²
De-propanizer column	9.0 Kg/cm²	13.0 Kg/cm²	14-17 Kg/cm²	18 Kg/cm²	21.0Kg/cm²
	45ºC	47 ºC	Top 48-68 ºC	69 ºC	90ºC
Balance tank 4	8 Kg/cm²	9 Kg/cm²	10-15 Kg/cm²	16Kg/cm²	18Kg/cm²
First naphtha separador tank	0.8Kg/cm²	2.0Kg/cm²	2.3-3.5 Kg/cm²	3.8Kg/cm²	5.6Kg/cm²
First naphtha separador column	0.8Kg/cm²	0.9Kg/cm²	1.0-5.3 Kg/cm²	5.4Kg/cm²	5.5Kg/cm²
	30ºC	45 ºC	Top 60-80 ºC	85 ºC	90ºC
Second naphtha separador column	2.5Kg/cm²	3.3Kg/cm²	3.5-4.2 Kg/cm²	4.5Kg/cm²	6.3Kg/cm²
	90ºC	95 ºC	Top 100-120 ºC	130 ºC	150ºC
2nd naphtha column furnace	0. 14Kg/cm²	0.55Kg/cm²	0.6-0.8 Kg/cm²	0.85Kg/cm²	2.0Kg/cm²
Balance tank 5	0. 6Kg/cm²	1.10Kg/cm²	1.2-1.3 Kg/cm²	1.40Kg/cm²	4.9Kg/cm²
Balance tank 6	2. 0Kg/cm²	2.3Kg/cm²	2.4-2.6 Kg/cm²	2.7 Kg/cm²	3Kg/cm²

Table A.7 Matlab confounding pattern of the Fractional Factorial Design for HCF factor screening.

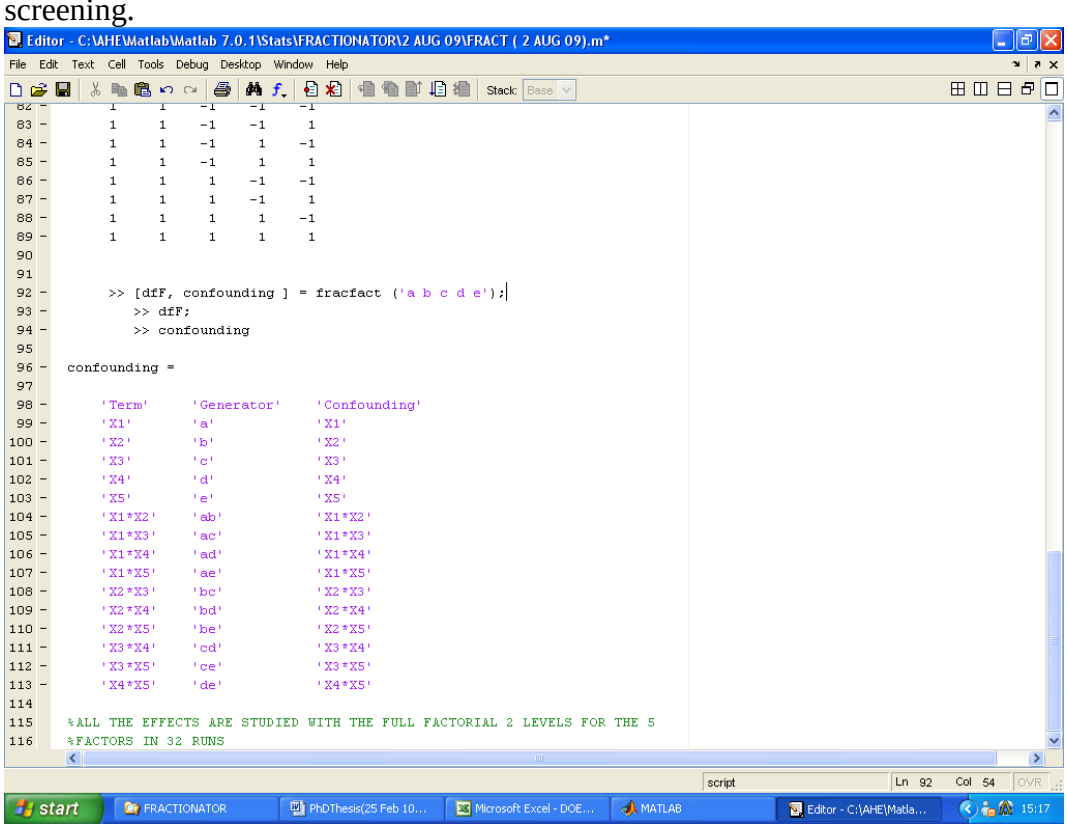

Table A.8 The two-level Fractional Factorial Design for HCF screening or factors.

Number	A	B	C	D	E
	X1	X2	X3	X4	X5
1	-1	-1	-1	-1	-1
2	1	-1	-1	-1	-1
3	-1	1	-1	-1	-1
4	1	1	-1	-1	-1
5	-1	-1	1	-1	-1
6	1	-1	1	-1	-1
7	-1	1	1	-1	-1
8	1	1	1	-1	-1
9	-1	-1	-1	1	-1
10	1	-1	-1	1	-1
11	-1	1	-1	1	-1
12	1	1	-1	1	-1
13	-1	-1	1	1	-1
14	1	-1	1	1	-1
15	-1	1	1	1	-1
16	1	1	1	1	-1
17	-1	-1	-1	-1	1

18	**1**	**-1**	**-1**	**-1**	**1**
19	**-1**	**1**	**-1**	**-1**	**1**
20	**1**	**1**	**-1**	**-1**	**1**
21	**-1**	**-1**	**1**	**-1**	**1**
22	**1**	**-1**	**1**	**-1**	**1**
23	**-1**	**1**	**1**	**-1**	**1**
24	**1**	**1**	**1**	**-1**	**1**
25	**-1**	**-1**	**-1**	**1**	**1**
26	**1**	**-1**	**-1**	**1**	**1**
27	**-1**	**1**	**-1**	**1**	**1**
28	**1**	**1**	**-1**	**1**	**1**
29	**-1**	**-1**	**1**	**1**	**1**
30	**1**	**-1**	**1**	**1**	**1**
31	**-1**	**1**	**1**	**1**	**1**
32	**1**	**1**	**1**	**1**	**1**